EXPLORATION OF DEVELOPMENTAL SIGNALING PATHWAYS IN TUMOR PROGRESSION AND TISSUE REGENERATION

A Dissertation

Presented to the Faculty of the Weill Cornell Graduate School

of Medical Sciences

in Partial Fulfillment of the Requirements for the Degree of

Doctor of Philosophy

by

Zhaohui Yang

May 2019

EXPLORATION OF DEVELOPMENTAL SIGNALING PATHWAYS IN TUMOR PROGRESSION AND TISSUE REGENERATION

Zhaohui Yang, Ph.D.

Cornell University, 2019

Developmental pathways, including Hedgehog (HH) and Hippo, are involved in cancer and tissue regeneration in various ways. HH signaling from the prostate epithelium was known to regulate mesenchyme expansion during development and regeneration. However, any role of HH signaling in stromal cells during prostate cancer (PCa) progression was poorly understood. I studied both mouse models and human PCa and observed paracrine HH signaling from epithelium to stroma. Genetic fate mapping suggested that the cancer-associated stroma derives from distinct cell types in different mouse models of PCa. Furthermore, I found that increasing HH signaling in the stroma results in decreased tumor progression and the presence of more smooth muscle, which correlated with lower grade PCa in human. Thus, we propose HH signaling restrains tumor progression by maintaining the smooth muscle and preventing invasion by tumor cells.

The Hippo pathway has been implicated in the repair of several tissue types. However, any possible role of the Hippo pathway in development or postnatal regeneration of the mouse cerebellum was unknown. I used genetic mouse models involving deletion of the transcriptional co-activators YAP and/or TAZ, and found that YAP, but not TAZ, is an essential regulator of effective recovery of the cerebellum after irradiation-induced injury at birth. Specifically, genetic ablation of *Yap* in the Nestin-expressing progenitors (NEPs), a progenitor

population central to cerebellar regeneration of granule cell precursors (GCPs) following injury, results in significantly impaired cerebellar growth and disruption in the cellular cytoarchitecture. The *Yap* mutant NEPs respond normally to the injury by migrating to the GCP niche, but then undergo increased cell death. Loss of YAP in NEPs or GCPs during normal development only mildly affects differentiation. Moreover, loss of TAZ does not alter development or regeneration of the cerebellum, or abrogate regeneration of GCPs by *Yap* mutant NEPs. Instead, *Taz* ablation seems to partially rescue the poor recovery of GCPs by *Yap* mutant NEPs, indicating that TAZ and YAP have distinct functions during cerebellar regeneration.

In summary, my thesis research provides new insights into the molecular signaling underlying PCa progression and the development and regeneration of the neonatal cerebellum.

BIOGRAPHICAL SKETCH

Zhaohui Yang was born in Chengde, Hebei, China and earned her Bachelor degree in Biotechnology from Nankai University, Tianjin in 2011. In 2012 Zhaohui joined the doctoral program in Biochemistry, Cell, and Molecular Biology at the Weill Cornell Graduate School of Medical Sciences in New York and did her graduate research in Dr. Alexandra L. Joyner's laboratory at Memorial Sloan Kettering Cancer Center. Her graduate studies focused on Hedgehog signaling in prostate cancer and Hippo signaling in cerebellum regeneration. During the course of her graduate research in Dr. Joyner's laboratory, Zhaohui presented her research at...Zhaohui published one part of her thesis research in a paper entitled "Stromal Hedgehog signaling maintains smooth muscle and hampers micro-invasive prostate cancer" in Disease Models & Mechanisms in 2017. A second manuscript on the other thesis research project entitled "YAP is involved in regeneration of the injured neonatal cerebellum" is in preparation.

My dissertation is dedicated to Sonic the Hedgehog, Gloria the Hippo,

Mickey and Minnie the Mice,

and all the friends of theirs and ours,

for kindly accepting us humans to this gorgeous planet.

ACKNOWLEDGEMENTS

I would like to express my gratitude to my mentor, Dr. Alexandra L. Joyner for all her guidance and mentorship. Her dedication to science has been my constant source of inspiration. I am truly grateful to have had the opportunity to work with such an incredible scientist and learn from her in various aspects of science and life.

I would like to thank the members of my thesis committee Drs. Danwei Huangfu and Yu Chen for their time and valuable suggestions on both research and my future career throughout the years.

Finally, I would like to thank past and present members of the Joyner laboratory for their generous support, insightful discussions and technical assistance. I am thankful to Drs. Yu-Ching Peng, Alexandre Wojcinski, whose scientific expertise and collegial support have been great help to my thesis research.

TABLE OF CONTENTS

LIST OF FIGURES

LIST OF TABLES

Chapter 1 Introduction

Signaling pathways that are essential for organ growth during development are often also exploited by cancer and utilized during tissue regeneration in a variety of different ways. The Hedgehog and Hippo pathways have important and usually distinct functions in organ development. Hedgehog signaling is known for exerting both mitogenic and morphogenic effects on organ growth and patterning, including the prostate and cerebellum. Hippo signaling is known to control the size of many organs, albeit with a less-defined role in the brain. Here I review the contribution of Hedgehog and Hippo pathways in development and their exploitation in tissue regeneration and cancer, particularly in the prostate and brain, respectively.

1.1 Hedgehog signaling

1.1.1 Overview of the Hedgehog pathway

Mammalian Hedgehog (HH) signaling has three secreted ligands that are homologs of the *Drosophila* HH polarity protein: Sonic Hedgehog (SHH), Indian Hedgehog (IHH), and Desert Hedgehog (DHH). HH signaling usually acts in a paracrine manner, in which HH ligands secreted from HH-producing cells act on neighboring or nearby HH-receiving cells of a different lineage. In HH-producing cells, the ligands undergo autoproteolytic cleavage and extensive post-translational modifications (Pepinsky et al., 1998; Perler, 1998; Taylor et al., 2001) before being exported by a membrane transporter protein named Dispatched (Briscoe and Therond, 2013). These modifications enable the ligands to travel and establish a protein gradient, and interact with the HH-

receiving cells to exert their functions (Beachy et al., 2010; Chuang and McMahon, 1999).

The HH-receiving cells carry out signal transduction through its receptor repertoire, including the twelve-pass transmembrane receptor Patched 1 (PTCH1) (Briscoe and Therond, 2013), and three co-receptors in vertebrates, CDO, BOC and GAS1 (Allen et al., 2007; Okada et al., 2006; Tenzen et al., 2006). Humans and mice have a second *Ptch* gene, *Ptch2*, with a different expression pattern and less defined function (Motoyama et al., 1998a; Motoyama et al., 1998b; Smyth et al., 1999). In the absence of HH ligand, PTCH1 uses its internal "tunnel" to export membrane cholesterol, which depletes cholesterol that is required for the activation of Smoothened (SMO), a seven-pass G-protein-coupled membrane protein (Sommer and Lemmon, 2018). When a HH ligand is present, two PTCH1 molecules bind to distinct sites of HH ligand in a steroid-dependent manner, resulting in the blockade of "tunnels" within PTCH1 (Gong et al., 2018; Qi et al., 2018; Sommer and Lemmon, 2018) (Fig. 1.1). Thus, abundant membrane cholesterol is free to traverse and bind with SMO, which induces a conformational change in SMO (Huang et al., 2018; Sommer and Lemmon, 2018; Zhang et al., 2018). With a structure that resembles activated G-protein-coupled receptors (Huang et al., 2018), SMO is able to activate Hedgehog signaling through the downstream GLI (glioma-associated oncogene family members) zinc-finger transcription factors.

The mammalian GLI protein family has three members – GLI1, GLI2, and GLI3, each with both distinct and overlapping functions in the nervous system

(Bai et al., 2002; Bai and Joyner, 2001; Bai et al., 2004; Motoyama et al., 2003; Park et al., 2000; Persson et al., 2002; Petrova et al., 2013) and in other organs (Drakopoulou et al., 2010; Rowbotham et al., 2009; Sabol et al., 2018; Solanki et al., 2017; Solanki et al., 2018; Theil et al., 1999). Upon HH ligand binding, SMO activation protects GLI2/GLI3 from proteasomal degradation, promoting GLI2, and to a lesser extent GLI3, to act as transcriptional activators. This in turn stimulates the expression of HH target genes including *Gli1* (Bai et al., 2004; Sasaki et al., 1999; Smelkinson et al., 2007), which forms a positive feedback on HH signaling (Bai et al., 2002; Park et al., 2000). Expression of another direct HH target gene *Ptch1* positively correlates with HH activity, imposing a negative feedback on HH signaling (Vokes et al., 2007; Vokes et al., 2008). When HH signaling is inactive, GLI2/GLI3 are phosphorylated and proteolytically processed, rendering GLI3, and to a lesser extent GLI2, to become transcriptional repressors (Bhatia et al., 2006; Pan et al., 2006; Wang et al., 2000; Wang and Li, 2006) (Fig. 1.1).

What is unique to mammalian HH signaling is the dependence on primary cilia. Primary cilia are slender microtubule-based cellular antennae that sense extracellular cues and convey intracellular signaling. They function as signaling hubs with concentration of several HH pathway components (Goetz and Anderson, 2010). The importance of primary cilia for proper mammalian HH signaling was first demonstrated by altered GLI protein activities in mutants of genes encoding ciliary proteins (Haycraft et al., 2005; Huangfu and Anderson, 2005; Liu et al., 2005). The dynamic translocation of PTCH and SMO into and out of the primary cilium is essential for proper modulation of mammalian HH signaling (Rohatgi et al., 2007). In the absence of HH, PTCH1

is enriched in the cilium and prevents SMO from entering the same location, thus downregulating SMO activity. When HH is present, SMO accumulates in the cilium and antagonizes SUFU (Suppressor of Fused), a negative regulator of HH signaling, which leads to the convertion of GLI2/3 into transcriptional activators to promote the expression of HH target genes (Cooper et al., 2005; Svard et al., 2006).

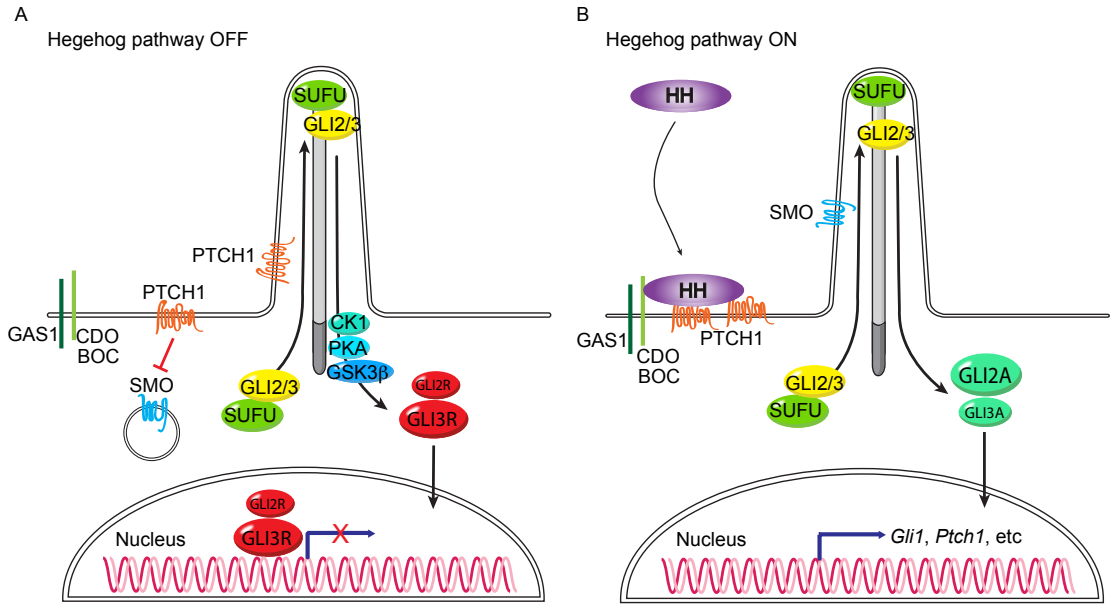

Figure 1.1 Schematics of the Hedgehog signaling pathway in mammals. (Adpated from (Peng and Joyner, 2015))

(A) In the absence of HH, PTCH1 prevents SMO from translocating to the primary cilium. GLI2/3 are associated with SUFU and phosphorylated by PKA, CK1, and GSK3β. GLI2/3 undergo proteolysis, leading to the conversion of GLI3, and to a lesser extent GLI2, into transcriptional repressors.
(B) In the presence of HH, the ligand binds with two PTCH1 molecules, alleviating the inhibition on SMO. SMO enters the cilium and promotes the dissociation of the SUFU-GLI2/3 complex. The proteolysis of GLI2/3 is inhibited, which promotes the formation of GLI2, and to a lesser extent GLI3, transcriptional activators, to induce expression of HH target genes including *Gli1* and *Ptch1*.

1.1.2 Hedgehog signaling in development of the prostate

HH signaling exerts crucial effects on the development of the prostate. The prostate is a male sex-accessory gland that originates from the endoderm-derived urogenital sinus (UGS). The first morphological event in prostate development occurs at embryonic day 16.5 (E16.5) in the mouse, when the urogenital sinus epithelium (UGE) starts to form solid epithelial buds that invade the surrounding urogenital sinus mesenchyme (UGM). This so-called budding is initiated by androgen signaling from the mesenchyme that specifies the epithelium (Cunha et al., 1986; Cunha and Lung, 1978). During embryonic development, the epithelial buds elongate and form unbranched ducts. After birth, these nascent epithelial ducts further elongate, canalize, and undergo extensive branching, to form an elaborate ductal system (Sugimura et al., 1986a). This branching morphogenesis starts by postnatal day 15 (P15) and is largely completed by P30 (Sugimura et al., 1986a). The mature mouse prostate consists of four pairs of lobes: anterior prostate (AP), dorsal prostate (DP), lateral prostate (LP), and ventral (VP) prostate, with each prostatic lobe having its distinct branching pattern (Sugimura et al., 1986a). In some studies, the DP and LP are collectively referred to as the dorsolateral prostate (DLP). Importantly, androgen signaling in the epithelium is essential for the production of prostate gland secretion (Cunha et al., 1987; Cunha and Lung, 1978).

During prostate development, *Shh* expression is enriched in the epithelium of nascent buds and the growing tips of elongating ducts (Lamm et al., 2002; Podlasek et al., 1999), while the surrounding mesenchyme has expression of HH targets including *Ptch1* and *Gli1* (Lamm et al., 2002; Pu et al., 2004), among many growth-inducing molecules (Yu and Bushman, 2013; Yu et al.,

2009). This points to a paracrine HH signaling from the epithelium to the mesenchyme. HH signaling was initially considered to be indispensible for prostate morphogenesis, since the use of a SHH neutralizing antibody abolished the growth and ductal morphogenesis of E15 UGS transplants that were grafted under the renal capsule of another adult male host mouse (Podlasek et al., 1999). Moreover, chemical inhibitor of SHH signaling using the SMO antagonist cyclopamine resulted in a severe inhibition of ductal budding in prostate organ cultures (Lamm et al., 2002). However, subsequent studies showed that UGS from *Shh*-null embryos had normal morphogenesis when it was grafted in male host mouse with normal androgen levels, or when UGS was treated with exogenous androgen (Berman et al., 2004; Freestone et al., 2003). This result seems to argue against the requirement of HH signaling for prostate development since the defects in *Shh*-null mutants could be rescued by androgens. But it is also possible that paracrine HH signaling in the mesenchyme induces androgen signaling in the epithelium in order for the prostate to grow. In the studies using chemical inhibition or SHH neutralizing antibody, paracrine HH signaling in the mesenchyme was inhibited, and thus prostate development was abrogated in the absence of exogenous androgens. In addition, elevated expression of *Ihh* was observed in *Shh*-null UGS, which potentially provided functional compensation for the loss of *Shh* (Doles et al., 2006).

Shh expression in the UGS epithelium is at its peak upon ductal budding and is maintained until ductal branching, then gradually decreases and eventually tapers off to a low but detectable level in the adult (Lamm et al., 2002; Podlasek et al., 1999) (Fig. 1.2). The effects of HH signaling on prostate ductal

morphogenesis are also stage-dependent (Yu and Bushman, 2013). Specifically, *in vitro* organ cultures showed that chemical inhibition of HH signaling reduced ductal tips in prenatal UGS explants but increased ductal tips in postnatal prostate explants. When explants were co-cultured with a SMO-overexpressing mesenchymal cell line, embryonic prostates had an increase in ductal growth while postnatal prostates had a decrease in ductal growth (Yu and Bushman, 2013). Furthermore, using transgenic mouse models with ectopic HH signaling in the mesenchyme from midgestation onwards, Yu and Bushman (2013) found that epithelial cell proliferation is enhanced in the embryonic prostate but reduced in postnatal prostates (Yu and Bushman, 2013). This elegant study reveals a growth-inducing effect of HH signaling during embryonic development of the prostate and a growth-inhibiting effect postnatally.

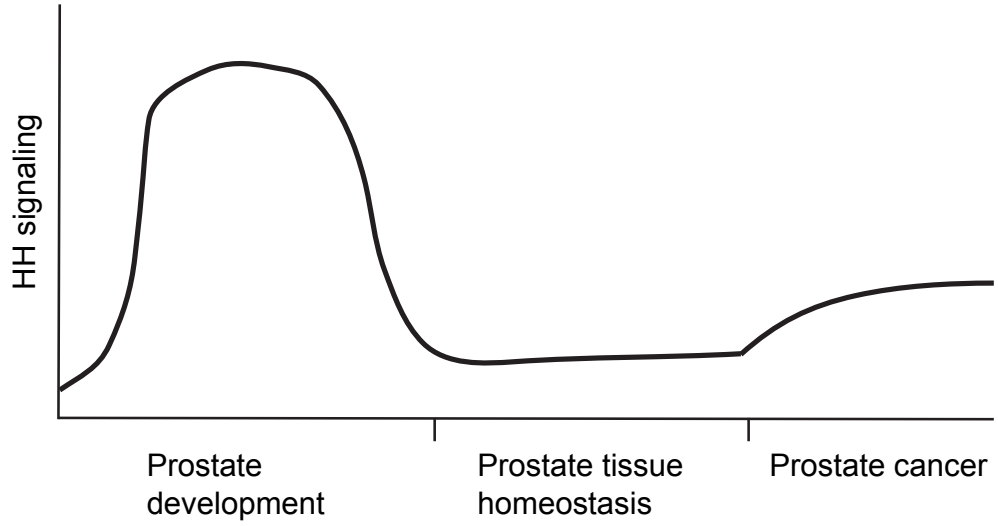

Figure 1.2 Schematic of HH signaling in the prostate during development, tissue homeostasis, and cancer

SHH signaling is at its peak during embryonic development of the prostate, and then gradually decreases and eventually tapers off to a low but detectable level in the adult. The signaling is increased in prostate cancer, and stromal HH signaling acts to inhibit tumor progression (this thesis).

1.1.3 Hedgehog signaling in regeneration of the prostate

The adult mouse prostate normally stays quiescent with sparse cell proliferation in distal duct tips (Sugimura et al., 1986c). Both development and maintenance of the prostate require androgen signaling. Castration of adult males causes a major glandular involution of the prostate due to widespread epithelial apoptosis and reduction in ductal tips and branching points (Sugimura et al., 1986b). Additionally, concurrent apoptotic death in both epithelial and stromal cells was observed in rat prostate following castration (Banerjee et al., 1995). However, administration of exogenous testosterone induces robust cell proliferation and branching morphogenesis in involuted prostates, which completely reconstitutes the architecture and restores the function of the prostate after only 14 days (Sugimura et al., 1986b). Amazingly, such cycles of involution and regeneration can be repeated over 30 times (Isaacs, 1985). The extensive regenerative capacity of the adult prostate has stimulated a general postulation of the existence of a population of castration-resistant stem or progenitor cells that are capable of self-renewal.

A potential role of HH signaling in prostate regeneration was indicated from an experiment involving inhibition of HH signaling by SMO inhibitors or HH-blocking antibodies that resulted in abrogation of the normal regeneration process (Karhadkar et al., 2004). This was interpreted to mean that HH signaling is important for stem cell-driven prostate regeneration, but the mode of action by HH signaling was not distinguished between aurocrine versus paracrine, and also the exact cell types that could respond to HH signaling were not identified. Contrary to the proposed positive role of HH signaling for

prostate regeneration, another study by the same group found that decreased HH activity in the epithelium enhanced ductal branching during prostate regeneration (Lim et al., 2014). Specifically, *Ihh* expression is enriched in epithelial cells between growing buds and focally decreased at ductal branching sites. Functional studies indicate that IHH downregulates the stromal expression of hepatocyte growth factor (HFG), which stimulates epithelial proliferation, and thus IHH negatively regulates epithelial bud formation during regeneration (Lim et al., 2014). Additional evidence is needed for a comprehensive understanding of the function of HH signaling, particularly in regard to its crosstalk with other regulators during prostate regeneration.

1.1.4 Hedgehog signaling in human cancers

Aberrant Hedgehog signaling is observed in a wide variety of human cancers. The mode of action for HH signaling can be categorized into two types. The first type involves cell autonomous HH signaling which results from somatic mutations in HH pathway genes including *Ptch1*, *Smo*, or *SuFu*. In this class, HH signaling is constitutively activated in cancer cells independent of HH ligands to drive tumor development. Reported human cancer types that fall into this class include basal cell carcinoma (BCC) (Hahn et al., 1996), medulloblastoma (Cavalli et al., 2017; Kool et al., 2014), rhabdomyosarcoma (Pressey et al., 2011; Tostar et al., 2006), and meningiomas (Aavikko et al., 2012; Clark et al., 2013; Kijima et al., 2012). For example, loss-of-function mutation in *PTCH1* directly associates with Gorlin syndrome, and patients with Gorlin syndrome develop medulloblastoma and BCC (Gorlin, 2004). Gain-of-function mutations of *SMO* are observed in BCCs (Epstein, 2001; Hahn et al., 1996; Johnson et al., 1996) and medulloblastomas (Kool et al., 2014).

Consistent with the human genetics, in mouse models where *Ptch1* is deleted or *SmoM2* (a constitutively active form of SMO) is expressed in the appropriate cell type, tumors form that are similar to Gorlin syndrome patients, BCCs and medulloblastomas (Mao et al., 2006; Xie et al., 1998). Vismodegib, a SMO inhibitor, has been approved by the FDA for the treatment of locally advanced and metastatic BCCs.

The second mode of action of HH signaling in cancer is cell non-autonomous paracrine signaling due to ectopic expression of HH ligands and the surrounding tumor stroma respond to the signaling. It is generally found that the HH receiving tumor stroma also returns reciprocal paracrine signals by secreting factors that stimulate the growth of tumor epithelium. A number of studies in human and mouse prostate cancer supported paracrine HH signaling from epithelium to stroma (Fan et al., 2004; Ibuki et al., 2013; Shaw et al., 2009). Several other studies reported the co-expression of SHH ligands and HH target genes such as *Gli1*, *Ptch1*, and *Hip* in prostate cancer epithelial cells (Chen et al., 2009; Karhadkar et al., 2004; Sanchez et al., 2004), particularly in advanced and metastatic cancers (Chen et al., 2009; Sheng et al., 2004; Tzelepi et al., 2011). However, these results are not sufficient to indicate autocrine HH signaling in prostate cancer due to the questionable reliability of antibodies to HH pathway components, the high heterogeneity of prostate cancer, and the fact that epithelium and stroma were not effectively separated in these analyses. In Chapter 2, I describe a paracrine mode of HH signaling in multiple mouse models of prostate cancer.

In addition, HH signaling may be activated in a non-canonical way, in which ligand binding of PTCH1 and activation of SMO is bypassed and GLI transcription factors are directly targeted, transcriptionally or epigenetically, by other molecules or signaling (Kasper et al., 2006). HH signaling may also synergize with other signaling pathways to regulate certain target genes (Kasper et al., 2006).

The functions of HH signaling for tumor progression are likely related to its mode of action. For example, in a mouse model of small cell lung cancer with cell autonomous HH signaling, ectopic expression of SmoM2 in tumor cells increased the tumor number and volume (Park et al., 2011). In other cancers dominated by paracrine HH signaling, HH activity was indicated to have negative effects on tumor progression. Recent studies in pancreas and bladder cancers showed that inhibition of HH signaling through genetic ablation of HH activating components in the stroma enhances tumor progression and decreases survival (Lee et al., 2014a; Rhim et al., 2014; Shin et al., 2014). Additionally, in mouse models of colon cancer, stroma-specific HH activation inhibits tumor progression, while decreased HH activity accelerates colon tumorigenesis (Gerling et al., 2016; Lee et al., 2016). Similarly in prostate cancer, SmoM2 expression in the epithelium was not sufficient to initiate tumorigenesis in mice (Mao et al., 2006). However, it was not tested in mouse models whether alteration of HH signaling in the stroma changes prostate tumor progression. In Chapter 2, I describe experiments in which we test whether HH signaling in the tumor stroma can alter prostate cancer progression in a mouse model, and found that excess HH signaling in prostate stromal cells has an inhibitory effect on cancer progression (Fig. 1.2).

Prostate cancer is the second leading cause of cancer-related death in men in the United States (Siegel et al., 2018) and the second most common malignancy in men worldwide (Torre et al., 2015). Currently, the dominant therapies for local prostate cancer are surgical removal and radiation. For advanced tumors, androgen deprivation is the primary treatment that effectively reduces tumor size. However, castration-resistant cancer eventually recurs and becomes refractory to any existing treatment (Ramamurthy et al., 2017). A popular idea is that cancer-initiating cells remain dormant and survive through therapies, then may awake and become active in repopulating tumor cells. In this process, many signaling pathways, including HH, have been proposed to play significant roles. Given the current diagnostic system that mainly relies on tumor histology assessment, a thorough characterization of the molecular signature for prostate cancer will be instrumental for the development of more effective diagnosis and treatments.

1.2 Hippo signaling

1.2.1 Overview of Hippo pathway

The Hippo pathway, first discovered through mosaic genetic screens for tissue growth related genes in *Drosophila melanogaster*, is evolutionarily conserved between mammals and fruit flies. In *Drosophila*, the Hippo pathway comprises a core kinase cascade of Ste20-like kinase Hippo (Hpo) (Harvey et al., 2003; Jia et al., 2003; Pantalacci et al., 2003; Udan et al., 2003; Wu et al., 2003) and NDR family kinase Warts (Wts) (Justice et al., 1995; Xu et al., 1995). Hpo directly binds with a scaffold protein Salvador (Sav) to phosphorylate and activate Wts, which then complexes with its regulatory protein Mats (Mob as

tumor suppressor) (Kango-Singh et al., 2002; Lai et al., 2005; Tapon et al., 2002). Downstream to the kinase cascade is a Wts-interacting protein Yorkie (Yki) that is directly subject to negative regulation by Wts (Dong et al., 2007; Huang et al., 2005). Yki is a Hippo pathway transcription co-activator with phosphorylation-dependent shuttling between the nucleus and cytoplasm. Specifically, when Hippo pathway is in the “on” state, Yki is phosphorylated by the Wts-Mats complex and binds with 14-3-3, which leads to its retention in the cytoplasm (Oh and Irvine, 2008; Ren et al., 2010). When the Hippo pathway is in the “off” state, unphosphorylated Yki translocates into the nucleus, and acts together with the transcription factor Scalloped (Sd) to initiate downstream target gene expression that promotes cell proliferation, survival, and growth (Mahoney et al., 2005; Vassilev et al., 2001).

In mammals, the core kinase components and transcription effectors are highly conserved as their *Drosophila* counterparts (Fig. 1.3). The mammalian orthologs of Hippo pathway components include the serine/threonine kinases MST1/2 (Mammalian Sterile 20-like kinases 1 and 2, Hpo homologs) and LATS1/2 (large tumor suppressor 1 and 2, Wts homologs), the scaffold proteins SAV1 (Salvador homolog 1, Sav homolog) and MOB1A/B (MOB kinase activator 1A and 1B, Mats homolog), the Yki homologs YAP (Yes-associated protein) and its paralog TAZ (transcriptional co-activator with PDZ-binding motif; also called WWTR1, for WW-domain containing transcription regulator 1), and the TEA domain-containing sequence-specific transcription factors TEAD1-4 (also referred to as TEFs, for transcriptional enhancer factors, Sd homologs). The pathway is considered to be in the active state when the MST and LATS kinases are active. Upon activation of the Hippo pathway, the

complex of MST1/2 and SAV1 phosphorylates and activates LATS1/2 and MOB1 cofactors (Callus et al., 2006; Chan et al., 2005; Praskova et al., 2008; Wei et al., 2007; Wu et al., 2003), which in turn directs multi-site phosphorylation of YAP/TAZ and hinders their nuclear transport, thereby inhibiting transcriptional activation of growth-promoting genes (Hao et al., 2008; Huang et al., 2005; Lei et al., 2008; Oka et al., 2008; Zhao et al., 2010). Phosphorylated YAP/TAZ are retained in the cytoplasm by 14-3-3 and undergo ubiquitin-dependent protein degradation (Kanai et al., 2000; Liu et al., 2010; Ren et al., 2010; Zhao et al., 2010). Conversely, when the Hippo pathway is inactive, dephosphorylated YAP/TAZ translocate into the nucleus, form complexes with the TEADs that can directly bind to DNA to drive transcriptional programs related to cell proliferation and organ growth (Vassilev et al., 2001; Zhao et al., 2008). In addition to the TEAD family transcription factors, YAP/TAZ can also interact with many other transcription factors including SMADs (Alarcon et al., 2009; Ferrigno et al., 2002; Varelas et al., 2008), RUNT-related transcription factors (RUNXs) (Cui et al., 2003; Hong et al., 2005; Yagi et al., 1999; Zaidi et al., 2004), T-box transcription factor 5 (TBX5) (Murakami et al., 2005; Rosenbluh et al., 2012) to regulate the transcription of a variety of downstream target genes.

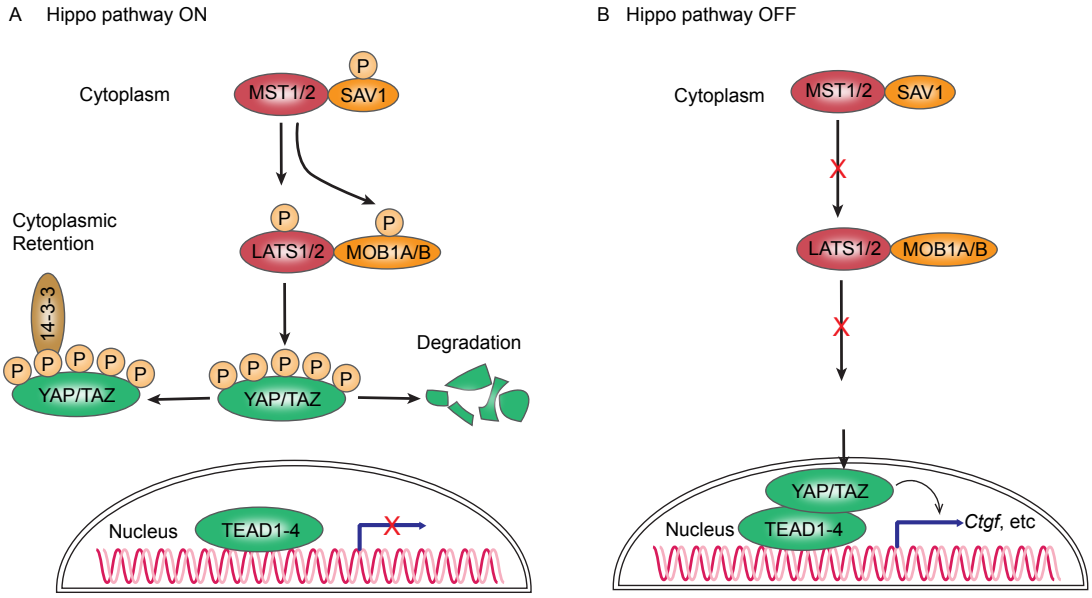

Figure 1.3 Schematic of the core Hippo signaling pathway in mammals. (Adapted from (Johnson and Halder, 2014))

(A) When the Hippo pathway is active, MST1/MST2 phosphorylates SAV1, and together they phosphorylate and activate LATS1/LATS2 kinases and MOB1A/MOB1B, which then phosphorylate YAP/TAZ. Phosphorylated YAP and TAZ are sequestered in the cytoplasm by the 14-3-3 protein and undergo proteasomal degradation. As a result, there is no expression of their target genes.
(B) When the Hippo pathway is inactive, the kinases MST1, MST2, LATS1 and LATS2 are inactive. Unphosphorylated YAP and TAZ enter the nucleus and form a complex with TEADs to promote the expression of target genes including *Ctgf*.

1.2.2 Hippo signaling in development of the brain and other organs

The function of the Hippo pathway in development has been extensively studied using genetically engineered mouse models. *Yap* null mutant mice have an embryonic lethal phenotype (Morin-Kensicki et al., 2006), and *Taz* null mutant mice show partial embryonic lethality (Hossain et al., 2007; Makita et al., 2008; Tian et al., 2007), suggesting that YAP, and to a lesser extent TAZ, are indispensible in embryonic development. Meanwhile, normal Hippo signaling controls organ size by preventing overgrowth such as the heart and liver (Camargo et al., 2007; Dong et al., 2007; Heallen et al., 2011).

Accumulating evidence shows that Hippo signaling controls organ growth through regulating the maintenance and differentiation of stem cells and progenitor cells. For example, YAP and TAZ have been reported to maintain ES cell self-renewal (Alarcon et al., 2009; Varelas et al., 2008). Consistently, *Yap* knockdown in mouse ES cells leads to loss of pluripotency, whereas overexpression of *Yap* inhibits ES cell differentiation (Lian et al., 2010). In the mouse fetal heart, genetic deletion of *Sav1* or activation of YAP stimulates cardiomyocyte proliferation (Heallen et al., 2011; von Gise et al., 2012). In liver, LATS1/2 are required for hepatocyte differentiation through inhibition of YAP/TAZ activities, while YAP overexpression suppresses normal hepatocyte maturation (Yi et al., 2016). Similarly in the skin, YAP overexpression causes expansion of basal epidermal progenitors and failure in terminal differentiation (Beverdam et al., 2013; Zhang et al., 2011).

The balance of progenitor expansion and terminal differentiation is presumably attributed to the subcellular localization-dependent transcriptional activities of

YAP/TAZ. For example, in the developing lungs, expression and subcellular localization of YAP controls progenitor cell behaviors through control of SOX2 expression (Mahoney et al., 2014). In particular, in the transition zone between airway and distal lung, YAP mainly accumulates in the nucleus of progenitors cells, which promotes TGF-β-dependent induction of SOX2 expression. In contrast, YAP remains in the cytoplasm of airway epithelial progenitors, which promotes cell differentiation and ultimately generates the airway epithelium (Mahoney et al., 2014). It has also been shown that nuclear YAP is required for branching morphogenesis through control of cell proliferation and physical properties of the epithelium (Lin et al., 2017). Similarly during skin development, nuclear YAP expression is high in skin progenitor cells, which correlates with the proliferative capacity and declines with age (Schlegelmilch et al., 2011; Zhang et al., 2011). Cytoplasmic YAP becomes evident upon skin progenitor cell differentiation. In addition, recent work revealed a non-canonical mechanism of YAP regulation on cardiomyocyte proliferation, where AMOTL1 (Angiomotin-like 1) directly binds with both YAP and FAT4 (FAT tumor suppressor homolog 4) to sequester YAP in the cytoplasm in a LATS1/2-independent manner, thereby inhibiting YAP-mediated cardiac growth (Ragni et al., 2017). In summary, nuclear YAP/TAZ promotes progenitor cell proliferation and proper organ growth through control of downstream transcriptional programs. In contrast, cytoplasmic YAP/TAZ drives progenitor differentiation during organ development.

During development, the brain requires rigorous control over the expansion of neural progenitors and the production of post-mitotic neurons and glial cells. Therefore, any disruption of the balance may result in severe consequences

on brain size and structure and neural functions. Several studies have implicated the Hippo pathway in regulating cell proliferation and differentiation in the nervous system. For example, YAP over-activation in the embryonic chick neural tube leads to expansion of neural progenitor cells (Cao et al., 2008), suggesting the importance of YAP in the maintenance of neural progenitor proliferation. A recent study in *Drosophila* showed that disruption of Hippo signaling through loss-of-function mutations of core kinases *Hpo* or *Wts* results in increased neuroblast proliferation and substantial brain overgrowth (Poon et al., 2016). In the postnatal mouse retina, shRNA against *Yap* was found to decrease proliferation and increase terminal differentiation of retinal progenitors, whereas ectopic expression of *Yap* promotes proliferation (Zhang et al., 2012). Conditional ablation of *Yap* alone from embryonic murine neural stem cells using a *Nestin-Cre* results in hydrocephalus with no reported major anatomical changes in the brain, and very subtle defects in the proliferation of radial glial progenitors (Park et al., 2016). Strikingly, genetic ablation of both *Yap* and *Taz* in radial glial progenitors of the dorsal telencephalon using an *Emx1-Cre* results in profound cortical defects, including significant thinning of cortical tissues and severe hydrocephalus, accompanied by a marked reduction of radial glial progenitors and intermediate progenitors (Kong, 2018). The phenotype is attributed to impaired proliferation and premature differentiation of neural progenitor cells (Kong, 2018). These two studies could indicate redundant functions of YAP and TAZ, but the same *Cre* transgene needs to be used to ablate *Yap* alone and *Yap*/*Taz* together to confirm this. Moreover, inactivation of LATS1/2 with *Nestin-Cre* in the neural progenitor population in the embryonic mouse brain leads to YAP/TAZ-driven global hypertranscription with upregulation of many target genes related to cell

growth and proliferation, as revealed by cell-number normalized transcriptome analysis, which in turn inhibits the differentiation of neural progenitors (Lavado et al., 2018). As for the cerebellum, one study using cultured granule cell precursors, which are the most abundant cell population in the brain and critical for the growth of cerebellum, showed that cell proliferation is increased by overexpression of *Yap* and decreased by shRNA knockdown of *Yap* (Fernandez et al., 2009). Given the lack of evidence for a function of the Hippo pathway in cerebellar development, in Chapter 3, I describe experiments in which we test the requirement for *Yap* and *Taz* in two critical cerebellar progenitor populations during development, and found that loss of YAP/TAZ did not affect the growth of the cerebellum but had mild effects on the differentiation of progenitor cells (Fig. 1.4).

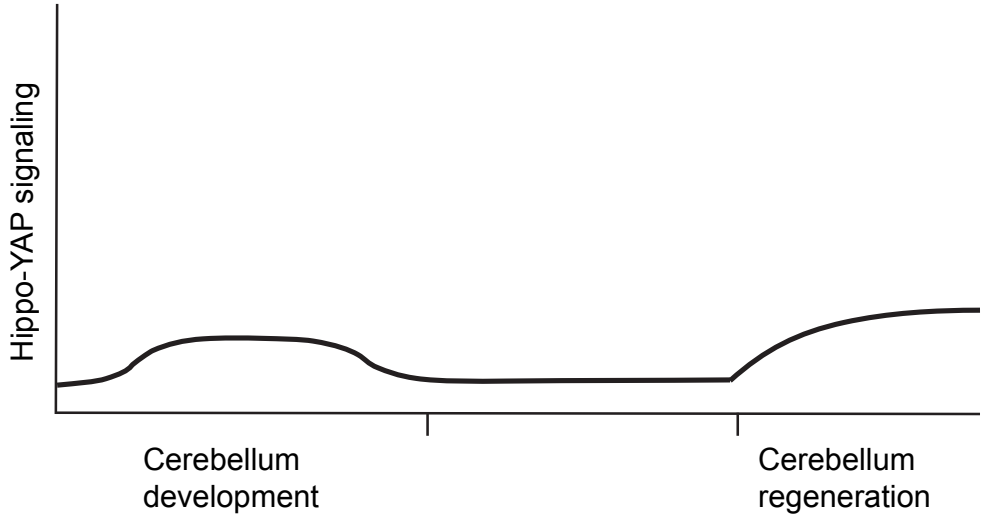

Figure 1.4 Schematic of Hippo signaling in the development and regeneration of the cerebellum.

YAP in the Hippo signaling pathway has a minor role in CB development, with a negative effect on the differentiation of progenitor cells. YAP has a major role in the regeneration of neonatal CB (this thesis).

1.2.3 Hippo signaling in regeneration of the brain and other tissues

There is very limited evidence for the function of Hippo signaling in the regeneration of the central nervous system (CNS), largely due to the fact that the CNS has a very limited capacity for self-renewal. One study using adult rat spinal cord showed elevated expression of YAP and TAZ after peripheral nerve injury (Li et al., 2013). Intriguingly, a recent study revealed a remarkable capacity of regeneration in the neonatal mouse cerebellum (Wojcinski et al., 2017), consistent with previous work that had a similar finding in the rat cerebellum (Altman et al., 1969). In Chapter 3, I describe the essential role of YAP in a population of plastic neural progenitors during recovery of the neonatal mouse cerebellum from irradiation-induced cell death of granule cell precursors, and show evidence that TAZ may have a divergent role from YAP during cerebellar regeneration.

The role of Hippo pathway in the regeneration of several other organs has been studied more extensively. For example, in the adult liver, *Yap* overexpression forces dedifferentiation of hepatocytes into progenitor-like cells, which is reversed by YAP inhibition (Yimlamai et al., 2014). Partial hepatectomy induces a higher level of nuclear localized YAP and increases YAP target gene expression, as well as a decrease in *Mst1/2*, *Lats1/2*, and *Mob1* (Grijalva et al., 2014). Livers with dual depletion of YAP and TAZ failed to restore liver mass due to defects in cell cycle entry during regeneration, indicating overlapping functions of the proteins (Lu et al., 2018). In the skin, small interfering RNA (siRNA)-mediated knockdown of *Yap* and *Taz* markedly delayed wound healing (Lee et al., 2014b). Moreover, YAP inhibition severely

impairs intestinal regeneration following chemical damage (Cai et al., 2010; Camargo et al., 2007). In a mouse model of colon regeneration induced by chemical insult, YAP/TAZ was shown to be required for repair of the epithelium (Yui et al., 2018). Interestingly, in a mouse incisor model, YAP and TAZ were found to be required to promote proliferation of transient-amplifying cells and inhibit differentiation (Hu et al., 2017). Together, these findings point to a positive role of YAP/TAZ for the survival and expansion of stem/progenitor cells during tissue regeneration.

1.2.4 Hippo signaling in human cancers

Extensive studies have established a prominent role of the Hippo pathway in human cancers. Considerable evidence indicates that loss of Hippo signaling is associated with tumor progression. For example, elevated YAP/TAZ protein levels and nuclear localization has been found in various human cancers, including liver, prostate, colon, lung, and breast cancers (Chan et al., 2008; Steinhardt et al., 2008; Zhao et al., 2007; Zhou et al., 2011). These results place YAP/TAZ as a potential prognostic parameter for certain human cancers (Xu et al., 2009). In mouse models, genetic ablation of LATS1 causes soft tissue sarcoma and ovarian tumors (St John et al., 1999). Deletion of *Sav1* or *Mst1/2* also leads to liver tumor formation (Lee et al., 2010; Song et al., 2010; Zhou et al., 2009). Brain tumors were also reported to be associated with decreased Hippo pathway activity. In a glioblastoma study, the overexpression of *Taz* or constitutive activation of nuclear TAZ was shown to increase tumor grade in a mouse model (Bhat et al., 2011). Amplification of the *YAP* gene locus has been reported in medulloblastomas, a pediatric brain tumor of the cerebellum (Fernandez et al., 2009).

Besides the genetic mutations of the Hippo pathway tumor suppressor genes, epigenetic silencing of Hippo components has been implicated in human cancers, including hypermethylation of *Mst1/2* in soft tissue sarcoma (Seidel et al., 2007) and *Lats1/2* in breast cancers (Takahashi et al., 2005). It is also worth noting that besides its role as a potential oncogene, YAP has been found to have tumor-suppressing functions in certain types of cancers. Specifically, loss of *YAP* is observed in human breast cancer and colon carcinomas (Barry et al., 2013; Yuan et al., 2008). In human head and neck cancers, cytoplasmic YAP is abundant while nuclear YAP overexpression results in cell death (Ehsanian et al., 2010). Together, the function of YAP in cancers appears dependent on the cell context. Thus it is crucial to determine the exact role of YAP as an oncoprotein versus a tumor suppressor in different cancers in order to conduct appropriate targeting of YAP as a cancer therapy.

REFERENCES

Aavikko, M., Li, S. P., Saarinen, S., Alhopuro, P., Kaasinen, E., Morgunova, E., Li, Y., Vesanen, K., Smith, M. J., Evans, D. G., et al. (2012). Loss of SUFU function in familial multiple meningioma. *American journal of human genetics* **91**, 520-526.

Alarcon, C., Zaromytidou, A. I., Xi, Q., Gao, S., Yu, J., Fujisawa, S., Barlas, A., Miller, A. N., Manova-Todorova, K., Macias, M. J., et al. (2009). Nuclear CDKs drive Smad transcriptional activation and turnover in BMP and TGF-beta pathways. *Cell* **139**, 757-769.

Allen, B. L., Tenzen, T. and McMahon, A. P. (2007). The Hedgehog-binding proteins Gas1 and Cdo cooperate to positively regulate Shh signaling during mouse development. *Genes & development* **21**, 1244-1257.

Altman, J., Anderson, W. J. and Wright, K. A. (1969). Early effects of x-irradiation of the cerebellum in infant rats: decimation and reconstitution of the external granular layer. *Experimental neurology* **24**, 196-216.

Bai, C. B., Auerbach, W., Lee, J. S., Stephen, D. and Joyner, A. L. (2002). Gli2, but not Gli1, is required for initial Shh signaling and ectopic activation of the Shh pathway. *Development (Cambridge, England)* **129**, 4753-4761.

Bai, C. B. and Joyner, A. L. (2001). Gli1 can rescue the in vivo function of Gli2. *Development (Cambridge, England)* **128**, 5161-5172.

Bai, C. B., Stephen, D. and Joyner, A. L. (2004). All mouse ventral spinal cord patterning by hedgehog is Gli dependent and involves an activator function of Gli3. *Developmental cell* **6**, 103-115.

Banerjee, P. P., Banerjee, S., Tilly, K. I., Tilly, J. L., Brown, T. R. and Zirkin, B. R. (1995). Lobe-specific apoptotic cell death in rat prostate after androgen ablation by castration. *Endocrinology* **136**, 4368-4376.

Barry, E. R., Morikawa, T., Butler, B. L., Shrestha, K., de la Rosa, R., Yan, K. S., Fuchs, C. S., Magness, S. T., Smits, R., Ogino, S., et al. (2013). Restriction of intestinal stem cell expansion and the regenerative response by YAP. *Nature* **493**, 106-110.

Beachy, P. A., Hymowitz, S. G., Lazarus, R. A., Leahy, D. J. and Siebold, C. (2010). Interactions between Hedgehog proteins and their binding partners come into view. *Genes & development* **24**, 2001-2012.

Berman, D. M., Desai, N., Wang, X., Karhadkar, S. S., Reynon, M., Abate-Shen, C., Beachy, P. A. and Shen, M. M. (2004). Roles for Hedgehog

signaling in androgen production and prostate ductal morphogenesis. *Developmental biology* **267**, 387-398.

Beverdam, A., Claxton, C., Zhang, X., James, G., Harvey, K. F. and Key, B. (2013). Yap controls stem/progenitor cell proliferation in the mouse postnatal epidermis. *The Journal of investigative dermatology* **133**, 1497-1505.

Bhat, K. P., Salazar, K. L., Balasubramaniyan, V., Wani, K., Heathcock, L., Hollingsworth, F., James, J. D., Gumin, J., Diefes, K. L., Kim, S. H., et al. (2011). The transcriptional coactivator TAZ regulates mesenchymal differentiation in malignant glioma. *Genes & development* **25**, 2594-2609.

Bhatia, N., Thiyagarajan, S., Elcheva, I., Saleem, M., Dlugosz, A., Mukhtar, H. and Spiegelman, V. S. (2006). Gli2 is targeted for ubiquitination and degradation by beta-TrCP ubiquitin ligase. *The Journal of biological chemistry* **281**, 19320-19326.

Briscoe, J. and Therond, P. P. (2013). The mechanisms of Hedgehog signalling and its roles in development and disease. *Nature reviews. Molecular cell biology* **14**, 416-429.

Cai, J., Zhang, N., Zheng, Y., de Wilde, R. F., Maitra, A. and Pan, D. (2010). The Hippo signaling pathway restricts the oncogenic potential of an intestinal regeneration program. *Genes & development* **24**, 2383-2388.

Callus, B. A., Verhagen, A. M. and Vaux, D. L. (2006). Association of mammalian sterile twenty kinases, Mst1 and Mst2, with hSalvador via C-terminal coiled-coil domains, leads to its stabilization and phosphorylation. *The FEBS journal* **273**, 4264-4276.

Camargo, F. D., Gokhale, S., Johnnidis, J. B., Fu, D., Bell, G. W., Jaenisch, R. and Brummelkamp, T. R. (2007). YAP1 increases organ size and expands undifferentiated progenitor cells. *Current biology : CB* **17**, 2054-2060.

Cao, X., Pfaff, S. L. and Gage, F. H. (2008). YAP regulates neural progenitor cell number via the TEA domain transcription factor. *Genes & development* **22**, 3320-3334.

Cavalli, F. M. G., Remke, M., Rampasek, L., Peacock, J., Shih, D. J. H., Luu, B., Garzia, L., Torchia, J., Nor, C., Morrissy, A. S., et al. (2017). Intertumoral Heterogeneity within Medulloblastoma Subgroups. *Cancer cell* **31**, 737-754.e736.

Chan, E. H., Nousiainen, M., Chalamalasetty, R. B., Schafer, A., Nigg, E. A. and Sillje, H. H. (2005). The Ste20-like kinase Mst2 activates the human large tumor suppressor kinase Lats1. *Oncogene* **24**, 2076-2086.

Chan, S. W., Lim, C. J., Guo, K., Ng, C. P., Lee, I., Hunziker, W., Zeng, Q. and Hong, W. (2008). A role for TAZ in migration, invasion, and tumorigenesis of breast cancer cells. *Cancer research* **68**, 2592-2598.

Chen, M., Tanner, M., Levine, A. C., Levina, E., Ohouo, P. and Buttyan, R. (2009). Androgenic regulation of hedgehog signaling pathway components in prostate cancer cells. *Cell cycle (Georgetown, Tex.)* **8**, 149-157.

Chuang, P. T. and McMahon, A. P. (1999). Vertebrate Hedgehog signalling modulated by induction of a Hedgehog-binding protein. *Nature* **397**, 617-621.

Clark, V. E., Erson-Omay, E. Z., Serin, A., Yin, J., Cotney, J., Ozduman, K., Avsar, T., Li, J., Murray, P. B., Henegariu, O., et al. (2013). Genomic analysis of non-NF2 meningiomas reveals mutations in TRAF7, KLF4, AKT1, and SMO. *Science (New York, N.Y.)* **339**, 1077-1080.

Cooper, A. F., Yu, K. P., Brueckner, M., Brailey, L. L., Johnson, L., McGrath, J. M. and Bale, A. E. (2005). Cardiac and CNS defects in a mouse with targeted disruption of suppressor of fused. *Development (Cambridge, England)* **132**, 4407-4417.

Cui, C. B., Cooper, L. F., Yang, X., Karsenty, G. and Aukhil, I. (2003). Transcriptional coactivation of bone-specific transcription factor Cbfa1 by TAZ. *Molecular and cellular biology* **23**, 1004-1013.

Cunha, G. R., Donjacour, A. A., Cooke, P. S., Mee, S., Bigsby, R. M., Higgins, S. J. and Sugimura, Y. (1987). The endocrinology and developmental biology of the prostate. *Endocrine reviews* **8**, 338-362.

Cunha, G. R., Donjacour, A. A. and Sugimura, Y. (1986). Stromal-epithelial interactions and heterogeneity of proliferative activity within the prostate. *Biochemistry and cell biology = Biochimie et biologie cellulaire* **64**, 608-614.

Cunha, G. R. and Lung, B. (1978). The possible influence of temporal factors in androgenic responsiveness of urogenital tissue recombinants from wild-type and androgen-insensitive (Tfm) mice. *The Journal of experimental zoology* **205**, 181-193.

Doles, J., Cook, C., Shi, X., Valosky, J., Lipinski, R. and Bushman, W. (2006). Functional compensation in Hedgehog signaling during mouse prostate development. *Developmental biology* **295**, 13-25.

Dong, J., Feldmann, G., Huang, J., Wu, S., Zhang, N., Comerford, S. A., Gayyed, M. F., Anders, R. A., Maitra, A. and Pan, D. (2007). Elucidation of a universal size-control mechanism in Drosophila and mammals. *Cell* **130**, 1120-1133.

Drakopoulou, E., Outram, S. V., Rowbotham, N. J., Ross, S. E., Furmanski, A. L., Saldana, J. I., Hager-Theodorides, A. L. and Crompton, T. (2010). Non-redundant role for the transcription factor Gli1 at multiple stages of thymocyte development. *Cell cycle (Georgetown, Tex.)* **9**, 4144-4152.

Ehsanian, R., Brown, M., Lu, H., Yang, X. P., Pattatheyil, A., Yan, B., Duggal, P., Chuang, R., Doondeea, J., Feller, S., et al. (2010). YAP dysregulation by phosphorylation or DeltaNp63-mediated gene repression promotes proliferation, survival and migration in head and neck cancer subsets. *Oncogene* **29**, 6160-6171.

Epstein, E., Jr. (2001). Genetic determinants of basal cell carcinoma risk. *Medical and pediatric oncology* **36**, 555-558.

Fan, L., Pepicelli, C. V., Dibble, C. C., Catbagan, W., Zarycki, J. L., Laciak, R., Gipp, J., Shaw, A., Lamm, M. L., Munoz, A., et al. (2004). Hedgehog signaling promotes prostate xenograft tumor growth. *Endocrinology* **145**, 3961-3970.

Fernandez, L. A., Northcott, P. A., Dalton, J., Fraga, C., Ellison, D., Angers, S., Taylor, M. D. and Kenney, A. M. (2009). YAP1 is amplified and up-regulated in hedgehog-associated medulloblastomas and mediates Sonic hedgehog-driven neural precursor proliferation. *Genes & development* **23**, 2729-2741.

Ferrigno, O., Lallemand, F., Verrecchia, F., L'Hoste, S., Camonis, J., Atfi, A. and Mauviel, A. (2002). Yes-associated protein (YAP65) interacts with Smad7 and potentiates its inhibitory activity against TGF-beta/Smad signaling. *Oncogene* **21**, 4879-4884.

Freestone, S. H., Marker, P., Grace, O. C., Tomlinson, D. C., Cunha, G. R., Harnden, P. and Thomson, A. A. (2003). Sonic hedgehog regulates prostatic growth and epithelial differentiation. *Developmental biology* **264**, 352-362.

Gerling, M., Buller, N. V., Kirn, L. M., Joost, S., Frings, O., Englert, B., Bergstrom, A., Kuiper, R. V., Blaas, L., Wielenga, M. C., et al. (2016). Stromal Hedgehog signalling is downregulated in colon cancer and its restoration restrains tumour growth. *Nature communications* **7**, 12321.

Goetz, S. C. and Anderson, K. V. (2010). The primary cilium: a signalling centre during vertebrate development. *Nature reviews. Genetics* **11**, 331-344.

Gong, X., Qian, H., Cao, P., Zhao, X., Zhou, Q., Lei, J. and Yan, N. (2018). Structural basis for the recognition of Sonic Hedgehog by human Patched1. *Science (New York, N.Y.)* **361**.

Gorlin, R. J. (2004). Nevoid basal cell carcinoma (Gorlin) syndrome. *Genetics in medicine : official journal of the American College of Medical Genetics* **6**, 530-539.

Grijalva, J. L., Huizenga, M., Mueller, K., Rodriguez, S., Brazzo, J., Camargo, F., Sadri-Vakili, G. and Vakili, K. (2014). Dynamic alterations in Hippo signaling pathway and YAP activation during liver regeneration. *American journal of physiology. Gastrointestinal and liver physiology* **307**, G196-204.

Hahn, H., Wicking, C., Zaphiropoulous, P. G., Gailani, M. R., Shanley, S., Chidambaram, A., Vorechovsky, I., Holmberg, E., Unden, A. B., Gillies, S., et al. (1996). Mutations of the human homolog of Drosophila patched in the nevoid basal cell carcinoma syndrome. *Cell* **85**, 841-851.

Hao, Y., Chun, A., Cheung, K., Rashidi, B. and Yang, X. (2008). Tumor suppressor LATS1 is a negative regulator of oncogene YAP. *The Journal of biological chemistry* **283**, 5496-5509.

Harvey, K. F., Pfleger, C. M. and Hariharan, I. K. (2003). The Drosophila Mst ortholog, hippo, restricts growth and cell proliferation and promotes apoptosis. *Cell* **114**, 457-467.

Haycraft, C. J., Banizs, B., Aydin-Son, Y., Zhang, Q., Michaud, E. J. and Yoder, B. K. (2005). Gli2 and Gli3 localize to cilia and require the intraflagellar transport protein polaris for processing and function. *PLoS genetics* **1**, e53.

Heallen, T., Zhang, M., Wang, J., Bonilla-Claudio, M., Klysik, E., Johnson, R. L. and Martin, J. F. (2011). Hippo pathway inhibits Wnt signaling to restrain cardiomyocyte proliferation and heart size. *Science (New York, N.Y.)* **332**, 458-461.

Hindley, C. J., Condurat, A. L., Menon, V., Thomas, R., Azmitia, L. M., Davis, J. A. and Pruszak, J. (2016). The Hippo pathway member YAP enhances human neural crest cell fate and migration. *Scientific reports* **6**, 23208.

Hong, J. H., Hwang, E. S., McManus, M. T., Amsterdam, A., Tian, Y., Kalmukova, R., Mueller, E., Benjamin, T., Spiegelman, B. M., Sharp,

P. A., et al. (2005). TAZ, a transcriptional modulator of mesenchymal stem cell differentiation. *Science (New York, N.Y.)* **309**, 1074-1078.

Hossain, Z., Ali, S. M., Ko, H. L., Xu, J., Ng, C. P., Guo, K., Qi, Z., Ponniah, S., Hong, W. and Hunziker, W. (2007). Glomerulocystic kidney disease in mice with a targeted inactivation of Wwtr1. *Proceedings of the National Academy of Sciences of the United States of America* **104**, 1631-1636.

Hu, J. K., Du, W., Shelton, S. J., Oldham, M. C., DiPersio, C. M. and Klein, O. D. (2017). An FAK-YAP-mTOR Signaling Axis Regulates Stem Cell-Based Tissue Renewal in Mice. *Cell stem cell* **21**, 91-106.e106.

Huang, J., Wu, S., Barrera, J., Matthews, K. and Pan, D. (2005). The Hippo signaling pathway coordinately regulates cell proliferation and apoptosis by inactivating Yorkie, the Drosophila Homolog of YAP. *Cell* **122**, 421-434.

Huang, P., Zheng, S., Wierbowski, B. M., Kim, Y., Nedelcu, D., Aravena, L., Liu, J., Kruse, A. C. and Salic, A. (2018). Structural Basis of Smoothened Activation in Hedgehog Signaling. *Cell* **174**, 312-324.e316.

Huangfu, D. and Anderson, K. V. (2005). Cilia and Hedgehog responsiveness in the mouse. *Proceedings of the National Academy of Sciences of the United States of America* **102**, 11325-11330.

Ibuki, N., Ghaffari, M., Pandey, M., Iu, I., Fazli, L., Kashiwagi, M., Tojo, H., Nakanishi, O., Gleave, M. E. and Cox, M. E. (2013). TAK-441, a novel investigational smoothened antagonist, delays castration-resistant progression in prostate cancer by disrupting paracrine hedgehog signaling. *Int J Cancer* **133**, 1955-1966.

Isaacs, J. T. (1985). Control of Cell Proliferation and Cell Death in the Normal and Neoplastic Prostate. In *Benign Prostatic Hyperplasia*, pp. 10.

Jia, J., Zhang, W., Wang, B., Trinko, R. and Jiang, J. (2003). The Drosophila Ste20 family kinase dMST functions as a tumor suppressor by restricting cell proliferation and promoting apoptosis. *Genes & development* **17**, 2514-2519.

Johnson, R. and Halder, G. (2014). The two faces of Hippo: targeting the Hippo pathway for regenerative medicine and cancer treatment. *Nature reviews. Drug discovery* **13**, 63-79.

Johnson, R. L., Rothman, A. L., Xie, J., Goodrich, L. V., Bare, J. W., Bonifas, J. M., Quinn, A. G., Myers, R. M., Cox, D. R., Epstein, E. H.,

Jr., et al. (1996). Human homolog of patched, a candidate gene for the basal cell nevus syndrome. *Science (New York, N.Y.)* **272**, 1668-1671.

Justice, R. W., Zilian, O., Woods, D. F., Noll, M. and Bryant, P. J. (1995). The Drosophila tumor suppressor gene warts encodes a homolog of human myotonic dystrophy kinase and is required for the control of cell shape and proliferation. *Genes & development* **9**, 534-546.

Kanai, F., Marignani, P. A., Sarbassova, D., Yagi, R., Hall, R. A., Donowitz, M., Hisaminato, A., Fujiwara, T., Ito, Y., Cantley, L. C., et al. (2000). TAZ: a novel transcriptional co-activator regulated by interactions with 14-3-3 and PDZ domain proteins. *The EMBO journal* **19**, 6778-6791.

Kango-Singh, M., Nolo, R., Tao, C., Verstreken, P., Hiesinger, P. R., Bellen, H. J. and Halder, G. (2002). Shar-pei mediates cell proliferation arrest during imaginal disc growth in Drosophila. *Development (Cambridge, England)* **129**, 5719-5730.

Karhadkar, S. S., Bova, G. S., Abdallah, N., Dhara, S., Gardner, D., Maitra, A., Isaacs, J. T., Berman, D. M. and Beachy, P. A. (2004). Hedgehog signalling in prostate regeneration, neoplasia and metastasis. *Nature* **431**, 707-712.

Kasper, M., Schnidar, H., Neill, G. W., Hanneder, M., Klingler, S., Blaas, L., Schmid, C., Hauser-Kronberger, C., Regl, G., Philpott, M. P., et al. (2006). Selective modulation of Hedgehog/GLI target gene expression by epidermal growth factor signaling in human keratinocytes. *Molecular and cellular biology* **26**, 6283-6298.

Kijima, C., Miyashita, T., Suzuki, M., Oka, H. and Fujii, K. (2012). Two cases of nevoid basal cell carcinoma syndrome associated with meningioma caused by a PTCH1 or SUFU germline mutation. *Familial cancer* **11**, 565-570.

Kong, S. (2018). Loss of YAP/TAZ impaired the proliferation and differentiation ability of neural progenitor cells. *bioRxiv*.

Kool, M., Jones, D. T., Jager, N., Northcott, P. A., Pugh, T. J., Hovestadt, V., Piro, R. M., Esparza, L. A., Markant, S. L., Remke, M., et al. (2014). Genome sequencing of SHH medulloblastoma predicts genotype-related response to smoothened inhibition. *Cancer cell* **25**, 393-405.

Lai, Z. C., Wei, X., Shimizu, T., Ramos, E., Rohrbaugh, M., Nikolaidis, N., Ho, L. L. and Li, Y. (2005). Control of cell proliferation and apoptosis by mob as tumor suppressor, mats. *Cell* **120**, 675-685.

Lamm, M. L., Catbagan, W. S., Laciak, R. J., Barnett, D. H., Hebner, C. M., Gaffield, W., Walterhouse, D., Iannaccone, P. and Bushman, W. (2002). Sonic hedgehog activates mesenchymal Gli1 expression during prostate ductal bud formation. *Developmental biology* **249**, 349-366.

Lavado, A., Park, J. Y., Pare, J., Finkelstein, D., Pan, H., Xu, B., Fan, Y., Kumar, R. P., Neale, G., Kwak, Y. D., et al. (2018). The Hippo Pathway Prevents YAP/TAZ-Driven Hypertranscription and Controls Neural Progenitor Number. *Developmental cell*.

Lee, J. J., Perera, R. M., Wang, H., Wu, D. C., Liu, X. S., Han, S., Fitamant, J., Jones, P. D., Ghanta, K. S., Kawano, S., et al. (2014a). Stromal response to Hedgehog signaling restrains pancreatic cancer progression. *Proc Natl Acad Sci U S A* **111**, E3091-3100.

Lee, J. J., Rothenberg, M. E., Seeley, E. S., Zimdahl, B., Kawano, S., Lu, W. J., Shin, K., Sakata-Kato, T., Chen, J. K., Diehn, M., et al. (2016). Control of inflammation by stromal Hedgehog pathway activation restrains colitis. *Proceedings of the National Academy of Sciences of the United States of America* **113**, E7545-e7553.

Lee, K. P., Lee, J. H., Kim, T. S., Kim, T. H., Park, H. D., Byun, J. S., Kim, M. C., Jeong, W. I., Calvisi, D. F., Kim, J. M., et al. (2010). The Hippo-Salvador pathway restrains hepatic oval cell proliferation, liver size, and liver tumorigenesis. *Proceedings of the National Academy of Sciences of the United States of America* **107**, 8248-8253.

Lee, M. J., Byun, M. R., Furutani-Seiki, M., Hong, J. H. and Jung, H. S. (2014b). YAP and TAZ regulate skin wound healing. *The Journal of investigative dermatology* **134**, 518-525.

Lei, Q. Y., Zhang, H., Zhao, B., Zha, Z. Y., Bai, F., Pei, X. H., Zhao, S., Xiong, Y. and Guan, K. L. (2008). TAZ promotes cell proliferation and epithelial-mesenchymal transition and is inhibited by the hippo pathway. *Molecular and cellular biology* **28**, 2426-2436.

Li, N., Lim, G., Chen, L., McCabe, M. F., Kim, H., Zhang, S. and Mao, J. (2013). Spinal expression of Hippo signaling components YAP and TAZ following peripheral nerve injury in rats. *Brain research* **1535**, 137-147.

Lian, I., Kim, J., Okazawa, H., Zhao, J., Zhao, B., Yu, J., Chinnaiyan, A., Israel, M. A., Goldstein, L. S., Abujarour, R., et al. (2010). The role of YAP transcription coactivator in regulating stem cell self-renewal and differentiation. *Genes & development* **24**, 1106-1118.

Lim, A., Shin, K., Zhao, C., Kawano, S. and Beachy, P. A. (2014). Spatially restricted Hedgehog signalling regulates HGF-induced branching of the adult prostate. *Nature cell biology* **16**, 1135-1145.

Lin, C., Yao, E., Zhang, K., Jiang, X., Croll, S., Thompson-Peer, K. and Chuang, P. T. (2017). YAP is essential for mechanical force production and epithelial cell proliferation during lung branching morphogenesis. *eLife* **6**.

Liu, A., Wang, B. and Niswander, L. A. (2005). Mouse intraflagellar transport proteins regulate both the activator and repressor functions of Gli transcription factors. *Development (Cambridge, England)* **132**, 3103-3111.

Liu, C. Y., Zha, Z. Y., Zhou, X., Zhang, H., Huang, W., Zhao, D., Li, T., Chan, S. W., Lim, C. J., Hong, W., et al. (2010). The hippo tumor pathway promotes TAZ degradation by phosphorylating a phosphodegron and recruiting the SCF{beta}-TrCP E3 ligase. *The Journal of biological chemistry* **285**, 37159-37169.

Lu, L., Finegold, M. J. and Johnson, R. L. (2018). Hippo pathway coactivators Yap and Taz are required to coordinate mammalian liver regeneration. *Experimental & molecular medicine* **50**, e423.

Mahoney, J. E., Mori, M., Szymaniak, A. D., Varelas, X. and Cardoso, W. V. (2014). The hippo pathway effector Yap controls patterning and differentiation of airway epithelial progenitors. *Developmental cell* **30**, 137-150.

Mahoney, W. M., Jr., Hong, J. H., Yaffe, M. B. and Farrance, I. K. (2005). The transcriptional co-activator TAZ interacts differentially with transcriptional enhancer factor-1 (TEF-1) family members. *The Biochemical journal* **388**, 217-225.

Makita, R., Uchijima, Y., Nishiyama, K., Amano, T., Chen, Q., Takeuchi, T., Mitani, A., Nagase, T., Yatomi, Y., Aburatani, H., et al. (2008). Multiple renal cysts, urinary concentration defects, and pulmonary emphysematous changes in mice lacking TAZ. *American journal of physiology. Renal physiology* **294**, F542-553.

Mao, J., Ligon, K. L., Rakhlin, E. Y., Thayer, S. P., Bronson, R. T., Rowitch, D. and McMahon, A. P. (2006). A novel somatic mouse model to survey tumorigenic potential applied to the Hedgehog pathway. *Cancer research* **66**, 10171-10178.

Mitani, A., Nagase, T., Fukuchi, K., Aburatani, H., Makita, R. and Kurihara, H. (2009). Transcriptional coactivator with PDZ-binding motif is essential for normal alveolarization in mice. *American journal of respiratory and critical care medicine* **180**, 326-338.

Morin-Kensicki, E. M., Boone, B. N., Howell, M., Stonebraker, J. R., Teed, J., Alb, J. G., Magnuson, T. R., O'Neal, W. and Milgram, S. L. (2006).

Defects in yolk sac vasculogenesis, chorioallantoic fusion, and embryonic axis elongation in mice with targeted disruption of Yap65. *Molecular and cellular biology* **26**, 77-87.

Motoyama, J., Heng, H., Crackower, M. A., Takabatake, T., Takeshima, K., Tsui, L. C. and Hui, C. (1998a). Overlapping and non-overlapping Ptch2 expression with Shh during mouse embryogenesis. *Mechanisms of development* **78**, 81-84.

Motoyama, J., Milenkovic, L., Iwama, M., Shikata, Y., Scott, M. P. and Hui, C. C. (2003). Differential requirement for Gli2 and Gli3 in ventral neural cell fate specification. *Developmental biology* **259**, 150-161.

Motoyama, J., Takabatake, T., Takeshima, K. and Hui, C. (1998b). Ptch2, a second mouse Patched gene is co-expressed with Sonic hedgehog. *Nature genetics* **18**, 104-106.

Murakami, M., Nakagawa, M., Olson, E. N. and Nakagawa, O. (2005). A WW domain protein TAZ is a critical coactivator for TBX5, a transcription factor implicated in Holt-Oram syndrome. *Proceedings of the National Academy of Sciences of the United States of America* **102**, 18034-18039.

Oh, H. and Irvine, K. D. (2008). In vivo regulation of Yorkie phosphorylation and localization. *Development (Cambridge, England)* **135**, 1081-1088.

Oka, T., Mazack, V. and Sudol, M. (2008). Mst2 and Lats kinases regulate apoptotic function of Yes kinase-associated protein (YAP). *The Journal of biological chemistry* **283**, 27534-27546.

Okada, A., Charron, F., Morin, S., Shin, D. S., Wong, K., Fabre, P. J., Tessier-Lavigne, M. and McConnell, S. K. (2006). Boc is a receptor for sonic hedgehog in the guidance of commissural axons. *Nature* **444**, 369-373.

Pan, Y., Bai, C. B., Joyner, A. L. and Wang, B. (2006). Sonic hedgehog signaling regulates Gli2 transcriptional activity by suppressing its processing and degradation. *Molecular and cellular biology* **26**, 3365-3377.

Pantalacci, S., Tapon, N. and Leopold, P. (2003). The Salvador partner Hippo promotes apoptosis and cell-cycle exit in Drosophila. *Nature cell biology* **5**, 921-927.

Park, H. L., Bai, C., Platt, K. A., Matise, M. P., Beeghly, A., Hui, C. C., Nakashima, M. and Joyner, A. L. (2000). Mouse Gli1 mutants are viable but have defects in SHH signaling in combination with a Gli2 mutation. *Development (Cambridge, England)* **127**, 1593-1605.

Park, K. S., Martelotto, L. G., Peifer, M., Sos, M. L., Karnezis, A. N., Mahjoub, M. R., Bernard, K., Conklin, J. F., Szczepny, A., Yuan, J., et al. (2011). A crucial requirement for Hedgehog signaling in small cell lung cancer. *Nature medicine* **17**, 1504-1508.

Park, R., Moon, U. Y., Park, J. Y., Hughes, L. J., Johnson, R. L., Cho, S. H. and Kim, S. (2016). Yap is required for ependymal integrity and is suppressed in LPA-induced hydrocephalus. *Nature communications* **7**, 10329.

Peng, Y. C. and Joyner, A. L. (2015). Hedgehog signaling in prostate epithelial-mesenchymal growth regulation. *Developmental biology* **400**, 94-104.

Pepinsky, R. B., Zeng, C., Wen, D., Rayhorn, P., Baker, D. P., Williams, K. P., Bixler, S. A., Ambrose, C. M., Garber, E. A., Miatkowski, K., et al. (1998). Identification of a palmitic acid-modified form of human Sonic hedgehog. *The Journal of biological chemistry* **273**, 14037-14045.

Perler, F. B. (1998). Protein splicing of inteins and hedgehog autoproteolysis: structure, function, and evolution. *Cell* **92**, 1-4.

Persson, M., Stamataki, D., te Welscher, P., Andersson, E., Bose, J., Ruther, U., Ericson, J. and Briscoe, J. (2002). Dorsal-ventral patterning of the spinal cord requires Gli3 transcriptional repressor activity. *Genes & development* **16**, 2865-2878.

Petrova, R., Garcia, A. D. and Joyner, A. L. (2013). Titration of GLI3 repressor activity by sonic hedgehog signaling is critical for maintaining multiple adult neural stem cell and astrocyte functions. *The Journal of neuroscience : the official journal of the Society for Neuroscience* **33**, 17490-17505.

Podlasek, C. A., Barnett, D. H., Clemens, J. Q., Bak, P. M. and Bushman, W. (1999). Prostate development requires Sonic hedgehog expressed by the urogenital sinus epithelium. *Developmental biology* **209**, 28-39.

Poon, C. L., Mitchell, K. A., Kondo, S., Cheng, L. Y. and Harvey, K. F. (2016). The Hippo Pathway Regulates Neuroblasts and Brain Size in Drosophila melanogaster. *Current biology : CB* **26**, 1034-1042.

Praskova, M., Xia, F. and Avruch, J. (2008). MOBKL1A/MOBKL1B phosphorylation by MST1 and MST2 inhibits cell proliferation. *Current biology : CB* **18**, 311-321.

Pressey, J. G., Anderson, J. R., Crossman, D. K., Lynch, J. C. and Barr, F. G. (2011). Hedgehog pathway activity in pediatric embryonal

rhabdomyosarcoma and undifferentiated sarcoma: a report from the Children's Oncology Group. *Pediatric blood & cancer* **57**, 930-938.

Pu, Y., Huang, L. and Prins, G. S. (2004). Sonic hedgehog-patched Gli signaling in the developing rat prostate gland: lobe-specific suppression by neonatal estrogens reduces ductal growth and branching. *Developmental biology* **273**, 257-275.

Qi, X., Schmiege, P., Coutavas, E. and Li, X. (2018). Two Patched molecules engage distinct sites on Hedgehog yielding a signaling-competent complex. *Science (New York, N.Y.)* **362**.

Ragni, C. V., Diguet, N., Le Garrec, J. F., Novotova, M., Resende, T. P., Pop, S., Charon, N., Guillemot, L., Kitasato, L., Badouel, C., et al. (2017). Amotl1 mediates sequestration of the Hippo effector Yap1 downstream of Fat4 to restrict heart growth. *Nature communications* **8**, 14582.

Ramamurthy, V. P., Ramalingam, S., Kwegyir-Afful, A. K., Hussain, A. and Njar, V. C. (2017). Targeting of protein translation as a new treatment paradigm for prostate cancer. *Current opinion in oncology*.

Reginensi, A., Enderle, L., Gregorieff, A., Johnson, R. L., Wrana, J. L. and McNeill, H. (2016). A critical role for NF2 and the Hippo pathway in branching morphogenesis. *Nature communications* **7**, 12309.

Reginensi, A., Scott, R. P., Gregorieff, A., Bagherie-Lachidan, M., Chung, C., Lim, D. S., Pawson, T., Wrana, J. and McNeill, H. (2013). Yap- and Cdc42-dependent nephrogenesis and morphogenesis during mouse kidney development. *PLoS genetics* **9**, e1003380.

Ren, F., Zhang, L. and Jiang, J. (2010). Hippo signaling regulates Yorkie nuclear localization and activity through 14-3-3 dependent and independent mechanisms. *Developmental biology* **337**, 303-312.

Rhim, A. D., Oberstein, P. E., Thomas, D. H., Mirek, E. T., Palermo, C. F., Sastra, S. A., Dekleva, E. N., Saunders, T., Becerra, C. P., Tattersall, I. W., et al. (2014). Stromal elements act to restrain, rather than support, pancreatic ductal adenocarcinoma. *Cancer Cell* **25**, 735-747.

Rohatgi, R., Milenkovic, L. and Scott, M. P. (2007). Patched1 regulates hedgehog signaling at the primary cilium. *Science (New York, N.Y.)* **317**, 372-376.

Rosenbluh, J., Nijhawan, D., Cox, A. G., Li, X., Neal, J. T., Schafer, E. J., Zack, T. I., Wang, X., Tsherniak, A., Schinzel, A. C., et al. (2012).

beta-Catenin-driven cancers require a YAP1 transcriptional complex for survival and tumorigenesis. *Cell* **151**, 1457-1473.

Rowbotham, N. J., Hager-Theodorides, A. L., Furmanski, A. L., Ross, S. E., Outram, S. V., Dessens, J. T. and Crompton, T. (2009). Sonic hedgehog negatively regulates pre-TCR-induced differentiation by a Gli2-dependent mechanism. *Blood* **113**, 5144-5156.

Sabol, M., Trnski, D., Musani, V., Ozretic, P. and Levanat, S. (2018). Role of GLI Transcription Factors in Pathogenesis and Their Potential as New Therapeutic Targets. *International journal of molecular sciences* **19**.

Sanchez, P., Hernandez, A. M., Stecca, B., Kahler, A. J., DeGueme, A. M., Barrett, A., Beyna, M., Datta, M. W., Datta, S. and Ruiz i Altaba, A. (2004). Inhibition of prostate cancer proliferation by interference with SONIC HEDGEHOG-GLI1 signaling. *Proc Natl Acad Sci U S A* **101**, 12561-12566.

Sasaki, H., Nishizaki, Y., Hui, C., Nakafuku, M. and Kondoh, H. (1999). Regulation of Gli2 and Gli3 activities by an amino-terminal repression domain: implication of Gli2 and Gli3 as primary mediators of Shh signaling. *Development (Cambridge, England)* **126**, 3915-3924.

Schlegelmilch, K., Mohseni, M., Kirak, O., Pruszak, J., Rodriguez, J. R., Zhou, D., Kreger, B. T., Vasioukhin, V., Avruch, J., Brummelkamp, T. R., et al. (2011). Yap1 acts downstream of alpha-catenin to control epidermal proliferation. *Cell* **144**, 782-795.

Seidel, C., Schagdarsurengin, U., Blumke, K., Wurl, P., Pfeifer, G. P., Hauptmann, S., Taubert, H. and Dammann, R. (2007). Frequent hypermethylation of MST1 and MST2 in soft tissue sarcoma. *Molecular carcinogenesis* **46**, 865-871.

Shaw, A., Gipp, J. and Bushman, W. (2009). The Sonic Hedgehog pathway stimulates prostate tumor growth by paracrine signaling and recapitulates embryonic gene expression in tumor myofibroblasts. *Oncogene* **28**, 4480-4490.

Sheng, T., Li, C., Zhang, X., Chi, S., He, N., Chen, K., McCormick, F., Gatalica, Z. and Xie, J. (2004). Activation of the hedgehog pathway in advanced prostate cancer. *Mol Cancer* **3**, 29.

Shin, K., Lim, A., Zhao, C., Sahoo, D., Pan, Y., Spiekerkoetter, E., Liao, J. C. and Beachy, P. A. (2014). Hedgehog signaling restrains bladder cancer progression by eliciting stromal production of urothelial differentiation factors. *Cancer Cell* **26**, 521-533.

Siegel, R. L., Miller, K. D. and Jemal, A. (2018). Cancer statistics, 2018. *CA: a cancer journal for clinicians* **68**, 7-30.

Smelkinson, M. G., Zhou, Q. and Kalderon, D. (2007). Regulation of Ci-SCFSlimb binding, Ci proteolysis, and hedgehog pathway activity by Ci phosphorylation. *Developmental cell* **13**, 481-495.

Smyth, I., Narang, M. A., Evans, T., Heimann, C., Nakamura, Y., Chenevix-Trench, G., Pietsch, T., Wicking, C. and Wainwright, B. J. (1999). Isolation and characterization of human patched 2 (PTCH2), a putative tumour suppressor gene inbasal cell carcinoma and medulloblastoma on chromosome 1p32. *Human molecular genetics* **8**, 291-297.

Solanki, A., Lau, C. I., Saldana, J. I., Ross, S. and Crompton, T. (2017). The transcription factor Gli3 promotes B cell development in fetal liver through repression of Shh. *The Journal of experimental medicine* **214**, 2041-2058.

Solanki, A., Yanez, D. C., Ross, S., Lau, C. I., Papaioannou, E., Li, J., Saldana, J. I. and Crompton, T. (2018). Gli3 in fetal thymic epithelial cells promotes thymocyte positive selection and differentiation by repression of Shh. *Development (Cambridge, England)* **145**.

Sommer, A. and Lemmon, M. A. (2018). Smoothening out the patches. *Science (New York, N.Y.)* **362**, 26-27.

Song, H., Mak, K. K., Topol, L., Yun, K., Hu, J., Garrett, L., Chen, Y., Park, O., Chang, J., Simpson, R. M., et al. (2010). Mammalian Mst1 and Mst2 kinases play essential roles in organ size control and tumor suppression. *Proceedings of the National Academy of Sciences of the United States of America* **107**, 1431-1436.

St John, M. A., Tao, W., Fei, X., Fukumoto, R., Carcangiu, M. L., Brownstein, D. G., Parlow, A. F., McGrath, J. and Xu, T. (1999). Mice deficient of Lats1 develop soft-tissue sarcomas, ovarian tumours and pituitary dysfunction. *Nature genetics* **21**, 182-186.

Steinhardt, A. A., Gayyed, M. F., Klein, A. P., Dong, J., Maitra, A., Pan, D., Montgomery, E. A. and Anders, R. A. (2008). Expression of Yes-associated protein in common solid tumors. *Human pathology* **39**, 1582-1589.

Sugimura, Y., Cunha, G. R. and Donjacour, A. A. (1986a). Morphogenesis of ductal networks in the mouse prostate. *Biology of reproduction* **34**, 961-971.

---- (1986b). Morphological and histological study of castration-induced degeneration and androgen-induced regeneration in the mouse prostate. *Biology of reproduction* **34**, 973-983.

Sugimura, Y., Cunha, G. R., Donjacour, A. A., Bigsby, R. M. and Brody, J. R. (1986c). Whole-mount autoradiography study of DNA synthetic activity during postnatal development and androgen-induced regeneration in the mouse prostate. *Biology of reproduction* **34**, 985-995.

Sun, Y., Yong, K. M., Villa-Diaz, L. G., Zhang, X., Chen, W., Philson, R., Weng, S., Xu, H., Krebsbach, P. H. and Fu, J. (2014). Hippo/YAP-mediated rigidity-dependent motor neuron differentiation of human pluripotent stem cells. *Nature materials* **13**, 599-604.

Svard, J., Heby-Henricson, K., Persson-Lek, M., Rozell, B., Lauth, M., Bergstrom, A., Ericson, J., Toftgard, R. and Teglund, S. (2006). Genetic elimination of Suppressor of fused reveals an essential repressor function in the mammalian Hedgehog signaling pathway. *Developmental cell* **10**, 187-197.

Takahashi, Y., Miyoshi, Y., Takahata, C., Irahara, N., Taguchi, T., Tamaki, Y. and Noguchi, S. (2005). Down-regulation of LATS1 and LATS2 mRNA expression by promoter hypermethylation and its association with biologically aggressive phenotype in human breast cancers. *Clinical cancer research : an official journal of the American Association for Cancer Research* **11**, 1380-1385.

Tapon, N., Harvey, K. F., Bell, D. W., Wahrer, D. C., Schiripo, T. A., Haber, D. and Hariharan, I. K. (2002). salvador Promotes both cell cycle exit and apoptosis in Drosophila and is mutated in human cancer cell lines. *Cell* **110**, 467-478.

Taylor, F. R., Wen, D., Garber, E. A., Carmillo, A. N., Baker, D. P., Arduini, R. M., Williams, K. P., Weinreb, P. H., Rayhorn, P., Hronowski, X., et al. (2001). Enhanced potency of human Sonic hedgehog by hydrophobic modification. *Biochemistry* **40**, 4359-4371.

Tenzen, T., Allen, B. L., Cole, F., Kang, J. S., Krauss, R. S. and McMahon, A. P. (2006). The cell surface membrane proteins Cdo and Boc are components and targets of the Hedgehog signaling pathway and feedback network in mice. *Developmental cell* **10**, 647-656.

Theil, T., Kaesler, S., Grotewold, L., Bose, J. and Ruther, U. (1999). Gli genes and limb development. *Cell and tissue research* **296**, 75-83.

Tian, Y., Kolb, R., Hong, J. H., Carroll, J., Li, D., You, J., Bronson, R., Yaffe, M. B., Zhou, J. and Benjamin, T. (2007). TAZ promotes PC2

degradation through a SCFbeta-Trcp E3 ligase complex. *Molecular and cellular biology* **27**, 6383-6395.

Torre, L. A., Bray, F., Siegel, R. L., Ferlay, J., Lortet-Tieulent, J. and Jemal, A. (2015). Global cancer statistics, 2012. *CA Cancer J Clin* **65**, 87-108.

Tostar, U., Malm, C. J., Meis-Kindblom, J. M., Kindblom, L. G., Toftgard, R. and Unden, A. B. (2006). Deregulation of the hedgehog signalling pathway: a possible role for the PTCH and SUFU genes in human rhabdomyoma and rhabdomyosarcoma development. *The Journal of pathology* **208**, 17-25.

Tzelepi, V., Karlou, M., Wen, S., Hoang, A., Logothetis, C., Troncoso, P. and Efstathiou, E. (2011). Expression of hedgehog pathway components in prostate carcinoma microenvironment: shifting the balance towards autocrine signalling. *Histopathology* **58**, 1037-1047.

Udan, R. S., Kango-Singh, M., Nolo, R., Tao, C. and Halder, G. (2003). Hippo promotes proliferation arrest and apoptosis in the Salvador/Warts pathway. *Nature cell biology* **5**, 914-920.

Varelas, X., Sakuma, R., Samavarchi-Tehrani, P., Peerani, R., Rao, B. M., Dembowy, J., Yaffe, M. B., Zandstra, P. W. and Wrana, J. L. (2008). TAZ controls Smad nucleocytoplasmic shuttling and regulates human embryonic stem-cell self-renewal. *Nature cell biology* **10**, 837-848.

Vassilev, A., Kaneko, K. J., Shu, H., Zhao, Y. and DePamphilis, M. L. (2001). TEAD/TEF transcription factors utilize the activation domain of YAP65, a Src/Yes-associated protein localized in the cytoplasm. *Genes & development* **15**, 1229-1241.

Vokes, S. A., Ji, H., McCuine, S., Tenzen, T., Giles, S., Zhong, S., Longabaugh, W. J., Davidson, E. H., Wong, W. H. and McMahon, A. P. (2007). Genomic characterization of Gli-activator targets in sonic hedgehog-mediated neural patterning. *Development (Cambridge, England)* **134**, 1977-1989.

Vokes, S. A., Ji, H., Wong, W. H. and McMahon, A. P. (2008). A genome-scale analysis of the cis-regulatory circuitry underlying sonic hedgehog-mediated patterning of the mammalian limb. *Genes & development* **22**, 2651-2663.

von Gise, A., Lin, Z., Schlegelmilch, K., Honor, L. B., Pan, G. M., Buck, J. N., Ma, Q., Ishiwata, T., Zhou, B., Camargo, F. D., et al. (2012). YAP1, the nuclear target of Hippo signaling, stimulates heart growth through cardiomyocyte proliferation but not hypertrophy. *Proceedings of*

the National Academy of Sciences of the United States of America **109**, 2394-2399.

Wang, B., Fallon, J. F. and Beachy, P. A. (2000). Hedgehog-regulated processing of Gli3 produces an anterior/posterior repressor gradient in the developing vertebrate limb. *Cell* **100**, 423-434.

Wang, B. and Li, Y. (2006). Evidence for the direct involvement of {beta}TrCP in Gli3 protein processing. *Proceedings of the National Academy of Sciences of the United States of America* **103**, 33-38.

Wei, X., Shimizu, T. and Lai, Z. C. (2007). Mob as tumor suppressor is activated by Hippo kinase for growth inhibition in Drosophila. *The EMBO journal* **26**, 1772-1781.

Wojcinski, A., Lawton, A. K., Bayin, N. S., Lao, Z., Stephen, D. N. and Joyner, A. L. (2017). Cerebellar granule cell replenishment postinjury by adaptive reprogramming of Nestin(+) progenitors. *Nature neuroscience* **20**, 1361-1370.

Wu, S., Huang, J., Dong, J. and Pan, D. (2003). hippo encodes a Ste-20 family protein kinase that restricts cell proliferation and promotes apoptosis in conjunction with salvador and warts. *Cell* **114**, 445-456.

Xie, J., Murone, M., Luoh, S. M., Ryan, A., Gu, Q., Zhang, C., Bonifas, J. M., Lam, C. W., Hynes, M., Goddard, A., et al. (1998). Activating Smoothened mutations in sporadic basal-cell carcinoma. *Nature* **391**, 90-92.

Xin, M., Kim, Y., Sutherland, L. B., Qi, X., McAnally, J., Schwartz, R. J., Richardson, J. A., Bassel-Duby, R. and Olson, E. N. (2011). Regulation of insulin-like growth factor signaling by Yap governs cardiomyocyte proliferation and embryonic heart size. *Science signaling* **4**, ra70.

Xu, M. Z., Yao, T. J., Lee, N. P., Ng, I. O., Chan, Y. T., Zender, L., Lowe, S. W., Poon, R. T. and Luk, J. M. (2009). Yes-associated protein is an independent prognostic marker in hepatocellular carcinoma. *Cancer* **115**, 4576-4585.

Xu, T., Wang, W., Zhang, S., Stewart, R. A. and Yu, W. (1995). Identifying tumor suppressors in genetic mosaics: the Drosophila lats gene encodes a putative protein kinase. *Development (Cambridge, England)* **121**, 1053-1063.

Yagi, R., Chen, L. F., Shigesada, K., Murakami, Y. and Ito, Y. (1999). A WW domain-containing yes-associated protein (YAP) is a novel transcriptional co-activator. *The EMBO journal* **18**, 2551-2562.

Yi, J., Lu, L., Yanger, K., Wang, W., Sohn, B. H., Stanger, B. Z., Zhang, M., Martin, J. F., Ajani, J. A., Chen, J., et al. (2016). Large tumor suppressor homologs 1 and 2 regulate mouse liver progenitor cell proliferation and maturation through antagonism of the coactivators YAP and TAZ. *Hepatology (Baltimore, Md.)* **64**, 1757-1772.

Yimlamai, D., Christodoulou, C., Galli, G. G., Yanger, K., Pepe-Mooney, B., Gurung, B., Shrestha, K., Cahan, P., Stanger, B. Z. and Camargo, F. D. (2014). Hippo pathway activity influences liver cell fate. *Cell* **157**, 1324-1338.

Yu, M. and Bushman, W. (2013). Differential stage-dependent regulation of prostatic epithelial morphogenesis by Hedgehog signaling. *Developmental biology* **380**, 87-98.

Yu, M., Gipp, J., Yoon, J. W., Iannaccone, P., Walterhouse, D. and Bushman, W. (2009). Sonic hedgehog-responsive genes in the fetal prostate. *The Journal of biological chemistry* **284**, 5620-5629.

Yuan, M., Tomlinson, V., Lara, R., Holliday, D., Chelala, C., Harada, T., Gangeswaran, R., Manson-Bishop, C., Smith, P., Danovi, S. A., et al. (2008). Yes-associated protein (YAP) functions as a tumor suppressor in breast. *Cell death and differentiation* **15**, 1752-1759.

Yui, S., Azzolin, L., Maimets, M., Pedersen, M. T., Fordham, R. P., Hansen, S. L., Larsen, H. L., Guiu, J., Alves, M. R. P., Rundsten, C. F., et al. (2018). YAP/TAZ-Dependent Reprogramming of Colonic Epithelium Links ECM Remodeling to Tissue Regeneration. *Cell stem cell* **22**, 35-49.e37.

Zaidi, S. K., Sullivan, A. J., Medina, R., Ito, Y., van Wijnen, A. J., Stein, J. L., Lian, J. B. and Stein, G. S. (2004). Tyrosine phosphorylation controls Runx2-mediated subnuclear targeting of YAP to repress transcription. *The EMBO journal* **23**, 790-799.

Zhang, H., Deo, M., Thompson, R. C., Uhler, M. D. and Turner, D. L. (2012). Negative regulation of Yap during neuronal differentiation. *Developmental biology* **361**, 103-115.

Zhang, H., Pasolli, H. A. and Fuchs, E. (2011). Yes-associated protein (YAP) transcriptional coactivator functions in balancing growth and differentiation in skin. *Proceedings of the National Academy of Sciences of the United States of America* **108**, 2270-2275.

Zhang, Y., Bulkley, D. P., Xin, Y., Roberts, K. J., Asarnow, D. E., Sharma, A., Myers, B. R., Cho, W., Cheng, Y. and Beachy, P. A. (2018). Structural Basis for Cholesterol Transport-like Activity of the Hedgehog Receptor Patched. *Cell*.

Zhao, B., Li, L., Tumaneng, K., Wang, C. Y. and Guan, K. L. (2010). A coordinated phosphorylation by Lats and CK1 regulates YAP stability through SCF(beta-TRCP). *Genes & development* **24**, 72-85.

Zhao, B., Wei, X., Li, W., Udan, R. S., Yang, Q., Kim, J., Xie, J., Ikenoue, T., Yu, J., Li, L., et al. (2007). Inactivation of YAP oncoprotein by the Hippo pathway is involved in cell contact inhibition and tissue growth control. *Genes & development* **21**, 2747-2761.

Zhao, B., Ye, X., Yu, J., Li, L., Li, W., Li, S., Yu, J., Lin, J. D., Wang, C. Y., Chinnaiyan, A. M., et al. (2008). TEAD mediates YAP-dependent gene induction and growth control. *Genes & development* **22**, 1962-1971.

Zhao, R., Fallon, T. R., Saladi, S. V., Pardo-Saganta, A., Villoria, J., Mou, H., Vinarsky, V., Gonzalez-Celeiro, M., Nunna, N., Hariri, L. P., et al. (2014). Yap tunes airway epithelial size and architecture by regulating the identity, maintenance, and self-renewal of stem cells. *Developmental cell* **30**, 151-165.

Zhou, D., Conrad, C., Xia, F., Park, J. S., Payer, B., Yin, Y., Lauwers, G. Y., Thasler, W., Lee, J. T., Avruch, J., et al. (2009). Mst1 and Mst2 maintain hepatocyte quiescence and suppress hepatocellular carcinoma development through inactivation of the Yap1 oncogene. *Cancer cell* **16**, 425-438.

Zhou, Z., Hao, Y., Liu, N., Raptis, L., Tsao, M. S. and Yang, X. (2011). TAZ is a novel oncogene in non-small cell lung cancer. *Oncogene* **30**, 2181-2186.

Chapter 2 Stromal Hedgehog signaling maintains smooth muscle and hampers micro-invasive prostate cancer [1]

INTRODUCTION

Prostate cancer (PCa) is the second leading cause of cancer-related mortality in men in the United States (Siegel et al., 2016) and the second most common malignancy in men worldwide (Torre et al., 2015). Although prostate carcinoma arises from the epithelium, numerous studies have revealed the potential influence of reciprocal interactions between prostate stromal cells (fibroblasts and smooth muscle cells or SMCs) and cancer epithelial cells on tumor progression (Barron and Rowley, 2012; Franco and Hayward, 2012). For example, human prostate carcinoma-associated fibroblasts, but not normal prostate fibroblasts, induce substantial growth and neoplasia of nonmalignant human prostate epithelial cell lines in tissue recombinants in mice (Olumi et al., 1999). Furthermore, the proportion of reactive stroma within human PCa samples has prognostic value for PCa-specific death (Ayala et al., 2003; Ayala et al., 2011). Unlike normal prostate stroma that is primarily composed of mature SMCs, the reactive stroma of human PCa has been described as enriched with myofibroblasts and fibroblasts, and depleted of mature SMCs (Tuxhorn et al., 2002). In the normal adult mouse prostate, our recent study identified four stromal subtypes: SMCs that express smooth

[1] **Yang, Z., Peng, Y. C., Gopalan, A., Gao, D., Chen, Y. and Joyner, A. L.** (2017). Stromal hedgehog signaling maintains smooth muscle and hampers micro-invasive prostate cancer. *Disease Models & Mechanisms* **10**, 39-52. Attribution of data: All experiments were designed and performed by Zhaohui Yang. Dr. Alexandra Joyner oversaw the design and interpretation of experimental results, provided scientific advice and assisted with the preparation of the manuscript. Drs. Yu-Ching Peng, Anuradha Gopalan, and Yu Chen provided valuable scientific advice.

muscle actin (SMA), fibroblasts scattered between prostate ducts, and two additional Vimentin-expressing ductal fibroblast-like cell types; “wrapping cells” that wrap the outside of the smooth muscle (SM) layer and “subepithelial cells” situated between the SM and the epithelium (Peng et al., 2013) (Fig. 2.1). Furthermore, genetic inducible fate mapping (GIFM) studies during regeneration of the adult prostate raised the possibility that each stromal subtype has a distinct stem/progenitor cell (Peng et al., 2013) (Fig. 2.1). The relationship between the different stromal lineages and cancer reactive stromal cells are not known, nor whether a particular subtype is tumor protective.

The Hedgehog (HH) signaling pathway plays a pivotal role in development and regeneration of the adult prostate, and abnormal HH signaling has been implicated in multiple carcinomas including PCa (Gonnissen et al., 2013; Lim et al., 2014; Peng and Joyner, 2015; Shaw and Bushman, 2007). In mammals, three HH ligands, Sonic (SHH), Indian (IHH), and Desert (DHH), exert their function by binding to the receptor Patched (PTCH), which relieves inhibition of the transmembrane protein Smoothened (SMO). SMO activation leads to the formation of GLI2 and GLI3 transcriptional activators, which induce target genes including *Gli1* and *Ptch1*. Because *Gli1* expression is dependent on GLI2 and GLI3 activators, it is a sensitive readout of high level HH signaling (Bai et al., 2002; Bai et al., 2004). The HH signaling pathway has stage-specific roles during prostate development (Berman et al., 2004; Peng and Joyner, 2015; Yu and Bushman, 2013). During embryonic development HH signaling acts on the mesenchyme to promote ductal extension and branching, whereas at the early postnatal stage HH plays an inhibitory role on ductal

morphogenesis. In the adult mouse prostate, our previous study showed that SHH is secreted by basal epithelial cells and signals to progenitors of all four stromal subtypes (Peng et al., 2013). A separate study using an *Ihh*^{CreER} knock-in allele revealed that during adult prostate regeneration *Ihh* is preferentially expressed by epithelial cells between growing buds, and functional studies indicate that IHH negatively regulates epithelial bud formation by down-regulating stromal *Hgf* (Lim et al., 2014). Any specific function of HH signaling in the stromal changes seen during PCa progression, however, has not been addressed experimentally.

Several studies have provided evidence for paracrine HH signaling in human and mouse PCa (Fan et al., 2004; Ibuki et al., 2013; Shaw et al., 2009), a cellular relationship resembling the epithelial-to-stromal HH signaling in developing and adult mouse prostates (Berman et al., 2004; Peng et al., 2013). Autocrine HH signaling in PCa epithelial cells has also been reported (Chen et al., 2009; Karhadkar et al., 2004; Sanchez et al., 2004), particularly in advanced and metastatic PCa specimens (Chen et al., 2009; Sheng et al., 2004; Tzelepi et al., 2011). Given the questionable reliability of antibodies to HH pathway components, the highly heterogeneous nature of PCa, and the difficulty of effectively separating tumor cells from the stroma, we have taken advantage of mouse genetic tools to study HH signaling *in vivo* during PCa progression in mouse models.

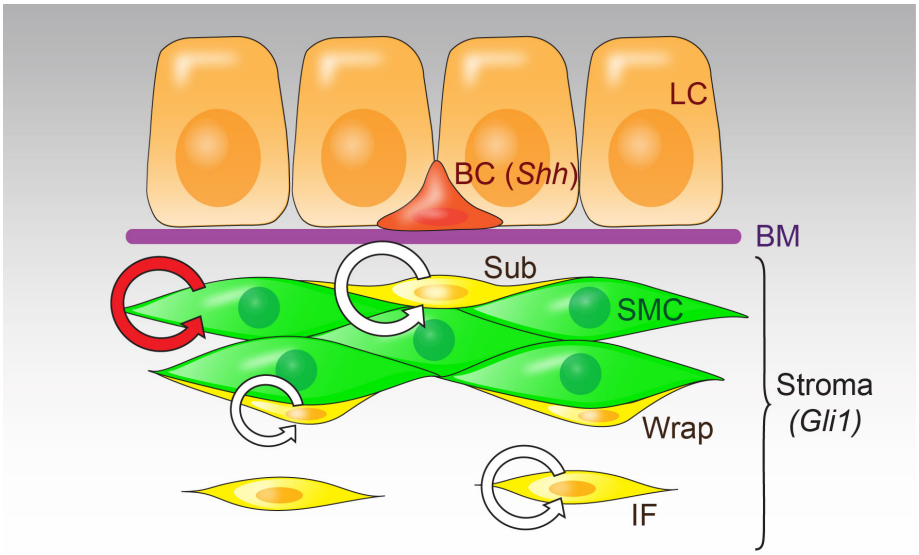

Figure 2.1 Schematic of SHH signaling in the adult prostate and model of stromal regeneration
(Adapted from (Peng et al., 2013))

Shh is expressed in the basal cells (BCs), while *Gli1* is expressed in all four stromal subtypes: subepithelial cell (Sub), smooth muscle cell (SMC), wrapping cell (Wrap), and interstitial fibroblast (IF). *Gli1* expression is enriched in Subs. Curved arrows indicate the proposed model that SHH signals to four lineage-restricted unipotent stromal stem/progenitor cells. SMCs are replenished by pre-existing SMCs (red arrow), and the other subtypes are replenished by distinct stem/progenitor cells (white arrows). BM, basement membrane; LC, luminal cell.

Several recent functional studies using mouse genetic carcinoma models found that stromal HH signaling reduces pancreas and bladder cancer progression (Lee et al., 2014; Mathew et al., 2014; Rhim et al., 2014; Shin et al., 2014), consistent with the poor outcomes of HH inhibitors in pancreas cancer clinical trials (Rosow et al., 2012). Specifically, genetic deletion of *Shh* in pancreatic cancer cells decreases survival and enhances tumor progression (Lee et al., 2014; Rhim et al., 2014), and deletion of *Smo* in bladder stromal cells promotes carcinogenesis (Shin et al., 2014). In addition, pharmacological modulation of the HH pathway in mice revealed accelerated or delayed pancreatic cancer development following SMO inhibitor or HH agonist treatment, respectively (Lee et al., 2014; Rhim et al., 2014). In a xenograft model, ablation of the HH co-receptors *Gas1* and *Boc* in mouse embryonic fibroblasts (MEFs) promoted the co-injected human pancreatic cancer cell lines to grow pancreatic tumors, whereas elimination of HH signaling by deletion of *Gas1*, *Boc*, and *Cdon* in MEFs inhibited pancreatic tumor growth, indicating a dose-dependent role of HH signaling in differentially regulating pancreatic cancer progression (Mathew et al., 2014). In PCa, however, functional studies using mouse models have not clarified the role of HH signaling in tumorigenesis. While conditional expression of oncogenic SmoM2 in the mouse prostate epithelium does not lead to mouse prostatic intraepithelial neoplasia (mPIN) or cancer (Mao et al., 2006), xenograft experiments using PCa cell lines have indicated a pro-tumor effect of HH signaling (Fan et al., 2004; Karhadkar et al., 2004), and one study using retroviral expression of SHH in the prostate reported cancer formation (Chen et al., 2006). Given the contradictory findings for the function of HH signaling

in PCa, it is important to test whether excess HH signaling in the stroma changes tumor progression in a mouse model of PCa.

We have characterized the phenotype of the stromal cells in three mouse models of PCa, and found that the proportions of cells with a SM- or fibroblast-like character were distinct to each model. In *PB-MYC* and to a lesser extent *ERG/PTEN*, but not *TRAMP* tumors, SMCs are greatly depleted, recapitulating a loss of mature SMCs seen in human PCa. Using genetic fate mapping, we found that SMCs are largely lost without contributing to the fibroblast-like reactive stroma that is increased between ducts in *PB-MYC* tumors, but contribute to the expanded SM and also give rise to a specific subset of intraductal stromal cells in *TRAMP* tumors. We found that HH signaling is increased in stromal cells in all three models, especially those adjacent to tumor cells. In *PB-MYC* and *TRAMP* tumors, *Ihh* and *Dhh* rather than *Shh* are the main ligands expressed by tumor cells. In human PCa, *IHH* is the highest expressed and the level of HH signaling positively correlates with the amount of stromal gene expression. To test whether stromal HH signaling can alter PCa progression, an activated form of the HH receptor was expressed in *Gli1*-expressing stromal cells of *PB-MYC* tumors. We found that excess HH signaling in prostate stromal cells has an inhibitory effect on cancer progression, potentially due to maintenance of SM that may prevent micro-invasion of tumors. Our studies provide new insights into the heterogeneity of stromal cells in three mouse models and in human PCa and the possible importance of particular stromal cell types in tumor progression, and also place the HH signaling pathway as a candidate of possible therapeutic value for treating PCa patients.

RESULTS

Advanced Human Prostate Tumors Show A Decrease In Smooth Muscle

In order to understand the degree to which mouse PCa models reflect the stromal changes seen in human PCa, since the proportions of SM and fibroblasts in the normal human prostate are different from mouse, we first characterized human PCa protein and RNA expression databases for changes in stromal markers. Using ACTA2 (SMA) and Calponin (CNN1) as SM markers in an analysis of human PCa specimens in the Human Protein Atlas (http://www.proteinatlas.org), we found the expected large proportion of SM in the normal human prostate, and disruption of the well organized SM layers in PCa samples, especially more advanced tumors (Fig. 2.2A-F; Fig. 2.3; Fig. 2.4). The mature SM marker CNN1 was consistently decreased (Fig. 2.2A-C; Fig. 2.3) as previously reported (Tuxhorn et al., 2002), and the area of ACTA2 expression seemed decreased in most but not all PCa samples (Fig. 2.2D-F; Fig. 2.4). However, the proportions of ACTA2-expressing and non-expressing cells varied both within samples from the same patient and between patients (Fig. 2.4H-J,H'-J'), thus it was difficult to determine if SMCs are depleted in tumors. Using Vimentin (VIM) as a fibroblast marker, we found that VIM was maintained in non-epithelial cells and possibly increased in some samples in the remaining stroma between glands (Fig. 2.2G-I; Fig. 2.5). Overall, higher-grade tumors appeared to have a greater disruption of the stromal cytoarchitecture (Fig. 2.2A-I; Fig. 2.3; Fig. 2.4; Fig. 2.5).

As a complementary approach to analyzing human PCa stromal content, we analyzed RNA-sequencing (RNA-seq) data from the TCGA dataset (n=27

normal and 330 primary PCa samples) (Abeshouse et al., 2015), and found a significant decrease in expression of the SM markers *ACTA2* and *CNN1*, as well as the fibroblast marker *VIM* in PCa compared to normal prostate samples (Fig. 2.2J). In addition, the expression levels of *CNN1* and *ACTA2* (but not *VIM*) were progressively lower in patients with higher Gleason scores, with a significant decrease seen in Gleason >=8 compared to most other stages (Fig. 2.2K; Fig. 2.6A). There was the expected corresponding decrease in basal cell markers (*KRT5* and *TP63*) and increase in expression of luminal cytokeratin markers in tumor cells (*KRT8* and *KRT18*) (Fig. 2.6B). There also was a greater correlation between tumors with high *ACTA2* or *CNN1* expression and basal cell gene expression (Pearson coefficient = 0.343 or 0.381 for *ACTA2* or *CNN1* with *KRT5*; = 0.299 or 0.319 for *ACTA2* or *CNN1* with *TP63*) than for *VIM* and basal markers (Pearson coefficient = 0.144 for *VIM-KRT5*; = 0.097 *VIM-TP63*), and a trend towards a negative correlation for the luminal marker *KRT18* with *ACTA2* and no correlation with *CNN1* (Pearson coefficient = -0.139 or -0.067 for *ACTA2* or *CNN1* with *KRT18*) (Table 2.1).

As an additional means to address stromal gene expression levels and clinical outcome, we analyzed RNA microarray data from the MSKCC Prostate Oncogenome Project (n=29 normal, 131 primary tumors, and 19 metastases) (Taylor et al., 2010). Interestingly metastatic PCa samples expressed significantly lower levels of *CNN1* and *ACTA2* compared to primary tumor samples and normal (Fig. 2.2L). Furthermore, Kaplan-Meier analysis revealed that patients with lower expression levels of *CNN1* and *ACTA2* but not *VIM* had a significantly shorter relapse-free time (Fig. 2.2M; Fig. 2.6C). All together,

these results show that more advanced PCa samples with a higher Gleason score or metastasis stage have lower levels of expression of two SM markers (*ACTA2* and *CNN1*), indicating either a reduction in the number of SMCs or the expression of these genes is decreased in the remaining cells.

Figure 2.2 Human prostate tumors show disruption of stromal architecture with a decrease in smooth muscle.

(A-I) Immunohistochemistry (IHC) of CNN1 (A-C), ACTA2 (D-F), and VIM (G-I) in human normal prostate, low- or medium-grade and high-grade prostate tumor samples from the Human Protein Atlas. Numbers on top right corner of each panel indicates the patient ID number. Scale bar, 100 μm. (J) The mRNA expressions of stromal marker genes (*CNN1*, *ACTA2*, and *VIM*) from TCGA RNA-seq data with 330 primary PCa samples (Tumor) and 27 normal controls (Normal). (K) The mRNA expression of *CNN1* in PCa samples graded with Gleason scores from TCGA RNA-seq data. (L) The mRNA expressions of stromal marker genes from MSKCC Prostate Oncogenome Project. (J-L) *P<0.05; **P<0.01; ****P<0.0001. Data are presented as mean ± s.d. Each data point represents one sample. (M) Kaplan-Meier relapse-free (months) analysis of patient data from PCa samples from MSKCC Prostate Oncogenome Project with *CNN1* low-expression (n = 38) and high-expression (n = 93); p value is calculated via Mantel-Cox (log rank) test.

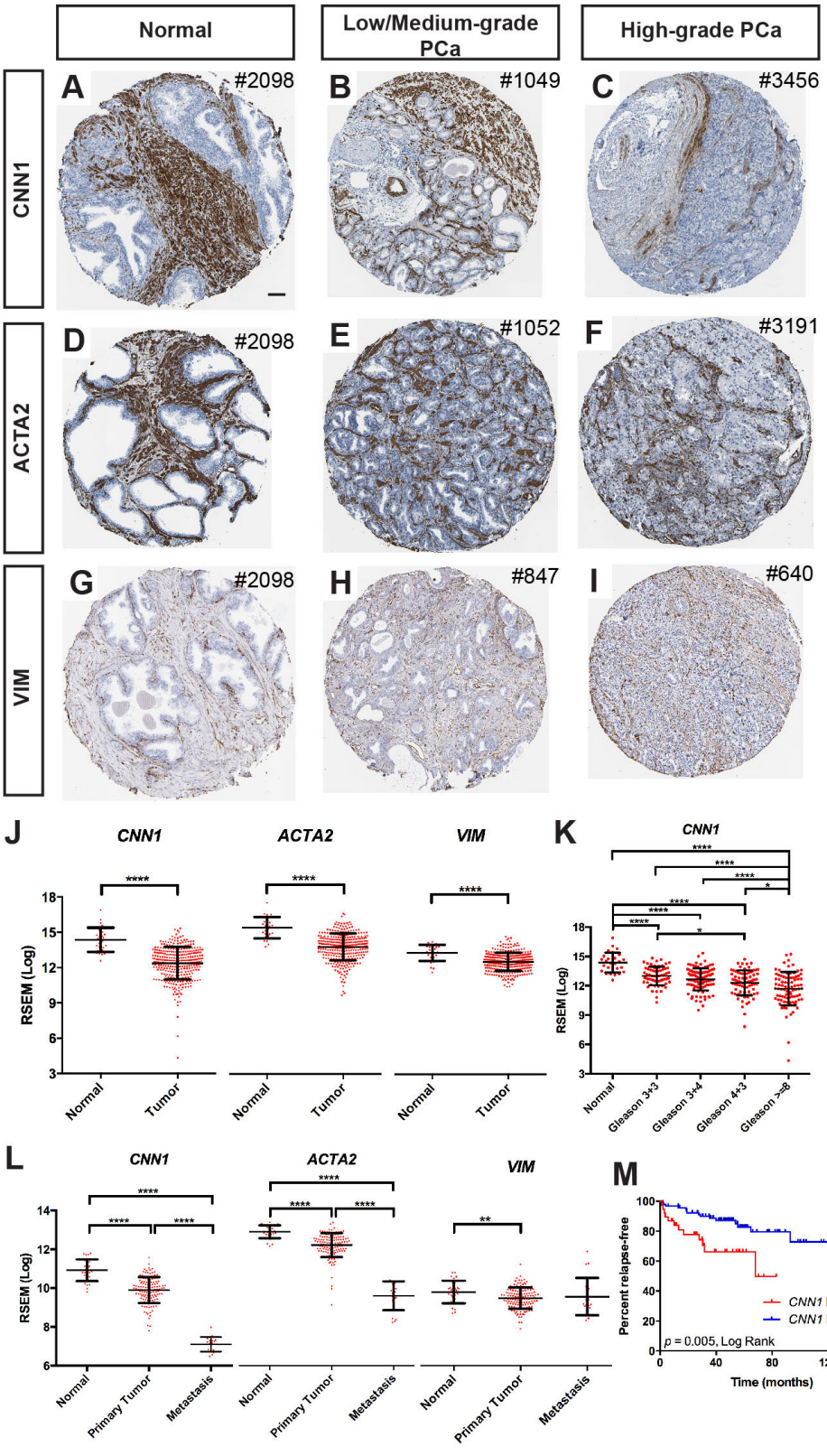
Normal
Low/Medium-grade PCa
High-grade PCa
CNN1
ACTA2
VIM
A
#2098
B
#1049
C
#3456
D
#2098
E
#1052
F
#3191
G
#2098
H
#847
I
#640
J
CNN1
ACTA2
VIM
RSEM (Log)
Normal
Tumor
K
CNN1
RSEM (Log)
Normal
Gleason 3+3
Gleason 3+4
Gleason 4+3
Gleason >=8
L
CNN1
ACTA2
VIM
RSEM (Log)
Normal
Primary Tumor
Metastasis
M
Percent relapse-free
CNN1 Low (n=38)
CNN1 High (n=93)
p = 0.005, Log Rank
Time (months)

Figure 2.3 CNN1 is consistently decreased in human PCa samples.

Immunohistochemistry (IHC) of CNN1 in human normal prostate (A, B), low-grade (C-G) and high-grade (H, I) prostate tumor samples from the Human Protein Atlas. Numbers on top right corner of each panel indicates the patient ID number. Scale bar, 100 μm.

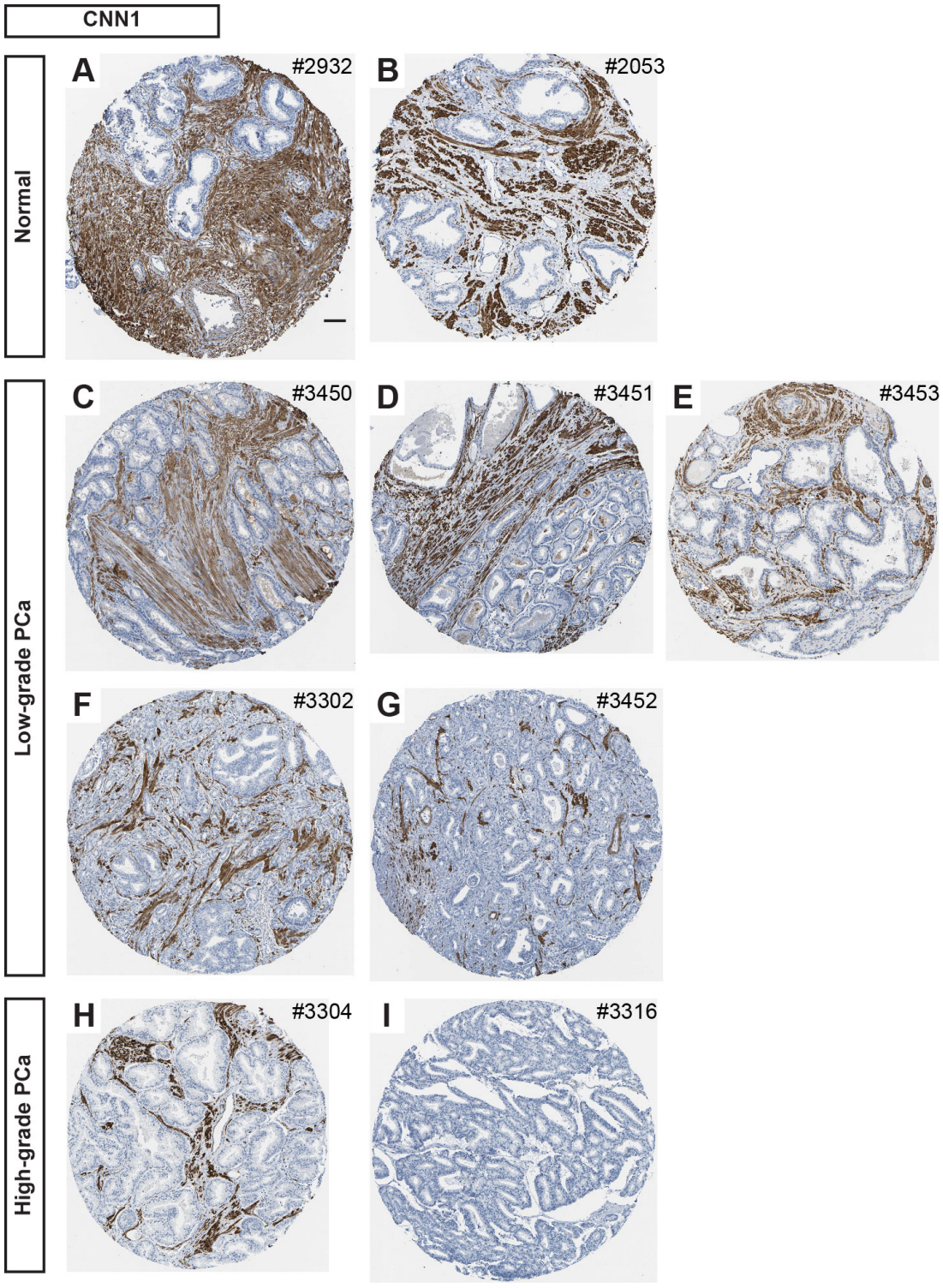
CNN1
Normal
A
#2932
B
#2053
Low-grade PCa
C
#3450
D
#3451
E
#3453
F
#3302
G
#3452
High-grade PCa
H
#3304
I
#3316

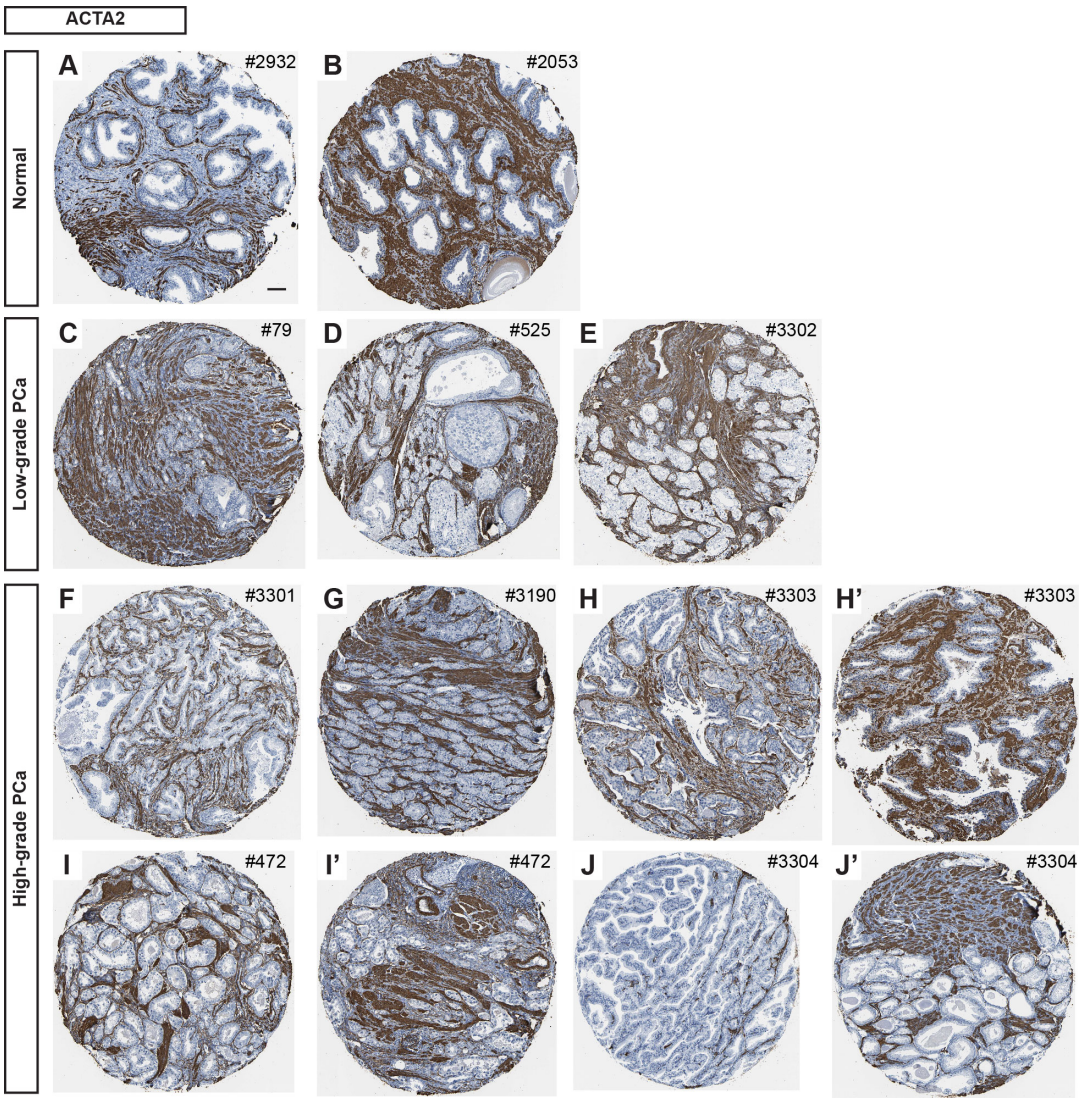

Figure 2.4 ACTA2 is decreased in most but not all human PCa samples.

IHC of ACTA2 in human normal prostate (A, B), low-grade (C-E) and high-grade (F-J) prostate tumor samples from the Human Protein Atlas. H', I', and J' are samples from the same patients with H, I, and J, respectively. Numbers on top right corner of each panel indicates the patient ID number. Scale bar, 100 μm.

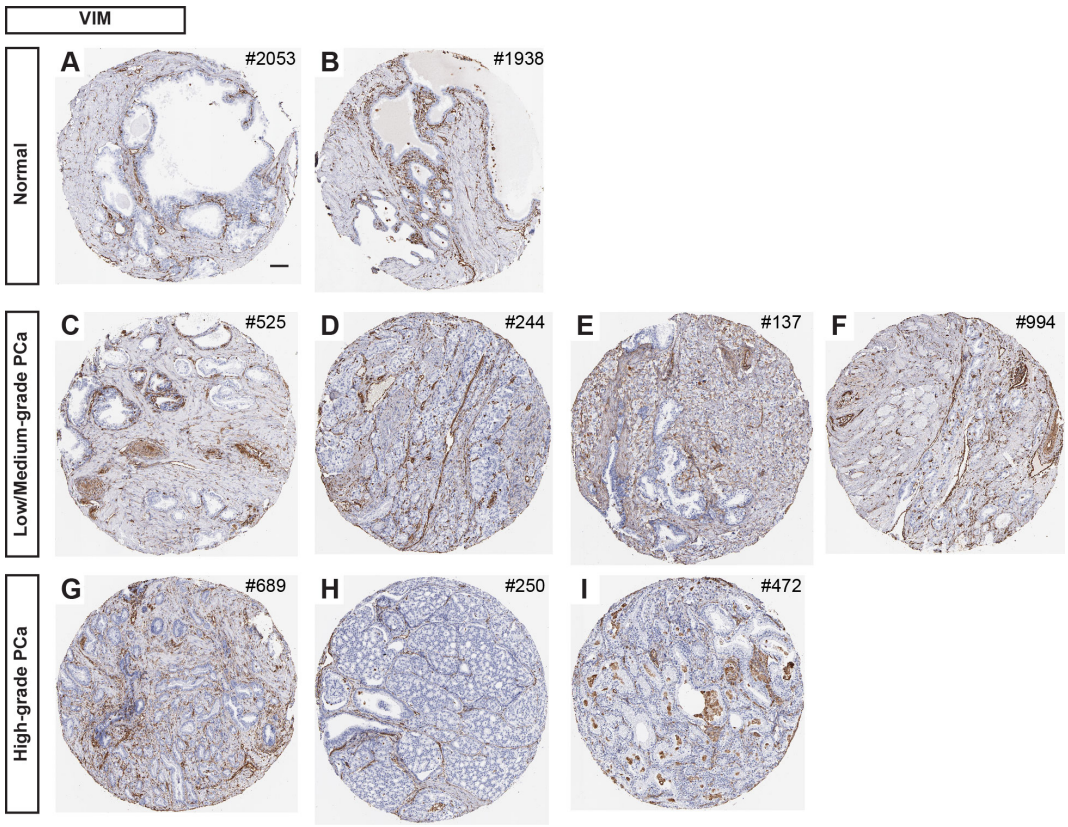

Figure 2.5 VIM is maintained in human PCa samples.

IHC of VIM in human normal prostate (A, B), low- or medium-grade (C-F) and high-grade (G-I) prostate tumor samples from the Human Protein Atlas. Numbers on top right corner of each panel indicates the patient ID number. Scale bar, 100 μm.

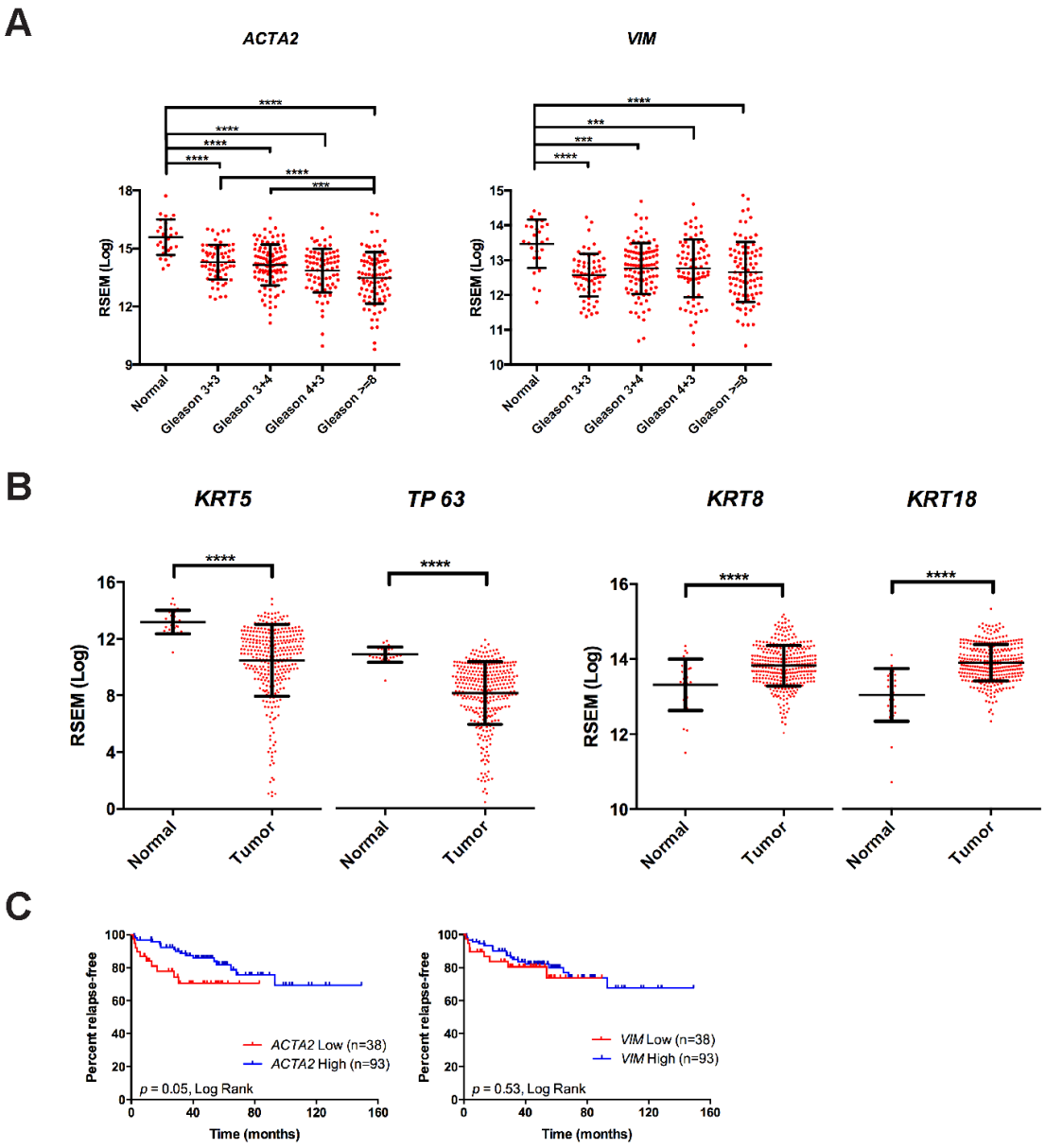

Figure 2.6 Stromal markers expressions are decreased in human primary PCa samples.

(A) The mRNA expressions of stromal cell marker genes in PCa samples graded with Gleason scores from TCGA RNA-seq data. (B) The mRNA expressions of basal and luminal cell marker genes in PCa samples from TCGA RNA-seq data with 330 primary PCa samples and 27 normal controls. (C) Kaplan-Meier relapse-free (months) analysis of patient data from PCa samples from MSKCC Prostate Oncogenome Project with stromal markers having low-expression (n = 38) and high-expression (n = 93); p values are calculated via Mantel-Cox (log rank) test.

Table 2.1 The Pearson correlation coefficient of gene expressions in the TCGA PCa dataset.

(A) Pearson correlation coefficient between stromal (SMC and fibroblast) and epithelial (basal and luminal) marker gene mRNA expressions.

Pearson coefficient	***CNN1***	***ACTA2***	***VIM***	***KRT5***	***TP63***	***KRT8***	***KRT18***
CNN1	1.000						
ACTA2	0.959	1.000					
VIM	0.555	0.628	1.000				
KRT5	0.381	0.343	0.144	1.000			
TP63	0.319	0.299	0.097	0.860	1.000		
KRT8	0.048	-0.018	-0.089	0.021	-0.154	1.000	
KRT18	-0.067	-0.139	-0.195	-0.116	-0.309	0.838	1.000

(B) Pearson correlation coefficient between HH pathway genes and prostate stromal and epithelial marker gene mRNA expressions.

Pearson correlation coefficient	***SHH***	***IHH***	***DHH***	***GLI1***
CNN1	-0.030	-0.072	0.450	0.379
ACTA2	-0.024	-0.076	0.422	0.483
VIM	0.126	-0.021	0.560	0.595
GLI1	0.181	0.189	0.309	1.000
KRT5	0.016	-0.082	0.001	0.047
TP63	0.014	-0.095	-0.017	0.045
KRT8	-0.040	0.083	0.025	-0.123
KRT18	-0.048	0.056	-0.054	-0.232

PB-MYC and *ERG/PTEN* but not *TRAMP* mouse PCa models display extensive disruption of smooth muscle

To investigate whether mouse PCa models have similar stromal alterations to those seen in human PCa, especially as mouse normal prostate has less SM than human, we analyzed the stromal characteristics of three distinct mouse lines. Two transgenic lines were investigated that use a Probasin gene regulatory element to drive expression of the oncogenes *MYC* (*PB-MYC*) (Ellwood-Yen et al., 2003) or SV40 large/small T antigen (*Tr*ansgenic *A*denocarcinoma *M*ouse *P*rostate or *TRAMP*) (Greenberg et al., 1995) in the dorsolateral epithelium of mouse prostate, and one conditional genetic model (*ERG/PTEN*) that mimics the *TMPRSS2-ERG* fusion loci that are seen in about fifty percent of human PCa (Clark et al., 2007; Hermans et al., 2006) by misexpressing the ETS transcription factor ERG (Chen et al., 2013) combined with *Pten* deletion in luminal cells (*Tmprss2*$^{CreER\text{-}GFP/+}$; *R26*$^{LSL\text{-}ERG\text{-}GFP/\ LSL\text{-}ERG\text{-}GFP}$; *Pten*$^{flox/flox}$ mice administered tamoxifen at 4 weeks of age). Unlike normal mouse prostates with a thin single layer of epithelium (Fig. 2.7A,A'; Fig. 2.8A), all three models displayed extensive mPIN featuring stratified epithelial cells with prominent nuclear atypia forming cribriform and/or tufting confined within the basement membrane. Such multifocal proliferative lesions were found to affect most of the dorsolateral ducts in *PB-MYC* (n=52 mice, 35-49 weeks old; Fig. 2.7B,B'; Fig. 2.8B) and almost all dorsolateral ducts in *ERG/PTEN* (n=9, 12-41 weeks old; Fig. 2.7D,D'; Fig, 2.7C). In late stage prostate tumors of *PB-MYC* mice (n=8 mice, 44-49 weeks old), micro-invasive carcinoma (MIC) was seen with nests of atypical tumor cells (EpCAM+ and CK5-) infiltrating into the stroma and forming irregular contours (Fig. 2.7C,C'; Fig. 2.8B). Using an SMA antibody to label SMCs, we found that the SM layer in *PB-MYC* tumors were

much thinner than normal and contained many gaps (Fig. 2.7G,H,I; Fig. 2.8E,F). In *ERG/PTEN* tumors, the disruption of the SM layers was less dramatic; the majority of ducts had an intact SM layer but some ducts had a discontinuous SM layer (Fig. 2.7J; Fig. 2.8G). In addition, in contrast to the normal prostate, VIM-positive fibroblast-like cells were abundant in both *PB-MYC* and *ERG/PTEN* prostates, filling up the space between tumor ducts (Fig. 2.7H-J). Furthermore, the interductal stromal cells showed an increase in expression of Collagen 1 (COL1) in *PB-MYC* and to a lesser extent in *ERG/PTEN* tumors (Fig. 2.9B-B",C-C") compared to WT (Fig. 2.9A-A"). Thus, these two models, and particularly *PB-MYC*, recapitulate many of the stromal alterations reported in human PCa, and therefore are valuable tools to study PCa stromal features and functions.

The tumors in *TRAMP* mutants had a distinct stromal character to that in *PB-MYC* and *ERG/PTEN* mice, even when the neuroendocrine tumors were not included in the analysis. In *TRAMP* prostates, most areas with mPIN (n=35 mice, 20-33 weeks old; Fig. 2.7E,E') showed an increase in the thickness of the SM layer surrounding the ducts (Fig. 2.7K; Fig. 2.8H) and SMA+ cells invaded between epithelial folds compared to normal prostates (Fig. 2.7G; Fig. 2.8E). Interestingly, in more advanced *TRAMP* tumors (28-33 weeks) there were regions with complex polypoid intraductal adenomatous-stromal proliferation with minimal cytologic atypia, referred to as Intraductal Adenoma with Stroma (IAS) as they contained proliferating masses of stromal cells that invaded between the epithelial layers within ducts (n=21 mice; Fig. 2.7F,F'; Fig. 2.8H). The majority of stromal cells in IAS expressed either SMA, VIM, and/or COL1 strongly (Fig. 2.7L; Fig. 2.9E-E'), indicating the stromal cells that

invaded IAS lesions of *TRAMP* prostates have features of SMCs and/or fibroblasts. Also unlike in the *PB-MYC* and *ERG/PTEN* models, *TRAMP* tumors had few VIM+ or COL1+ interductal fibroblasts (Fig. 2.9D). The exception was in rare areas where the SM layer was partially disrupted (Fig. 2.10H). Thus, only in some areas of *TRAMP* tumors did the stromal character have similarities to the *PB-MYC* and *ERG/PTEN* models. Unlike human PCa, however, in all three PCa models CNN1 expression largely overlapped with SMA expression (Fig. 2.8I-L).

Figure 2.7 *PB-MYC*, *ERG/PTEN*, and *TRAMP* PCa models have distinct stromal characteristics.

(A-F) H&E staining of dorsolateral prostate (DLP) sections from tissues of WT (A), *PB-MYC/+* (B, C), *ERG/PTEN* (D), and *TRAMP/+* (E, F) mice. (A'-F') Magnification of areas within dashed lines in A-F. (G-L) Immunofluorescent (IF) staining of DLP sections for SMA (green), Vimentin (VIM, red), and DAPI (blue). Arrows in K indicate SMCs invading between epithelial folds. *= Infiltrating nests of tumor cells; plus symbols (+) indicate blood vessels Scale bars, 50 μm.

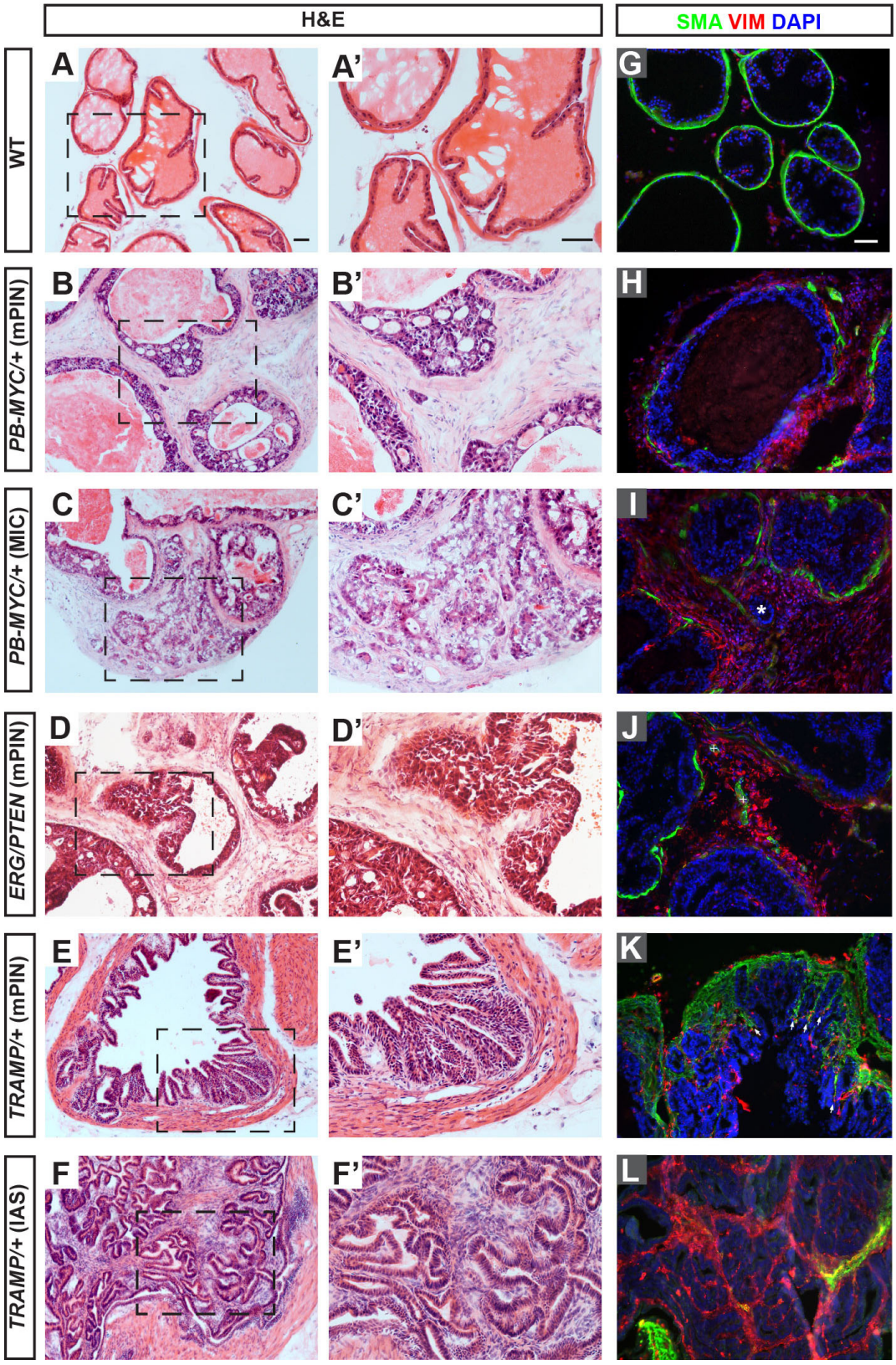
H&E
SMA VIM DAPI
WT
PB-MYC/+ (mPIN)
PB-MYC/+ (MIC)
ERG/PTEN (mPIN)
TRAMP/+ (mPIN)
TRAMP/+ (IAS)
A
A'
G
B
B'
H
C
C'
I
D
D'
J
E
E'
K
F
F'
L

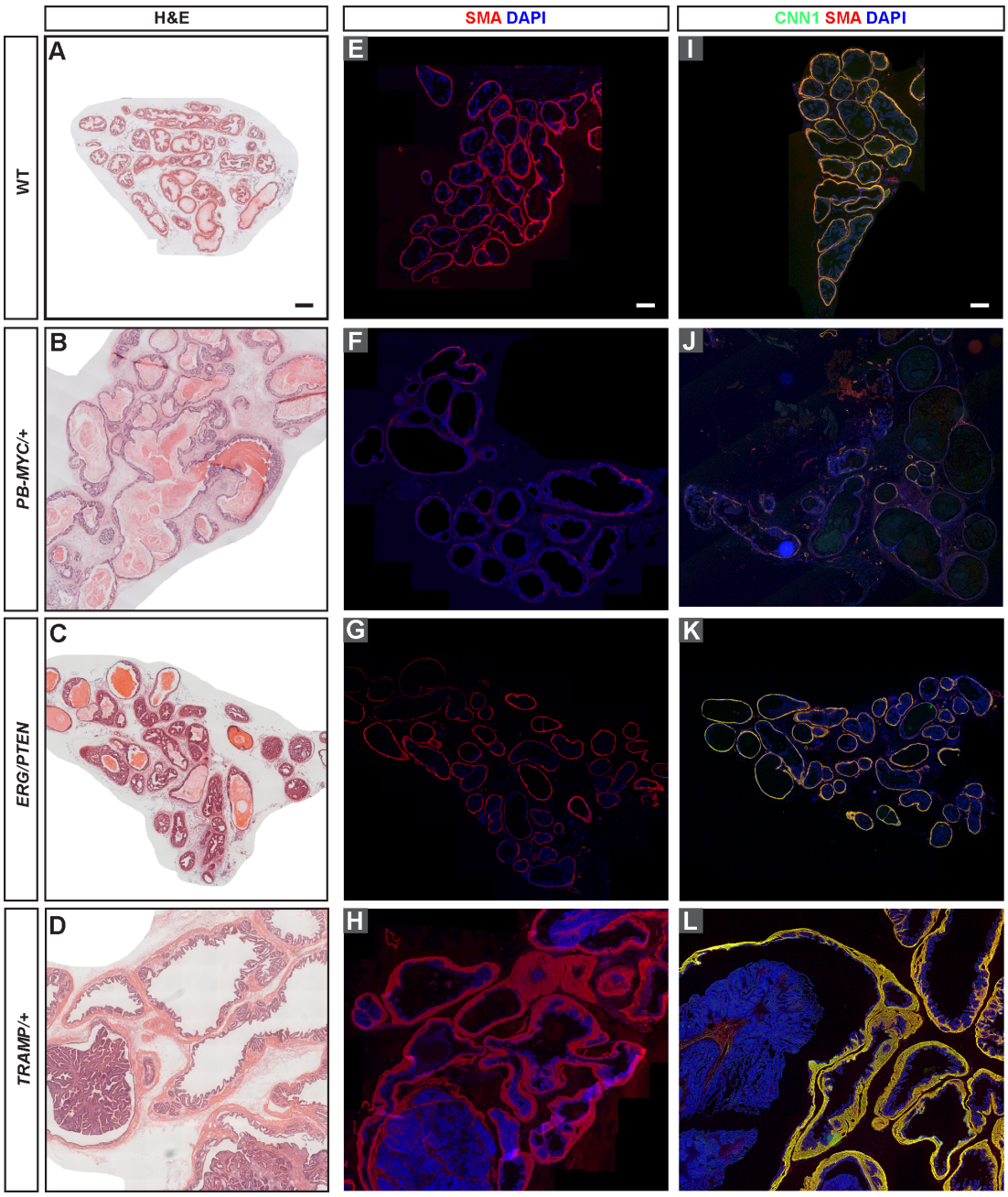

Figure 2.8 *PB-MYC*, *ERG/PTEN*, and *TRAMP* PCa models have distinct cytoarchitecture and stromal cell contents.

(A-D) H&E staining of DLP sections from tissues of WT (A), *PB-MYC/+* (B), *ERG/PTEN* (C), and *TRAMP/+* (D) mice. (E-L) Immunofluorescent (IF) staining of DLP sections for (E-H) SMA (red) and DAPI (blue); (I-L) CNN1 (green), SMA (red), and DAPI (blue). Scale bars, 200 μm.

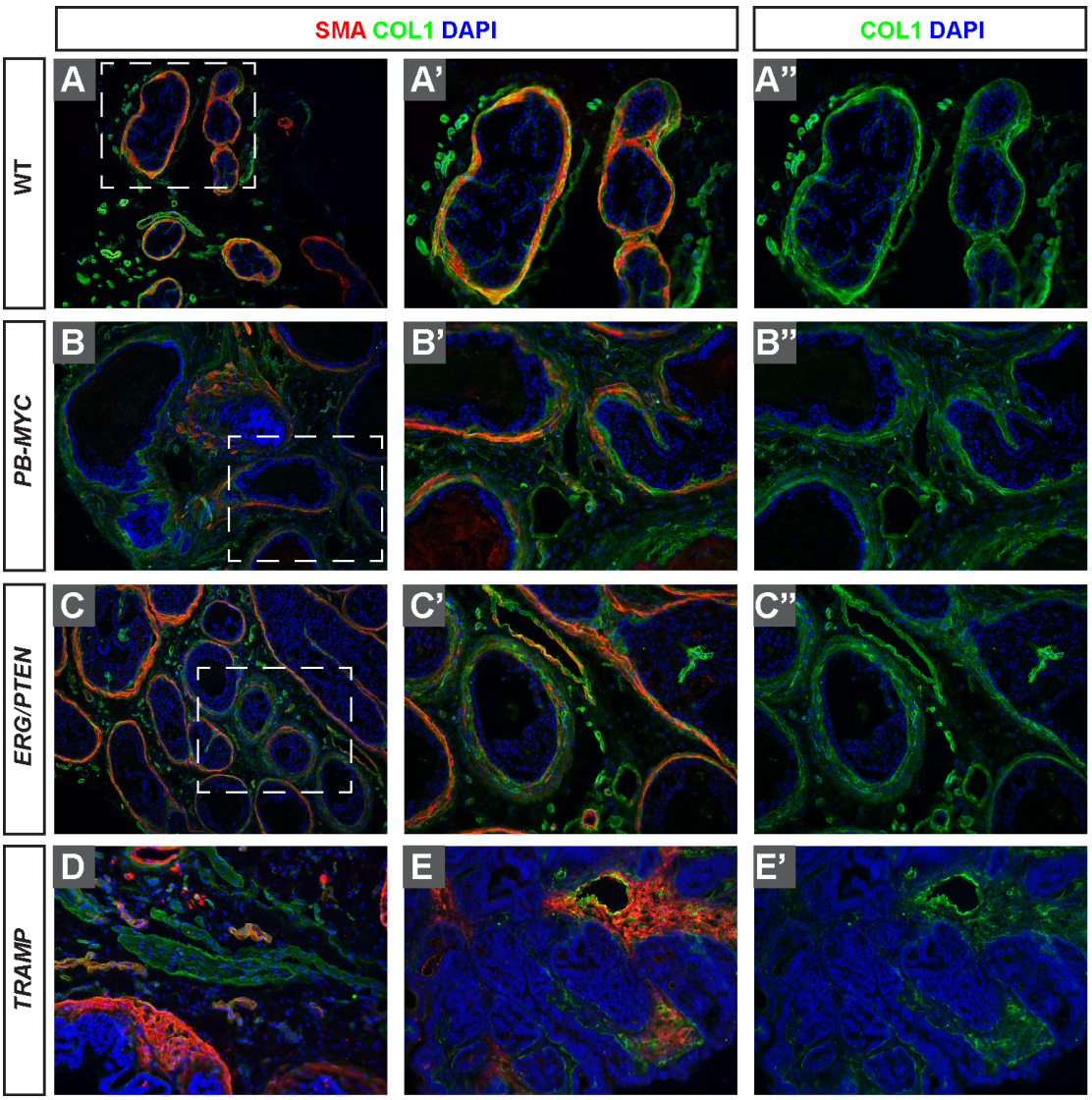

Figure 2.9 Interductal reactive stroma in *PB-MYC* and *ERG/PTEN* and IAS stroma in *TRAMP* tumors have an increased expression of Collagen 1 compared to normal interductal fibroblasts.

IF staining of DLP sections from tissues of (A-A") 30-week old WT, (B-B") 45-week old *PB-MYC,* (C-C") 22-week old *ERG/PTEN,* and (D,E-E') 30-week old *TRAMP* mice, for (A-A") SMA (red), COL1 (green), and DAPI (blue). (B-D) show regions of mPIN; (E-E') shows a region of IAS. Scale bars, 50 μm.

SMCs are largely lost in *PB-MYC* prostate tumors whereas some form the stroma in *TRAMP* IAS lesions

Since SM is significantly reduced in *PB-MYC* tumors, we used GIFM to test whether SMA+ cells are lost or change fate into cancer reactive stroma. Tamoxifen was administered to *Sma-CreER/+*;*R26*$^{tdTomato/+}$*;PB-MYC/+* (*Sma*-GIFM;*PB-MYC*) mice and control *Sma-CreER/+*;*R26*$^{tdTomato/+}$ (*Sma*-GIFM;WT) littermates at 4 weeks of age (Fig. 2.10A). In prostates of *Sma*-GIFM;*PB-MYC* mice at 6 weeks of age, soon after the initiation of *MYC* transgene expression and two weeks after administration of tamoxifen, the histology and distribution of tdT+ cells was comparable to that of control *Sma*-GIFM;WT mice (Fig.2.9), and tdT specifically labeled the majority of SMCs (Fig. 2.10C). Strikingly, *Sma*-GIFM;*PB-MYC* mice at 45 weeks had a huge reduction in the number of tdT-labeled SMA+/COL1+ cells surrounding the mPIN or MIC lesions (Fig. 2.10D,E; Fig. 2.11). There were only rare tdT+ reactive stromal cells interspersed between ducts, and they all expressed VIM+ and a rare subset expressed SMA weakly (Fig. 2.11A-A'',B-B''). This result indicates that SMA-positive lineage cells were prominently reduced in number during tumor progression, and they are not a major cell-of-origin for reactive stroma in *PB-MYC* tumors.

Since *TRAMP* have a large increase in SM and stromal cells invade into IASs, we also fate mapped the SMA-lineage cells in *TRAMP* to test whether they expand only in the SM layer or give rise to other cancer reactive stroma. The increased SM layers surrounding mPIN and most IASs remained largely positive for tdT and SMA (Fig. 2.10F,G). In addition to expanding the SM, some cells marked by *Sma*-GIFM (many positive for COL1 and negative or

only weakly positive for SMA) extended into subepithelial folds of mPIN lesions (Fig. 2.10F) and were present within IASs (Fig. 2.10G; Fig. 2.12A-A'',E-E"). 71% of the intraductal masses (15/21 from 5 mice) had extensive tdT labeling (Fig. 2.12A-A",B; Table 2.2) while 29% did not (Fig. 2.12C,D), indicating that SMCs are a major cell-of-origin of the stromal cells within IASs in *TRAMP* tumors. However, none of the fibroblasts between the ducts were labeled with tdT, indicating that as in *PB-MYC* tumors, the interductal cancer stromal cells have a separate cell-of-origin. In addition, in rare regions where the SM layer was diminished there were few fate-mapped cells (Fig. 2.10H). Among the tdT+ IASs, 10/15 expressed SMA (Table 2.2), suggesting that some SMA-expressing cells turned off SMA while giving rise to cancer reactive stroma. In summary, our two fate-mapping studies indicate that the character of the epithelial tumor cells could regulate the fate of SMCs in prostate tumor stroma.

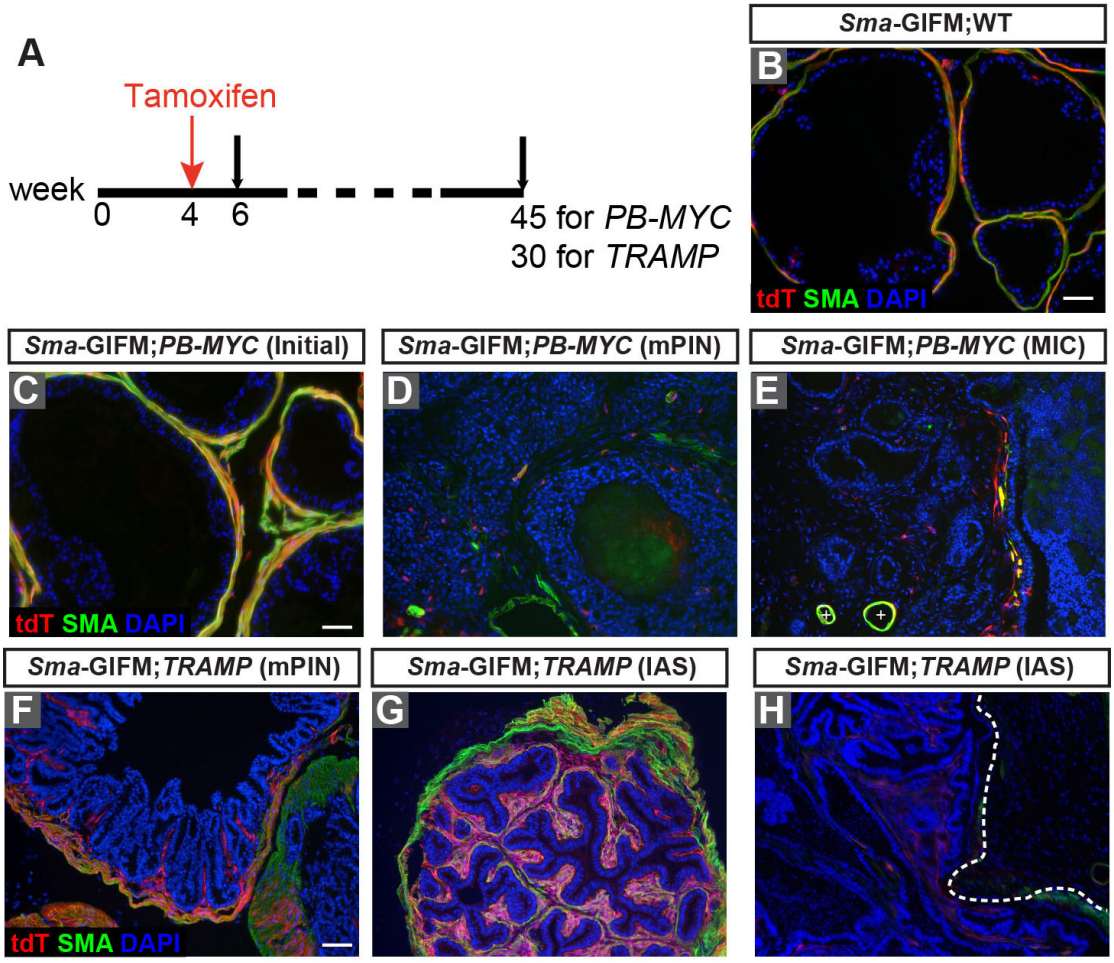

Figure 2.10 SMA-expressing cells are largely lost in *PB-MYC* tumors while some transform into cancer stroma in *TRAMP* IAS lesions.

(A) Schematic showing experimental design. (B) IF staining of DLP sections from 30 week old *Sma-CreER/+*;*R26*$^{tdTomato/+}$ (*Sma*-GIFM;WT) mice for tdT (red), SMA (green), and DAPI (blue). (C-E) IF staining of 6 week old (C) and 45 week old (D,E) *Sma-CreER/+*;*R26*$^{tdTomato/+}$;*PB-MYC/+* (*Sma*-GIFM;*PB-MYC*) mice for tdT (red), SMA (green), and DAPI (blue). Plus symbols (+) indicate blood vessels. (F-H) IF staining of DLP sections from 30 week old *Sma*-GIFM;WT (*Sma-CreER/+;R26*$^{tdTomato/+}$) (F) and *Sma*-GIFM;*TRAMP* (*Sma-CreER/+;R26*$^{tdTomato/+}$*;TRAMP/+*) (G,H) mice for tdTomato (tdT, red), SMA (green), and DAPI (blue). Dashed line in H indicates a region where the SM layer is diminished. Scale bar, 50 μm.

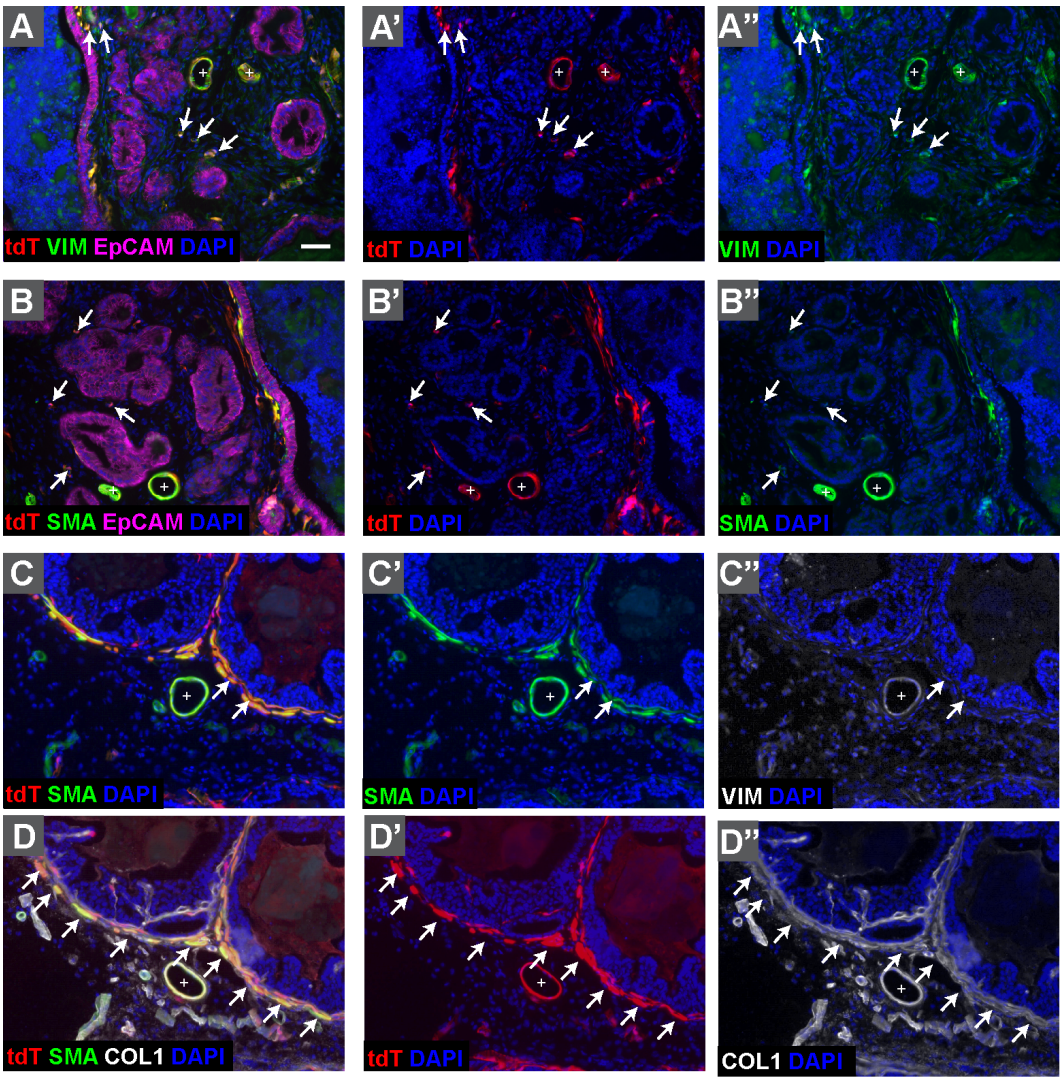

Figure 2.11 SMA-expressing cells are mostly lost in *PB-MYC*.

IF staining of DLP sections from tissues of 45-week old *Sma*-GIFM;*PB-MYC* mice. (A-A") tdT (red), VIM (green), EpCAM (magenta), and DAPI (blue). Arrows indicate the rare tdT+ VIM+ EpCAM- stromal cells in the center of the image where many VIM+ fibroblast-like cells are present. (B-B'') tdT (red), SMA (green), EpCAM (magenta), and DAPI (blue). Arrows indicate rare stromal cells expressing tdT that are weakly SMA+ and EpCAM-. (C-C") tdT (red), SMA (green), VIM (white), and DAPI (blue). Arrows indicate rare SM-like cells that express tdT and are weakly VIM+. (D-D") tdT (red), SMA (green), COL1 (white), and DAPI (blue). Arrows indicate fate mapped stromal cells in the SM layer expressing tdT that are COL1+. Plus symbols (+) indicate blood vessels. Scale bar, 50 μm.

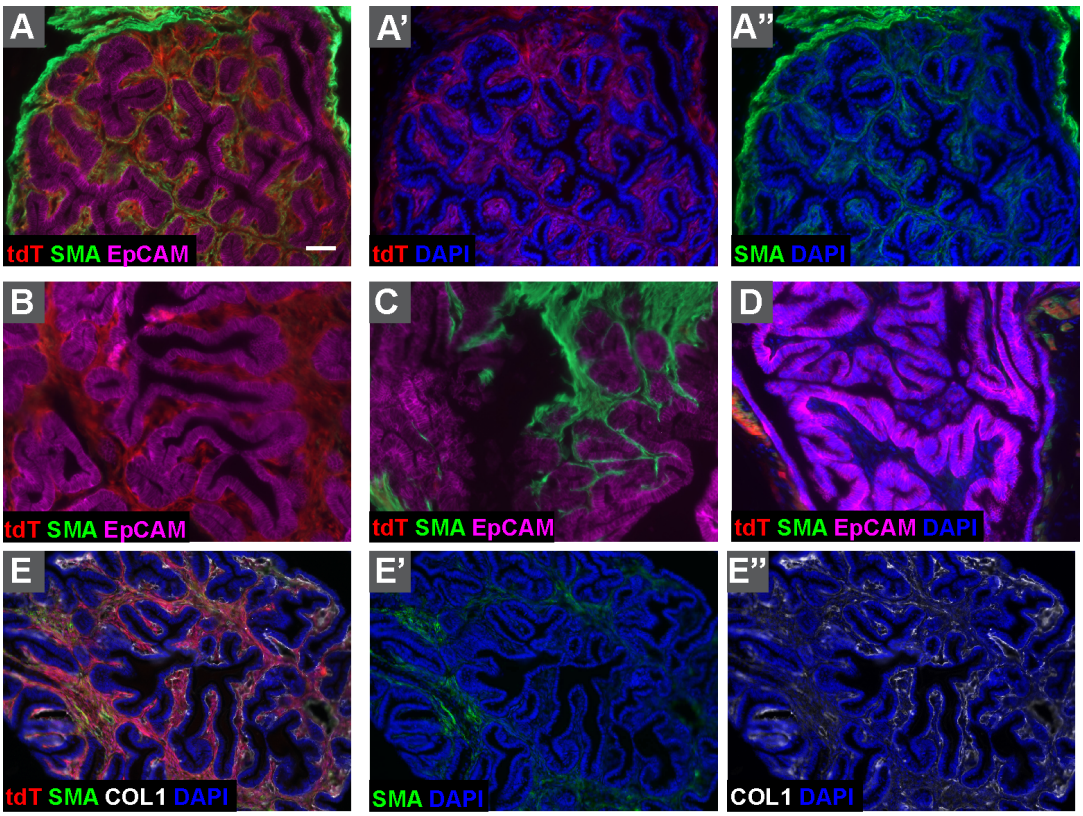

Figure 2.12 Some SMA-expressing cells contribute to the stroma in IAS of *TRAMP* tumors.

IF staining of DLP sections from tissues of 30-week old *Sma*-GIFM;*TRAMP* mice. (A-A", B-D) tdT (red), SMA (green), EpCAM (magenta), and DAPI (blue). (E-E") tdT (red), SMA (green), COL1 (white), and DAPI (blue). Scale bar, 50 μm.

Table 2.2 The SMA+ lineage is a major cell-of-origin for stromal cells in IAS of *TRAMP* PCa.

Quantification of IAS ducts from five *Sma*-GIFM; *TRAMP* (*Sma-CreER/+; R26*$^{tdTomato/+}$*; TRAMP/+*) mice.

Animal ID	#IAS Ducts in *Sma*-GIFM; *TRAMP*				
	tdT+ SMA+	tdT+ SMA-	tdT- SMA+	tdT- SMA-	Subtotal
T67	2	1	0	0	3
T171	0	2	1*	2	5
T183	1	0	0	0	1
T213	2**	1***	0	2****	5
T800	5	1	0	1	7
Sum	10	5	1	5	21
	GIFM+ 15/21; 10/15 SMA+, 5/15 SMA-		GIFM- 6/21; 1/6 SMA+, 5/6 SMA-		

* This IAS duct has ~60% of the intraductal stromal cells that are SMA+.
** In one out of the two IAS ducts, ~50% of the intraductal stromal cells are tdT+.
*** This IAS duct has only 30% of the intraductal stromal cells that are SMA+, and thus is considered as SMA-.
**** In one out of the two IAS ducts, only 30% of the intraductal stromal cells are SMA+, and thus is considered as SMA-.

Gli1 is increased and restricted to stromal cells in PCa

Given the correlation between reduced SM layers and higher-grade tumors and functional relationship in the prostate between SHH and expansion of the stroma during development, we next asked whether HH signaling is altered in mouse PCa compared to the normal adult prostate. Our previous study using knock-in reporter mice revealed that *Gli1*^{nlacZ} (Bai et al., 2002) is expressed by a subset of all four stromal subtypes in normal adult mouse prostate (Peng et al., 2013) (Fig.2.12A,A'; Fig. 2.14A). Unlike previous studies using RNA *in situ* hybridization or questionable antibodies to analyze human tumors samples (Fan et al., 2004; Sanchez et al., 2004), the nuclear-localized lacZ protein allows the cell type expressing *Gli1* to be unambiguously identified. In areas of mPIN (n=12 mice, 35-49 weeks; Fig. 2.13B,B'; Fig. 2.14B) or MIC (n= 6 mice, 45-49 weeks, Fig. 2.13C,C'; Fig. 2.14C) of *PB-MYC* tumors, *Gli1*^{nlacZ} was expressed in scattered cells in the stroma, primarily adjacent to the tumor epithelium. As in wild-type (WT) mice, all *Gli1*+ cells were negative for the epithelial marker EpCAM (Fig. 2.14A-C), demonstrating that *Gli1*+ cells are stromal cells. We also examined *Gli1* expression in the prostate stroma of *ERG/PTEN* mice carrying a *Gli1*^{GFP} allele (referred to as *Gli1*^{GFP}*;ERG/PTEN*). Although almost all epithelial cells express a high level of nuclear-localized GFP (ERG-GFP and CreER-GFP), any stromal GFP+ cells should reflect expression of *Gli1*, since *ERG/PTEN* alone has no GFP+ stromal cells (n= 5 mice, 12-41 weeks; Fig. 2.14F-F"). As in *PB-MYC* tumors, a high proportion of *ERG/PTEN* tumor stromal cells near mPIN lesions expressed *Gli1*^{GFP}, including SMCs (Fig. 2.14G-G").

In *TRAMP* mPIN lesions, *Gli1*^{nlacZ} expression was enriched in the stromal cells closest to the tumor epithelium, including the SMCs cells invading between epithelial folds (n=8 mice, 25-33 weeks; Fig. 2.13D,D'; Fig. 2.14D). Strikingly, many tumor stromal cells in IASs expressed *Gli1*^{nlacZ}, although cells at a distance from tumor cells did not (n=4 mice, 28-33 weeks; Fig. 2.13E,E'; Fig. 2.14E). Thus, an increase in HH signaling specifically in the stroma (SMCs and fibroblasts) near tumor cells appears to be a consistent finding in mouse models of PCa.

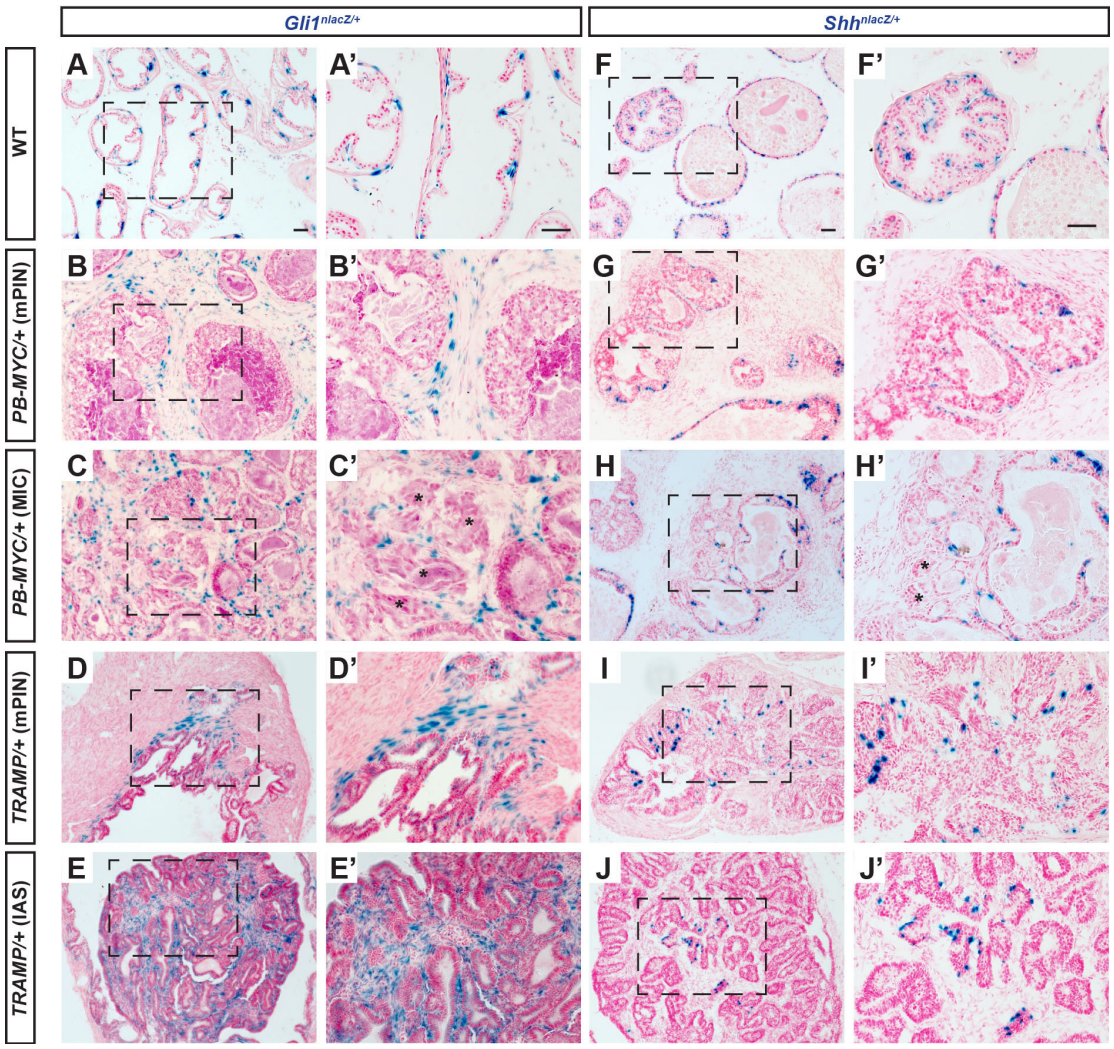

Figure 2.13 *Gli1*^{nlacZ} is expressed in the stromal cells and *Shh*^{nlacZ} is expressed in the basal epithelial cells in both *PB-MYC* and *TRAMP* prostate tumors.

(A-E) X-Gal staining (blue) of DLP sections from tissues of *Gli1*$^{nlacZ/+}$ (A), *Gli1*$^{nlacZ/+}$*;PB-MYC/+* (B, C), and *Gli1*$^{nlacZ/+}$*;TRAMP/+* (D, E) mice. (A'-E') Magnification of areas within dashed lines in A-E. (F-J) X-Gal staining (blue) of DLP sections from tissues of *Shh*$^{nlacZ/+}$ (F), *Shh*$^{nlacZ/+}$*;PB-MYC/+* (G, H), and *Shh*$^{nlacZ/+}$*;TRAMP/+* (I, J) mice. (F'-J') Magnification of areas of dashed lines in F-J. *= Infiltrating nests of tumor cells. Scale bars, 50 μm.

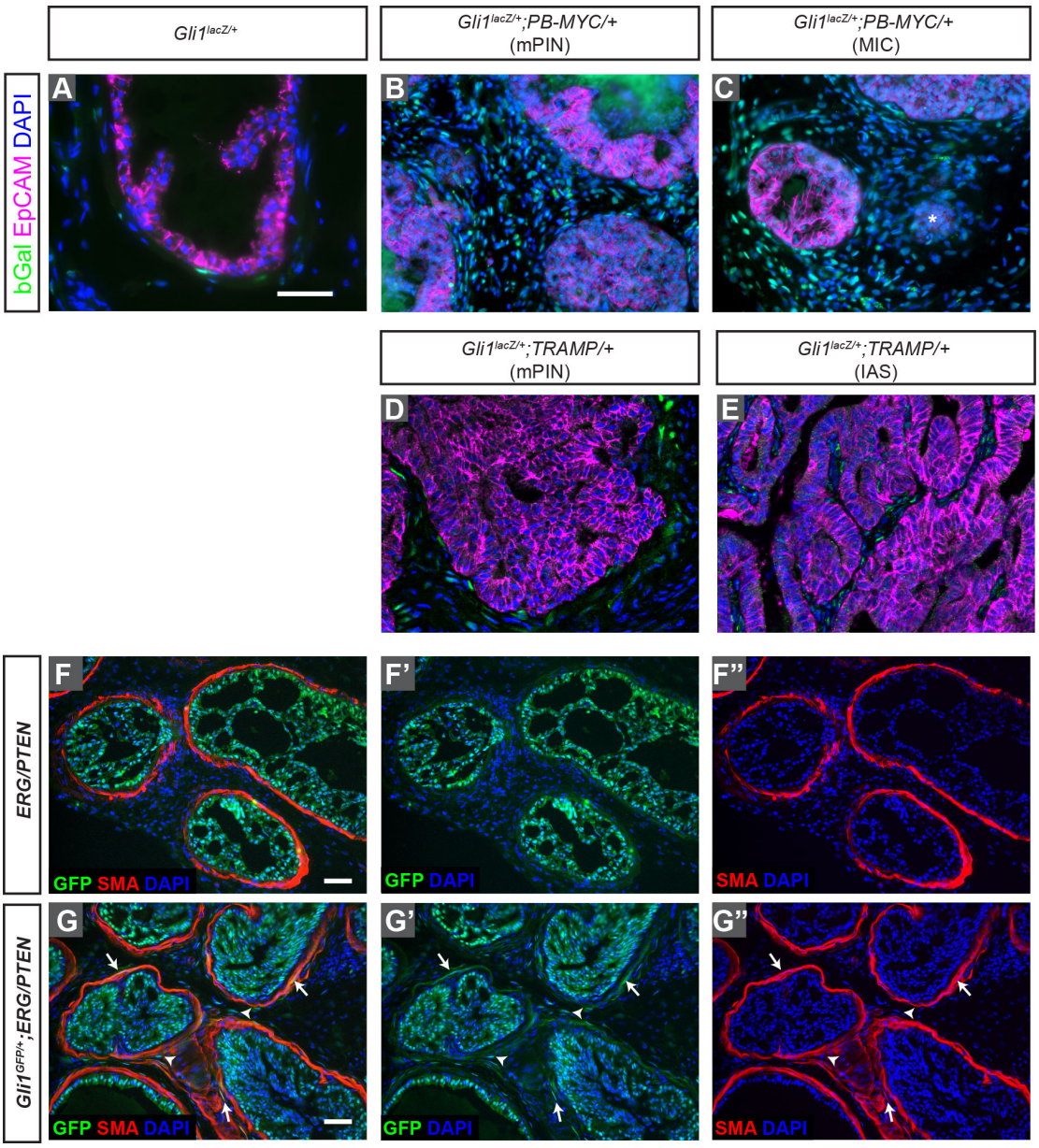

Figure 2.14 Gli1 expresssion is restricted to the stroma in all three PCa models.

(A-E) IF staining for bGAL (green), the enzyme product of lacZ, EpCAM (magenta), and DAPI (blue), showing that *Gli1*+ cells are non-epithelial cells in *PB-MYC* and *TRAMP* tumors. *= Infiltrating nests of tumor cells. (F-F", G-G") IF staining of DLP sections from *ERG/PTEN* (F-F") and *Gli1^{Gfp};ERG/PTEN* (G-G") mice for GFP (green), SMA (red), and DAPI (blue). Arrows indicate GFP+ SMA+ stromal cells, and arrowheads indicate GFP+ SMA- stromal cells. Scale bars, 50 μm.

IHH and DHH contribute to HH signaling to the stroma of mouse PCa

We next tested whether SHH could be the ligand responsible for *Gli1* expression near tumor cells by examining Shh^{nlacZ} (Gonzalez-Reyes et al., 2012) expression in *PB-MYC* and *TRAMP* tumors. As in WT prostate (Peng et al., 2013) (Fig. 2.13F,F'; Fig. 2.15A,F), Shh^{nlacZ} expression was detected in the majority of CK5+ basal cells in *PB-MYC* mPIN lesions, although a few cells were only positive for either CK5 or Shh^{nlacZ} (n=6 mice, 35-42 weeks; Fig. 2.13G,G'; Fig. 2.15B,G). In areas of MICs, Shh^{nlacZ} expressing cells were rare (n=5 mice, 35-42 weeks; Fig. 2.13H,H'), consistent with the loss of cells with a basal phenotype, as indicated by few CK5-expressing cells (Fig. 2.15C,H). Similarly in *TRAMP* mPIN lesions, Shh^{lacZ} expression was detected in CK5+ basal cells, (n=5 mice, 20-32 weeks; Fig. 2.13I,I'). The number of basal cells, however, was greatly diluted out by the increase in CK8+ luminal cells (Fig. 2.15D,I). In IASs, Shh^{lacZ} expression was detected only in the rare CK5+ basal cells that remained (n=5 mice, 20-32 weeks, Fig. 2.13J,J'; Fig. 2.15E,J).

Our results from *PB-MYC* and *TRAMP* PCa models suggest that paracrine HH signaling is retained in tumors, but raises the question of whether SHH is the primary ligand since few Shh^{nlacZ}-expressing cells remained in tumors. One possible explanation for the extensive *Gli1* expression despite little *Shh* in both PCa models is that another HH ligand is expressed. Using *in situ* hybridization (ISH), we first confirmed an increase in cells expressing *Gli1* (Fig. 2.16A-C,A'-C'; Fig. 2.17A-C,A'-C'), and also found that *Shh* expression was maintained in *PB-MYC* tumors (Fig. 2.16E,E'; Fig. 2.17E,E') but almost absent in *TRAMP* tumors (Fig. 2.16F,F'; Fig. 2.17F,F') compared with WT (Fig. 2.16D,D'; Fig.

2.17D,D'). As expected, *Sma* mRNA in stromal cells was markedly decreased in *PB-MYC* tumors (Fig. 2.16N; Fig. S9N) and increased in *TRAMP* tumors (Fig. 2.16O; Fig. 2.17O) compared to WT (Fig. 2.16M; Fig. 2.17M). Interestingly, whereas we detected little expression of *Ihh* or *Dhh* in the epithelium of normal prostates (Fig. 2.16G,G',J,J'), *Ihh* was abundant in *PB-MYC* (Fig. 2.16H,H'; Fig. 2.17H,H') and somewhat increased in *TRAMP* (Fig. 2.16I,I'; Fig. 2.17I,I') tumor epithelium, and *Dhh* was detected in the tumor epithelium of both *PB-MYC* and *TRAMP* models, especially in *TRAMP* mPIN lesions (Fig. 2.16K,K',L,L'; Fig. 2.17K,K',L,L'). qRT-PCR analysis of RNA isolated from whole dorsal prostates of WT, *TRAMP*, and *PB-MYC* tumors confirmed that *Ihh* expression is highest in *PB-MYC* and *Dhh* is highest in *TRAMP* tumors and both are increased compared to normal prostate (Fig. 2.18). In summary, our results have uncovered that *Ihh* and *Dhh* expression are increased in the epithelium of two mouse PCa models as compared to the normal prostates, with *Ihh* increased more in *PB-MYC* than *TRAMP* tumors.

Figure 2.15 *Shh*^{nlacZ} is expressed in the few basal epithelial cells in both *PB-MYC* and *TRAMP* prostate tumors.

(A-E) IF staining of DLP sections from tissues of *Shh*$^{nlacZ/+}$ (A), *Shh*$^{nlacZ/+}$*; PB-MYC/+* (B, C), and *Shh*$^{nlacZ/+}$*; TRAMP/+* (D, E) mice for CK5 (green), a basal epithelial cell marker, bGAL (red), and DAPI (blue), showing that *Shh*+ cells are basal cells. (F-J) IF staining for CK8 (red), a luminal epithelial marker, CK5 (green), and DAPI (blue), showing the proportion of basal cells is greatly decreased in tumor lesions. Note that red staining in E is background. Arrows indicate CK5+/bGAL+ cells; arrowheads indicate CK5+/bGAL- cells. * = infiltrating nests of tumor cells. Scale bars, 50 μm.

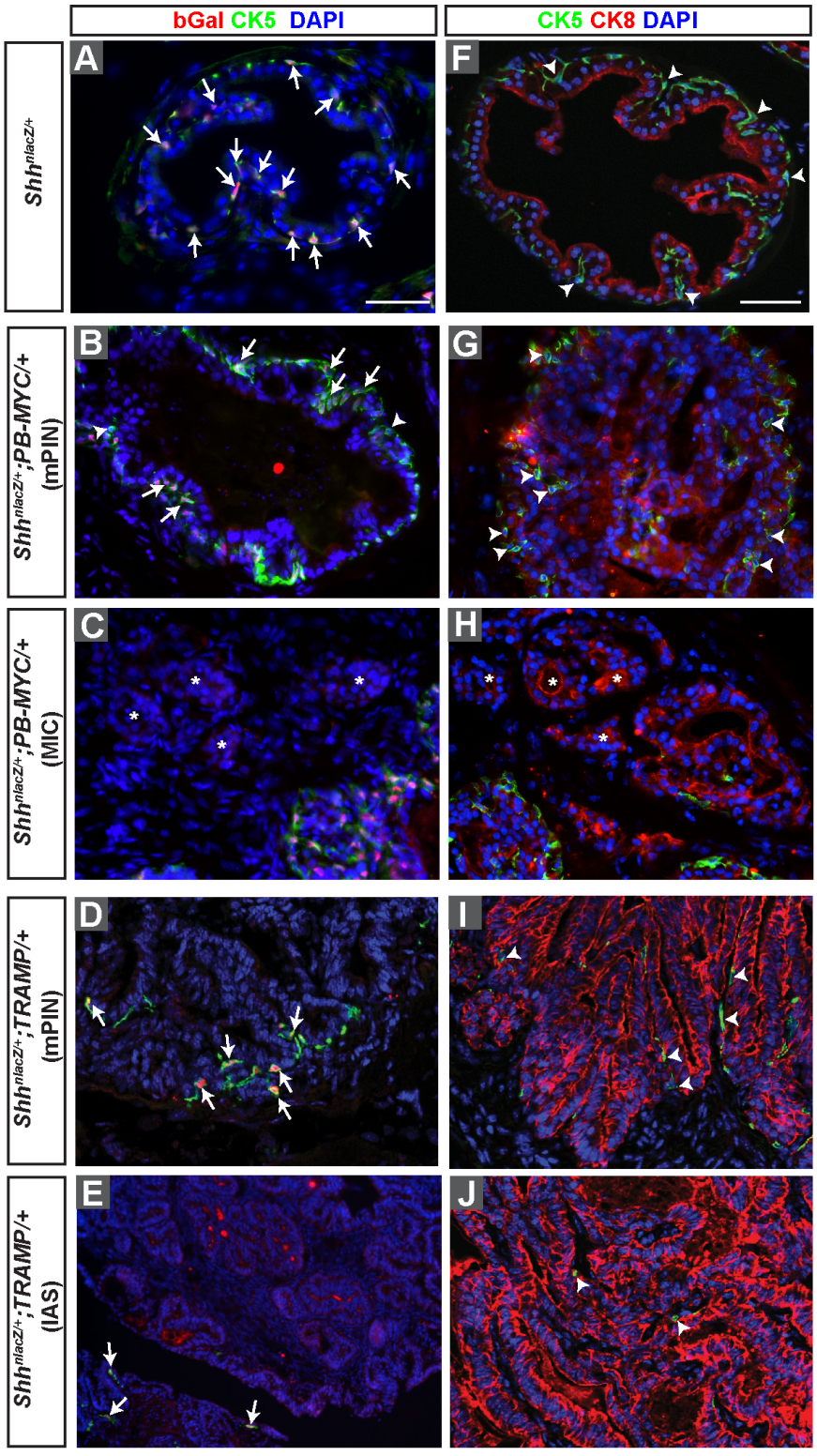
bGal CK5 DAPI
CK5 CK8 DAPI
Shh^nlacZ/+
Shh^nlacZ/+;PB-MYC/+ (mPIN)
Shh^nlacZ/+;PB-MYC/+ (MIC)
Shh^nlacZ/+;TRAMP/+ (mPIN)
Shh^nlacZ/+;TRAMP/+ (IAS)
A
B
C
D
E
F
G
H
I
J

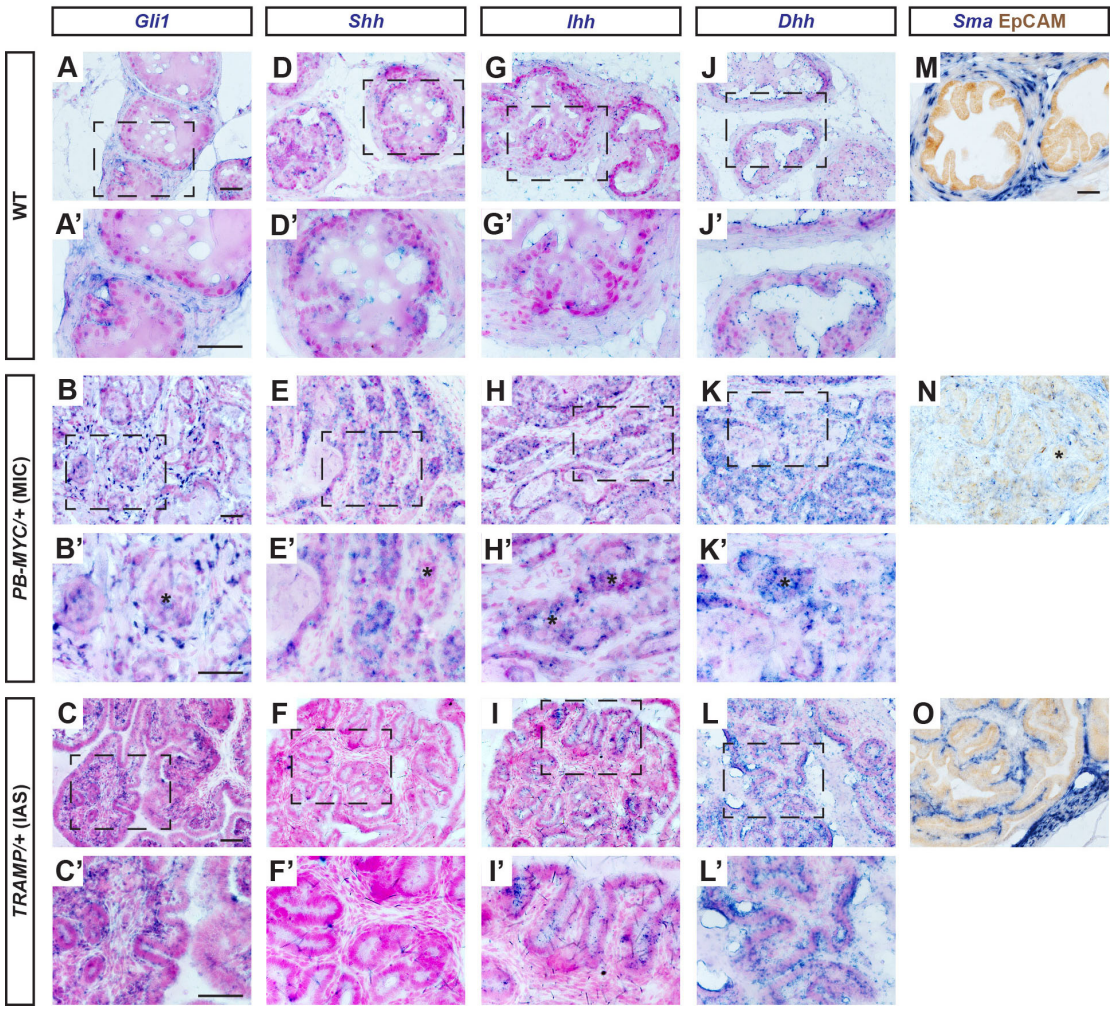

Figure 2.16 *Ihh* and *Dhh* are upregulated in tumor epithelium of *PB-MYC* and *TRAMP* PCa models.

mRNA *in situ* hybridization (blue) of *Gli1* (A-C), *Shh* (D-F), *Ihh* (G-I), *Dhh* (J-L) on DLP sections from WT (A, D, G, J), *PB-MYC/+* MIC lesions (B, E, H, K), and *TRAMP/+* IAS lesions (C, F, I, L), counter-stained with fast red. (A'-L') - Magnifications of areas of dashed lines in A-L. (M-O) *Sma* mRNA *in situ* hybridization (blue) co-stained with IHC of EpCAM. * = infiltrating nests of tumor cells. Scale bars, 50 µm.

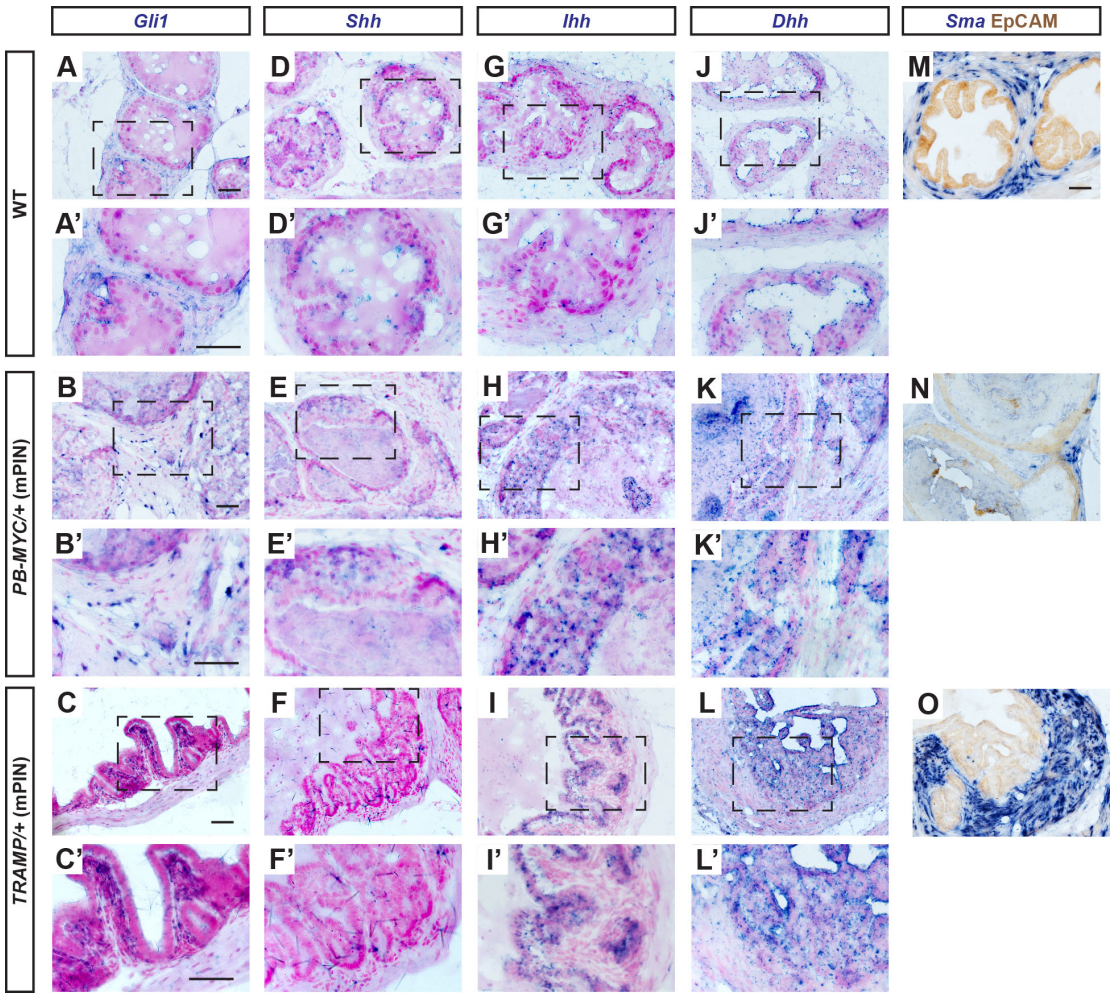

Figure 2.17 *Ihh* and *Dhh* are upregulated in tumor mPIN epithelium of both *PB-MYC* and *TRAMP*.

mRNA *in situ* hybridization (blue) of *Gli1* (A-C), *Shh* (D-F), *Ihh* (G-I), *Dhh* (J-L) on DLP sections from WT (A, D, G, J), *PB-MYC/+* mPIN lesions (B, E, H, K), and *TRAMP/+* mPIN lesions (C, F, I, L), counter-stained with fast red. (A'-L') - Magnifications of areas of dashed lines in A-L. (M-O) *Sma* mRNA *in situ* hybridization (blue) co-stained with immunohistochemistry (IHC) of EpCAM. Scale bars, 50 µm.

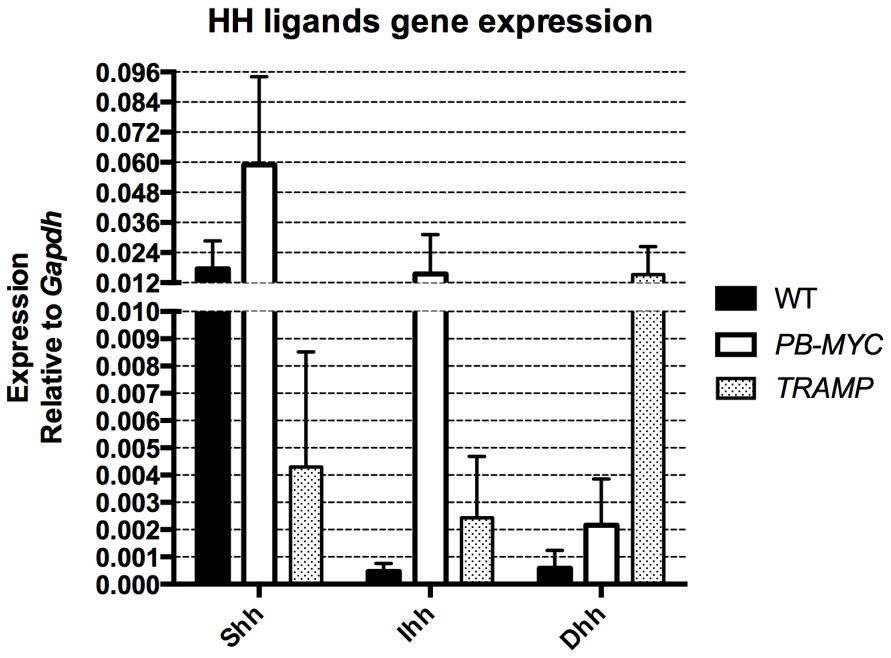

Figure 2.18 *Ihh* and *Dhh* are upregulated in *PB-MYC* and *TRAMP* tumors compared to normal prostate.

Gene expression levels of *Shh*, *Ihh*, and *Dhh* in WT, *PB-MYC*, and *TRAMP* prostates measured by qRT-PCR.

HH signaling in human PCa correlates with stromal content and is driven mainly by *DHH*

Our expression studies using mouse tumor sections raise the question of whether the genes encoding any of the HH ligands and *GLI1* are increased in a subset of human PCa. Analysis of the TCGA dataset (n=330) of primary PCa samples (Abeshouse et al., 2015) and the MSKCC Prostate Oncogenome Project (n=29 normal, 131 primary tumors, and 19 metastases) (Taylor et al., 2010) revealed that the overall expression of *IHH*, but not *SHH* or *DHH* is significantly increased in tumor samples compared to normal prostate samples (Fig. 2.19A). However, there were no significant differences in the expression of HH genes between tumor samples with various Gleason scores (Fig. 2.19B) or between primary and metastasis tumors (Fig. 2.19C). *GLI1* expression was the same in normal prostate and all types of tumor samples (Fig. 2.19), which could indicate an actual increase in stromal expression since the proportion of stromal cells is reduced. Indeed, there was a positive correlation between tumors with high expression of stromal markers and *GLI1* (Pearson coefficient = 0.483 or 0.379 or 0.595 for *ACTA2* or *CNN1* or *VIM* with *GLI1*; Table 2.1B). There was also a correlation between *DHH* expression, and to a lesser extent *IHH* or *SHH*, with *GLI1* expression levels (Pearson coefficient = 0.309 or 0.198 or 0.181 for *DHH* or *IHH* or *SHH* with *GLI1*; Table 2.1B). There was also a strong correlation between *DHH* and *ACTA* or *VIM* (Pearson coefficient = 0.422 or 0.560 for *ACTA2* or *VIM* with *DHH*). Curiously, there were poor correlations between the levels of *DHH* and luminal markers (Pearson coefficient = 0.025 or -0.054 for *KRT8* or *KRT18* with *DHH*) or basal markers (Pearson coefficient = 0.001 or -0.017 for *KRT5* or *TP63* with *DHH*) in tumor samples (Table 2.1B), indicating that *DHH*

expression is induced in a tumor context-dependent manner. Thus, mRNA expression data from human primary PCa samples indicate that the level of HH signaling (*GLI1* expression) correlates with the proportion of stromal cells in a tumor, and *IHH* is increased more than the other HH ligands in tumors compared to normal prostate.

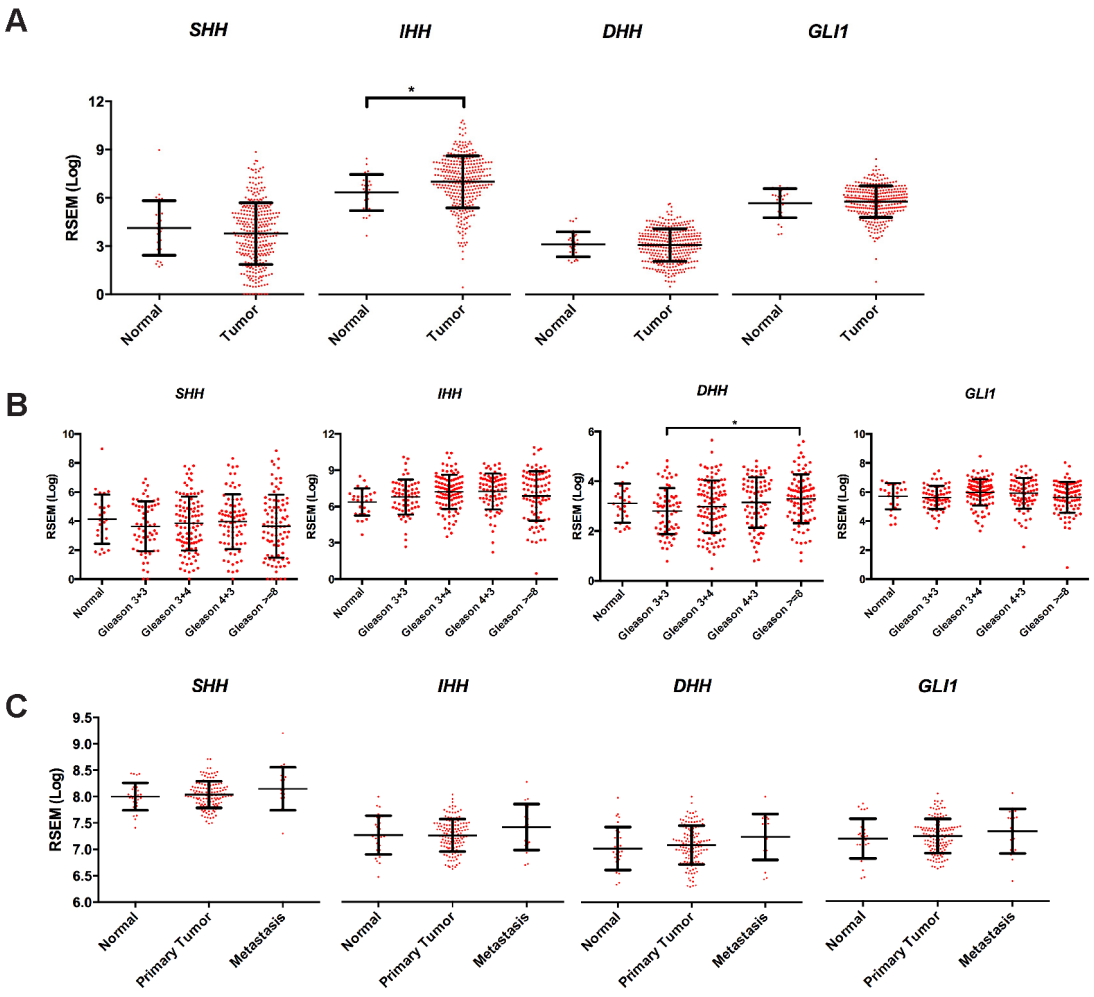

Figure 2.19 *IHH* is increased in the TCGA human primary PCa samples.

(A, B) The mRNA expressions of HH pathway genes in human PCa from TCGA RNA-seq data with 330 primary PCa samples (Tumor) and 27 normal controls (Normal) (A), or PCa samples categorized by Gleason scores (Gleason 3+3, 3+4, 4+3, and >=8) (B). (C) The mRNA expressions of HH pathway genes in human PCa from the MSKCC Prostate Oncogenome Project with 131 primary PCa samples (Primary Tumor), 19 Metastasis samples (Metastasis), and 27 normal controls (Normal). *P<0.05. Data are presented as mean ± s.d. Each data point represents one sample.

Gene expression profile of *Gli1*-expressing stromal cells is altered in *PB-MYC* tumors

In order to analyze the expression profile of mouse PCa stromal cells, we used the *Gli1*$^{GFP/+}$ knock-in reporter line (Brownell et al., 2011) to isolate the subset of stromal cells undergoing HH signaling to compare the transcriptomes between *PB-MYC* PCa and normal prostate (~45 weeks of age) using RNA-seq. Unsupervised hierarchical clustering of all genes with significant differences in gene expression showed a clear separation between the two populations (Fig. 2.20A). Analysis of variance correcting for multiple hypothesis testing identified 243 genes with significantly different expression ($p<0.05$ and FDR<0.05) between WT and *PB-MYC* cells expressing *Gli1*^{GFP} at a level of $\geqslant$ 2 fold (281 genes $\geqslant$ 1.5 fold) (Table 2.3A), with the majority of the genes expressed more strongly in WT cells (Fig. 2.20A). Interestingly, *Acta2* and *Cnn1* were decreased by 21 and 12 fold, respectively, in stromal *Gli1*-expressing tumor cells compared to WT, and VIM was not significantly altered (Table 2.3B). The decrease in SM gene expression likely reflects the decrease in the proportion of SMCs in *PB-MYC* tumors. Consistent with our conclusions based on RNA *in situ* analysis, the three *Hh* genes were not expressed in stromal *Gli1*-expressing cells (Table 2.3B). Pathway analysis ($p<0.1$ and FDR<0.1) identified 6 pathway differences (Fig. S14B), with a top pathway being focal adhesion that was reduced in *PB-MYC Gli1*^{GFP}-expressing cells (Fig. 2.20B,C), consistent with the greater dispersion of stromal cells in tumors.

A

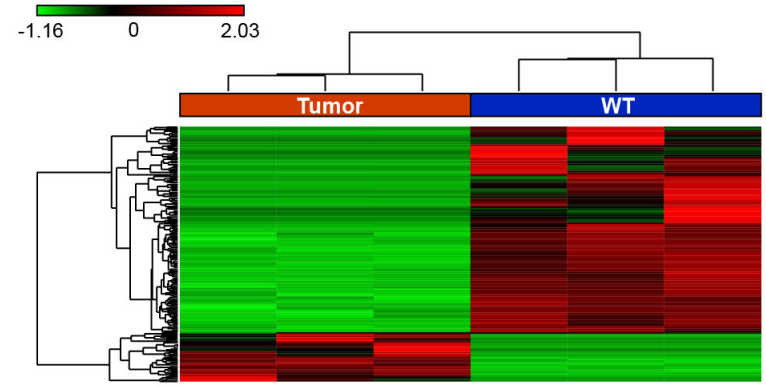

B

#	Pathway	Gene Count	%	P Value	Fold Enrichment
1	Focal adhesion	11	2.86	0.01	2.75
2	Cell adhesion molecules (CAMs)	8	2.08	0.03	2.57
3	Arrhythmogenic right ventricular cardiomyopathy (ARVC)	6	1.56	0.02	3.96
4	ECM-receptor interaction	6	1.56	0.02	3.58
5	Hypertrophic cardiomyopathy (HCM)	6	1.56	0.03	3.53
6	Dilated cardiomyopathy	6	1.56	0.04	3.23

C

#	Gene Symbol	Gene Name	Fold Change	P Value	FDR
1	Col6a1	Collagen, type VI, alpha 1	-2.12	0.00025	0.027
2	Ppp1ca	Protein phosphatase 1, catalytic subunit, alpha isoform	-2.27	0.00156	0.068
3	Ccnd2	Cyclin D2	-2.45	0.00054	0.041
4	Ilk	Integrin linked kinase	-2.45	0.00202	0.076
5	Actg1	Actin, gamma, cytoplasmic 1	-2.80	0.00012	0.019
6	Itgb4	Integrin beta 4	-3.39	0.00143	0.065
7	Ccnd1	Cyclin D1	-4.03	0.00067	0.045
8	Cav1	Caveolin 1, caveolin protein	-7.38	0.00004	0.009
9	Comp	Cartilage oligomeric matrix protein	-7.80	0.00017	0.023
10	Kdr	Kinase insert domain protein receptor	-8.84	0.00002	0.005
11	Itga8	Integrin alpha 8	-29948.47	0.00012	0.019

Figure 2.20 Altered gene expression profile of *Gli1*-expressing stromal cells in *PB-MYC* tumors.

(A) Analysis of Variance correcting for multiple hypothesis testing identified 288 genes with significantly different expression between WT and *PB-MYC* *Gli1*^{GFP}-expressing cells (q<0.05). (B) Pathway analysis (q<0.1) identified 6 differentially represented ($\geqslant$2 fold). %, percentage of genes in pathway that are differentially expressed; FDR, false discovery rate. (C) Genes in the focal adhesion pathway that are differentially detected (p<0.05, q<0.1) between WT and *PB-MYC* *Gli1*^{GFP}-expressing cells.

Table 2.3 List of differentially expressed genes between WT and *PB-MYC Gli1^{GFP}*-expressing cells.

(A) List of genes with significant differential expressions (p<0.05, FDR<0.05, fold change >1.5)
See Appendix Table 2.3A.

(B) Stromal marker genes and HH pathway genes

#	Gene Symbol	P-value (Tumor vs. WT)	FDR step up (Tumor vs. WT)	Fold change (Tumor vs. WT)
1	*Cnn1*	0.0121	0.1631	-11.92
2	*Acta2*	0.0072	0.1339	-21.16
3	*Vim*	0.4523	0.6558	-1.17
4	*Shh*	0.1183	0.3998	-3604.97
5	*Ihh*	0.7145	0.8515	-5.99
6	*Dhh*	0.4274	0.6368	-15.16
7	*Gli1*	0.2558	0.5693	1.28

Enhanced HH signaling in the *PB-MYC* stroma impedes PCa progression and maintains the SM

Given the extensive reduction of SM and presence of local MIC in advanced *PB-MYC* tumors, and reduction in SM gene expression in more advanced human PCa samples, we reasoned that the damaged SM layers could facilitate the invasion of prostate tumor cells, since they must cross the SM layer surrounding the ductal glands. Furthermore, given the correlation between high *DHH* and *GLI1* expression and higher stromal content of human PCa samples, we hypothesized that increasing stromal HH signaling would decrease tumor progression by maintaining or increased SM. To test this hypothesis, we used Cre/loxP to genetically increase HH signaling in the stroma of *PB-MYC* tumors by administering tamoxifen to *Gli1*$^{CreER/+}$;*R26*$^{LSL\text{-}SmoM2\text{-}YFP/+}$;*PB-MYC/+* (*SmoM2;PB-MYC*) and *R26*$^{LSL\text{-}SmoM2\text{-}YFP/+}$;*PB-MYC/+* (*PB-MYC*) littermates at 4 weeks to induce expression of a constitutively active SMO (SmoM2) (Mao et al., 2006) in a subset of stromal cells (Fig. 2.21A). The severity of tumors was assessed at 44 to 46 weeks in a blinded fashion based on tissue pathology. Four categories of mPIN lesions and MIC were graded according to the degree of architectural and cytologic abnormalities and the extent of ducts affected. Low-grade mPIN (LGPIN) was defined as having 1 to 2 layers of cells and mild nuclear atypia (Fig. 2.21B,B'). High grade mPIN lesions were divided into three grades: HGPIN1 lesions were focal and had increased nuclear atypia with 2 or more layers of cells often in papillary, tufting, or cribriform arrangements (Fig. 2.21C,C'). HGPIN2 lesions were more extensive and had obvious nuclear atypia and the cells filled or almost filled the ductal lumens in papillary or cribriform patterns (Fig. 2.21D,D'). HGPIN3 lesions were the most extensive and had more severe atypia, filled the ductal

lumens, and some cells bulged into the surrounding stroma but without the clear invasion seen in MIC (Fig. 2.21E,E'). Strikingly, mice with active HH signaling in the stroma (*SmoM2;PB-MYC*) showed a significant decrease in tumor grade compared with *PB-MYC* littermates (Fig. 2.21G) (Mann-Whitney U test: U=53, n_1=n_2=14, p=0.0096 two-tailed). Thus increased HH signaling in *PB-MYC* stroma can suppress progression of PCa.

Since MIC is less likely to occur in *PB-MYC* tumors with increased stromal HH signaling (Fig. 2.13F), we then asked whether the SMC content of tumors was altered by HH activation. The SMA+ area was quantified in *SmoM2;PB-MYC* mice and *PB-MYC* littermates (N=6 mice, 44-45 weeks), as well as their non-tumor littermate controls, $Gli1^{CreER/+};R26^{LSL\text{-}SmoM2\text{-}YFP/+}$ (SmoM2) (N=5 mice, 45 weeks) and $R26^{LSL\text{-}SmoM2\text{-}YFP/+}$ (WT) mice (N=3 mice, 45 weeks). Whereas *PB-MYC* tumors had the expected large decrease in SMCs and gaps in the SM layer compared with normal prostates (Fig. 2.22A,A',C,C'), *PB-MYC* tumors with stromal SmoM2-expression had strikingly more normal SM layers (Fig. 2.22C-D,C'-D'). Quantification of the SMA+ area with respect to total cell number (estimated from the number of DAPI+ nuclei) showed an increase (p=0.049) in *SmoM2;PB-MYC* mice compared with *PB-MYC* mice (Fig. 2.22E), although SMA+ area relative to stromal cell number (EpCAM-) did not show a significant increase (Fig. 2.22F). This result could in part be due to a contribution of immune cells to the stromal cell count. The increase of SM in *SmoM2;PB-MYC* tumors is unlikely due to enhanced HH signaling via *SmoM2* expression as the SMCs are not specifically enriched with SmoM2-YFP-positive cells, and both SMA+ and SMA- stromal cells expressed SmoM2-YFP (Fig. 2.23). These results suggest that HH signaling maintains the SM layers in

PCa and has an inhibitory effect on invasive cancer, possibly via maintaining the SM layers as barriers to prevent tumor epithelial cells from invading into the stroma.

Figure 2.21 Ectopic HH signaling in the stroma reduces *PB-MYC* prostate tumor progression.

(A-E) H&E staining of DLP sections from tissues of either *SmoM2;PB-MYC* (*Gli1*$^{CreER/+}$;*R26*$^{LSL\text{-}SmoM2\text{-}YFP/+}$;*PB-MYC/+*) or *PB-MYC* (*R26*$^{LSL\text{-}SmoM2\text{-}YFP/+}$;*PB-MYC/+*) mice, representing lesions of different severity; low-grade mPIN (LGPIN or LG) (A), high-grade 1 mPIN (HGPIN grade 1 or HG 1) (B), high-grade 2 mPIN (HGPIN grade 2 or HG 2) (C), high-grade 3 mPIN (HGPIN grade 3 or HG 3) (D), and MIC (E). (A'-E') Magnification of areas of dashed lines in A-E. Arrows= micro-invasive carcinoma. Scale bars, 50 μm. (F) Dot plot of each mouse with a certain grade of tumor lesion, showing inverse correlation between tumor severity and HH signaling. Each dot represents one mouse. ** P<0.01; N=14 mice for each of *SmoM2;PB-MYC* and *PB-MYC* groups.

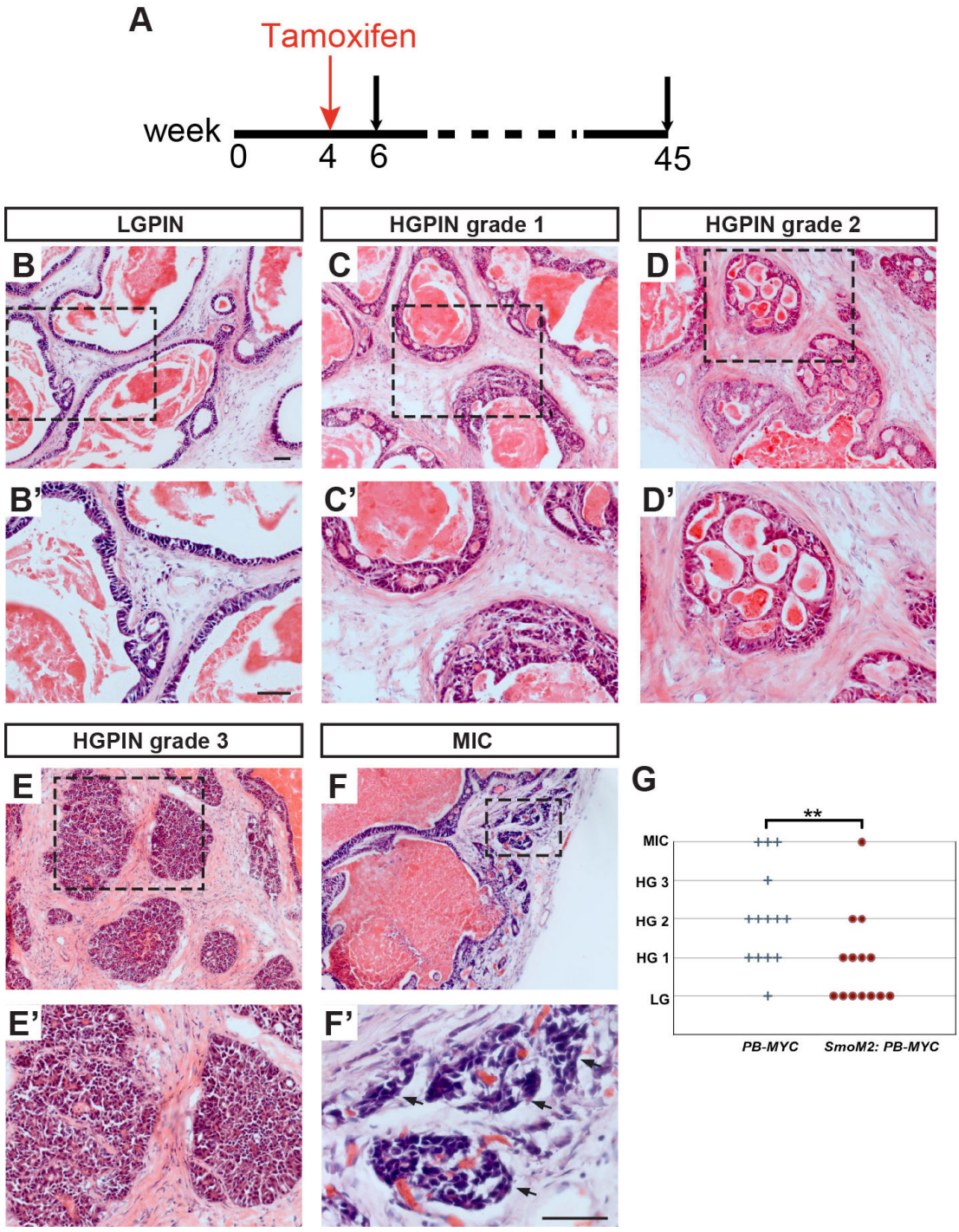
A
Tamoxifen
week
0
4
6
45
LGPIN
HGPIN grade 1
HGPIN grade 2
B
C
D
B'
C'
D'
HGPIN grade 3
MIC
E
F
G
E'
F'
**
MIC
HG 3
HG 2
HG 1
LG
PB-MYC
SmoM2: PB-MYC

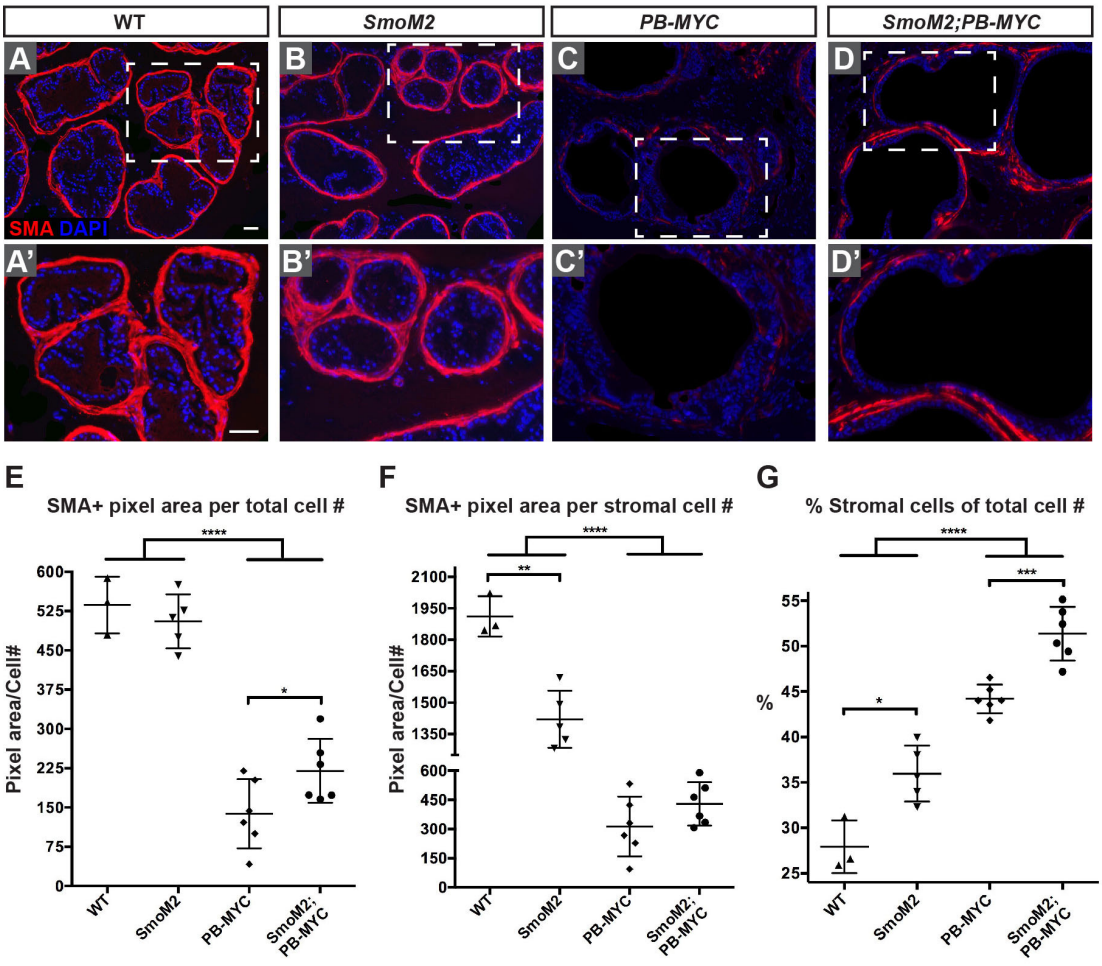

Figure 2.22 Enhanced HH signaling in the stroma of *PB-MYC* prostates increases stromal cells including SMCs.

(A-D) IF staining of DLP sections from WT (*R26*$^{LSL\text{-}SmoM2\text{-}YFP/+}$) (A), SmoM2 (*Gli1*$^{CreER/+}$; *R26*$^{LSL\text{-}SmoM2\text{-}YFP/+}$) (B), *PB-MYC* (*R26*$^{LSL\text{-}SmoM2\text{-}YFP/+}$; *PB-MYC*/+) (C), and *SmoM2;PB-MYC* (*Gli1*$^{CreER/+}$; *R26*$^{LSL\text{-}SmoM2\text{-}YFP/+}$; *PB-MYC*/+) (D) mice for SMA (red) and DAPI (blue). Scale bars, 50 μm. (E-F) Quantification of the SMA+ area per total cell number (E) or per stromal cell number (F). (G) The percentage of stromal cells within total cells. *P<0.05; **P<0.01; ***P<0.001; ****P<0.0001. Data are presented as mean ± s.d. Each data point represents the average of 4 sections from one mouse.

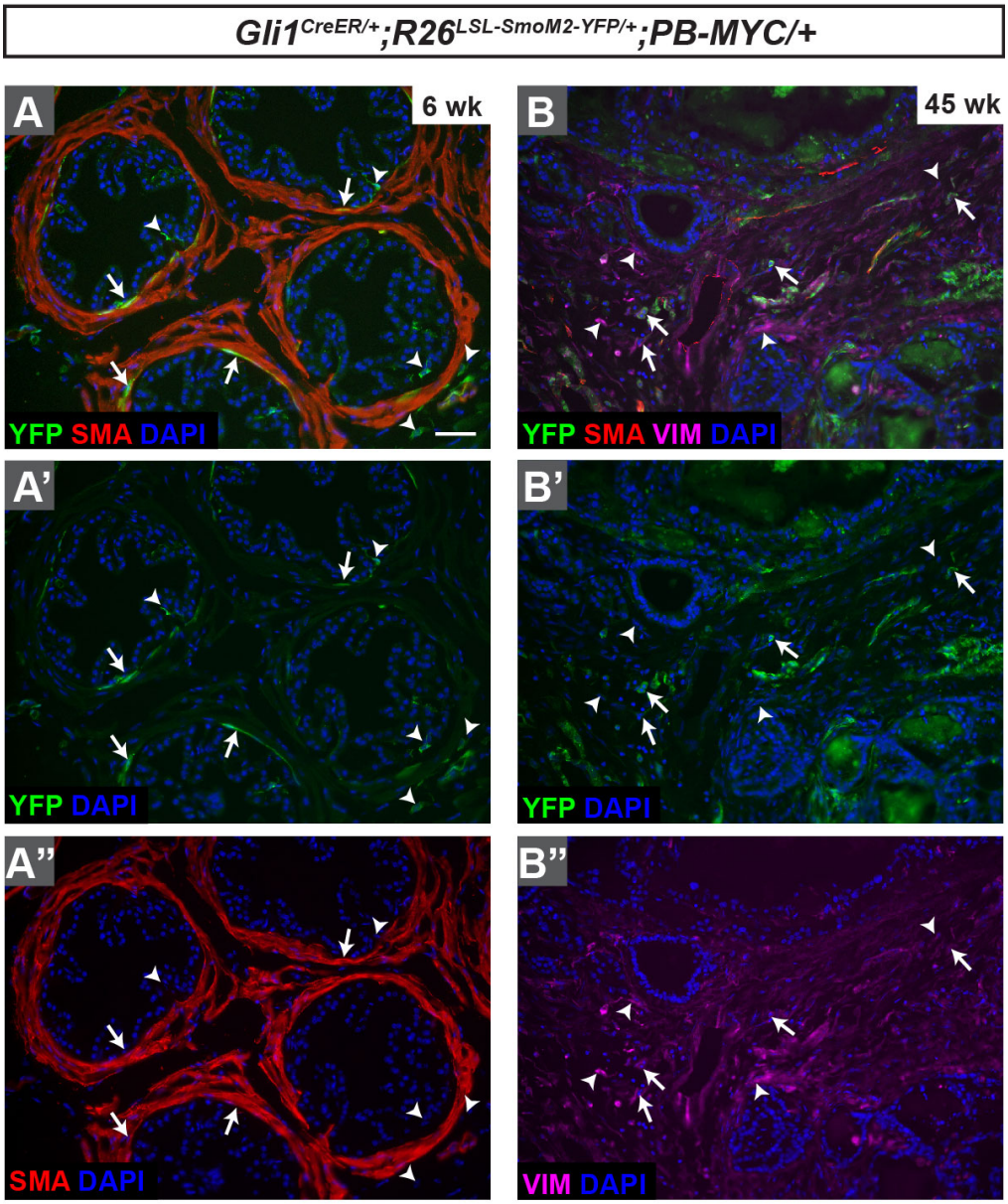

Figure 2.23 *SmoM2* is expressed in both SMA+ and SMA- stromal cells of *PB-MYC* prostate tumors.

IF staining of DLP sections from tissues of 6-week old (A-A'') and 45-week old (B-B'') *SmoM2;PB-MYC* (*Gli1*$^{CreER/+}$; *R26*$^{LSL-SmoM2-YFP/+}$; *PB-MYC*/+) mice for YFP (green), DAPI (blue), and SMA (red) or VIM (magenta). Arrows indicate YFP+ VIM+ (A-A'') or YFP+ SMA+ (B-B'') stromal cells. Arrowheads indicate YFP+ SMA- (A-A'') or YFP- VIM+ (B-B'') stromal cells. Scale bar, 50 μm.

Enhanced HH signaling in the stroma of *PB-MYC* tumors increases the stromal cell number

Although *PB-MYC* tumors have a prominent reduction of SMCs, the proportion of all cells (epithelial + stromal) that were stromal (EpCAM-) was significantly increased in both *SmoM2;PB-MYC* ($p<0.0001$) and *PB-MYC* ($p<0.0001$) prostates compared to non-tumor controls, and was significantly higher in *SmoM2;PB-MYC* than *PB-MYC* tumors ($p=0.0004$) (Fig. 2.22G). There was also a small increase in the proportion of stromal cells in *SmoM2* non-tumor prostates compared with WT ($p=0.01$) (Fig. 2.22G). These results indicate that the major effect of increasing HH signaling in the stroma of *PB-MYC* is to increase the proportion of stromal cells.

The observed increase in stromal cells in *SmoM2;PB-MYC* prostates could be due to an increase in proliferation (1 hr pulse EdU) or decrease in cell death induced by HH activation. In *SmoM2* and WT prostates, few EdU+ cells were detected (Fig. 2.24A,B,E,F), whereas *SmoM2;PB-MYC* and *PB-MYC* tumors had the expected significantly higher level of cell proliferation ($p=0.001$ and $p=0.0007$, respectively). Curiously, the percentage of EdU+ stromal cells was significantly reduced ($p=0.018$) in the stroma of *SmoM2;PB-MYC* mice compared to *PB-MYC* in late stage tumors (Fig. 2.24C,D,E), and in epithelial cells was slightly but not significantly ($p=0.37$) lower (Fig. 2.24F). TUNEL labeling of dying cells did not reveal an obvious difference between *SmoM2;PB-MYC* and *PB-MYC* tumors (Fig. 2.24G,H). Thus, the main cellular changes that lead to the increase in PCa stroma likely occur at an earlier stage in tumor progression, or represent mainly that stromal cells are maintained when HH signaling is increased.

Figure 2.24 Enhanced stromal HH signaling in *PB-MYC* prostates does not increase stromal cell proliferation in late stage tumors.

(A-D) IF staining of DLP sections from WT (A), SmoM2 (B), *PB-MYC* (C), and *SmoM2;PB-MYC* (D) mice for EdU (green), SMA (red), and DAPI (blue). Scale bar, 50 μm. Arrows indicate EdU+ epithelial cells; arrowheads indicate EdU+ stromal cells. (E-F) Quantification of the percentage of EdU+ stromal cells (E) or EdU+ epithelial cells (F). *P<0.05; **P<0.01; ***P<0.001. (G-H) TUNEL staining (green) with SMA (red) and DAPI (blue) of DLP sections from *PB-MYC* (G) and *SmoM2;PB-MYC* (H) mice. Arrows indicate TUNEL+ epithelial cells; arrowheads indicate TUNEL+ stromal cells.

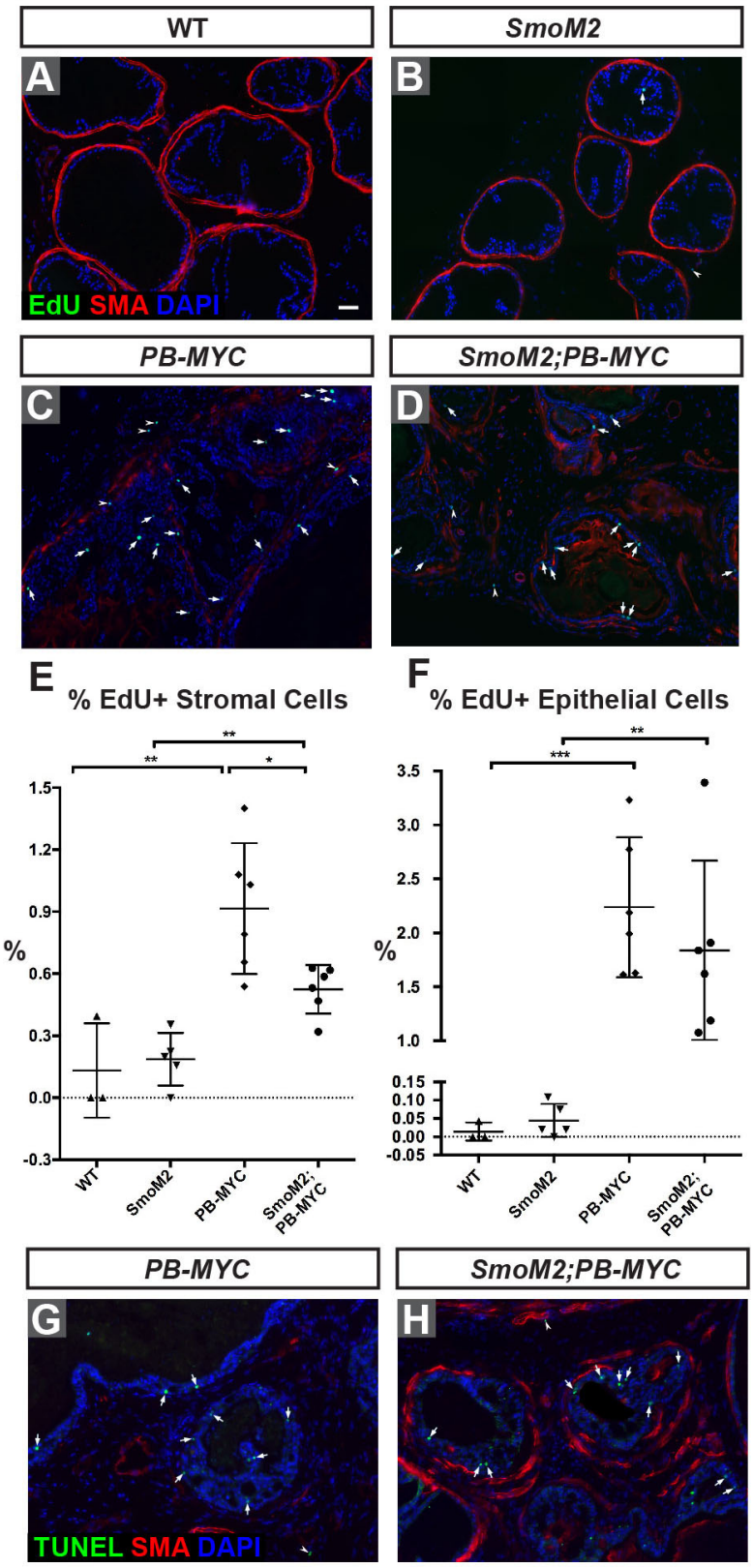
WT
SmoM2
A
B
EdU SMA DAPI
PB-MYC
SmoM2;PB-MYC
C
D
E
% EdU+ Stromal Cells
F
% EdU+ Epithelial Cells
%
WT
SmoM2
PB-MYC
SmoM2; PB-MYC
PB-MYC
SmoM2;PB-MYC
G
H
TUNEL SMA DAPI

DISCUSSION

In three mouse models of PCa, including one with highly recurrent mutations in human PCa (*ERG/PTEN*), we found distinct contributions of SM-like and fibroblast-like cells to the stroma, yet HH signaling (*Gli1*^{nlacZ} expression) was restricted to stromal cells, especially near the tumor epithelium. Whereas *TRAMP* tumors had an increase in SMCs and little change in interductal fibroblasts, *PB-MYC* and to a lesser extent *ERG/PTEN* had a decrease in SMCs and an accompanying increase in fibroblast-like stromal cells between the ducts. RNA-seq analysis of *Gli1*^{GFP}-labeled cells of *PB-MYC* and normal prostate similarly revealed a major decrease in SM genes, and the fibroblast gene *Vim* was not altered. Based on the Human Protein Atlas and RNA data analysis, we confirmed that human PCa tumors have a dramatic disruption of the SM layers and a clear decrease in the mature SM marker Calponin (CNN1) in advanced tumors, consistent with a previous report (Tuxhorn et al., 2002). ACTA2 (SMA) staining revealed the SM layers were disrupted and the proportion of cells were decreased in most advanced tumor samples, whereas VIM was maintained in the remaining stromal cells. Analysis of TCGA, the largest RNA-seq dataset of primary PCa samples (Abeshouse et al., 2015), revealed a decrease in *ACTA2* and *CNN1* but not *VIM* expression in more advanced tumors (higher Gleason score), suggesting the proportion of SMCs in human tumors, or at least the expression levels of the cell type specific genes are decreased. In a separate RNA expression data set (Taylor et al., 2010) *ACTA2* and *CNN1* but not *VIM* expression were found to be significantly lower in metastatic samples compared to primary tumors. In addition, we found correlations between higher luminal or lower basal cell gene expression and lower SM gene expression. Our study thus demonstrates that PCa in *PB-*

MYC mice nicely models the decrease in SM layers seen in more advanced human PCa.

Using GIFM, we traced the fate of SMA-expressing cells *in vivo* during mouse tumor progression and found that the labeled cells are largely lost in *PB-MYC* tumors without changing fate and giving rise to cancer reactive stroma. In *TRAMP* tumors, in contrast, labeled SMCs not only expand the SM layers, but also contribute to cancer stromal cells, specifically in IAS and not between ducts. Thus, in *TRAMP* tumors, some labeled SMCs change their fate to fibroblasts and/or myofibroblast-like cells and migrate into IASs. However, SMCs in *TRAMP* tumors, as in *PB-MYC* tumors, do not contribute to interductal stromal cells. We propose that the fate of SMC is likely determined by the molecular character of the tumor epithelial cells. It will be interesting to determine if the cell-of-origin of interductal stroma is the stem/progenitor cell that a fate mapping study indicates is restricted to the interductal fibroblast lineage (Peng et al., 2013). Furthermore, if each stromal lineage has a distinct expression signature, it should be possible to predict the cell of origin of reactive stroma in human PCa samples.

In both *TRAMP* and *PB-MYC* models of PCa, we found that the proportion of epithelial cells expressing Shh^{nlacZ} decreases greatly during tumor progression, whereas the two alternate ligands, *Ihh* and *Dhh* are prominently expressed by tumor cells but not normal prostate luminal cells (Fig. 2.16; Fig. 2.14). Consistent with this result, *Shh* expression is decreased and *Ihh* increased in the *LADY* prostate tumor model compared to normal prostate based on qRT-PCR of whole tumor tissue (Gipp et al., 2007; Kasper et al., 1998). Analysis of

TCGA RNA-seq data revealed that *IHH* is increased in human PCa compared to normal prostate (Fig. 2.6). Furthermore, the level of *DHH*, and to a lesser extent *IHH*, is positively correlated with *GLI1* (HH signaling), as well as the level of stromal gene expression (Table 2.1B). Thus, HH signaling appears to be a predictor of the amount of stroma in a tumor. Finally, our examination of gene expression on mouse sections revealed a paracrine mode of HH signaling from tumor cells to stroma.

A majority of the studies on the role of HH signaling using PCa cell lines have suggested that HH pathway blockade via cyclopamine treatment suppresses tumor growth. Using an *in vivo* genetic mouse model that reflects the changes in stromal content of human PCa, however, we found that aberrant activation of HH signaling in the *Gli1*-expressing subset of stromal cells in *PB-MYC* tumors results in decreased tumor progression, revealing that tumor stroma can restrain PCa progression. We propose that the partially restored SM layers act as a barrier to prevent epithelial cells from invading into the stroma (Fig. 2.25). It is also possible that SMCs secrete factors, such as pro-differentiation proteins, that restrain tumor progression (Fig. 2.25). Together with several recent studies showing that inhibition of HH signaling in the stroma of pancreas and bladder cancers decreases survival (Lee et al., 2014; Rhim et al., 2014; Shin et al., 2014), our findings offer an explanation for the unsuccessful clinical trials using small-molecule HH antagonists for PCa. Further research in genetic models that represent later stages of human PCa will provide additional evidence for the value of altering HH function for PCa patients.

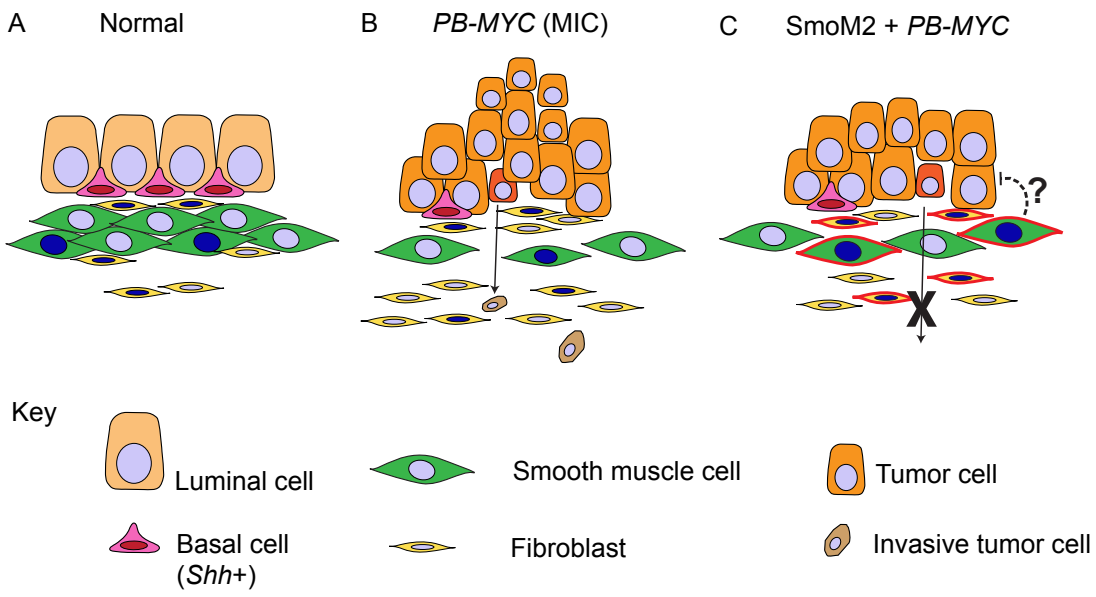

Figure 2.25 Schematic diagram of the proposed model mechanism for enhanced HH signaling in *PB-MYC* stroma to restrain prostate tumor progression.

(A) In the normal prostate, the epithelium has a single layer of luminal cells and basal cells, and the surrounding stroma is composed of smooth muscle cells and fibroblasts. *Shh* is expressed in basal epithelial cells, and *Gli1* expression (indicated by dark blue color of cell nuclei) is restricted in a subset of each subtype of stromal cells.
(B) In the *PB-MYC* tumor with micro-invasive carcinoma (MIC) lesions, tumor epithelial cells hyper-proliferate and form multi-layer tumor epithelium. The amount of smooth muscle is largely reduced, and the fibroblast-like subtypes increase in number. Some invasive tumor cells invade into the surrounding stroma (indicated by arrow) and form the MIC lesions.
(C) When HH signaling in the stroma is enhanced through over-expression of *SmoM2* (indicated by red outline of cell membrane) in the *Gli1*-expressing subset of the stromal cells in the *PB-MYC* tumor, the smooth muscle layer is partially restored, which may act as a barrier to prevent tumor epithelial cells from invading into the stroma (indicated by the arrow and red X) and forming MIC lesions. An alternative possible mechanism is that smooth muscle cells can secret certain factors to inhibit the tumor epithelial cell expansion or dedifferentiation that can restrain tumor progression (indicated by the dashed line).

MATERIALS AND METHODS

Mice

The following mouse lines were used: *TRAMP/+* (Greenberg et al., 1995), *PB-MYC/+* (Ellwood-Yen et al., 2003), $Shh^{nlacZ/+}$ (Gonzalez-Reyes et al., 2012), $Gli1^{nlacZ/+}$ (Bai et al., 2002), $Gli1^{GFP/+}$ (Brownell et al., 2011), $Gli1^{CreER/+}$ (Ahn and Joyner, 2005), *Sma-CreER/+* (Wendling et al., 2009), $Pten^{flox/flox}$ (Trotman et al., 2003), $R26^{LSL\text{-}ERG\text{-}GFP/\ LSL\text{-}ERG\text{-}GFP}$ (Chen et al., 2013), *Rosa26* (*R26*) reporter mice (Madisen et al., 2010; Soriano, 1999; Srinivas et al., 2001), and $Tmprss2^{CreER\text{-}GFP/+}$ was generated by knock-in of a $CreER^{T2}$*-IRES-EGFP* cassette with a splice acceptor into the first intron of the *Tmprss2* gene, after exon 1 which is non-coding (Gao et. al. in press). Tamoxifen (Sigma, T5648) was dissolved in corn oil and administered by oral gavage (250 μg g^{-1}). Mouse husbandry and all experiments were performed in accordance with MSKCC IACUC-approved protocols.

Tissue Processing

Animals were anesthetized and transcardially perfused with PBS followed by chilled 4% paraformaldehyde. Prostates were harvested and postfixed for 15-20 min (normal prostate) or 2–3 h (tumor) or overnight (RNA *in situ* and some IHC), and cryoprotected in 30% sucrose before freezing in Cryo-OCT. Frozen prostates were sectioned at either 8 μm (pathology) or 12 μm on a cryostat, and sections of the dorsolateral prostates were used for all analyses.

Microscopy

Mosaic fluorescence images were taken on an inverted microscope (Zeiss, Observer.Z1) using Zen software (Zeiss). Bright-field images were taken with 10X or 20X objectives.

Immunofluorescent staining

Cryosections were stained with the following primary antibodies: SMA (1:500; Sigma-Aldrich; F3777, C6198), Vimentin (1:500; Cell Signaling; 5741), Calponin (1:500; Abcam; ab46794), Collagen type I alpha 2 (1:500; Rockland; 600-401-103-0.1), bGAL (1:1,000; Thermo Fisher Scientific; PA1-21477), EpCAM (1:200; eBioscience; 14–5791-82), GFP/YFP (1:1,000; Nacalai Tesque; 0440484), CK5 (1:2,000; Covance; PRB-160P), and CK8 (1:500; Developmental Studies Hybridoma Bank; TROMA-1). Secondary antibodies for double labeling were donkey anti-species conjugated with Alexa Fluor 488 or 555 (1:1,000; Molecular Probes). Nuclei were counterstained with DAPI.

X-GAL Staining

Sections were post-fixed with paraformaldehyde for 5 min, washed twice in X-GAL buffer (2 mM $MgCl_2$, 0.1% Igepal Ca-30, 0.05% sodium deoxycholate in PBS) for 10 min, and stained in X-GAL staining solution (1 mg ml^{-1} X-GAL, 0.2 mM potassium ferricyanide, 0.17 mM potassium ferrocyanide in X-GAL buffer) for 12–14 h at 37 °C. X-GAL–stained sections were counterstained with 0.1% Nuclear Fast Red (Poly Scientific, s248).

Flow Cytometry and RNA-sequencing

To isolate HH-responding (*Gli1*-expressing) stromal cells, prostates of *Gli1*$^{GFP/+}$*; PB-MYC/+* and *Gli1*$^{GFP/+}$ mice were freshly harvested and processed into a single cell suspension, and then subject to FACS (fluorescence activated cell sorting) to isolate GFP+ cells. RNA was extracted from GFP+ cells from individual prostates, then pooled to have a minimum of 4 ng and subject to RNA-sequencing analysis (MSKCC Genomics Core Facility). Alignment of raw data, principal component analysis, and unsupervised hierarchical clustering were performed in Partek Flow. Pathway analysis was performed in DAVID.

Quantification and statistical analysis

To quantify the area of cells expressing SMA, 20x mosaic photographs of four region-matched dorsolateral prostate sections were taken from each male mouse, and the SMA+ pixel area was measured using Photoshop. The numbers of DAPI+ nuclei in the epithelium (EpCAM+) and stroma (EpCAM-) were measured using Cell Profiler. To quantify the EdU+ cells in each compartment, 20x mosaic photographs of four region-matched dorsolateral prostate sections were taken from each male, and EdU+/EpCAM+ and EdU+/EpCAM- cells were counted manually using Stereo Investigator (MBF Bioscience). At least three mice were analyzed for each group in each experiment. Data are presented as mean ± s.d. (standard deviation). Statistical analyses were performed using GraphPad Prism version 6.0.

EdU (5-ethynyl-2'-deoxyuridine) Injection and Staining

For assessing cell proliferation, EdU (Invitrogen, E10187) was given at 100 mg g^{-1} by i.p. injection 1 h before euthanasia. Click-it EdU assay with Alexa Fluor 488 (Invitrogen, C10337) was used according to the protocol of the manufacturer.

TUNEL Staining

For TUNEL staining, slides were permeabilized with 0.5% TritonX-100, pre-incubated with Tdt buffer (30 mM Tris·HCl, 140 mM sodium cacodylate and 1 mM $CoCl_2$) for 15 min at room temperature, and incubated for I h at 37 °C in TUNEL reaction solution (Tdt buffer containing TUNEL enzyme and dUTPbiotin; Roche Applied Science). Then slides were incubated with Streptavidin Alexa Fluoro 647 (Invitrogen, S-32357) for 1 h.

mRNA *in situ* hybridization

RNA *in situ* hybridization analysis was performed based on standard protocols (Birren et al., 1993; Keil et al., 2012) with minor modifications, using antisense RNA probes for *Shh, Dhh and Ihh* (Echelard et al., 1993), *Gli1* (Hui et al., 1994), and a *Sma* probe made using RT-PCR and the following primers: 5'-TGG CTT CGC TGT CTA CCT TC-3' and 5'- CGA TGT TAA TAC GAC TCA CTA TAG GGT GAA GTC AGT GTC GAT TTT TCC-3'.

RNA isolation and real-time polymerase chain reaction (qRT-PCR)

Total RNA from dorsal prostates was isolated using miRNeasy mini kit (QIAGEN, 217004). For reverse transcription-PCR reactions, 8 µg total RNA was reverse transcribed using iScript cDNA systhesis kit (Bio Rad, 170-8891).

qRT-PCR was performed using PowerUp SYBR Green Master Mix (ThermoFisher Scientific, A25742) and GAPDH as an internal control. Each PCR was run in duplicate. Primer sequences were as follows: *Shh* forward 5'-AAAGCTGACCCCTTTAGCCTA-3', *Shh* reverse 5'-TTCGGAGTTTCTTGTGATCTTCC-3', *Ihh* forward 5'-CTCTTGCCTACAAGCAGTTCA-3', *Ihh* reverse 5'-CCGTGTTCTCCTCGTCCTT-3', *Dhh* forward 5'-CTTGGCACTCTTGGCACTATC-3', *Dhh* reverse 5'-GACCCCCTTGTTACCCTCC-3', *Gapdh* forward 5'-CCAAGGTGTCCGTCGTGGATCT-3', and *Gapdh* reverse 5'-GTTGAAGTCGCAGGAGACAACC-3'.

REFERENCES

Abeshouse, A., Ahn, J., Akbani, R., Ally, A., Amin, S., Andry, C. D., Annala, M., Aprikian, A., Armenia, J., Arora, A., et al. (2015). The Molecular Taxonomy of Primary Prostate Cancer. *Cell* **163**, 1011-1025.

Ahn, S. and Joyner, A. L. (2005). In vivo analysis of quiescent adult neural stem cells responding to Sonic hedgehog. *Nature* **437**, 894-897.

Ayala, G., Tuxhorn, J. A., Wheeler, T. M., Frolov, A., Scardino, P. T., Ohori, M., Wheeler, M., Spitler, J. and Rowley, D. R. (2003). Reactive stroma as a predictor of biochemical-free recurrence in prostate cancer. *Clin Cancer Res* **9**, 4792-4801.

Ayala, G. E., Muezzinoglu, B., Hammerich, K. H., Frolov, A., Liu, H., Scardino, P. T., Li, R., Sayeeduddin, M., Ittmann, M. M., Kadmon, D., et al. (2011). Determining prostate cancer-specific death through quantification of stromogenic carcinoma area in prostatectomy specimens. *Am J Pathol* **178**, 79-87.

Bai, C. B., Auerbach, W., Lee, J. S., Stephen, D. and Joyner, A. L. (2002). Gli2, but not Gli1, is required for initial Shh signaling and ectopic activation of the Shh pathway. *Development* **129**, 4753-4761.

Bai, C. B., Stephen, D. and Joyner, A. L. (2004). All mouse ventral spinal cord patterning by hedgehog is Gli dependent and involves an activator function of Gli3. *Dev Cell* **6**, 103-115.

Barron, D. A. and Rowley, D. R. (2012). The reactive stroma microenvironment and prostate cancer progression. *Endocr Relat Cancer* **19**, R187-204.

Berman, D. M., Desai, N., Wang, X., Karhadkar, S. S., Reynon, M., Abate-Shen, C., Beachy, P. A. and Shen, M. M. (2004). Roles for Hedgehog signaling in androgen production and prostate ductal morphogenesis. *Developmental biology* **267**, 387-398.

Birren, S. J., Lo, L. and Anderson, D. J. (1993). Sympathetic neuroblasts undergo a developmental switch in trophic dependence. *Development* **119**, 597-610.

Brownell, I., Guevara, E., Bai, C. B., Loomis, C. A. and Joyner, A. L. (2011). Nerve-derived sonic hedgehog defines a niche for hair follicle stem cells capable of becoming epidermal stem cells. *Cell Stem Cell* **8**, 552-565.

Chen, B. Y., Lin, D. P., Liu, J. Y., Chang, H., Huang, P. H., Chen, Y. L. and Chang, H. H. (2006). A mouse prostate cancer model induced by Hedgehog overexpression. *J Biomed Sci* **13**, 373-384.

Chen, M., Tanner, M., Levine, A. C., Levina, E., Ohouo, P. and Buttyan, R. (2009). Androgenic regulation of hedgehog signaling pathway components in prostate cancer cells. *Cell cycle (Georgetown, Tex.)* **8**, 149-157.

Chen, Y., Chi, P., Rockowitz, S., Iaquinta, P. J., Shamu, T., Shukla, S., Gao, D., Sirota, I., Carver, B. S., Wongvipat, J., et al. (2013). ETS factors reprogram the androgen receptor cistrome and prime prostate tumorigenesis in response to PTEN loss. *Nature medicine* **19**, 1023-1029.

Clark, J., Merson, S., Jhavar, S., Flohr, P., Edwards, S., Foster, C. S., Eeles, R., Martin, F. L., Phillips, D. H., Crundwell, M., et al. (2007). Diversity of TMPRSS2-ERG fusion transcripts in the human prostate. *Oncogene* **26**, 2667-2673.

Echelard, Y., Epstein, D. J., St-Jacques, B., Shen, L., Mohler, J., McMahon, J. A. and McMahon, A. P. (1993). Sonic hedgehog, a member of a family of putative signaling molecules, is implicated in the regulation of CNS polarity. *Cell* **75**, 1417-1430.

Ellwood-Yen, K., Graeber, T. G., Wongvipat, J., Iruela-Arispe, M. L., Zhang, J., Matusik, R., Thomas, G. V. and Sawyers, C. L. (2003). Myc-driven murine prostate cancer shares molecular features with human prostate tumors. *Cancer Cell* **4**, 223-238.

Fan, L., Pepicelli, C. V., Dibble, C. C., Catbagan, W., Zarycki, J. L., Laciak, R., Gipp, J., Shaw, A., Lamm, M. L., Munoz, A., et al. (2004). Hedgehog signaling promotes prostate xenograft tumor growth. *Endocrinology* **145**, 3961-3970.

Franco, O. E. and Hayward, S. W. (2012). Targeting the tumor stroma as a novel therapeutic approach for prostate cancer. *Adv Pharmacol* **65**, 267-313.

Gipp, J., Gu, G., Crylen, C., Kasper, S. and Bushman, W. (2007). Hedgehog pathway activity in the LADY prostate tumor model. *Mol Cancer* **6**, 19.

Gonnissen, A., Isebaert, S. and Haustermans, K. (2013). Hedgehog signaling in prostate cancer and its therapeutic implication. *Int J Mol Sci* **14**, 13979-14007.

Gonzalez-Reyes, L. E., Verbitsky, M., Blesa, J., Jackson-Lewis, V., Paredes, D., Tillack, K., Phani, S., Kramer, E. R., Przedborski, S. and Kottmann, A. H. (2012). Sonic hedgehog maintains cellular and neurochemical homeostasis in the adult nigrostriatal circuit. *Neuron* **75**, 306-319.

Greenberg, N. M., DeMayo, F., Finegold, M. J., Medina, D., Tilley, W. D., Aspinall, J. O., Cunha, G. R., Donjacour, A. A., Matusik, R. J. and Rosen, J. M. (1995). Prostate cancer in a transgenic mouse. *Proc Natl Acad Sci U S A* **92**, 3439-3443.

Hermans, K. G., van Marion, R., van Dekken, H., Jenster, G., van Weerden, W. M. and Trapman, J. (2006). TMPRSS2:ERG fusion by translocation or interstitial deletion is highly relevant in androgen-dependent prostate cancer, but is bypassed in late-stage androgen receptor-negative prostate cancer. *Cancer Res* **66**, 10658-10663.

Hui, C. C., Slusarski, D., Platt, K. A., Holmgren, R. and Joyner, A. L. (1994). Expression of three mouse homologs of the Drosophila segment polarity gene cubitus interruptus, Gli, Gli-2, and Gli-3, in ectoderm- and mesoderm-derived tissues suggests multiple roles during postimplantation development. *Developmental biology* **162**, 402-413.

Ibuki, N., Ghaffari, M., Pandey, M., Iu, I., Fazli, L., Kashiwagi, M., Tojo, H., Nakanishi, O., Gleave, M. E. and Cox, M. E. (2013). TAK-441, a novel investigational smoothened antagonist, delays castration-resistant progression in prostate cancer by disrupting paracrine hedgehog signaling. *Int J Cancer* **133**, 1955-1966.

Karhadkar, S. S., Bova, G. S., Abdallah, N., Dhara, S., Gardner, D., Maitra, A., Isaacs, J. T., Berman, D. M. and Beachy, P. A. (2004). Hedgehog signalling in prostate regeneration, neoplasia and metastasis. *Nature* **431**, 707-712.

Kasper, S., Sheppard, P. C., Yan, Y., Pettigrew, N., Borowsky, A. D., Prins, G. S., Dodd, J. G., Duckworth, M. L. and Matusik, R. J. (1998). Development, progression, and androgen-dependence of prostate tumors in probasin-large T antigen transgenic mice: a model for prostate cancer. *Lab Invest* **78**, i-xv.

Keil, K. P., Mehta, V., Branam, A. M., Abler, L. L., Buresh-Stiemke, R. A., Joshi, P. S., Schmitz, C. T., Marker, P. C. and Vezina, C. M. (2012). Wnt inhibitory factor 1 (Wif1) is regulated by androgens and enhances androgen-dependent prostate development. *Endocrinology* **153**, 6091-6103.

Lee, J. J., Perera, R. M., Wang, H., Wu, D. C., Liu, X. S., Han, S., Fitamant, J., Jones, P. D., Ghanta, K. S., Kawano, S., et al. (2014). Stromal response to Hedgehog signaling restrains pancreatic cancer progression. *Proc Natl Acad Sci U S A* **111**, E3091-3100.

Lim, A., Shin, K., Zhao, C., Kawano, S. and Beachy, P. A. (2014). Spatially restricted Hedgehog signalling regulates HGF-induced branching of the adult prostate. *Nat Cell Biol* **16**, 1135-1145.

Madisen, L., Zwingman, T. A., Sunkin, S. M., Oh, S. W., Zariwala, H. A., Gu, H., Ng, L. L., Palmiter, R. D., Hawrylycz, M. J., Jones, A. R., et al. (2010). A robust and high-throughput Cre reporting and characterization system for the whole mouse brain. *Nat Neurosci* **13**, 133-140.

Mao, J., Ligon, K. L., Rakhlin, E. Y., Thayer, S. P., Bronson, R. T., Rowitch, D. and McMahon, A. P. (2006). A novel somatic mouse model to survey tumorigenic potential applied to the Hedgehog pathway. *Cancer Res* **66**, 10171-10178.

Mathew, E., Zhang, Y., Holtz, A. M., Kane, K. T., Song, J. Y., Allen, B. L. and Pasca di Magliano, M. (2014). Dosage-dependent regulation of pancreatic cancer growth and angiogenesis by hedgehog signaling. *Cell reports* **9**, 484-494.

Olumi, A. F., Grossfeld, G. D., Hayward, S. W., Carroll, P. R., Tlsty, T. D. and Cunha, G. R. (1999). Carcinoma-associated fibroblasts direct tumor progression of initiated human prostatic epithelium. *Cancer Res* **59**, 5002-5011.

Peng, Y. C. and Joyner, A. L. (2015). Hedgehog signaling in prostate epithelial-mesenchymal growth regulation. *Developmental biology* **400**, 94-104.

Peng, Y. C., Levine, C. M., Zahid, S., Wilson, E. L. and Joyner, A. L. (2013). Sonic hedgehog signals to multiple prostate stromal stem cells that replenish distinct stromal subtypes during regeneration. *Proc Natl Acad Sci U S A* **110**, 20611-20616.

Rhim, A. D., Oberstein, P. E., Thomas, D. H., Mirek, E. T., Palermo, C. F., Sastra, S. A., Dekleva, E. N., Saunders, T., Becerra, C. P., Tattersall, I. W., et al. (2014). Stromal elements act to restrain, rather than support, pancreatic ductal adenocarcinoma. *Cancer Cell* **25**, 735-747.

Rosow, D. E., Liss, A. S., Strobel, O., Fritz, S., Bausch, D., Valsangkar, N. P., Alsina, J., Kulemann, B., Park, J. K., Yamaguchi, J., et al. (2012). Sonic Hedgehog in pancreatic cancer: from bench to bedside, then back to the bench. *Surgery* **152**, S19-32.

Sanchez, P., Hernandez, A. M., Stecca, B., Kahler, A. J., DeGueme, A. M., Barrett, A., Beyna, M., Datta, M. W., Datta, S. and Ruiz i Altaba, A. (2004). Inhibition of prostate cancer proliferation by interference with SONIC HEDGEHOG-GLI1 signaling. *Proc Natl Acad Sci U S A* **101**, 12561-12566.

Shaw, A. and Bushman, W. (2007). Hedgehog signaling in the prostate. *J Urol* **177**, 832-838.

Shaw, A., Gipp, J. and Bushman, W. (2009). The Sonic Hedgehog pathway stimulates prostate tumor growth by paracrine signaling and

recapitulates embryonic gene expression in tumor myofibroblasts. *Oncogene* **28**, 4480-4490.

Sheng, T., Li, C., Zhang, X., Chi, S., He, N., Chen, K., McCormick, F., Gatalica, Z. and Xie, J. (2004). Activation of the hedgehog pathway in advanced prostate cancer. *Mol Cancer* **3**, 29.

Shin, K., Lim, A., Zhao, C., Sahoo, D., Pan, Y., Spiekerkoetter, E., Liao, J. C. and Beachy, P. A. (2014). Hedgehog signaling restrains bladder cancer progression by eliciting stromal production of urothelial differentiation factors. *Cancer Cell* **26**, 521-533.

Siegel, R. L., Miller, K. D. and Jemal, A. (2016). Cancer statistics, 2016. *CA Cancer J Clin* **66**, 7-30.

Soriano, P. (1999). Generalized lacZ expression with the ROSA26 Cre reporter strain. *Nature genetics* **21**, 70-71.

Srinivas, S., Watanabe, T., Lin, C. S., William, C. M., Tanabe, Y., Jessell, T. M. and Costantini, F. (2001). Cre reporter strains produced by targeted insertion of EYFP and ECFP into the ROSA26 locus. *BMC Dev Biol* **1**, 4.

Taylor, B. S., Schultz, N., Hieronymus, H., Gopalan, A., Xiao, Y., Carver, B. S., Arora, V. K., Kaushik, P., Cerami, E., Reva, B., et al. (2010). Integrative genomic profiling of human prostate cancer. *Cancer Cell* **18**, 11-22.

Torre, L. A., Bray, F., Siegel, R. L., Ferlay, J., Lortet-Tieulent, J. and Jemal, A. (2015). Global cancer statistics, 2012. *CA Cancer J Clin* **65**, 87-108.

Trotman, L. C., Niki, M., Dotan, Z. A., Koutcher, J. A., Di Cristofano, A., Xiao, A., Khoo, A. S., Roy-Burman, P., Greenberg, N. M., Van Dyke, T., et al. (2003). Pten dose dictates cancer progression in the prostate. *PLoS biology* **1**, E59.

Tuxhorn, J. A., Ayala, G. E., Smith, M. J., Smith, V. C., Dang, T. D. and Rowley, D. R. (2002). Reactive stroma in human prostate cancer: induction of myofibroblast phenotype and extracellular matrix remodeling. *Clin Cancer Res* **8**, 2912-2923.

Tzelepi, V., Karlou, M., Wen, S., Hoang, A., Logothetis, C., Troncoso, P. and Efstathiou, E. (2011). Expression of hedgehog pathway components in prostate carcinoma microenvironment: shifting the balance towards autocrine signalling. *Histopathology* **58**, 1037-1047.

Wendling, O., Bornert, J. M., Chambon, P. and Metzger, D. (2009). Efficient temporally-controlled targeted mutagenesis in smooth muscle cells of the adult mouse. *Genesis (New York, N.Y. : 2000)* **47**, 14-18.

Yu, M. and Bushman, W. (2013). Differential stage-dependent regulation of prostatic epithelial morphogenesis by Hedgehog signaling. *Developmental biology* **380**, 87-98.

Chapter 3 YAP is involved in regeneration of the injured neonatal cerebellum [2]

INTRODUCTION

The cerebellum (CB) not only has a principal role in motor coordination and balance control (Huang et al., 2013), but also is linked with a wide range of higher order cognitive and social functions (Fatemi et al., 2012; Marek et al., 2018; Steinlin, 2007; Stoodley et al., 2017; Tavano et al., 2007; Tsai et al., 2012; Tsai et al., 2018; Wang et al., 2014). Development of the CB in both human and mouse is a protracted process, much of which spans from late embryonic to early postnatal stages (Altman and Bayer, 1997; Dobbing and Sands, 1973; Rakic and Sidman, 1970). Therefore, the CB is particularly vulnerable to clinical and environmental insults. Indeed, preterm birth has been linked to cerebellar hypoplasia and multiple neurological dysfunctions (Allen, 2008; Tam, 2013; Wang et al., 2009; Wang et al., 2014). Thus it is crucial to determine whether the CB has the capability of self-repair, and if so to dissect the molecular mechanisms that underlie such a recovery process.

The mouse CB originates from the anterior hindbrain and undergoes substantial growth in the first two postnatal weeks. Prior to birth, the *Atoh1*-expressing granule cell precursors (GCPs) migrate over the surface of the CB at embryonic day (E) 13.5 – 15.5. After birth, GCPs rapidly proliferate in the

[2] Attribution of data: All experiments were designed and performed by Zhaohui Yang. Daniel Stephen helped with sectioning some of the samples. Dr. Alexandra Joyner oversaw the design and interpretation of experimental results, provided scientific advice and assisted with the preparation of the manuscript. Dr. Alexander Wojcinski assisted with the interpretation of some of the results.

external granule cell layer (EGL) in response to Sonic Hedgehog (SHH) secreted by Purkinje cells (PCs) (Corrales et al., 2006; Lewis et al., 2004; Sillitoe and Joyner, 2007). Until approximately postnatal day (P) 15, post-mitotic GCPs migrate past the underlying Purkinje cell layer (PCL) towards the internal granule cell layer (IGL) where they complete differentiation and maturation (Sillitoe and Joyner, 2007) (Fig. 3.1).

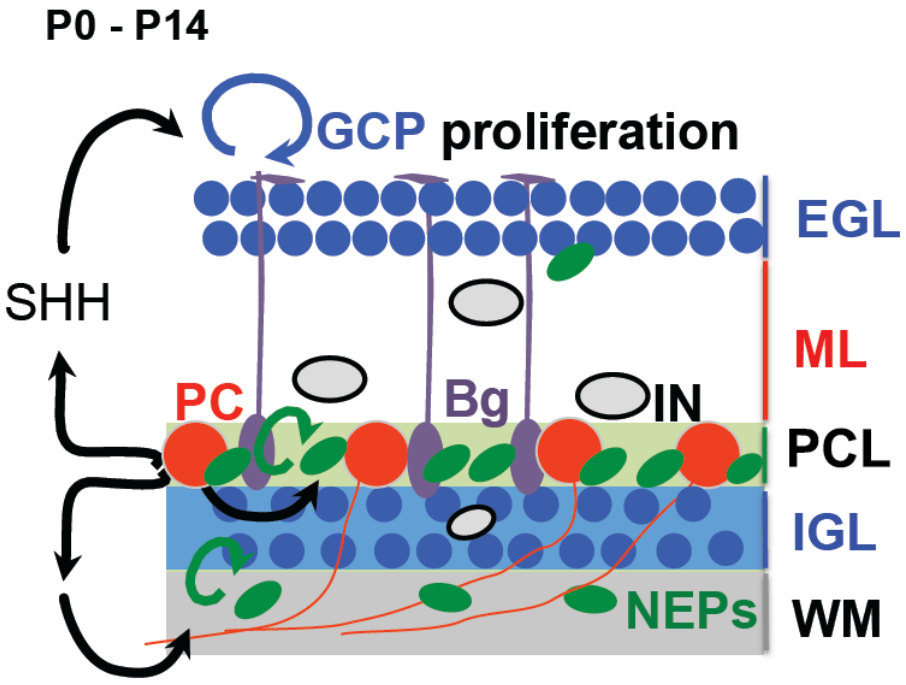

Figure 3.1 Schematic of early postnatal cerebellar cytoarchitecture.

In the first two postnatal weeks, Granule Cell Precursors (GCPs) rapidly proliferate in the External Granule cell Layer (EGL) in response to Sonic Hedgehog (SHH) secreted by Purkinje cells (PCs). Post-mitotic GCPs then migrate along Bergmann glial fibers and past the underlying Purkinje Cell Layer (PCL) into the Internal Granule cell Layer (IGL) where they complete differentiation and maturation. *Nestin*-expressing progenitors are located in three sites, PCL, White Matter (WM), and right beneath the EGL. SHH stimulates proliferation of PCL and WM NEPs, which generate astrocytes and Bergmann glia or astrocytes and interneurons, respectively.

Recent studies uncovered a previously unappreciated regenerative ability of the murine CB. It was first shown in the infant rat that the EGL undergoes a major reconstitution several days after depletion by irradiation, but the long term consequences were not determined (Altman et al., 1969). More recently, we showed that the CB of neonatal mouse is capable of substantial recovery of its adult size and morphology after significant ablation of GCPs in the EGL or PCs soon after birth (Bayin et al., 2018; Wojcinski et al., 2017). The regeneration of GCPs after depletion via irradiation is dependent on the *Nestin*-expressing progenitors (NEPs) derived from the ventricular zone during mid-embryogenesis that proliferate in the postnatal CB (Buffo and Rossi, 2013; Fleming et al., 2013; Milosevic and Goldman, 2004). There are two main subsets of NEPs residing in PCL and white matter (WM) (Fleming et al., 2013; Li et al., 2013; Wojcinski et al., 2017) (Fig. 3.1; Fig. 3.2). Under normal conditions, NEPs in the PCL give rise to astroglia (astrocytes and Bergmann glia) *in vivo*, whereas NEPs in the WM produce interneurons and astroglia (Parmigiani et al., 2015; Wojcinski et al., 2017). However, when GCPs in the EGL are depleted by irradiation at P1, NEPs in the PCL sense the injury and respond by increasing cell proliferation and then migrating into the EGL where they switch cell fate to produce GCs that contribute to the IGL (Fig. 3.2) (Wojcinski et al., 2017). At the same time, NEPs in WM and IGL transiently reduce their production of interneurons and astrocytes (Fig. 3.2). Although it has been shown that SHH signaling is required for NEPs to replenish the injured EGL (Wojcinski et al., 2017), and a SHH agonist protects the neonatal CB by preserving its volume and inhibiting Purkinje cell death (Nguyen et al., 2018), the full molecular repertoire underlying the regenerative capacity of NEPs is not known.

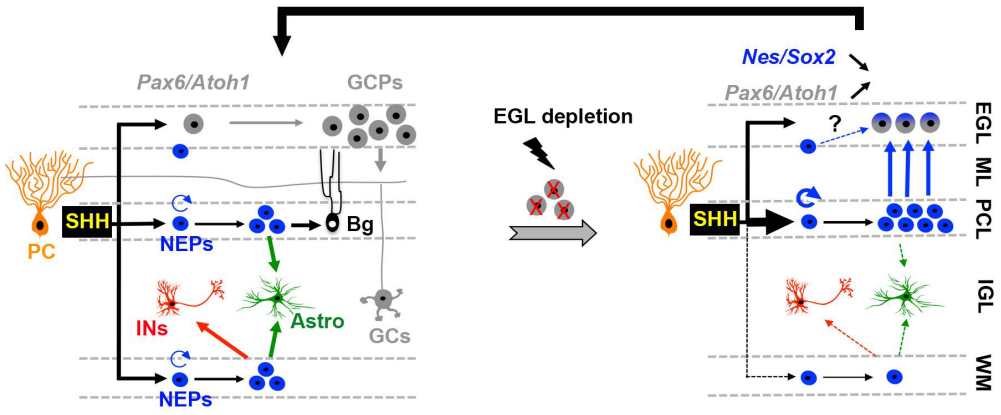

Figure 3.2 Model of the cellular responses during regeneration of the developing cerebellum after irradiation at P1.
(Adopted from (Wojcinski et al., 2017))

Depletion of the External Granule Layer (EGL) during the first days of postnatal cerebellar development results in upregulation of Sonic Hedgehog (SHH) signaling in the Purkinje Cell Layer (PCL), which leads to the expansion and migration of *Nestin*-Expressing Progenitors (NEPs) in the PCL that normally produce Astrocytes (Astro) and Bergmann Glia (Bg). Once in the EGL, NEP-derived cells progressively lose their Neural Stem Cell markers (SOX2 and Nestin), initiate expression of Granule Cell lineage-specific genes (*Pax6* and *Atoh1*) and expand to replenish the EGL. Concomitantly, White Matter (WM) NEPs likely have reduced SHH resulting in a transient reduction in production of interneurons and astrocytes. Thus, injury of the EGL stimulates a cell-cell communication system that coordinates the responses of the different NEP populations during recovery, leading to a reset of the postnatal developmental clock of the cerebellum to re-establish the correct proportions of cerebellar cell types and ensure normal cerebellar circuit formation.

The Hippo signaling pathway is a key regulator of size control of many organs (Halder and Johnson, 2011; Pan, 2010) through regulating cell proliferation and apoptosis (Udan et al., 2003; Wu et al., 2003). In mammals, upon activation of a conserved kinase cascade consisting of the serine/threonine kinases MST1/2 (mammalian Ste2-like kinases) and LATS1/2 (large tumor suppressor kinase 1/2), the transcriptional cofactor Yes-associated protein (YAP) is phosphorylated, sequestered by 14-3-3 in the cytoplasm, and targeted for degradation in a ubiquitin-proteasome-dependent manner (Callus et al., 2006; Chan et al., 2005; Wu et al., 2003; Zhao et al., 2010). Conversely, in the absence of Hippo signaling, dephosphorylated YAP translocates into the nucleus and forms complexes with the TEAD/TEF family transcription factors to activate downstream transcriptional programs that promote cell proliferation and organ growth (Wang et al., 2009). TAZ (transcriptional coactivator with PDZ binding motif; also called WWTR1, for WW-domain containing transcription regulator 1), a paralog of YAP in mammals, is regulated in a similar manner. Although YAP is known to regulate the renewal of many tissue types, including liver, incisors, and the colonic epithelium (Hu et al., 2017; Lu et al., 2018; Yui et al., 2018), the role of YAP in mammalian brain development and regeneration remains poorly studied. Conditional genetic ablation of *Yap* in radial glial progenitor cells (using *Nestin-cre*) was found to cause hydrocephalus and a subtle defect in the proliferation of cortical neural progenitors, but no major anatomical changes in the brain (Park et al., 2016). On the other hand, inactivation of LATS1/2 from the same (Nestin+) neural progenitor population during brain development in mouse results in YAP/TAZ-driven global hypertranscription with upregulation of many target genes related to cell growth and proliferation as revealed by cell-number normalized

transcriptome analysis, which in turn inhibits the differentiation of neural progenitors and promotes a transient over-proliferation (Lavado et al., 2018). In an *ex vivo* model, it was shown that *Yap* over-expression increases the proliferation of cultured GCPs, while shRNA knockdown of *Yap* decreases proliferation (Fernandez et al., 2009). Moreover, *Yap* over-expression seemed to protect cultured GCPs from irradiation-induced damage by sustaining their proliferation and survival (Fernandez et al., 2012). However, the potential functions of YAP and TAZ in development and regeneration of the neonatal CB have not been tested *in vivo*.

Here we utilized genetic modulations of YAP and TAZ in mice and revealed an essential role of YAP in mammalian CB regeneration and mild cellular effects during CB development. Loss of YAP at P0 in NEPs or GCPs in conditional knockout (cKO) mice resulted in only mild alterations of differentiation of NEPs and GCPs and no alteration of the size or morphology of the adult CB. In contrast, YAP was found to play a prominent role in injury-induced regeneration of the CB. Loss of YAP in NEPs disrupted restoration of cerebellar size with pronounced reduction in the IGL and disorganization of PCs and Bergmann glial fibers. The poor recovery of the CB was associated with elevated death of the NEPs in the PCL 1 day after irradiation and later death of NEPs after they entered the EGL. Surprisingly, loss of *Taz* in addition to *Yap* at P0 in NEPs did not alter development or restrict the recovery of the CB after EGL injury. Rather, TAZ ablation appeared to partially rescue the poor recovery of the CB observed in *Yap Nes*-cKO, indicating that TAZ and YAP have distinct functions during CB regeneration. Our study identified Hippo as a key molecular signaling pathway underlying regeneration of the postnatal

CB. Our discovery also raises the possibility that inhibiting the Hippo signaling pathway could potentially reverse cerebellar hypoplasia after injury through structural and functional restoration.

RESULTS

YAP and TAZ expressions are enriched in NEPs in the neonatal CB

As a first step in studying the function of YAP in the developing and regenerating CB, we characterized the expression of the protein in *Nestin-CFP* reporter mice using immunofluorescence (IF). It was previously reported that YAP is expressed in GCPs (Fernandez et al., 2009), but expression in NEPs was not addressed. In the CB of normal P4 mice, a low level of nuclear YAP was detected in some NEPs (CFP+ cells) whereas in GCPs in the EGL little or no YAP was detected (Fig. 3.3A,A',A"). Since NEPs contribute to regeneration of the irradiated (IR) mouse CB, we asked whether YAP expression changes in NEPs during their adaptive reprogramming following irradiation of the CB. When the cerebella of mice were irradiated at P1 (IR mice) and analyzed at P4, nuclear YAP was detected mainly in NEPs (CFP+ cells) and little expression was seen in GCPs (Fig. 3.3B,B',B"). Intriguingly, in IR mice most of the CFP+ NEPs that had entered the EGL showed nuclear expression of YAP (Fig. 3.3B,B',B"), indicating that YAP could play a role in the adaptive reprogramming response of NEPs to EGL ablation. Unlike YAP, nuclear located TAZ expression was obvious in NEPs of both Non-IR and IR cerebella, in addition to in the NEPs that had entered the EGL (Fig. 3.3C-D,C'-D',C"-D").

To confirm that *Yap* and *Taz* are expressed at higher levels in NEPs than GCPs, we carried out quantitative RT-PCR (qRT-PCR) of mRNA from FACS-

sorted Nestin-CFP+ NEPs and Atoh1-GFP+ GCPs from P4 IR and Non-IR mice. Indeed, *Yap* and *Taz* mRNA were significantly lower in GCPs than in NEPs of Non-IR and IR mice, and there were no significant changes after irradiation (Fig. 3.3E,F). Consistent with the antibody staining and qRT-PCR results, analysis of RNA-seq data from Nestin-CFP+ NEPs isolated by FACS from P5 IR and Non-IR mice (Wojcinski et al., 2017) showed the *Yap* and *Taz* transcripts were present in NEPs, with no significant changes after irradiation and lower numbers of reads for *Taz* (Table 3.1). The DNA-binding TEAD family transcription factors *Tead1* and *Tead2* transcripts were abundant while *Tead3* was minimal (Table 3.1), indicating that TEAD1/2 are the main binding partners for YAP/TAZ in neonatal NEPs. The Hippo target gene *Birc5* was present and appears to be slightly upregulated in irradiated NEPs, but a second target gene *Ctgf* had little expression (Table 3.1). Together, these data demonstrate that the cell type that predominantly expresses *Yap* and *Taz* is NEPs, and thus YAP and TAZ could play a role in the regeneration of the EGL by NEPs following irradiation.

Figure 3.3 Nuclear YAP and TAZ are mainly detected in NEPs in the postnatal CB.

(A-D) Immunofluorescence (IF) detection of YAP (A-B) and TAZ (C-D), co-stained for CFP and DAPI, on midsagittal sections of cerebella from Non-IR and IR *Nestin-CFP* reporter mice at P4. Arrows and arrowheads indicate *Nestin* (CFP) positive cells in the Purkinje cell layer (PCL) or EGL, respectively that also have nuclear YAP or TAZ. Scale bar, 50 mm. (E-F) qRT-PCR analysis of the mRNA expression of *Yap* (E) and *Taz* (F) relative to *Gapdh* in FACS isolated NEPs (Nestin-CFP+) and GCPs (Atoh1-GFP+) from Non-IR and IR mice at P4. Data are presented as mean ± S.D., and statistical analysis by two-way ANOVA. Each data point represents one animal.

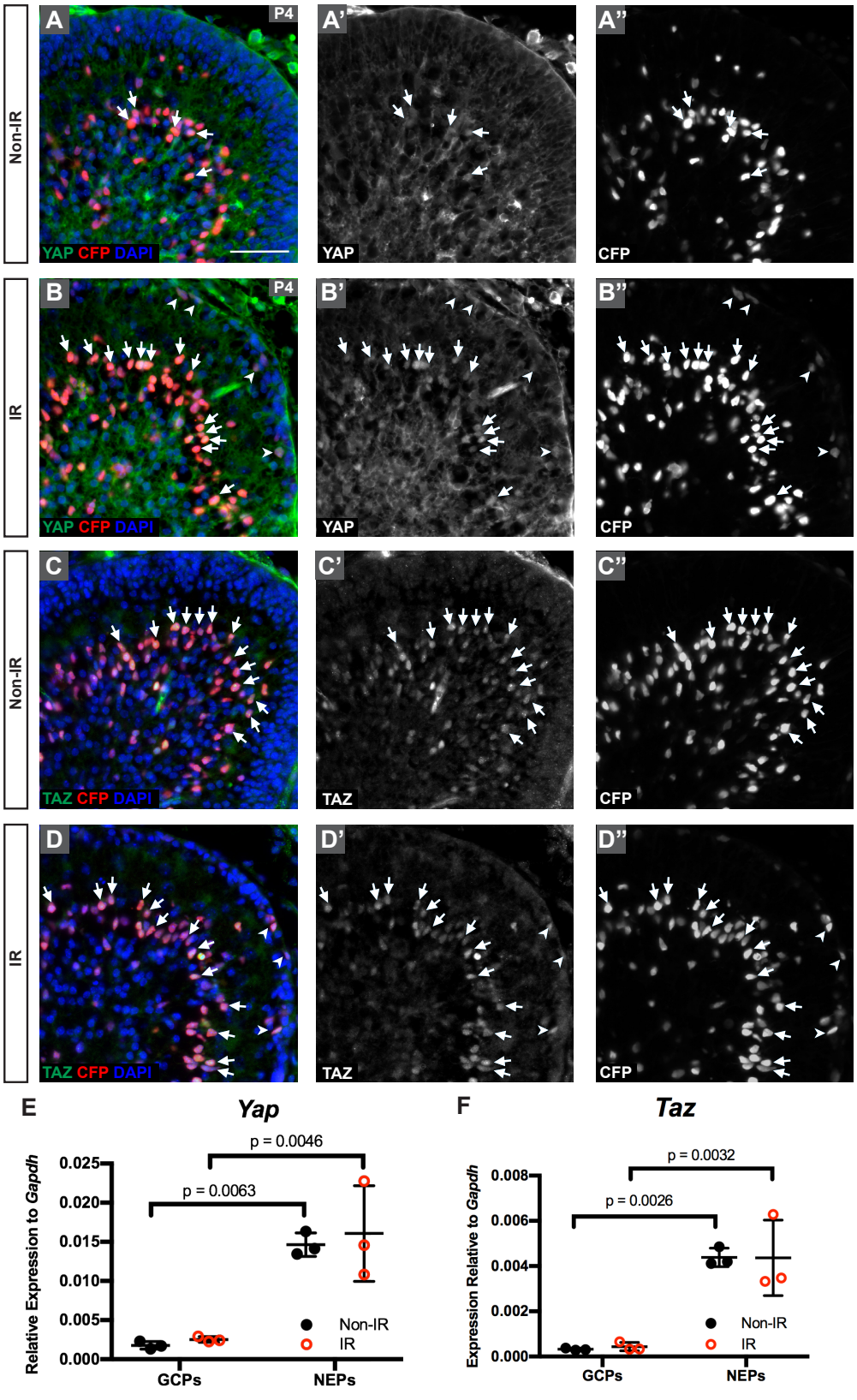
Non-IR
A
P4
YAP CFP DAPI
A'
YAP
A''
CFP
IR
B
P4
YAP CFP DAPI
B'
YAP
B''
CFP
Non-IR
C
TAZ CFP DAPI
C'
TAZ
C''
CFP
IR
D
TAZ CFP DAPI
D'
TAZ
D''
CFP
E
Yap
Relative Expression to Gapdh
0.025
0.020
0.015
0.010
0.005
0.000
p = 0.0046
p = 0.0063
Non-IR
IR
GCPs
NEPs
F
Taz
Expression Relative to Gapdh
0.008
0.006
0.004
0.002
0.000
p = 0.0032
p = 0.0026
Non-IR
IR
GCPs
NEPs

Table 3.1 Read number of Hippo pathway genes from RNA-sequencing of Non-IR and IR NEPs from P5 *Nes-CFP* mice.

Gene	Non-IR NEPs	IR NEPs	Unadjusted p value
Yap	3203	3051	0.88
Taz	2129	2211	0.73
Tead1	8018	8137	0.91
Tead2	7219	7587	0.64
Tead3	648	490	0.08
Ctgf	72	86	0.50
Birc5	2687	3125	0.19
Gapdh	2081	2212	0.60

YAP regulates differentiation of NEPs during normal CB development

Given the potential role of YAP in NEPs during development and/or regeneration, we determined whether *Yap* is required for growth or differentiation of the CB. *Yap* was mutated in NEPs at P0 using a mosaic mutant analysis approach (MASTR, mosaic mutant analysis with spatial and temporal control of recombination) (Lao et al., 2012; Wojcinski et al., 2017) (Fig. 3.4A). An inducible FLP site-specific recombinase expressed from a Nestin transgene was used to induce sustained expression of a protein fusion between GFP and CRE (referred to as GFPcre) following injection of tamoxifen (Tm), which then induces recombination of a *Yap* floxed allele (Reginensi et al., 2013), resulting in visualization of the mutant cells and their descendants based on GFP expression (Fig. 3.4A). Tm was administered to *Nes-FlpoER/+;R26*$^{FSF\text{-}GFPcre/+}$*;Yap*$^{flox/flox}$ *(Nes-mYap* cKO*)* mice and littermate controls (*Nes-FlpoER/+;Yap*$^{flox/flox}$, or *R26*$^{FSF\text{-}GFPcre/+}$*;Yap*$^{flox/flox}$, or *Yap*$^{flox/flox}$) at P0, and the size of the adult CB was measured based on the area of midline sections at P30 (Fig. 3.4B). Despite the obvious expression of YAP in most of the NEPs, the size of *Nes-mYap* cKO cerebella was similar to controls (Fig. 3.4C,D,E).

Since the loss of YAP in NEPs did not affect the size of the P30 CB, we tested whether it affected differentiation of NEPs in the developing CB at P8 by determining the distribution of NEPs and their descendants in different layers of the CB. Quantification of the GFPcre+ NEPs in lobule 4/5 of P8 *Nes-mYap* cKOs and controls (*Nes-FlpoER/+;R26*$^{FSF\text{-}GFPcre/+}$ or *Nes-m*) indicated an increase in the number of mutant cells present at P8, and demonstrated a significant increase in the number of GFP+ cells in the molecular layer (ML)

normalized to the area of the lobule analyzed, as well as the percentage of cells in the layer (Fig. 3.4H,I; Fig. 3.5A,B). There was a concomitant decrease in the percentage of cells in the IGL+WM layers, but not the total number of cells, indicating that the significant change in *Nes-mYap* cKOs is an increase in the production of cells destined to the ML (Fig. 3.4J; Fig. 3.5A,B). Consistent with the GFP+ cells in the ML being interneurons produced by WM NEPs, there was also a significant increase in the number of cells in the ML that expressed PAX2, a marker of differentiating interneurons (Fig. 3.4K). The number of PAX2+ cells was slightly higher in the IGL and WM, consistent with an overall increase in production of interneurons in the absence of *Yap* (Fig. 3.4L; Fig. 3.5C,D). Quantification of S100β+ astrocytes among the GFP+ populations in lobule 4/5 revealed an increase in the number of astrocytes in the PCL (Fig. 3.4M; Fig. 3.5E,F). These data suggest that YAP normally plays a role in attenuating production of interneurons and astrocytes.

Figure 3.4 YAP affects differentiation of NEPs during normal postnatal CB development.

(A) Schematic of the MASTR technique. (B) Schematic showing experimental design. (C-D) Hematoxylin and eosin (H&E) stained midsagittal sections of *Nes-mYap* cKO and control cerebella at P30. Scale bar, 500 μm. (E) Graph of the area of midsagittal sections from *Nes-mYap* cKOs (n = 6) and littermate controls (n = 4) at P30. p = 0.1309. (F-G) Representative images from lobule 4/5 showing IF staining of GFP and DAPI on midsagittal sections from a *Nes-m* control and a *Nes-mYap* cKO at P8. Shades of highlights indicate the partition of different layers (EGL, ML, PCL, IGL and WM) within the lobule. Scale bar, 100 μm. (H-M) Graphs of the number of GFP+ cells in all the layers (H) or in the ML (I) or IGL+WM (J), the number of PAX2+ GFP+ cells in the ML (K) and IGL+WM (L), and the number of S100β+ GFP+ cells in the PCL (M), per 0.1 mm^2 of the total area analyzed in lobule 4/5 from *Nes-m* controls (n = 3) and *Nes-mYap* cKOs (n = 4) at P8. (H) p = 0.1996;; (J) p = 0.6065; (L) P = 0.3548; (M) P = 0.0791. Statistical analysis is conducted by unpaired t test. Data are presented as mean ± standard deviation (S.D.), and each data point represents one animal.

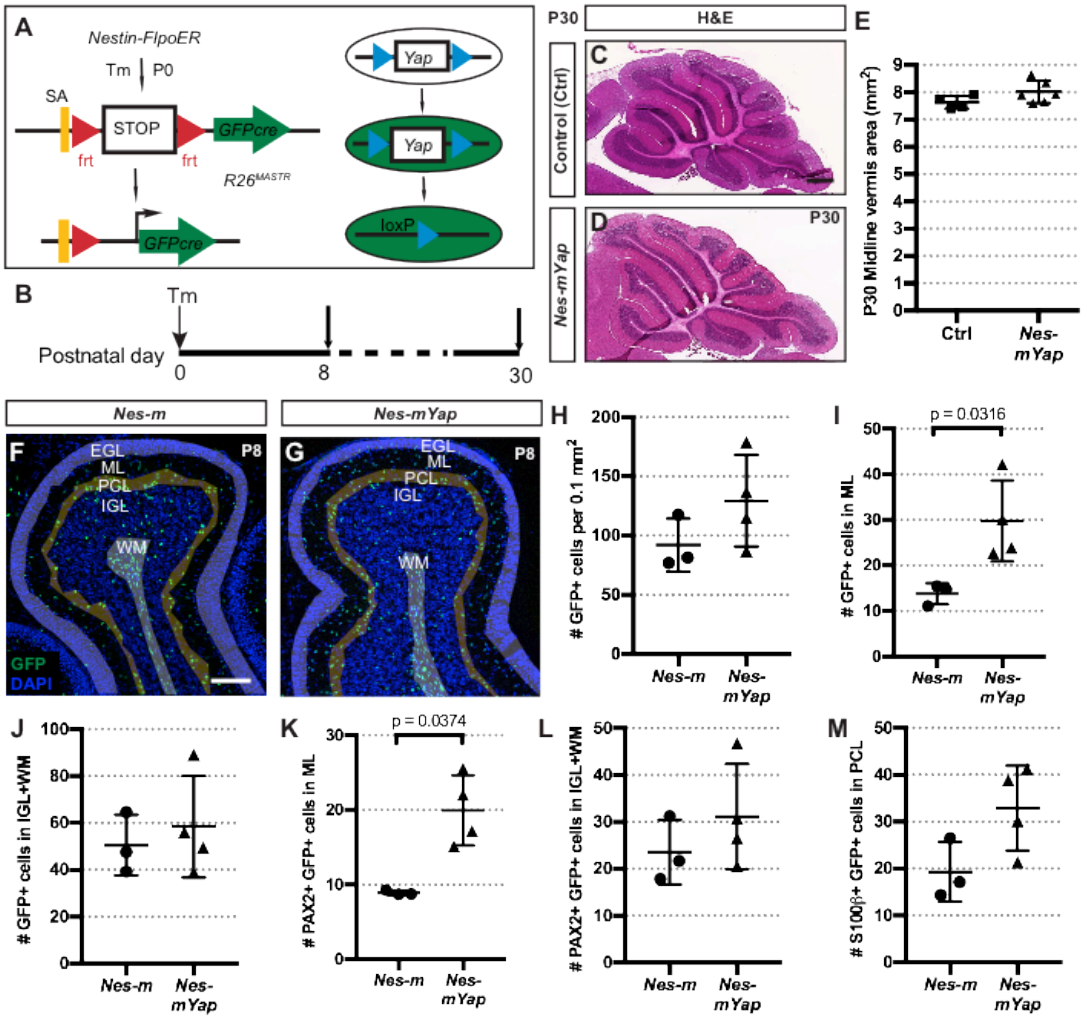
A
Nestin-FlpoER
Tm
P0
SA
STOP
GFPcre
frt
frt
R26MASTR
GFPcre
Yap
Yap
loxP
B
Tm
Postnatal day
0
8
30
P30
H&E
Control (Ctrl)
Nes-mYap
C
D
P30
E
P30 Midline vermis area (mm2)
Ctrl
Nes-mYap
Nes-m
Nes-mYap
F
G
P8
EGL
ML
PCL
IGL
WM
GFP
DAPI
H
GFP+ cells per 0.1 mm2
I
p = 0.0316
# GFP+ cells in ML
J
GFP+ cells in IGL+WM
K
p = 0.0374
# PAX2+ GFP+ cells in ML
L
PAX2+ GFP+ cells in IGL+WM
M
S100β+ GFP+ cells in PCL

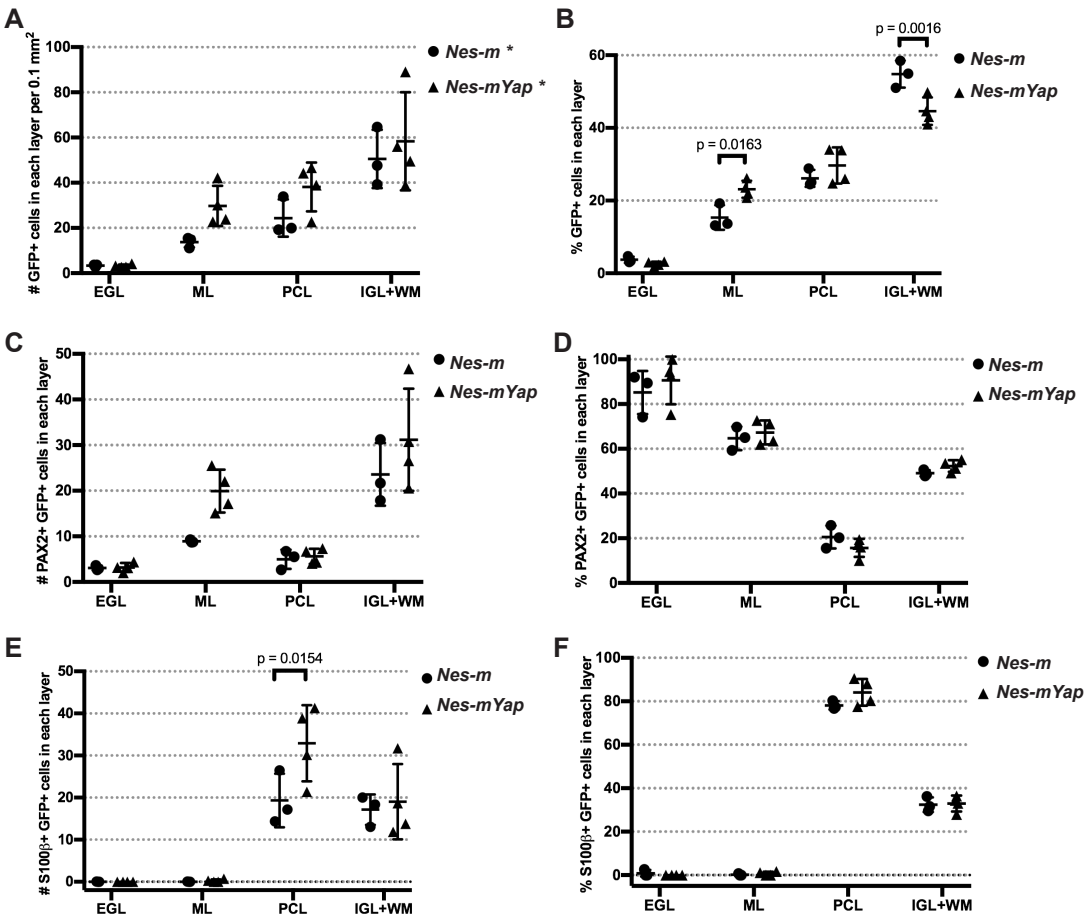

Figure 3.5 YAP has mild effects on differentiation of NEPs during normal postnatal CB development.

Graphs of the normalized number and percentage of GFP+ cells in different layers (A,B), the number and percentage of PAX2+ GFP+ double cells (C,D) or S100β+ GFP+ double cells (E,F) within each layer, per 0.1 mm^2 of the total area analyzed in lobule 4/5 of midsagittal sections from *Nes-m* controls (n=3) and *Nes-mYap* cKOs (n = 4) at P8. (A) * p = 0.0217, F (5, 15) = 3.722. Data are presented as mean ± S.D., and statistical analysis by two-way ANOVA. Each data point represents one animal.

YAP regulates differentiation of GCPs during normal development

In order to determine whether YAP plays a role in GCPs during CB development, we generated two mutants. First, we deleted *Yap* from the ATOH1-expressing rhombic lip lineage when GCPs and the cerebellar nuclei neurons are generated in the embryo and analyzed the size of the P30 CB in *Atoh1-Cre/+;Yap*$^{flox/flox}$ *(Atoh1-Yap* cKO*)* mice compared to *Yap*$^{flox/flox}$ littermate controls. Consistent with the weak expression of *Yap* mRNA in GCPs (Fig. 3.3A-B,A'-B',A"-B"), P30 *Atoh1-Yap* cKOs showed no reduction in the area of the midline, or the IGL area or IGL/CB ratio (Fig. 3.6A-G). This lack of a phenotype is similar to mice lacking *Yap* in NEPs (Fig. 3.4C-E), showing that loss of YAP in the *Atoh1*-lineage does not have a major effect on growth of the CB during development.

We next used the MASTR approach with an *Atoh1-FlpoER* to determine whether differentiation of GCPs is altered when *Yap* is removed. Tm was administered at P0 to *Atoh1-FlpoER/+;R26*$^{FSF-GFPcre/+}$*;Yap*$^{flox/flox}$ (*Atoh1-mYap* cKO) mice and controls (*Atoh1-FlpoER/+; R26*$^{FSF-GFPcre/+}$ or *Atoh1-m*), and then EdU was injected 1 hour prior to sacrifice at P8. The EdU+ outer EGL (oEGL) consists of actively proliferating GCPs, and the percentage of post-mitotic GFP+ GCs in the EdU-negative "inner layers" including inner EGL (iEGL), ML, IGL, and WM was determined amongst all GFP+ cells (Fig. 3.6H-I, H'-I'). Interestingly, we found that the percentage of GFP+ cells in the "inner layers" was significantly higher in *Atoh1-mYap* cKOs compared to controls (Fig. 3.6J), indicating an increase in differentiation, or decrease in self-renewal of GCPs. The proliferation index (percent of EdU+ GFP+ cells among all GFP+ cells in the oEGL) was similar between *Atoh1-mYap* cKO and controls

(Fig. 3.6K), showing that *Yap* does not regulate the proliferation rate. Taken together, these data indicate YAP plays a minor but negative role on differentiation of GCPs into granule neurons. Given this role, all be it mild, of *Yap* in promoting GCP self-renewal, one might have expected a growth defect in *Atoh1-Yap* cKOs. One possibility is that this phenotype is only expressed in a mosaic situation, where there is completion between the scattered mutant cells and their surrounding wild type neighbors.

In order to determine whether TAZ plays a redundant role in GCPs during CB development, we deleted both *Taz* and *Yap* from the ATOH1-expressing lineage and analyzed the size of the P30 CB in *Atoh1-Cre/+;Yap*$^{flox/flox}$*;Taz*$^{flox/flox}$ *(Atoh1-YapTaz* cKO*)* mice compared to *Yap*$^{flox/flox}$*;Taz*$^{flox/flox}$ littermate controls. Similar to *Yap* mutant alone, P30 *Atoh1-YapTaz* cKOs showed no reduction in the area of the midline, or the IGL area or IGL/CB ratio (Fig. 3.6L-R). This result suggests that neither YAP nor TAZ in the *Atoh1*-lineage has a major role on growth of the CB during development.

Figure 3.6 YAP regulates differentiation of GCPs during normal development of CB.

(A-D) H&E staining (A-B) and IF detection of the granule cells marker NeuN (C-D) on midsagittal sections of cerebella from *Atoh1-Yap* cKOs and littermate control (Ctrl) mice at P30. Scale bars, 500 μm. (E-G) Graphs of the area of the midline of the CB (E), the area of the IGL (F), and IGL/CB area ratio (G) in *Atoh1-Yap* cKO (n = 4) and littermate controls (n = 4) at P30. (E) p = 0.8554; (F) p = 0.1727; (G) p = 0.1155. (H-I) Representative images from lobule 4/5 showing IF staining for GFP, EdU, and DAPI on midsagittal sections from an *Atoh1-m* control and *Atoh1-mYap* cKO at P8. (H'-I') Magnification of areas within dotted lines in H-I. Yellow dashed lines indicate the EGL and the border of the outer- and inner-EGL. Scale bars, 100 μm. (J-K) Graphs of the percent of differentiated GFP+ cells (in all layers except the oEGL) among all GFP+ cells (J) and proliferation index (G) in the midline of the CB in *Atoh1-m* controls (n = 3) and *Atoh1-mYap* cKOs (n = 3) at P8. (K) p = 0.4670. (L-O) H&E staining (L-M) and IF detection of NeuN (N-O) on midsagittal sections of cerebella from *Atoh1-YapTaz* cKOs and littermate control (Ctrl) mice at P30. Scale bars, 500 μm. (P-R) Graphs of the area of the midline of the CB (P), the area of the IGL (Q), and IGL/CB area ratio (R) in *Atoh1-YapTaz* cKO (n = 6) and littermate controls (n = 6) at P30. (P) p = 0.3110; (Q) p = 0.4977; (R) p = 0.1807. Data are presented as mean ± S.D., and statistical analysis by unpaired t test. Each data point represents one animal.

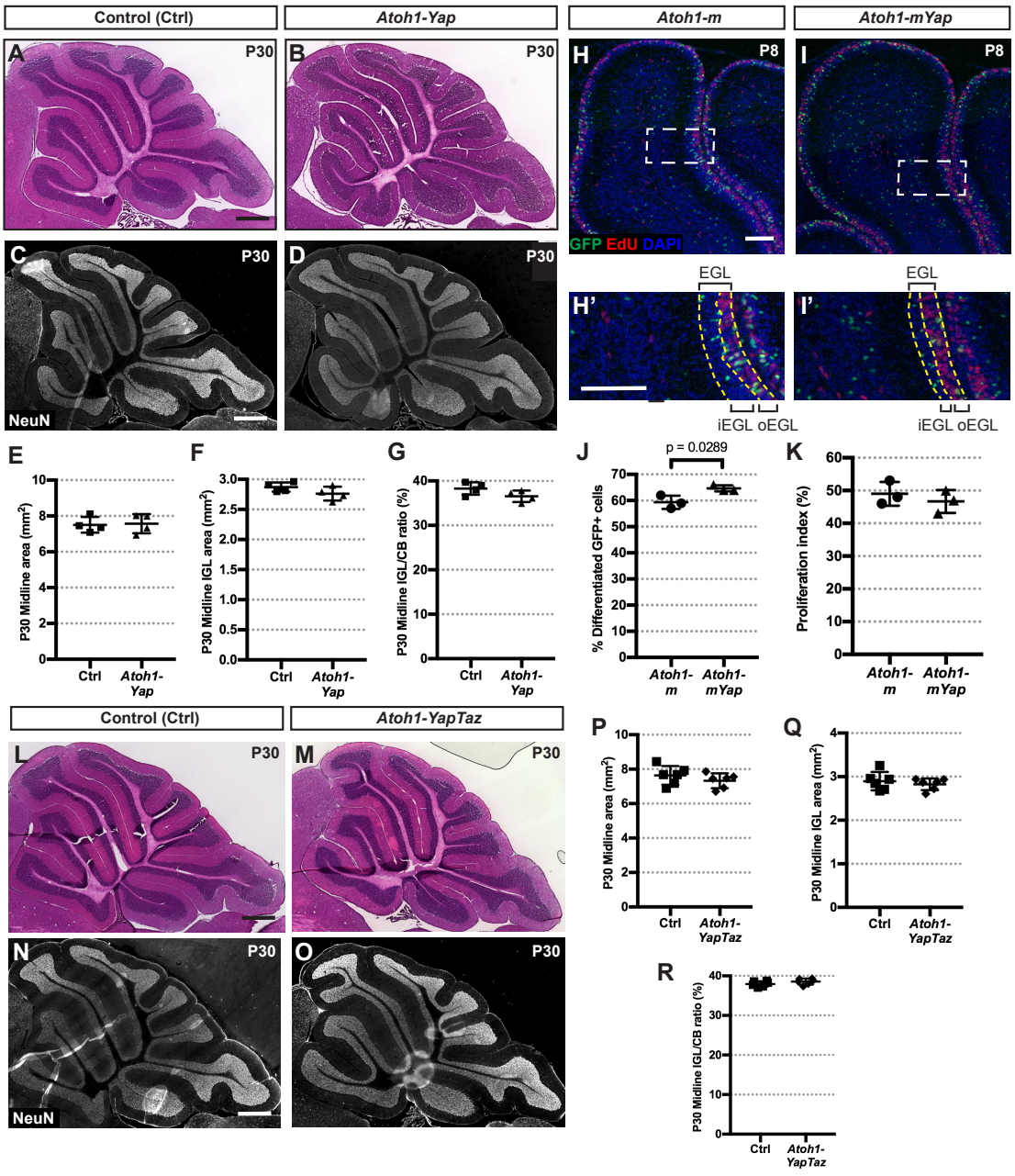
Control (Ctrl)
Atoh1-Yap
Atoh1-m
Atoh1-mYap
A
P30
B
P30
H
P8
I
P8
C
P30
NeuN
D
P30
GFP EdU DAPI
EGL
H'
I'
iEGL oEGL
E
P30 Midline area (mm²)
Ctrl
Atoh1-Yap
F
P30 Midline IGL area (mm²)
G
P30 Midline IGL/CB ratio (%)
J
p = 0.0289
% Differentiated GFP+ cells
Atoh1-m
Atoh1-mYap
K
Proliferation index (%)
Control (Ctrl)
Atoh1-YapTaz
L
M
N
O
P
Q
R

Loss of YAP in the NEP lineage hampers postnatal cerebellum regeneration

To determine any role of YAP in NEPs during injury-induced regeneration of the EGL, we mutated *Yap* in NEPs by administering Tm to *Nes-mYap* cKOs and littermate controls P0 and X-ray irradiating them at P1, and then measuring the size of CB at P30 (Fig. 3.7A). Significantly, although *Yap* deletion does not reduce CB growth during development (Fig. 3.4A-E; Fig. 3.7), *Nes-mYap* cKO showed a significant reduction in recovery after irradiation compared to IR littermate controls (Fig. 3.7). The size of the CB (area of the midline) of IR mutants was reduced to 41.3 ± 2.10% of Non-IR littermate mutants compared to 50.4 ± 2.75% for IR littermate controls compared to Non-IR controls ($p = 0.0403$) (Fig. 3.7B-F; Fig. 3.8A). Even more prominent was a significant reduction in the area of the IGL ($p = 0.0005$), and IGL/CB ratio ($p < 0.0001$) in *Nes-mYap* cKOs compared to controls (Fig. 3.7G-L; Fig. 3.8B-C). Furthermore, the Calbindin+ Purkinje cells failed to form a single cell layer in the *Nes-mYap* cKO CB; instead, the individual Purkinje cells were disorganized and dispersed throughout the entire WM-IGL-ML layers (Fig. 3.8D-G,D'-G'). The GFAP+ Bergmann glial fibers also appeared disorganized and disoriented in the *Nes-mYap* cKO CB (Fig. 3.8H-K, H'-K'). Furthermore, by measuring the IGL area of the CB at P12 and P16, we found that *Nes-mYap* cKOs and littermate controls had a similar IR/Non-IR ratio in IGL area at P12 and the CB appeared to be getting smaller at P16 (Fig. 3.9). Together, these data indicate a crucial role of YAP in NEPs at a late stage in the recovery of postnatal CB growth and cellular organization after IR-induced injury to the EGL.

Figure 3.7 Loss of YAP in the NEP lineage hampers postnatal cerebellum regeneration.

(A) Schematic showing experimental design. (B-E) H&E staining of midsagittal sections of the CB from Non-IR and IR animals at P30. Scale bar, 500 μm. (F) Graph of the area of midline sections of the CB as a percentage of IR/Non-IR animals. P = 0.0403. (G-J) IF detection of NeuN on midsagittal sections of the CB from Non-IR and IR animals at P30. Scale bar, 500 μm. (K-L) Graphs of the ratio of the area of the midline IGL of IR/Non-IR animals (K) and IGL/CB ratio (L) from *Nes-mYap* cKOs (Non-IR, n = 6; IR, n = 4) and littermate controls (Non-IR, n = 4; IR, n = 5) at P30. Data are presented as mean ± S.D., and statistical analysis by unpaired t test. Each data point represents one animal, and is calculated as the value for each IR mouse (average of 3 sections) divided by the mean for all the Non-IR littermates, X 100.

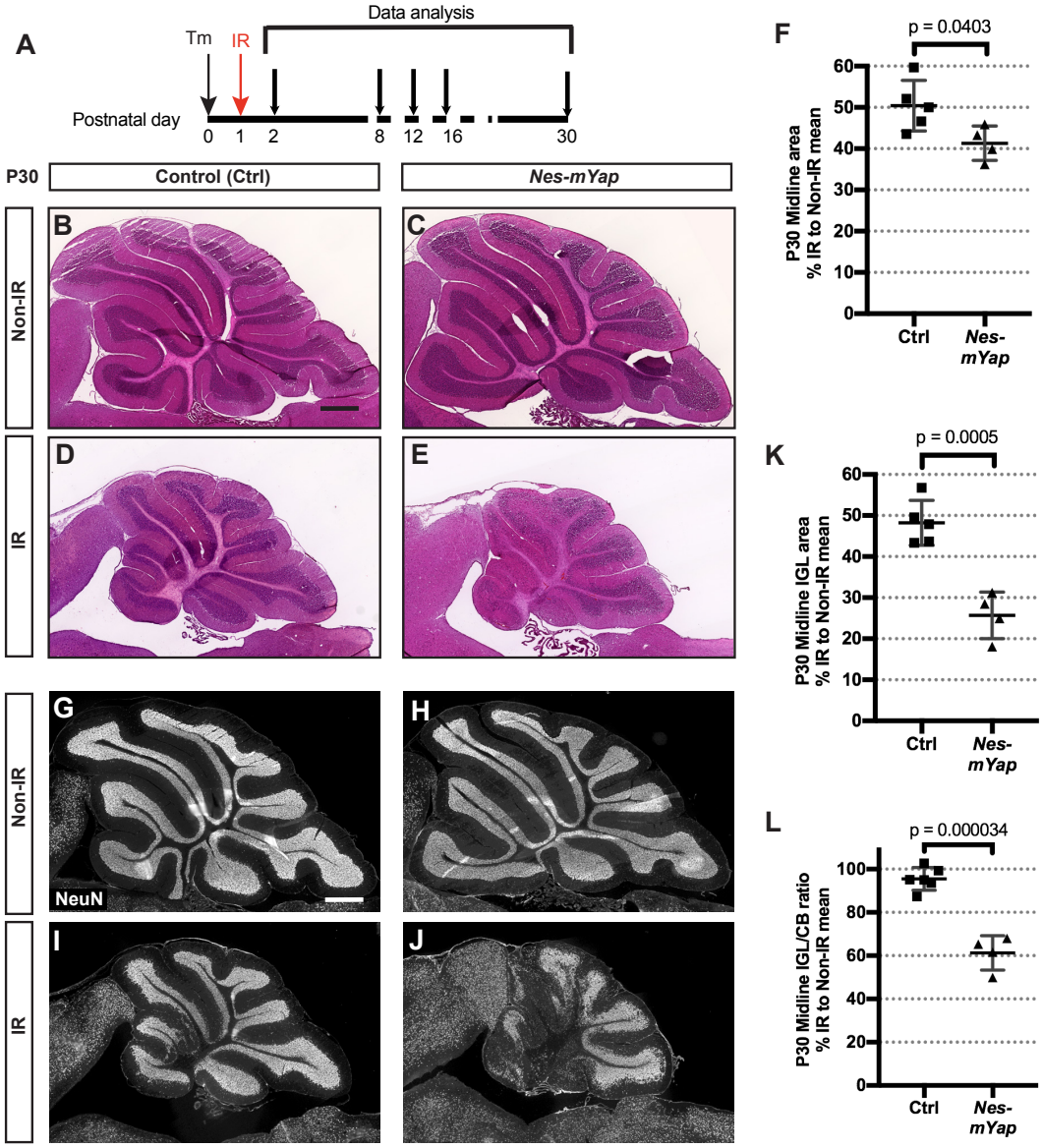
A
Data analysis
Tm
IR
Postnatal day
0 1 2 8 12 16 30
P30
Control (Ctrl)
Nes-mYap
Non-IR
IR
B
C
D
E
G
H
I
J
NeuN
F
p = 0.0403
P30 Midline area
% IR to Non-IR mean
Ctrl
Nes-
mYap
K
p = 0.0005
P30 Midline IGL area
% IR to Non-IR mean
L
p = 0.000034
P30 Midline IGL/CB ratio
% IR to Non-IR mean

Figure 3.8 Loss of YAP hinders injury-induced regeneration of the CB and disrupts the layered cytoarchitecture.

(A-C) Graphs of the midline CB area (A), the IGL area (B), and IGL/CB area ratio (C) from *Nes-mYap* cKOs (Non-IR, n = 6; IR, n = 4) and littermate controls (Non-IR, n = 4; IR, n = 5) at P30. Data are presented as mean ± S.D., and statistical analysis by two-way ANOVA. Each data point represents one animal. (D-K) Representative images from lobule 4/5 showing IF staining for Calbindin (CALB) (D-G) and GFAP (H-K) on midsagittal sections from *Nes-mYap* cKOs and littermate controls at P30. (D'-G') Magnification of areas within dotted lines in D-G. (H'-K', H"-K") Magnification of areas within dotted lines in H-K. Scale bars, 50 μm.

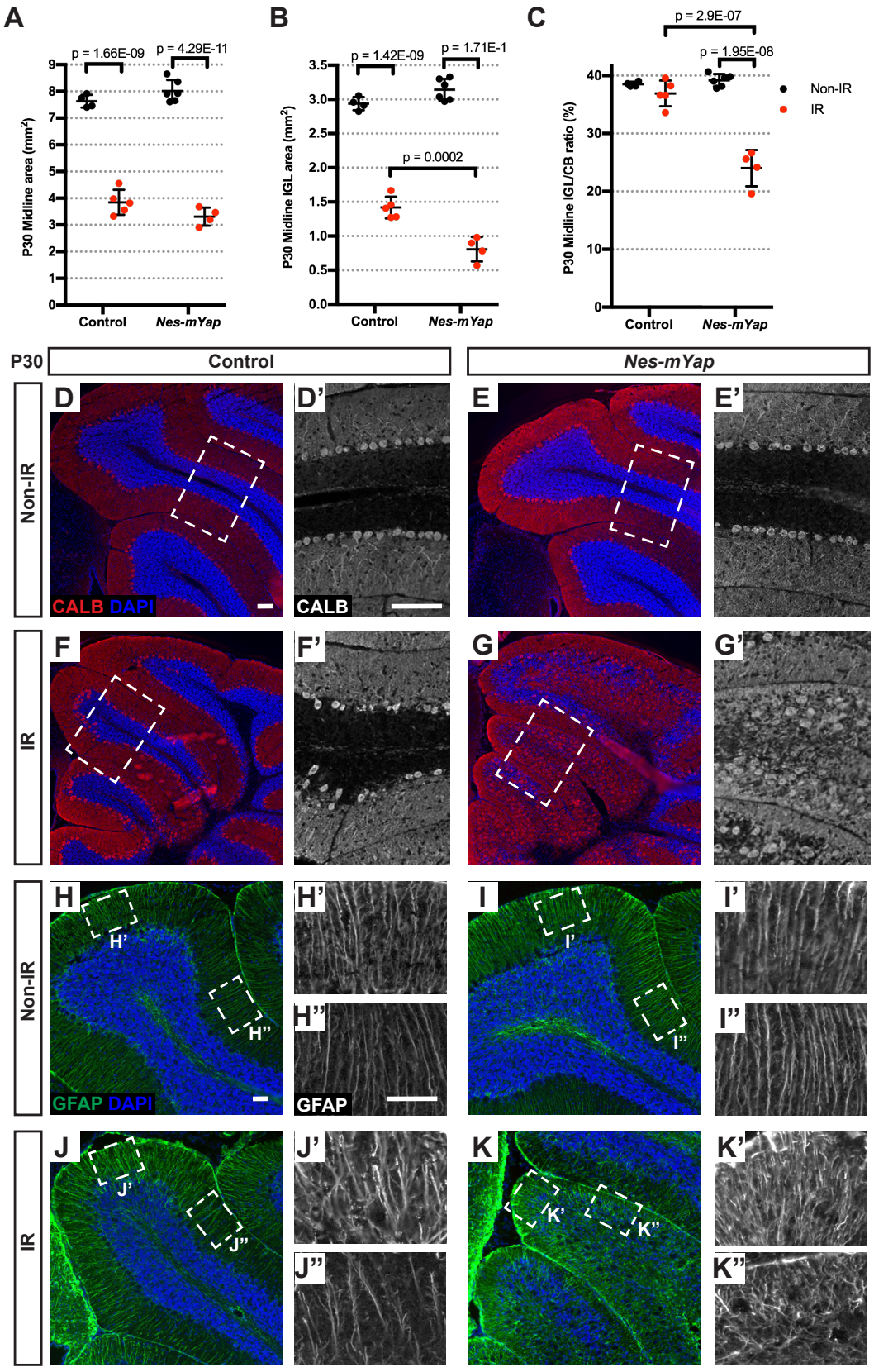
A
p = 1.66E-09
p = 4.29E-11
P30 Midline area (mm²)
Control
Nes-mYap
B
p = 1.42E-09
p = 1.71E-1
p = 0.0002
P30 Midline IGL area (mm²)
Control
Nes-mYap
C
p = 2.9E-07
p = 1.95E-08
P30 Midline IGL/CB ratio (%)
Non-IR
IR
Control
Nes-mYap
P30
Control
Nes-mYap
Non-IR
IR
D
D'
E
E'
F
F'
G
G'
H
H'
H"
I
I'
I"
J
J'
J"
K
K'
K"
CALB DAPI
CALB
GFAP DAPI
GFAP

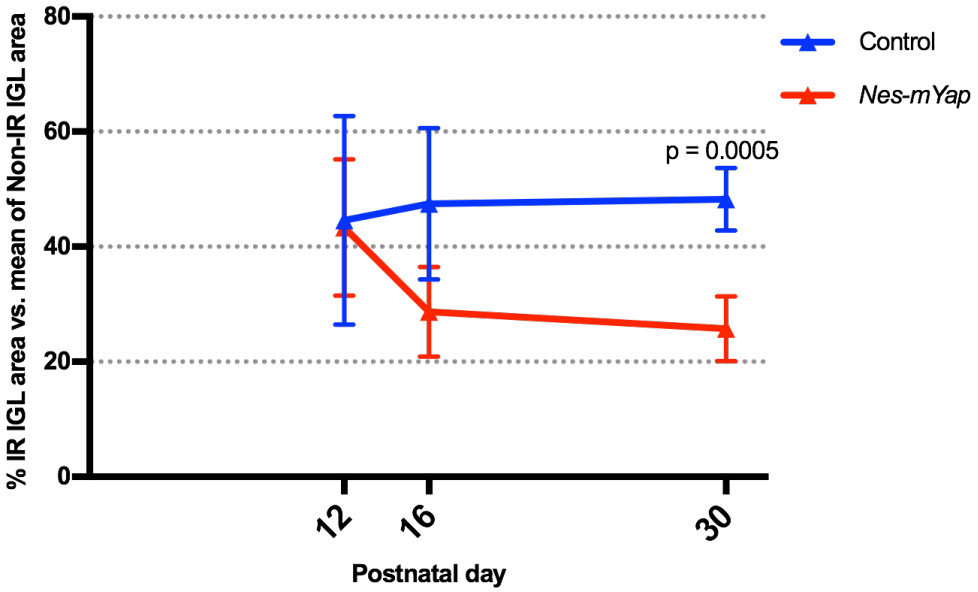

Figure 3.9 The defect in recovery from IR in *Yap* mutants occurs late.

Graph showing the IGL area of IR mice as a percentage of the mean of Non-IR littermates for *Nes-mYap* cKOs (red) and controls (blue) at three developmental ages (P12, P16, and P30). P12, p = 0.9150; P16, p = 0.1002. P12 *Nes-mYap* cKO: Non-IR, n = 4; IR, n = 4; P12 littermate control: n = 3; IR, n = 4; P16 *Nes-mYap* cKO: Non-IR, n = 3; IR, n = 3; P16 littermate control: n = 3; IR, n = 3; P30 *Nes-mYap* cKO: Non-IR, n = 6; IR, n = 4; P16 littermate control: n = 4; IR, n = 5. Data are presented as mean ± S.D., and statistical analysis by unpaired t-test. Each data point represents one animal.

Loss of YAP results in an increase in cell death in NEPs at P2 and in the EGL at P12 following IR-induced injury at P1

To dissect the cellular mechanism underlying the reduced recovery of *Nes-mYap* cKOs after IR, we first examined whether YAP plays a role in maintaining the survival of NEPs in the PCL following IR. As expected, cell death (TUNEL+ particles) was minimal in the CB of Non-IR *Nes-mYap* cKOs and littermate controls given Tm at P0, and cell death was prominent in the EGL of IR mice (Fig. 3.10A-F). In addition, *Nes-mYap* cKOs showed a 1.6-fold increase ($p = 0.0039$) in the density of TUNEL+ cells within the PCL compared to IR controls (Fig. 3.10D,E,F). This result indicates that YAP protects NEPs from apoptosis following IR, similar to what was observed for GCPs in culture (Fernandez et al., 2012).

Next we examined whether YAP is required for migration of NEPs into the EGL. The distribution of GFP+ NEP-lineage cells in the different layers of lobule 4/5 was quantified in both *Nes-mYap* cKO and *Nes-m* control mice at P8 (Fig. 3.10A). Unlike the increase in production of interneurons and astrocytes in Non-IR *Nes-mYap* cKOs compared to controls (Fig. 3.4; Fig. 3.5), the distribution of NEPs in the different layers of the CB in IR mice was similar between the two genotypes, including in the EGL, with a slight change in the total number of GFP+ cells (Fig. 3.10G-L; Fig. 3.11A-C). This result suggests that the initial response of NEPs to irradiation does not depend on YAP, including the migration of NEPs from the PCL into the EGL to repopulate the GCPs.

Figure 3.10 Loss of YAP results in more cell death in the PCL after IR-induced injury.

(A) Schematic showing experimental design. (B-E) Representative images from lobule 4/5 showing IF staining of TUNEL, SOX2, and DAPI on midsagittal sections from *Nes-mYap* cKOs and littermate controls at P2. Grey shadow highlights the PCL of the lobule. Arrows indicate TUNEL+ particles in the PCL. Scale bar, 100 μm. (F) Graph of the number of TUNEL+ particles in the PCL of the midline CB from *Nes-mYap* cKOs (Non-IR, n = 3; IR, n = 3) and littermate controls (Non-IR, n = 3; IR, n = 3) at P2. (G-J) Representative images from lobule 4/5 showing IF staining of GFP and DAPI on midsagittal CB sections from *Nes-m* controls and *Nes-mYap* cKOs at P8. Grey shadow highlights the EGL of the lobule. Scale bar, 100 μm. (K-L) Graphs of the number of GFP+ cells normalized to total area measured in the EGL (K) and the percent of GFP+ cells in the EGL among the total number of GFP+ cells (L) from *Nes-m* controls (Non-IR, n = 3; IR, n = 3) and *Nes-mYap* cKOs (Non-IR, n = 4; IR, n = 3) at P8. Data are presented as mean ± S.D., and statistical analysis by two-way ANOVA. Each data point represents one animal.

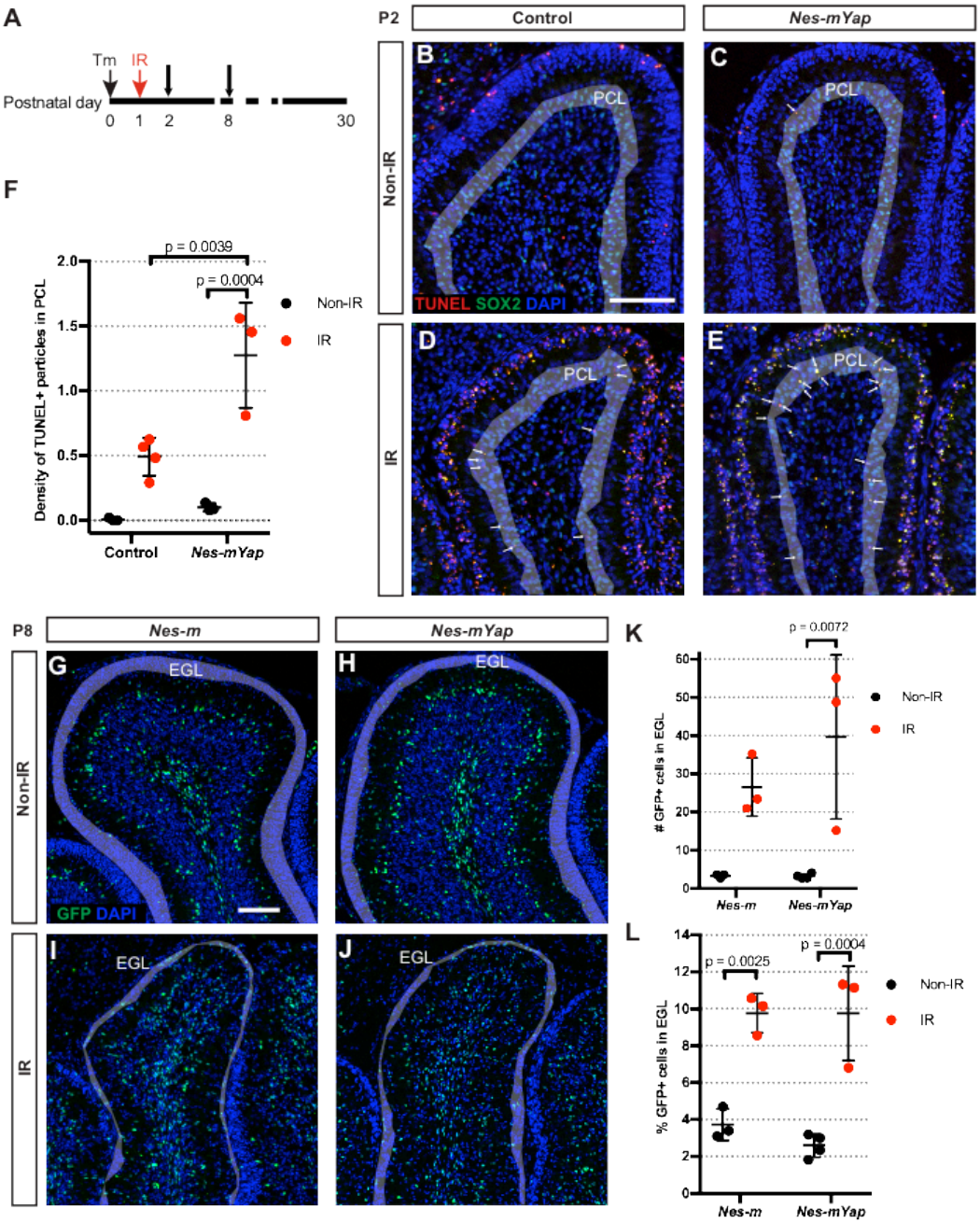
A
Tm
IR
Postnatal day
0
1
2
8
30
F
p = 0.0039
p = 0.0004
Density of TUNEL+ particles in PCL
2.0
1.5
1.0
0.5
0.0
Non-IR
IR
Control
Nes-mYap
P2
Control
Nes-mYap
Non-IR
IR
B
C
D
E
PCL
TUNEL SOX2 DAPI
P8
Nes-m
Nes-mYap
G
H
I
J
EGL
GFP DAPI
K
p = 0.0072
# GFP+ cells in EGL
60
50
40
30
20
10
0
Non-IR
IR
Nes-m
Nes-mYap
L
p = 0.0025
p = 0.0004
% GFP+ cells in EGL
14
12
10
8
6
4
2
0
Non-IR
IR
Nes-m
Nes-mYap

Figure 3.11 Injury of EGL overrides the requirement for YAP in differentiation of NEPs.

(A) Graph of the total number of GFP+ cells per 0.1 mm^2 of the total area analyzed in lobule 4/5. (B-G) Graphs of the number and percentage of GFP+ cells in different layers (B,C), the number and percentage of PAX2+ GFP+ double cells (D,E) or S100β+ GFP+ double cells (F,G) within each layer per 0.1 mm^2 of the total area analyzed in lobule 4/5 from midsagittal sections of *Nes-m* controls (n=3) and *Nes-mYap* cKOs (n = 3) at P8. (A) P = 0.2816. (B) * P = 0.0180, F (4, 12) = 4.562. (D) * P = 0.0290, F (4, 12) = 3.927. Data are presented as mean ± S.D., and statistical analysis by two-way ANOVA. Each data point represents one animal.

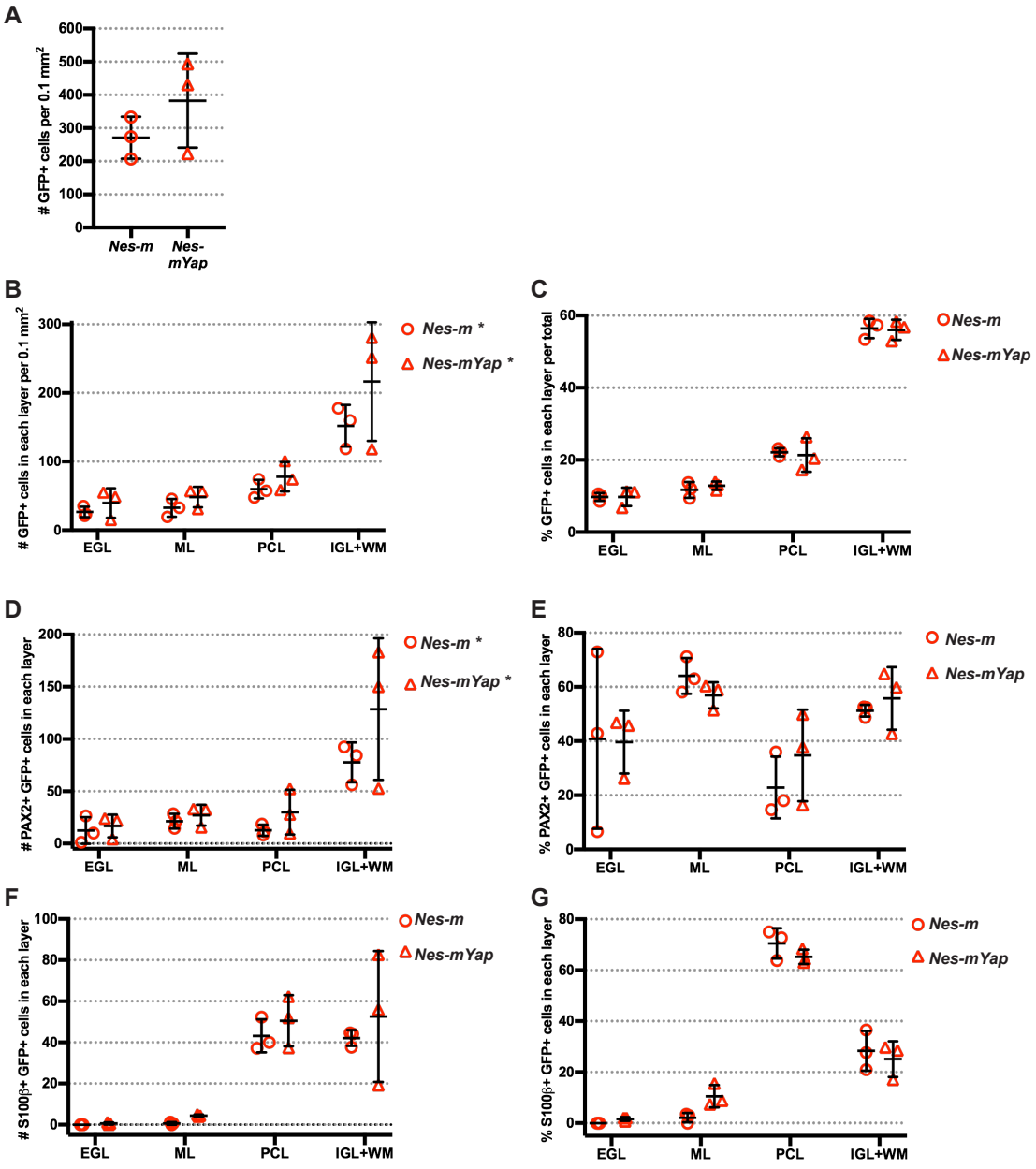
A
GFP+ cells per 0.1 mm2
600
500
400
300
200
100
0
Nes-m
Nes-mYap
B
GFP+ cells in each layer per 0.1 mm2
300
200
100
0
EGL
ML
PCL
IGL+WM
Nes-m *
Nes-mYap *
C
% GFP+ cells in each layer per total
60
40
20
0
EGL
ML
PCL
IGL+WM
Nes-m
Nes-mYap
D
PAX2+ GFP+ cells in each layer
200
150
100
50
0
EGL
ML
PCL
IGL+WM
Nes-m *
Nes-mYap *
E
% PAX2+ GFP+ cells in each layer
80
60
40
20
0
EGL
ML
PCL
IGL+WM
Nes-m
Nes-mYap
F
S100β+ GFP+ cells in each layer
100
80
60
40
20
0
EGL
ML
PCL
IGL+WM
Nes-m
Nes-mYap
G
% S100β+ GFP+ cells in each layer
80
60
40
20
0
EGL
ML
PCL
IGL+WM
Nes-m
Nes-mYap

To determine whether the loss of YAP alters the differentiation of NEPs into interneurons and astrocytes during irradiation-induced recovery of the CB, we quantified the normalized number and the percentage of GFP+ cells that were PAX2+ interneurons or S100β+ astrocytes in each layer of lobule 4/5. Unlike in Non-IR mice, although the number of PAX2+ interneurons showed a significant difference between *Yap* mutant and control mice, no difference was observed in the number or percentage of PAX2+ in any of the layers (Fig. 3.11D,E). Additionally, there was no difference in the production of S100β+ astrocytes between *Yap* mutant and control mice (Fig. 3.11F,G). These results indicate that the requirement for YAP in differentiation of NEPs is over-ridden when the EGL of the CB is injured.

We next analyzed the CB at P12, when the EGL is being diminished due to increased production of GCs. Given the reduction of the IGL in mutants compared to control IR P30 mice, we asked whether YAP plays a role in cell survival of GCPs. Strikingly, TUNEL staining in the EGL revealed a significant increase in the density of TUNEL+ cells within the EGL of *Nes-mYap* cKOs compared to littermate controls after IR ($p = 0.0306$; Fig. 3.12). The density of TUNEL+ cells within the EGL at P8 was similar between controls and mutants, consistent with the similar distribution of GFP+ cells (Fig. 3.13). These results indicate that YAP is required for the GCPs to maintain cell survival in the EGL during injury-induced recovery.

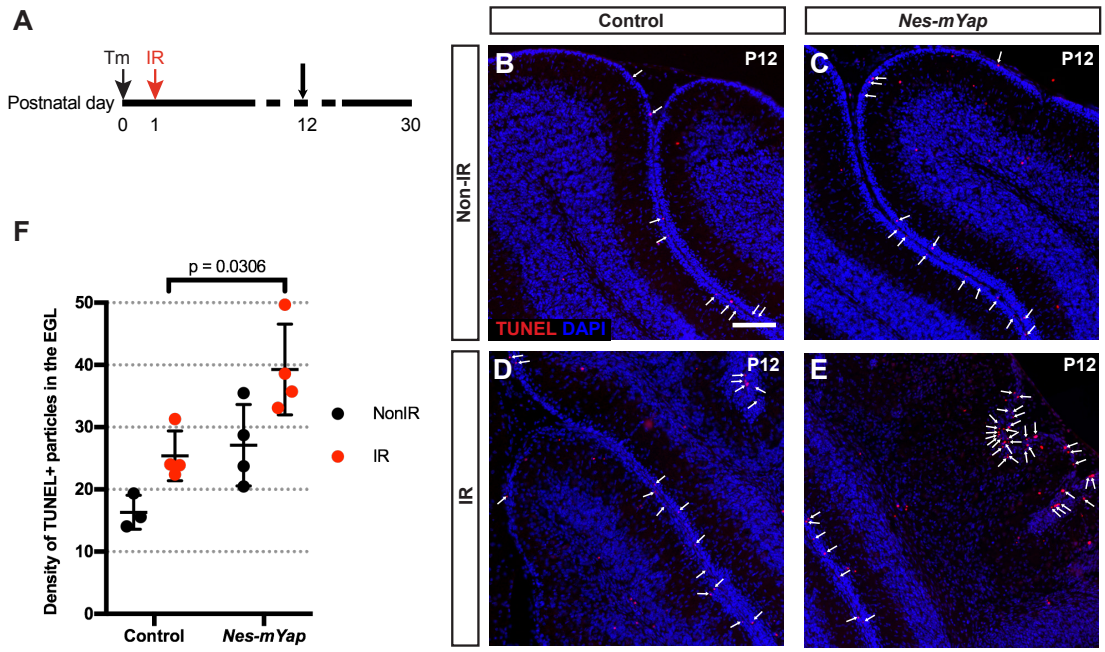

Figure 3.12 Loss of YAP results in more cell death in the EGL at P12 after IR-induced injury.

(A) Schematic showing experimental design. (B-E) Representative images showing IF staining of TUNEL and DAPI on midsagittal sections from *Nes-mYap* cKO and littermate controls at P12. Arrows indicate TUNEL+ particles in the EGL. Scale bars, 100 μm. (F) Graph of the density of TUNEL+ particles in the EGL (the number of TUNEL+ particles per 0.1 mm^2 of EGL area) in midline CB sections from *Nes-mYap* cKOs (Non-IR, n = 3; IR, n = 4) and littermate controls (Non-IR, n = 4; IR, n = 4) at P12. Data are presented as mean ± S.D., and statistical analysis by two-way ANOVA. Each data point represents one animal.

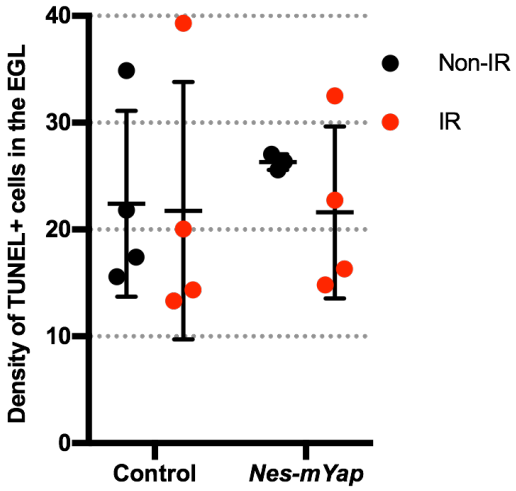

Figure 3.13 Loss of YAP does not alter cell death in the EGL at P8.

Graph of the density of TUNEL+ particles in the EGL (the number of TUNEL+ particles per 0.1 mm^2 of EGL area) in midline CB sections from *Nes-mYap* cKOs and littermate controls at P8. Controls: Non-IR, n = 4; IR, n = 4. *Nes-mYap* cKO: Non-IR, n = 3; IR, n = 4. Data are presented as mean ± S.D., and statistical analysis by two-way ANOVA. Each data point represents one animal.

Loss of *Taz* in *Yap* mutants does not abrogate NEP-driven recovery after irradiation

Since TAZ and YAP have been found to have both similar and distinct requirements in the development or regeneration of various organs (Deng et al., 2016; Hossain et al., 2007; Makita et al., 2008; Morin-Kensicki et al., 2006; Reginensi et al., 2013; Tian et al., 2007), and TAZ is expressed in NEPs and possibly upregulated in the nucleus after irradiation (Fig. 3.3C-D,C'-D'), we asked whether TAZ contributes to the regenerative response following irradiation in *Nes-mYap* cKOs. We first tested any requirement for *Taz* in development of the CB and replenishment of the CB after IR by administering Tm at P0 to *Nes-FlpoER/+;R26*$^{FSF\text{-}GFPcre/+}$*;Taz*$^{flox/flox}$ (*Nes-mTaz* cKO) mice and littermate controls (*Nes-FlpoER/+;Taz*$^{flox/flox}$, or *R26*$^{FSF\text{-}GFPcre/+}$*;Taz*$^{flox/flox}$, or *Taz*$^{flox/flox}$). Similar to *Nes-mYap* cKOs, conditional deletion of *Taz* did not affect the size or IGL of the P30 CB (Fig. 3.14; Fig. 3.16). However, unlike *Nes-mYap* cKOs, *Nes-mTaz* cKOs recovered almost as well as littermate control mice after IR (Fig. 3.14; Fig. 3.16). We next ablated both *Yap* and *Taz* from NEPs using *Nes-FlpoER/+;R26*$^{FSF\text{-}GFPcre/+}$*;Yap*$^{flox/flox}$*;Taz*$^{flox/flox}$ (*Nes-mYapTaz* cKO) mice and littermate controls (*Nes-FlpoER/+;Yap*$^{flox/flox}$*;Taz*$^{flox/flox}$, or *R26*$^{FSF\text{-}GFPcre/+}$*;Yap*$^{flox/flox}$*;Taz*$^{flox/flox}$, or *Yap*$^{flox/flox}$*;Taz*$^{flox/flox}$) given Tm at P0. Surprisingly, ablation of both *Yap* and *Taz* did not result in a worse recovery of the CB after injury compared to *Nes-mYap* cKOs. On the contrary, *Nes-mYapTaz* cKOs had no significant reduction in the area of the midline CB or IGL, but had a significant, although small reduction in the IGL/CB area ratio compared to controls (Fig. 3.17; Fig. 3.18). The genetic loss of *Yap* and *Taz* was confirmed via qRT-PCR analysis of the *Yap* mRNA levels in GFPcre+ NEPs of *Nes-mYapTaz* cKOs compared

to *Nes-m* control mice at P8 (Fig. 3.15). Significantly, the mRNA expression of both genes was greatly reduced. The apparent better recovery of *Nes-mYapTaz* cKOs compared to *Nes-mYap* cKOs could indicate that loss of *Taz* partially rescues the poor recovery observed in *Nes-mYap* cKOs (Fig. 3.18). This result would point to an opposing functional role of TAZ towards YAP, consistent with a similar finding in chondrocytes where TAZ competes with YAP in interacting with a regulator protein that can modulate cell maturation (Deng et al., 2016). Alternatively, the difference in genetic backgrounds of the single and double mutants could contribute to the degree of recovery of *Yap* mutant NEPs after IR.

Since YAP mildly affects the differentiation of NEPs during normal development of the CB, we next examined whether TAZ also has a function in regulation of differentiation of NEPs. The distribution of GFP+ NEP-lineage cells in the different layers of lobule 4/5 was quantified in both *Nes-mYapTaz* cKO and *Nes-m* control mice at P8. Similar to *Yap* single mutants, *Nes-mYapTaz* had a slight change in the number of GFP+ cells compared to controls (Fig. 3.19A-C). The number and percentage of PAX2+ interneurons were also significantly different between mutants and controls (Fig. 3.19D,E), however not specifically in the ML as in *Yap* mutants, suggesting that TAZ plays little role in the differentiation of NEPs into interneurons. The number and percentage of S100β+ were similar between mutants and controls (Fig. 3.19F,G), unlike *Yap* single mutants that have an increase in astrocytes in the PCL, indicating that TAZ antagonizes YAP in the function of NEPs in the PCL.

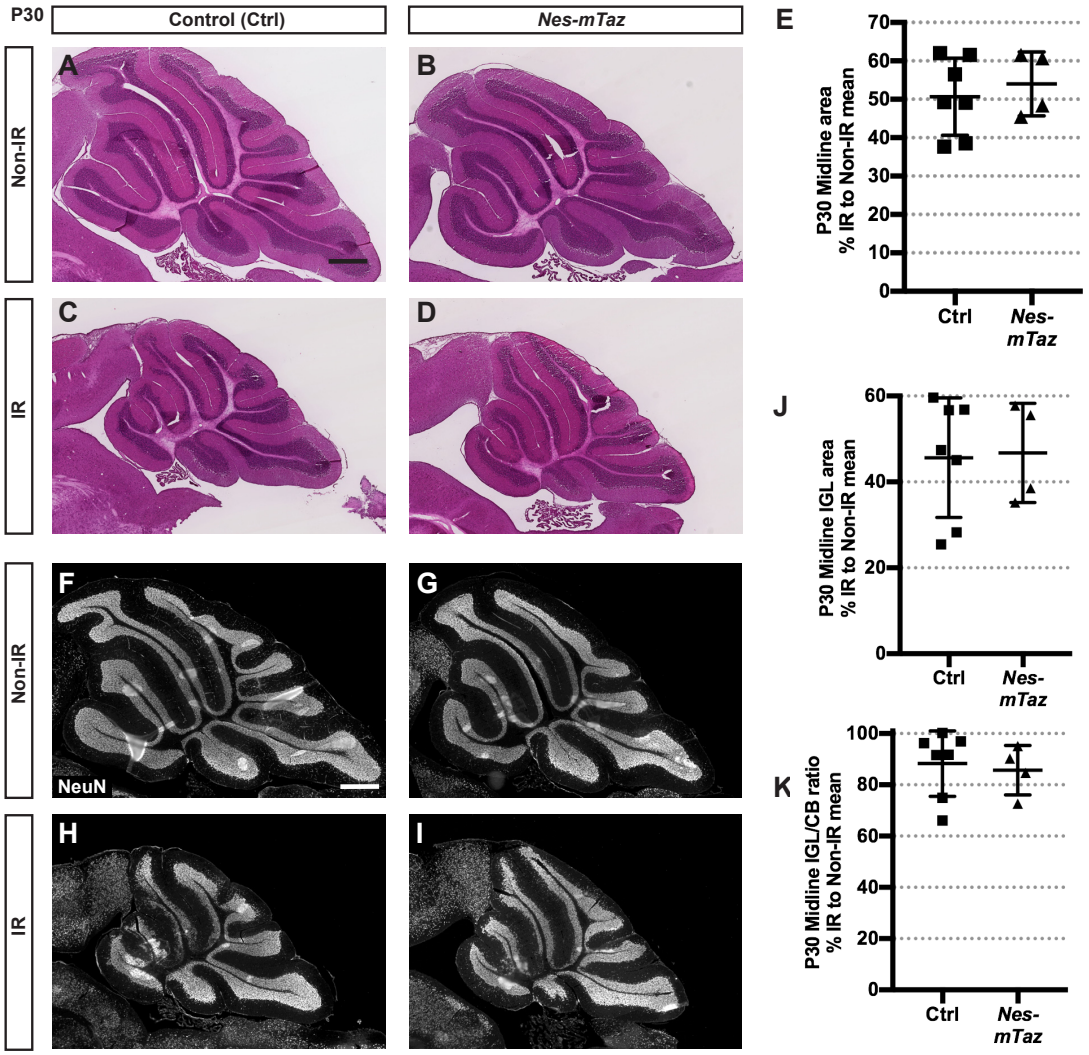

Figure 3.14 Loss of *Taz* does not affect cerebellar growth during development and regeneration.

(A-D) H&E staining of midsagittal sections of cerebella from Non-IR and IR animals at P30. Scale bars, 500 μm. (E) Graph of the ratio of the area of the CB of IR/Non-IR animals in midline sections. p = 0.5866. (F-I) IF detection of NeuN on midsagittal sections of the CB from Non-IR and IR animals at P30. Scale bar, 500 μm. (J,K) Graphs of the ratio of IGL area of IR/Non-IR mice (J) and IGL/CB area (K) from *Nes-mTaz* cKOs (Non-IR, n = 6; IR, n = 4) and littermate controls (Non-IR, n = 4; IR, n = 7) at P30. (J) p = 0.8945; (K) p = 0.7335. Data are presented as mean ± S.D., and statistical analysis by unpaired t test. Each data point represents one animal, and is calculated using each IR measurement divided by the mean of Non-IR mice.

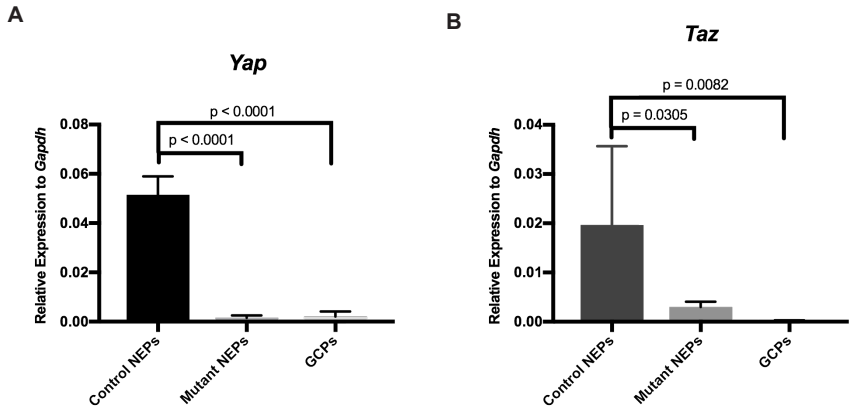

Figure 3.15 *Yap* and *Taz* mRNA are greatly reduced in *YapTaz*-mutant NEPs.

(A-B) qRT-PCR analysis of the mRNA expression of *Yap* (A) and *Taz* (B) relative to *Gapdh* in NEPs isolated by FACS (GFP+ cells) from *Nes-m* (Control NEPs) and *Nes-mYapTaz* (Mutant NEPs) at P8, as well as GCPs (GFP+ cells) from *Atoh1-Gfp* mice. Data are presented as mean ± S.D., and statistical analysis by one-way ANOVA.

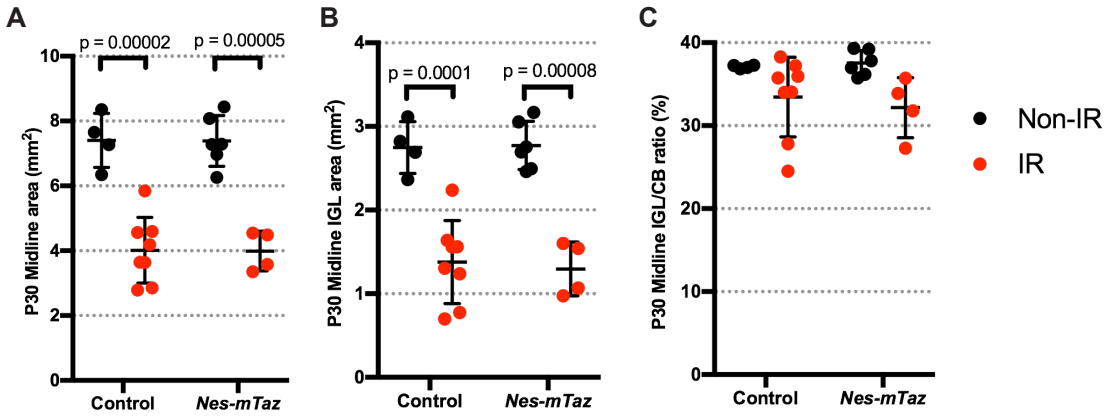

Figure 3.16 Loss of *Taz* does not affect cerebellar growth during development and regeneration.

(A-C) Graphs of the CB area (A), the IGL area (B), and IGL/CB area ratio (C) of midline CB sections from *Nes-mTaz* cKOs (Non-IR, n = 6; IR, n = 4) and littermate controls (Non-IR, n = 4; IR, n = 8) at P30. Data are presented as mean ± S.D., and statistical analysis by two-way ANOVA. Each data point represents one animal.

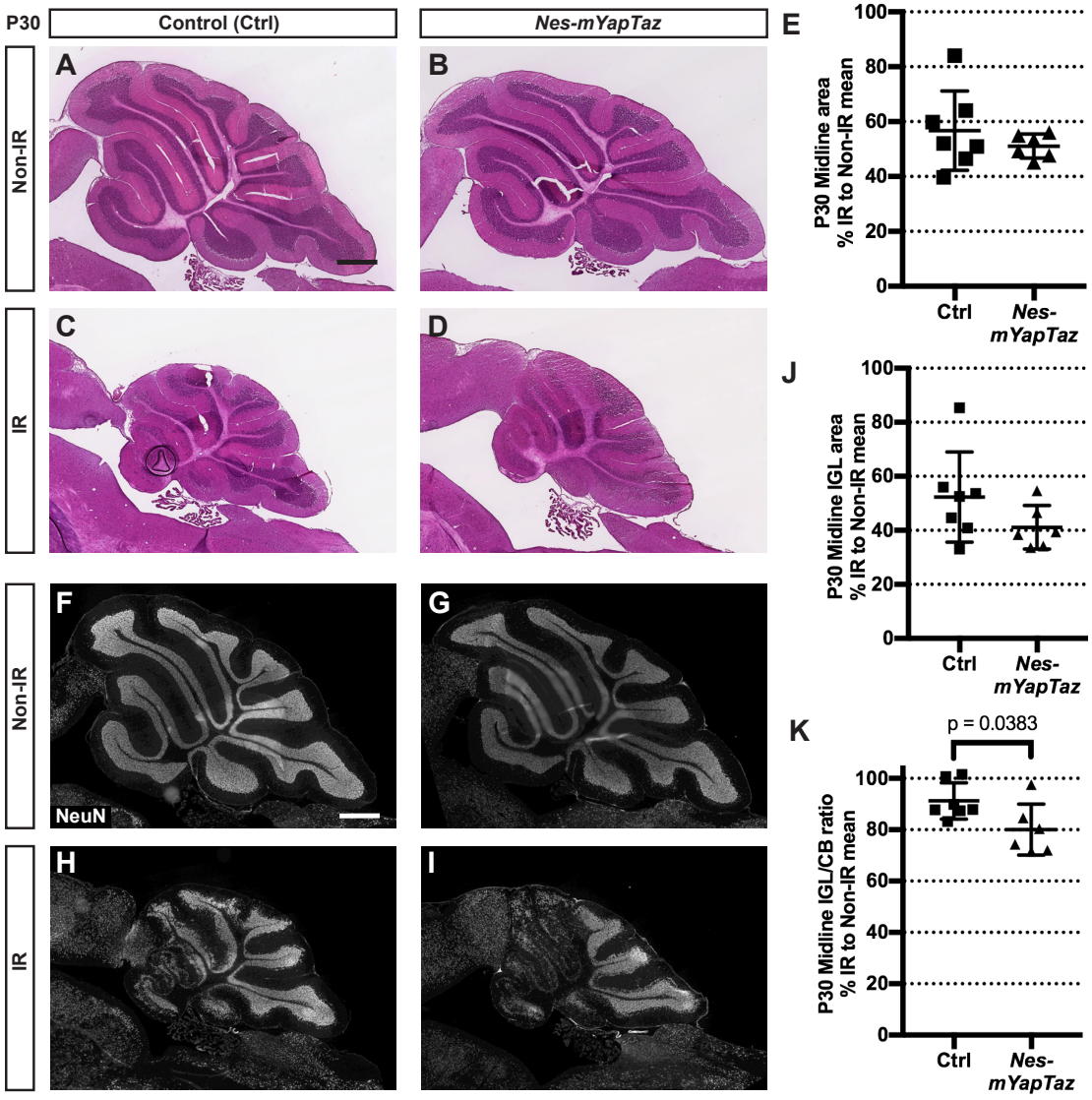

Figure 3.17 Loss of *Taz* in *Yap* mutants does not abrogate NEP-driven recovery after irradiation.

(A-D) H&E staining of midsagittal sections of the CB from Non-IR and IR animals at P30. Scale bars, 500 μm. (E) Graph of the ratio of the midline CB area IR mice as a ratio of Non-IR littermates of the same genotype. p = 0.3815. (F-I) IF detection of NeuN on midsagittal sections of the CB from non-IR and IR animals at P30. Scale bar, 500 μm. (J,K) Graphs of the area of the IGL (J) and IGL/CB area (K) as a ratio of Non-IR littermates of the same genotype in midsaggital sections from *Nes-mYapTaz* cKOs (Non-IR, n = 7; IR, n = 6) and littermate controls (Non-IR, n = 4; IR, n = 7) at P30. (J) p = 0.1637; (K) p = 0.0383. Data are presented as mean ± S.D., and statistical analysis by unpaired t test. Each data point represents one animal, and is calculated using each IR divided by the mean of Non-IR X 100.

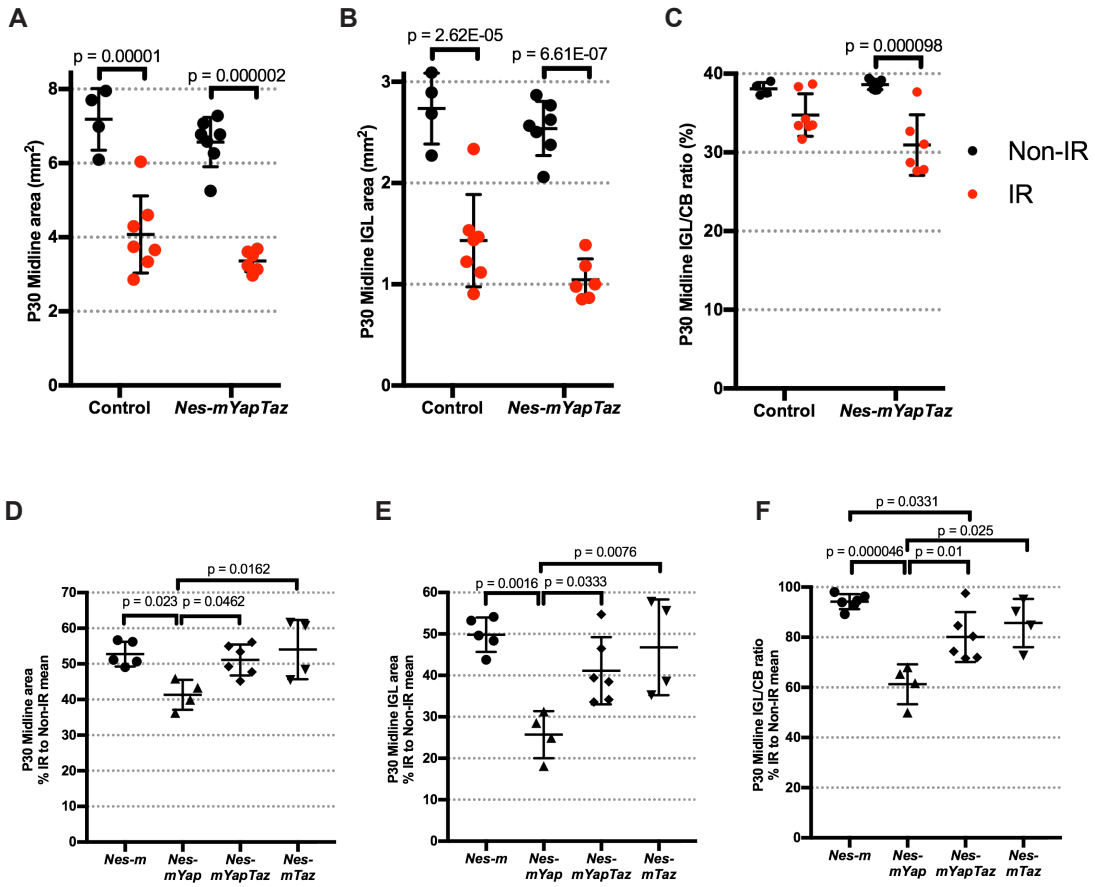

Figure 3.18 Loss of *Taz* in *Yap* mutants does not abrogate NEP-driven recovery after irradiation.

(A-C) Graphs of the midline CB area (A), the IGL area (B), and IGL/CB area as a percentage (C) for IR mice as a ratio of Non-IR littermates of the same genotype. *Nes-mYazTaz* cKOs (Non-IR, n = 7; IR, n = 6) and littermate controls (Non-IR, n = 4; IR, n = 7) at P30. Data are presented as mean ± S.D., and statistical analysis by two-way ANOVA. Each data point represents one animal. (D-F) Graphs of the ratio of IR/Non-IR animals as a percentage for midline CB area (D), the IGL area (E), and IGL/CB area ratio (F) from *Nes-m* controls (Non-IR, n = 6; IR, n = 5), *Nes-mYap* cKO (Non-IR, n = 6; IR, n = 4), *Nes-mYazTaz* cKO (Non-IR, n = 7; IR, n = 6), and *Nes-mTaz* cKO (Non-IR, n = 6; IR, n = 4), at P30. Data are presented as mean ± S.D., and statistical analysis by one-way ANOVA. Each data point represents one animal.

Figure 3.19 Loss of Yap and *Taz* mildly affects differentiation of NEPs during normal development of CB.

(A) Graph of the total number of GFP+ cells per 0.1 mm^2 of the total area analyzed in lobule 4/5. (B-G) Graphs of the number and percentage of GFP+ cells in different layers (B,C), the number and percentage of PAX2+ GFP+ double cells (D,E) or S100β+ GFP+ double cells (F,G) within each layer per 0.1 mm^2 of the total area analyzed in lobule 4/5 from midsagittal sections of *Nes-m* controls (n=3) and *Nes-mYapTaz* cKOs (n = 3) at P8. (A) P = 0.3430. (B) * P = 0.0108, F (4, 12) = 5.294. (D) * P = 0.0353, F (4, 12) = 3.681. (E) * P = 0.0405, F (4, 12) = 3.511. Data are presented as mean ± S.D., and statistical analysis by two-way ANOVA. Each data point represents one animal.

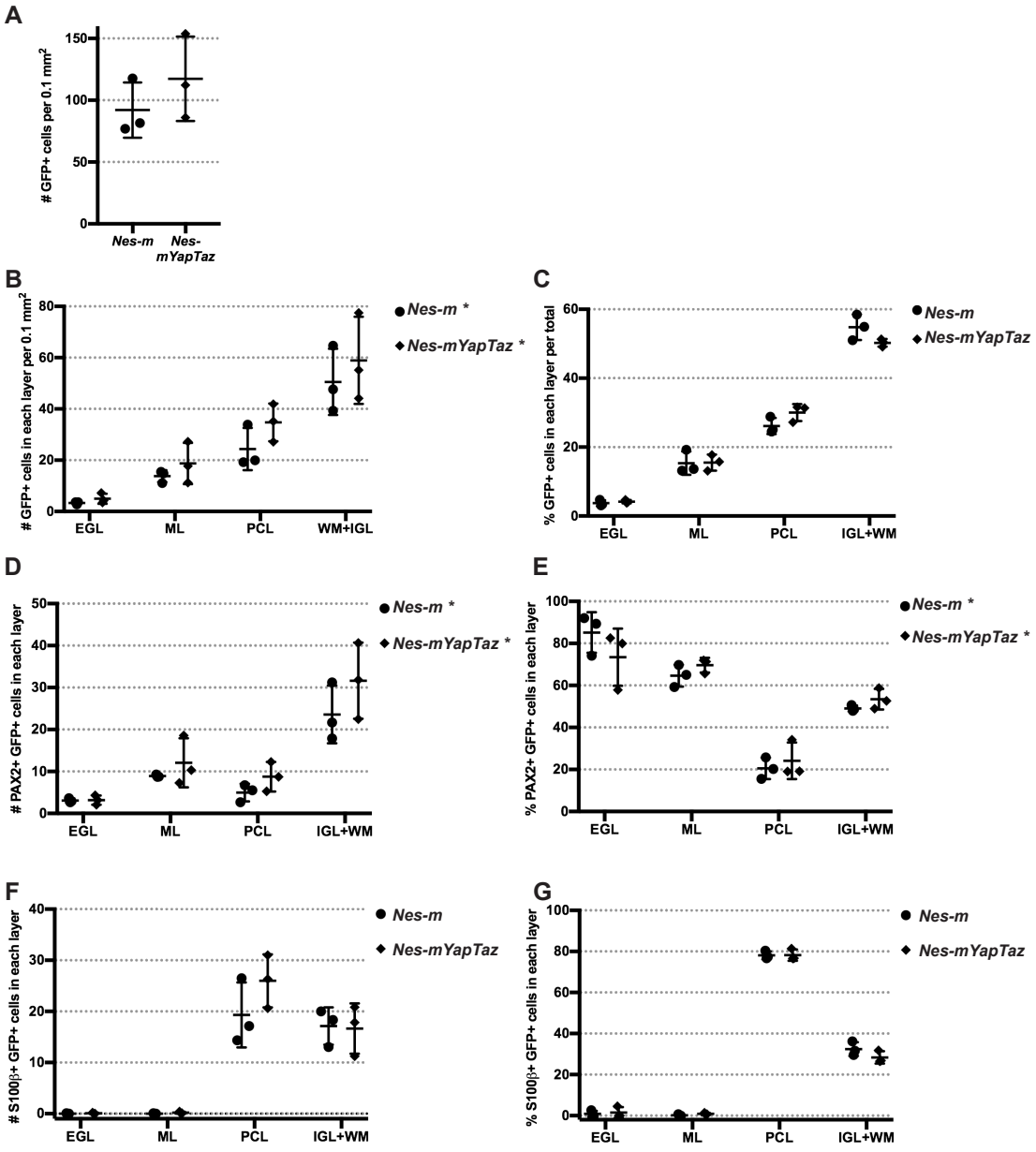
A
GFP+ cells per 0.1 mm2
150
100
50
0
Nes-m
Nes-mYapTaz
B
GFP+ cells in each layer per 0.1 mm2
80
60
40
20
0
EGL
ML
PCL
WM+IGL
Nes-m *
Nes-mYapTaz *
C
% GFP+ cells in each layer per total
60
40
20
0
EGL
ML
PCL
IGL+WM
Nes-m
Nes-mYapTaz
D
PAX2+ GFP+ cells in each layer
50
40
30
20
10
0
EGL
ML
PCL
IGL+WM
Nes-m *
Nes-mYapTaz *
E
% PAX2+ GFP+ cells in each layer
100
80
60
40
20
0
EGL
ML
PCL
IGL+WM
Nes-m *
Nes-mYapTaz *
F
S100β+ GFP+ cells in each layer
40
30
20
10
0
EGL
ML
PCL
IGL+WM
Nes-m
Nes-mYapTaz
G
% S100β+ GFP+ cells in each layer
100
80
60
40
20
0
EGL
ML
PCL
IGL+WM
Nes-m
Nes-mYapTaz

DISCUSSION

The pivotal role of the Hippo signaling pathway in brain development has been extensively studied in *Drosophila*, a model organism in which the Hippo pathway itself was first discovered. For example, disruption of Hippo signaling, through either loss-of-function mutations in several core kinases or over-expression of the *Drosophila* YAP homolog Yorkie, results in increased neuroblast proliferation and substantial brain overgrowth (Poon et al., 2016). In the mouse, loss of YAP in cortical neural progenitors leads to subtle defects in cortical development (Park et al., 2016), whereas genetic ablation of both *Yap* and *Taz* in radial glial progenitors results in profound cortical defects, (Kong, 2018). The more severe phenotype in *YapTaz* double mutants suggests functional redundancy between YAP and TAZ, or that the time difference in the onset of genetic ablation with the different Cre lines used in the two studies is critical. In this study, we explored the roles of YAP and TAZ in development and postnatal regeneration of the mouse cerebellum. Consistent with the subtle role of YAP in cortical development (Park et al., 2016), YAP ablation from NEPs or GCPs did not affect the overall size of the adult CB. We nevertheless observed minor defects in the differentiation of NEPs and GCPs (Fig. 3.20). Unlike in cortical development, genetic ablation of both *Yap* and *Taz* in NEPs or GCPs did not affect growth of the CB, suggesting that YAP and TAZ might have distinct functions in different brain regions. The difference in severity of the phenotypes, however, could be due to the later time of Cre activity onset in our study of the CB. It is likely that additional pathways or regulatory cues cooperate with Hippo signaling to ultimately ensure normal growth of the CB.

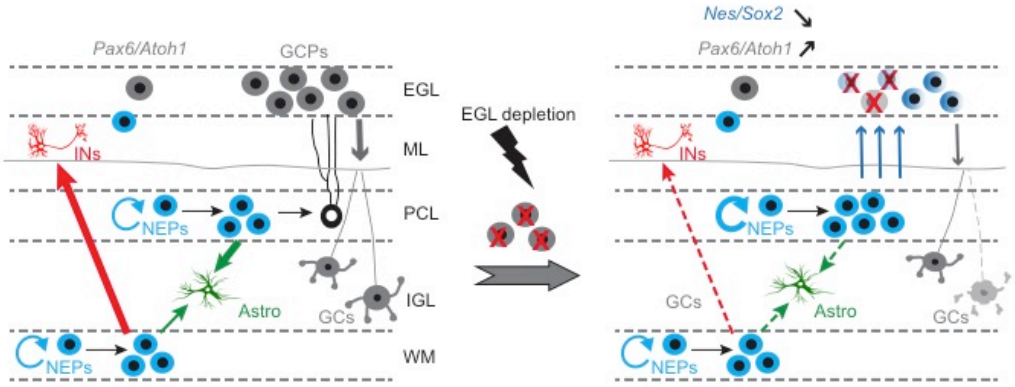

Figure 3.20 Model of the cellular responses during the development and impaired regeneration of the neonatal cerebellum in *Nes-mYap* mouse after irradiation at P1.
(Adapted from (Wojcinski et al., 2017))

In Non-IR *Nes-mYap* mice, the growth of cerebella is not altered during development, with normal CB size and Internal Granule Layer (IGL). Genetic ablation of *Yap* from *Nestin*-Expressing Progenitors (NEPs) promotes the differentiation of White Matter (WM) NEPs into interneurons (INs) in the Molecular Layer (ML), and the differentiation of Purkinje Cell Layer (PCL) NEPs into astrocytes (Astro).
In IR *Nes-mYap* mice, depletion of the External Granule Layer (EGL) during the first days of postnatal cerebellar development leads to the expansion and migration of NEPs in the PCL that normally produce Astrocytes (Astro) and Bergmann Glia (Bg) to the EGL. At P12 in IR *Nes-mYap* mice have an increase in GCP cell death compared to that in control mice that likely accounts for the poor recovery of the IGL and much fewer Granule Cells (GCs). The differentiation of NEPs, however, is overridden in IR cerebella.

Although YAP does not have a major role in growth of the CB during development, we demonstrated that it has a minor role in differentiation of GCPs and NEPs, and a major requirement for postnatal regeneration following irradiation. A similar paradigm has also shown to be true in the liver, as YAP seems dispensable for the growth of liver to achieve relatively normal liver to body weight ratios during normal development, but is required for its proper regeneration (Lu et al., 2018). Moreover, mechanical changes of normal and diseased tissues have been shown to alter YAP/TAZ activities and thereby change proliferation and differentiation of progenitor cells (Vining and Mooney, 2017). In particular, YAP activity depends on force-dependent nuclear translocation (Elosegui-Artola et al. Cell 2017). Thus it is possible that YAP is activated by drastic mechanical changes of tissues caused by acute injury and then acts to promote regeneration.

Several lines of evidence suggest an intersection or coupling of the Hedgehog (HH) and Hippo pathways in *Drosophila* and mice (Fernandez et al., 2009; Huang and Kalderon, 2014). Specifically, in flies elevated Hh signaling (*ptc* mutants) induces Yorkie target gene activities, while additional Yorkie deletion abolishes the effects of excess Hh signaling on cell proliferation and survival (Huang and Kalderon, 2014). In cultured mouse GCPs, SHH treatment increases the transcription and nuclear localization of YAP protein (Fernandez et al., 2009). Our previous study showed that SHH signaling is required for NEPs to regenerate the mouse CB (Wojcinski et al., 2017). Thus it is possible that SHH signaling activates YAP to promote the survival of GCPs derived from NEPs. On the other hand, comparison of *Nes-Smo* cKO and *Nes-Yap* cKO phenotypes after irradiation of the CB reveals an immediate defect in

recovery in the *Nes-Smo* cKOs, compared to the late defect in *Nes-Yap* cKOs. One possibility is that SHH has other target genes besides *Yap* that are required for proliferation and migration of NEPs.

Using genetic knockout of *Yap* in the Nestin-expressing NEPs and *Atoh1*-expressing GCPs, we found that YAP restricts differentiation of neural progenitors and thus likely maintains self-renewal. In particular, loss of YAP results in an increase in differentiation of NEPs (PCL NEPs to produce astrocytes and WM NEPs to produce interneurons) and GCPs (to produce granule cells) between P1 and P8. This finding is consistent with recent studies that emphasize the functional role of YAP in modulating a timely transition from cell proliferation into differentiation. For example, YAP over-activation in mouse intestine or chick neural tube leads to expansion of progenitor cells and loss of differentiated cells (Camargo et al., 2007; Cao et al., 2008). It was also shown that cultured myoblasts with YAP overexpression failed to differentiate and form myotubes (Watt et al., 2010), and reduced Hippo signaling in mouse results in hyper-proliferation and failure of differentiation in multiple epithelial cell types (Lee et al., 2008). In a recent study, loss of the Hippo pathway kinases LATS1/2 was found to result in YAP/TAZ-driven hypertranscription, which resulted in impaired cortical neural progenitor differentiation and promotion of a transient over-proliferation (Lavado et al., 2018). Together, these lines of evidence provide an explanation for the increase in differentiation at the likely expense of self-renewal when *Yap* is removed from NEPs or GCPs in a mosaic manner.

YAP and TAZ have often been found to have overlapping functions, consistent with their significant homology and common binding partners, but some recent studies point to distinct roles in addition to overlapping functions of YAP and TAZ that appear to be context dependent. For example, *Yap* null mutant mice are embryonical lethals (Morin-Kensicki et al., 2006), whereas *Taz* nulls only show partial embryonic lethality and surviving mice have lung defects and kidney disease (Hossain et al., 2007; Makita et al., 2008; Tian et al., 2007). It has also been shown that TAZ competes with YAP in an interaction with a regulator protein that modulates the maturation of chondrocytes, a critical step for skeletal development and bone repair (Deng et al., 2016). Similarly in our study, *Yap* ablation from NEPs leads to poor recovery of the postnatal CB following acute injury, but deletion of *Taz* does not abrogate regeneration. Double conditional *Yap* and *Taz* mutants instead show a milder phenotype than *Yap* cKOs, indicating that loss of *Taz* partially rescues the *Yap* mutant phenotype. This finding raises the possibility of antagonizing functions between YAP and TAZ in the CB as in the bone compared to overlapping functions under other circumstances. Thus it will be important to dissect the distinct downstream molecular pathways of the two co-activators to reveal context-dependent functions of the Hippo pathway. Leveraging this knowledge will pave the road for potential therapeutic intervention for cerebellar hypoplasias caused by injury.

MATERIALS AND METHODS

Mice

The following mouse lines were used: *Nes-CFP* (Mignone et al., 2004), *Atoh1-GFP* (Chen et al., 2002), *Nestin-FlpoER* (Wojcinski et al., 2017), *Atoh1-FlpoER*, *Rosa26*$^{MASTR(frt\text{-}STOP\text{-}frt\text{-}GFPcre)}$ (Lao et al., 2012), *Yap*$^{flox/flox}$ and *Yap*$^{flox/flox}$*;Taz*$^{flox/flox}$ (Reginensi et al., 2013), and *Atoh1-Cre* (Matei et al., 2005). Tamoxifen (Sigma, T5648) was dissolved in corn oil at 20 mg/mL and a single dose of 200 µg/g was administered to P0 animals by subcutaneous injection. Mouse husbandry and all experiments were performed in accordance with MSKCC IACUC-approved protocols.

Irradiation

P1 mice were anesthetized by hypothermia and received a single dose of 4 Gy irradiation in an X-RAD 225Cx (Precision X-ray) Microirradiator in the MSKCC Small-Animal Imaging Core Facility. A 5-mm diameter collimator was used to target the CB from the left side of the animal.

Tissue Processing

For animals younger than P4, brains were dissected out and fixed in 4% paraformaldehyde overnight at 4°C. Animals P4-30 were anesthetized and transcardially perfused with PBS followed by chilled 4% paraformaldehyde. Brains were harvested and post-fixed overnight and cryoprotected in 30% sucrose before freezing in Cryo-OCT. Frozen brains were sectioned at 12 µm on a cryostat, and sagittal sections of the midline of the CB were used for all analyses.

Immunofluorescent (IF) staining

Cryosections were stained overnight at 4°C with the following primary antibodies: mouse anti-YAP (Abcam, AB56701), rabbit anti-TAZ (Santa Cruz, sc-48805), rat anti-GFP (1:1,000; Nacalai Tesque; 0440484), mouse anti-NeuN (Millipore, MAB377), rabbit anti-Calbindin D-28K (Swant, CB38), rabbit anti-GFAP (Dako, Z0334), rabbit anti-S100β (Dako, Z0311), rabbit anti-PAX2 (Invitrogen, 71600), and goat anti-SOX2 (R&D System, AF2018). Secondary antibodies for double labeling were donkey anti-species conjugated with Alexa Fluor 488 or 555 (1:1,000; Molecular Probes). Nuclei were counterstained with Hoechst 33258 (Invitrogen, H3569).

Microscopy

Images were collected either on a DM6000 Leica microscope using Zen software (Zeiss), or NanoZoomer 2.0 HT slide scanner (Hamamatsu Photonics) using NDP.scan software. All images were taken with 20X objectives, and processed using NDP.view2 and Photoshop software.

Flow Cytometry

Cerebella of *Atoh1-GFP* and *Nes-CFP* mice were dissected out under a dissecting microscope. Tissues were digested in Trypsin/DNase, and then subjected to FACS (fluorescence activated cell sorting) to isolate GFP+ or CFP+ cells. RNA was extracted from GFP+ or CFP+ cells of individual cerebella and then subject to qRT-PCR analysis.

qRT-PCR

RNA was isolated from FACS-isolated GFP+ cells from P4 *Atoh1-GFP* mice, FACS-isolated CFP+ cells from P4 *Nestin-CFP* mice, FACS-isolated GFP+ cells from *Nes-m* and *Nes-mYap* mice at P8, using a miRNeasyMicro Kit (Qiagen) according to the manufacturer's protocol. cDNA was prepared using iScript cDNA synthesis kit (Bio-Rad). qRT-PCR was performed using PowerUp Sybr Green Master Mix (Applied Biosystems). Fold changes in expression were calculated using the ΔΔCt method. The *Gapdh* gene was used to normalize the results. The following primer pairs were used: *Yap* forward 5′-ACCCTCGTTTTGCCATGAAC-3′, *Yap* reverse 5′-TGTGCTGGGATTGATATTCCGTA-3′, *Gapdh* forward 5′-CCAAGGTGTCCGTCGTGGATCT-3′, and *Gapdh* reverse 5′-GTTGAAGTCGCAGGAGACAACC-3'.

Quantification and statistical analysis

ImageJ software was used to measure the area (mm^2) of cerebellar section near the midline. For all IF staining, cell counts were obtained using Stereo Investigator Software. Three sections per animal and at least three animals per genotype and condition were analyzed for quantification. Statistical analyses were performed using Prism software (GraphPad) and significance was determined at $P < 0.05$. All statistical analyses were two-tailed. For two-group comparisons with equal variance as determined by the F-test, an unpaired Student's t test was used. For comparisons among four independent groups with equal variance, an unpaired one-way ANOVA was used. For comparisons between groups that are split with two independent variables, an unpaired two-way ANOVA was used. P values and degrees of freedom are

given in the figure legends. Data are presented as mean ± S.D. (standard deviation). No statistical methods were used to predetermine the sample size, but our sample sizes are similar to those generally employed in the field. No randomization was used. Data collection and analysis were not performed blind to the conditions of the experiments.

EdU (5-ethynyl-2'-deoxyuridine) Injection and Staining

For assessing cell proliferation, EdU (Invitrogen, E10187) was given at 100 mg/g by i.p. injection 1 h before euthanasia. Click-it EdU assay with Sulfo-Cyanine5 azide (Lumiprobe corporation, A3330) was used according to the protocol of the manufacturer.

TUNEL Staining

For TUNEL staining, slides were permeabilized with 0.5% TritonX-100, pre-incubated with Tdt buffer (30 mM Tris·HCl, 140 mM sodium cacodylate and 1 mM $CoCl_2$) for 15 min at room temperature, and incubated for 1 h at 37 °C in TUNEL reaction solution containing Terminal Transferase (Roche, 03333574001) and Digoxigenin-11-dUTP (Sigma-Aldrich, 11093088910). Then slides were incubated with anti-digoxigenin-rhodamine (Sigma-Aldrich, 11207750910) for 1 h.

REFERENCES

Allen, M. C. (2008). Neurodevelopmental outcomes of preterm infants. *Current opinion in neurology* **21**, 123-128.

Altman, J., Anderson, W. J. and Wright, K. A. (1969). Early effects of x-irradiation of the cerebellum in infant rats: decimation and reconstitution of the external granular layer. *Experimental neurology* **24**, 196-216.

Altman, J. and Bayer, S. A. (1997). Development of the cerebellar system in relation to its evolution, structure, and functions. *Boca Raton: CRC Press*.

Bayin, N. S., Wojcinski, A., Mourton, A., Saito, H., Suzuki, N. and Joyner, A. L. (2018). Age-dependent dormant resident progenitors are stimulated by injury to regenerate Purkinje neurons. *eLife* **7**.

Buffo, A. and Rossi, F. (2013). Origin, lineage and function of cerebellar glia. *Progress in neurobiology* **109**, 42-63.

Callus, B. A., Verhagen, A. M. and Vaux, D. L. (2006). Association of mammalian sterile twenty kinases, Mst1 and Mst2, with hSalvador via C-terminal coiled-coil domains, leads to its stabilization and phosphorylation. *The FEBS journal* **273**, 4264-4276.

Camargo, F. D., Gokhale, S., Johnnidis, J. B., Fu, D., Bell, G. W., Jaenisch, R. and Brummelkamp, T. R. (2007). YAP1 increases organ size and expands undifferentiated progenitor cells. *Current biology : CB* **17**, 2054-2060.

Cao, X., Pfaff, S. L. and Gage, F. H. (2008). YAP regulates neural progenitor cell number via the TEA domain transcription factor. *Genes & development* **22**, 3320-3334.

Chan, E. H., Nousiainen, M., Chalamalasetty, R. B., Schafer, A., Nigg, E. A. and Sillje, H. H. (2005). The Ste20-like kinase Mst2 activates the human large tumor suppressor kinase Lats1. *Oncogene* **24**, 2076-2086.

Chen, P., Johnson, J. E., Zoghbi, H. Y. and Segil, N. (2002). The role of Math1 in inner ear development: Uncoupling the establishment of the sensory primordium from hair cell fate determination. *Development (Cambridge, England)* **129**, 2495-2505.

Corrales, J. D., Blaess, S., Mahoney, E. M. and Joyner, A. L. (2006). The level of sonic hedgehog signaling regulates the complexity of cerebellar foliation. *Development (Cambridge, England)* **133**, 1811-1821.

Deng, Y., Wu, A., Li, P., Li, G., Qin, L., Song, H. and Mak, K. K. (2016). Yap1 Regulates Multiple Steps of Chondrocyte Differentiation during Skeletal Development and Bone Repair. *Cell reports* **14**, 2224-2237.

Dobbing, J. and Sands, J. (1973). Quantitative growth and development of human brain. *Archives of disease in childhood* **48**, 757-767.

Fatemi, S. H., Aldinger, K. A., Ashwood, P., Bauman, M. L., Blaha, C. D., Blatt, G. J., Chauhan, A., Chauhan, V., Dager, S. R., Dickson, P. E., et al. (2012). Consensus paper: pathological role of the cerebellum in autism. *Cerebellum (London, England)* **11**, 777-807.

Fernandez, L. A., Northcott, P. A., Dalton, J., Fraga, C., Ellison, D., Angers, S., Taylor, M. D. and Kenney, A. M. (2009). YAP1 is amplified and up-regulated in hedgehog-associated medulloblastomas and mediates Sonic hedgehog-driven neural precursor proliferation. *Genes & development* **23**, 2729-2741.

Fernandez, L. A., Squatrito, M., Northcott, P., Awan, A., Holland, E. C., Taylor, M. D., Nahle, Z. and Kenney, A. M. (2012). Oncogenic YAP promotes radioresistance and genomic instability in medulloblastoma through IGF2-mediated Akt activation. *Oncogene* **31**, 1923-1937.

Fleming, J. T., He, W., Hao, C., Ketova, T., Pan, F. C., Wright, C. C., Litingtung, Y. and Chiang, C. (2013). The Purkinje neuron acts as a central regulator of spatially and functionally distinct cerebellar precursors. *Developmental cell* **27**, 278-292.

Halder, G. and Johnson, R. L. (2011). Hippo signaling: growth control and beyond. *Development (Cambridge, England)* **138**, 9-22.

Hossain, Z., Ali, S. M., Ko, H. L., Xu, J., Ng, C. P., Guo, K., Qi, Z., Ponniah, S., Hong, W. and Hunziker, W. (2007). Glomerulocystic kidney disease in mice with a targeted inactivation of Wwtr1. *Proceedings of the National Academy of Sciences of the United States of America* **104**, 1631-1636.

Hu, J. K., Du, W., Shelton, S. J., Oldham, M. C., DiPersio, C. M. and Klein, O. D. (2017). An FAK-YAP-mTOR Signaling Axis Regulates Stem Cell-Based Tissue Renewal in Mice. *Cell stem cell* **21**, 91-106.e106.

Huang, C. C., Sugino, K., Shima, Y., Guo, C., Bai, S., Mensh, B. D., Nelson, S. B. and Hantman, A. W. (2013). Convergence of pontine and proprioceptive streams onto multimodal cerebellar granule cells. *eLife* **2**, e00400.

Huang, J. and Kalderon, D. (2014). Coupling of Hedgehog and Hippo pathways promotes stem cell maintenance by stimulating proliferation. *The Journal of cell biology* **205**, 325-338.

Kong, S. (2018). Loss of YAP/TAZ impaired the proliferation and differentiation ability of neural progenitor cells. *bioRxiv*.

Lao, Z., Raju, G. P., Bai, C. B. and Joyner, A. L. (2012). MASTR: a technique for mosaic mutant analysis with spatial and temporal control of recombination using conditional floxed alleles in mice. *Cell reports* **2**, 386-396.

Lavado, A., Park, J. Y., Pare, J., Finkelstein, D., Pan, H., Xu, B., Fan, Y., Kumar, R. P., Neale, G., Kwak, Y. D., et al. (2018). The Hippo Pathway Prevents YAP/TAZ-Driven Hypertranscription and Controls Neural Progenitor Number. *Developmental cell*.

Lee, J. H., Kim, T. S., Yang, T. H., Koo, B. K., Oh, S. P., Lee, K. P., Oh, H. J., Lee, S. H., Kong, Y. Y., Kim, J. M., et al. (2008). A crucial role of WW45 in developing epithelial tissues in the mouse. *The EMBO journal* **27**, 1231-1242.

Lewis, P. M., Gritli-Linde, A., Smeyne, R., Kottmann, A. and McMahon, A. P. (2004). Sonic hedgehog signaling is required for expansion of granule neuron precursors and patterning of the mouse cerebellum. *Developmental biology* **270**, 393-410.

Li, P., Du, F., Yuelling, L. W., Lin, T., Muradimova, R. E., Tricarico, R., Wang, J., Enikolopov, G., Bellacosa, A., Wechsler-Reya, R. J., et al. (2013). A population of Nestin-expressing progenitors in the cerebellum exhibits increased tumorigenicity. *Nature neuroscience* **16**, 1737-1744.

Lu, L., Finegold, M. J. and Johnson, R. L. (2018). Hippo pathway coactivators Yap and Taz are required to coordinate mammalian liver regeneration. *Experimental & molecular medicine* **50**, e423.

Makita, R., Uchijima, Y., Nishiyama, K., Amano, T., Chen, Q., Takeuchi, T., Mitani, A., Nagase, T., Yatomi, Y., Aburatani, H., et al. (2008). Multiple renal cysts, urinary concentration defects, and pulmonary emphysematous changes in mice lacking TAZ. *American journal of physiology. Renal physiology* **294**, F542-553.

Marek, S., Siegel, J. S., Gordon, E. M., Raut, R. V., Gratton, C., Newbold, D. J., Ortega, M., Laumann, T. O., Adeyemo, B., Miller, D. B., et al. (2018). Spatial and Temporal Organization of the Individual Human Cerebellum. *Neuron*.

Matei, V., Pauley, S., Kaing, S., Rowitch, D., Beisel, K. W., Morris, K., Feng, F., Jones, K., Lee, J. and Fritzsch, B. (2005). Smaller inner ear sensory epithelia in Neurog 1 null mice are related to earlier hair cell cycle exit. *Developmental dynamics : an official publication of the American Association of Anatomists* **234**, 633-650.

Mignone, J. L., Kukekov, V., Chiang, A. S., Steindler, D. and Enikolopov, G. (2004). Neural stem and progenitor cells in nestin-GFP transgenic mice. *The Journal of comparative neurology* **469**, 311-324.

Milosevic, A. and Goldman, J. E. (2004). Potential of progenitors from postnatal cerebellar neuroepithelium and white matter: lineage specified vs. multipotent fate. *Molecular and cellular neurosciences* **26**, 342-353.

Morin-Kensicki, E. M., Boone, B. N., Howell, M., Stonebraker, J. R., Teed, J., Alb, J. G., Magnuson, T. R., O'Neal, W. and Milgram, S. L. (2006). Defects in yolk sac vasculogenesis, chorioallantoic fusion, and embryonic axis elongation in mice with targeted disruption of Yap65. *Molecular and cellular biology* **26**, 77-87.

Nguyen, V., Sabeur, K., Maltepe, E., Ameri, K., Bayraktar, O. and Rowitch, D. H. (2018). Sonic Hedgehog Agonist Protects Against Complex Neonatal Cerebellar Injury. *Cerebellum (London, England)* **17**, 213-227.

Pan, D. (2010). The hippo signaling pathway in development and cancer. *Developmental cell* **19**, 491-505.

Park, R., Moon, U. Y., Park, J. Y., Hughes, L. J., Johnson, R. L., Cho, S. H. and Kim, S. (2016). Yap is required for ependymal integrity and is suppressed in LPA-induced hydrocephalus. *Nature communications* **7**, 10329.

Parmigiani, E., Leto, K., Rolando, C., Figueres-Onate, M., Lopez-Mascaraque, L., Buffo, A. and Rossi, F. (2015). Heterogeneity and Bipotency of Astroglial-Like Cerebellar Progenitors along the Interneuron and Glial Lineages. *The Journal of neuroscience : the official journal of the Society for Neuroscience* **35**, 7388-7402.

Poon, C. L., Mitchell, K. A., Kondo, S., Cheng, L. Y. and Harvey, K. F. (2016). The Hippo Pathway Regulates Neuroblasts and Brain Size in Drosophila melanogaster. *Current biology : CB* **26**, 1034-1042.

Rakic, P. and Sidman, R. L. (1970). Histogenesis of cortical layers in human cerebellum, particularly the lamina dissecans. *The Journal of comparative neurology* **139**, 473-500.

Reginensi, A., Scott, R. P., Gregorieff, A., Bagherie-Lachidan, M., Chung, C., Lim, D. S., Pawson, T., Wrana, J. and McNeill, H. (2013). Yap-

and Cdc42-dependent nephrogenesis and morphogenesis during mouse kidney development. *PLoS genetics* **9**, e1003380.

Sillitoe, R. V. and Joyner, A. L. (2007). Morphology, molecular codes, and circuitry produce the three-dimensional complexity of the cerebellum. *Annual review of cell and developmental biology* **23**, 549-577.

Steinlin, M. (2007). The cerebellum in cognitive processes: supporting studies in children. *Cerebellum (London, England)* **6**, 237-241.

Stoodley, C. J., D'Mello, A. M., Ellegood, J., Jakkamsetti, V., Liu, P., Nebel, M. B., Gibson, J. M., Kelly, E., Meng, F., Cano, C. A., et al. (2017). Altered cerebellar connectivity in autism and cerebellar-mediated rescue of autism-related behaviors in mice. *Nature neuroscience* **20**, 1744-1751.

Tam, E. W. (2013). Potential mechanisms of cerebellar hypoplasia in prematurity. *Neuroradiology* **55 Suppl 2**, 41-46.

Tavano, A., Grasso, R., Gagliardi, C., Triulzi, F., Bresolin, N., Fabbro, F. and Borgatti, R. (2007). Disorders of cognitive and affective development in cerebellar malformations. *Brain : a journal of neurology* **130**, 2646-2660.

Tian, Y., Kolb, R., Hong, J. H., Carroll, J., Li, D., You, J., Bronson, R., Yaffe, M. B., Zhou, J. and Benjamin, T. (2007). TAZ promotes PC2 degradation through a SCFbeta-Trcp E3 ligase complex. *Molecular and cellular biology* **27**, 6383-6395.

Tsai, P. T., Hull, C., Chu, Y., Greene-Colozzi, E., Sadowski, A. R., Leech, J. M., Steinberg, J., Crawley, J. N., Regehr, W. G. and Sahin, M. (2012). Autistic-like behaviour and cerebellar dysfunction in Purkinje cell Tsc1 mutant mice. *Nature* **488**, 647-651.

Tsai, P. T., Rudolph, S., Guo, C., Ellegood, J., Gibson, J. M., Schaeffer, S. M., Mogavero, J., Lerch, J. P., Regehr, W. and Sahin, M. (2018). Sensitive Periods for Cerebellar-Mediated Autistic-like Behaviors. *Cell reports* **25**, 357-367.e354.

Udan, R. S., Kango-Singh, M., Nolo, R., Tao, C. and Halder, G. (2003). Hippo promotes proliferation arrest and apoptosis in the Salvador/Warts pathway. *Nature cell biology* **5**, 914-920.

Vining, K. H. and Mooney, D. J. (2017). Mechanical forces direct stem cell behaviour in development and regeneration. *Nature reviews. Molecular cell biology* **18**, 728-742.

Wang, K., Degerny, C., Xu, M. and Yang, X. J. (2009). YAP, TAZ, and Yorkie: a conserved family of signal-responsive transcriptional coregulators in animal development and human disease. *Biochemistry and cell biology = Biochimie et biologie cellulaire* **87**, 77-91.

Wang, S. S., Kloth, A. D. and Badura, A. (2014). The cerebellum, sensitive periods, and autism. *Neuron* **83**, 518-532.

Watt, K. I., Judson, R., Medlow, P., Reid, K., Kurth, T. B., Burniston, J. G., Ratkevicius, A., De Bari, C. and Wackerhage, H. (2010). Yap is a novel regulator of C2C12 myogenesis. *Biochemical and biophysical research communications* **393**, 619-624.

Wojcinski, A., Lawton, A. K., Bayin, N. S., Lao, Z., Stephen, D. N. and Joyner, A. L. (2017). Cerebellar granule cell replenishment postinjury by adaptive reprogramming of Nestin(+) progenitors. *Nature neuroscience* **20**, 1361-1370.

Wu, S., Huang, J., Dong, J. and Pan, D. (2003). hippo encodes a Ste-20 family protein kinase that restricts cell proliferation and promotes apoptosis in conjunction with salvador and warts. *Cell* **114**, 445-456.

Yui, S., Azzolin, L., Maimets, M., Pedersen, M. T., Fordham, R. P., Hansen, S. L., Larsen, H. L., Guiu, J., Alves, M. R. P., Rundsten, C. F., et al. (2018). YAP/TAZ-Dependent Reprogramming of Colonic Epithelium Links ECM Remodeling to Tissue Regeneration. *Cell stem cell* **22**, 35-49.e37.

Zhao, B., Li, L., Tumaneng, K., Wang, C. Y. and Guan, K. L. (2010). A coordinated phosphorylation by Lats and CK1 regulates YAP stability through SCF(beta-TRCP). *Genes & development* **24**, 72-85.

Chapter 4 Conclusions and future directions

The Hedgehog and Hippo pathways are two master regulators with divergent effects on tissue growth during development. Active HH signaling promotes cell expansion and morphogenesis, while active Hippo signaling contains organ growth. Thus, it would be intriguing to investigate further how the HH and Hippo pathways coordinate and fine-tune within a network of signaling molecules to ensure complete development of organs or organisms and that they attain their proper sizes. One possibility is that the HH and Hippo pathways exert their functions in a stepwise manner, such that HH stimulates major cell expansion of cell number and tissue growth, followed by Hippo downregulating or putting the breaks on growth to avoid overgrowth. It is also possible that both the HH and Hippo pathways act simultaneously and continuously maintain a growth equilibrium throughout the whole developmental process, so the growth of organs move on steadily at the correct pace until it is halted. Interestingly, the activities of both signaling pathways tend to decline with the completion of embryonic development and are maintained at low but detectable levels in adults, to regulate tissue homeostasis. Even though SHH and Hippo activities remain relatively quiescent in normal adult organs, they can be exploited in different biological contexts that require rapid cell proliferation and tissue growth, for example, organ regeneration and cancer. The work described in my thesis investigated both processes, specifically the role of HH signaling in prostate cancer and Hippo signaling in cerebellar regeneration. Our findings provide new insights into the complex modes of action and functions that developmental signaling pathways have in cancer progression and tissue regeneration.

Hedgehog signaling in the tumor stroma restrains prostate cancer progression in a mouse model

A majority of the tumor xenograft studies using prostate cancer cell lines suggested that HH pathway blockade by cyclopamine suppresses tumor growth (Fan et al., 2004; Karhadkar et al., 2004). However, in my thesis work, a genetic mouse model showed that ectopic activation of HH signaling in the *Gli1*-expressing subset of stromal cells leads to decreased tumor progression, suggesting that the tumor stroma can restrain PCa progression (Yang et al., 2017). This finding is consistent with several other studies in pancreas and bladder cancers, which showed that inhibition of HH signaling in the stroma decreases survival (Lee et al., 2014; Rhim et al., 2014; Shin et al., 2014). Additionally, in mouse models of colon cancer, stroma-specific HH activation inhibits tumor progression, while decreased HH activity accelerates colon tumourigenesis (Gerling et al., 2016; Lee et al., 2016). One difference between *in vitro* cell line studies and *in vivo* mouse studies may rest on the differential functions of HH signaling in cancer cells and its surrounding stromal cells. HH signaling activation in cancer cells may promote tumorigenesis through cell-autonomous functions, while HH signaling activation in stromal cells may exert cell-non-autonomous effects and inhibit the growth of cancer cells via reciprocal signaling. Thus, it will be interesting to systematically dissect the functions and interplay of HH signaling in cancer cells and its various types of stromal cells through *in vivo* mouse genetics. Although *in vivo* models have obvious superiorities to *in vitro* models, caution is still needed for the interpretation of studies using mouse models. As demonstrated in the three mouse models used in my thesis research, each mouse model exhibits a

distinct tumor microenvironment, and the models likely only represent a certain subset or a particular stage of the environment in human prostate tumors. Indeed, most genetically modified mouse models only simulate a limited part of normal cancer progression. Given the lack of reliable and robust prostate cancer metastasis mouse models, the effects of HH signaling in tumor metastasis are hard to determine.

Besides the extrinsic signaling coming from the stromal microenvironment in response to SHH signaling that acts as a brake on overgrowth of prostate cancer, an alternative mechanism for size control is intrinsic signaling cues. The Hippo pathway is a very appealing potential candidate. Tissue regeneration is also a process that requires strict control on cell expansion and organ growth. The adult prostate gland has a remarkable capability for regeneration with the addition of exogenous testosterone after castration-induced glandular involution (Isaacs, 1985). Amazingly, such cycles of involution and regeneration can be repeated over 30 times, and regenerated prostates always appear to completely reconstitute the architecture and restore the proper size. Such a precise control on the size of regenerated prostates raises an intriguing possibility that the Hippo pathway is likely responsible during regeneration to stop growth at the correct time. This idea can also be tested in other organs that have similar behavioral patterns of regeneration, for example, the liver.

YAP is essential for regeneration of the neonatal cerebellum after injury

In Chapter 3, I showed that YAP is required for a thorough restoration of cerebellum size and structure following irradiation at postnatal day 1 (P1).

However, it was not tested whether functional recovery of the cerebellar circuits is also affected by YAP ablation. A variety of behavioral tests for motor functions could be conducted, including footprint analysis, rotarod test, and fore limb grip strength test.

Although my thesis research focused on biological functions of YAP in cerebellar regeneration, it is possible that a mechanical force dependent mechanism of YAP signaling also plays a role during injury-induced recovery. Recently, emerging evidence indicates that the Hippo pathway plays a mechano-sensitive signaling mechanism to sense and convert physical changes into biochemical, cellular, and morphogenetic events (Elbediwy et al., 2018; Elosegui-Artola et al., 2017; Koser et al., 2016). Mechanical force is transmitted through extracellular matrix-nuclear coupling to stretch the nuclear pore resulting in nuclear translocation of YAP (Elosegui-Artola et al., 2017), which triggers downstream transcriptional programs for cell proliferation. Although the mechanical force-mediated cell proliferation changes are mostly documented in epithelial cells *in vitro* (Benham-Pyle et al., 2015; Gudipaty et al., 2017), it is increasingly appreciated that neurodevelopmental processes create diverse physical environments and may also take advantage of physical changes to direct tissue morphogenesis (Barnes et al., 2017; Vining and Mooney, 2017). For example, differential local tissue stiffness guides the axonal growth of retinal ganglion cells towards softer tissues in the developing *Xenopus* brain (Koser et al., 2016). Beyond normal biological contexts, tissue stiffness also plays a key role in carcinogenesis to mediate brain tumor progression (Barnes et al., 2017). Thus, it is possible that irradiation-induced injury creates an acute change in the physical environment in the neonatal

cerebellum. Consequently, Nestin-expressing progenitors (NEPs) may sense such changes through YAP activity and undergo over-proliferation to repair tissue damage.

My results showed that ablation of YAP in the irradiated cerebellum resulted in pronounced disorganization of Purkinje cells and Bergmann glial fibers in the adult stage. This phenotype is likely a secondary effect of the failure of the GCPs to generate an internal granule cell layer (IGL) in *Yap* mutants. Alternatively, *Yap* depletion results in a cell autonomous defect in Bergamnn glia, which in turn hinders the migration of GCPs into the IGL. This possibility is consistent with the observation that cell death in the Purkinje cell layer of *Yap* mutants is significantly elevated 1 day after irradiation compared to littermate controls (Fig. 3.10). Since Bergmann glial cells are situated in the Purkinje cell layer, it is possible that the elevated cell death is in the Bergmann glial population. Staining using a Bergmann glial markers BLBP can test this hypothesis, and the number of + Bergmann glial cells at P3 can be quantified to examined whether *Yap* mutant has less number of Bergmann glial cells.

Although YAP deletion did not affect the initial migration of NEPs into the EGL (at P8) after irradiation, it is possible that the migration of NEP-derived GCPs into the IGL is defective in *Yap* mutants. Indeed, YAP has been shown to regulate the migration of vascular tip cells and human glioma cells (Sakabe et al., 2017; Zhang et al., 2018). Therefore, the poor cerebellar recovery of *Yap* mutants may also be attributed to impairment in migration of NEP progenies into the IGL after they reached the EGL. In order to test this hypothesis, live imaging of GFP+ NEPs at P12 and P14 can be conducted such that migration

of NEPs can be observed directly. In addition, co-staining of centrosome markers and GFP in P12-P14 cerebella can be used to indicate the direction of migration. Alternatively, potential morphological defects in the leading processes of *Yap*-mutant NEPs might also be directly observed.

REFERENCES

Barnes, J. M., Przybyla, L. and Weaver, V. M. (2017). Tissue mechanics regulate brain development, homeostasis and disease. *Journal of cell science* **130**, 71-82.

Benham-Pyle, B. W., Pruitt, B. L. and Nelson, W. J. (2015). Cell adhesion. Mechanical strain induces E-cadherin-dependent Yap1 and beta-catenin activation to drive cell cycle entry. *Science (New York, N.Y.)* **348**, 1024-1027.

Elbediwy, A., Vanyai, H., Diaz-de-la-Loza, M. D., Frith, D., Snijders, A. P. and Thompson, B. J. (2018). Enigma proteins regulate YAP mechanotransduction. *Journal of cell science*.

Elosegui-Artola, A., Andreu, I., Beedle, A. E. M., Lezamiz, A., Uroz, M., Kosmalska, A. J., Oria, R., Kechagia, J. Z., Rico-Lastres, P., Le Roux, A. L., et al. (2017). Force Triggers YAP Nuclear Entry by Regulating Transport across Nuclear Pores. *Cell* **171**, 1397-1410.e1314.

Fan, L., Pepicelli, C. V., Dibble, C. C., Catbagan, W., Zarycki, J. L., Laciak, R., Gipp, J., Shaw, A., Lamm, M. L., Munoz, A., et al. (2004). Hedgehog signaling promotes prostate xenograft tumor growth. *Endocrinology* **145**, 3961-3970.

Gerling, M., Buller, N. V., Kirn, L. M., Joost, S., Frings, O., Englert, B., Bergstrom, A., Kuiper, R. V., Blaas, L., Wielenga, M. C., et al. (2016). Stromal Hedgehog signalling is downregulated in colon cancer and its restoration restrains tumour growth. *Nature communications* **7**, 12321.

Gudipaty, S. A., Lindblom, J., Loftus, P. D., Redd, M. J., Edes, K., Davey, C. F., Krishnegowda, V. and Rosenblatt, J. (2017). Mechanical stretch triggers rapid epithelial cell division through Piezo1. *Nature* **543**, 118-121.

Isaacs, J. T. (1985). Control of Cell Proliferation and Cell Death in the Normal and Neoplastic Prostate. IN: Benigh Prostatic Hyperplasia, Volume II (C. H. Rodgers, D. S. Coffey, G. Cunha, J. T. Grayhack, F. Hinman, Jr. and R. Horton, Eds.). NIH Publication No. 87-2881, pp. 2885-2894.

Karhadkar, S. S., Bova, G. S., Abdallah, N., Dhara, S., Gardner, D., Maitra, A., Isaacs, J. T., Berman, D. M. and Beachy, P. A. (2004). Hedgehog signalling in prostate regeneration, neoplasia and metastasis. *Nature* **431**, 707-712.

Koser, D. E., Thompson, A. J., Foster, S. K., Dwivedy, A., Pillai, E. K., Sheridan, G. K., Svoboda, H., Viana, M., Costa, L. D., Guck, J., et al. (2016). Mechanosensing is critical for axon growth in the developing brain. *Nature neuroscience* **19**, 1592-1598.

Lee, J. J., Perera, R. M., Wang, H., Wu, D. C., Liu, X. S., Han, S., Fitamant, J., Jones, P. D., Ghanta, K. S., Kawano, S., et al. (2014). Stromal response to Hedgehog signaling restrains pancreatic cancer progression. *Proc Natl Acad Sci U S A* **111**, E3091-3100.

Lee, J. J., Rothenberg, M. E., Seeley, E. S., Zimdahl, B., Kawano, S., Lu, W. J., Shin, K., Sakata-Kato, T., Chen, J. K., Diehn, M., et al. (2016). Control of inflammation by stromal Hedgehog pathway activation restrains colitis. *Proceedings of the National Academy of Sciences of the United States of America* **113**, E7545-e7553.

Rhim, A. D., Oberstein, P. E., Thomas, D. H., Mirek, E. T., Palermo, C. F., Sastra, S. A., Dekleva, E. N., Saunders, T., Becerra, C. P., Tattersall, I. W., et al. (2014). Stromal elements act to restrain, rather than support, pancreatic ductal adenocarcinoma. *Cancer Cell* **25**, 735-747.

Sakabe, M., Fan, J., Odaka, Y., Liu, N., Hassan, A., Duan, X., Stump, P., Byerly, L., Donaldson, M., Hao, J., et al. (2017). YAP/TAZ-CDC42 signaling regulates vascular tip cell migration. *Proceedings of the National Academy of Sciences of the United States of America* **114**, 10918-10923.

Shin, K., Lim, A., Zhao, C., Sahoo, D., Pan, Y., Spiekerkoetter, E., Liao, J. C. and Beachy, P. A. (2014). Hedgehog signaling restrains bladder cancer progression by eliciting stromal production of urothelial differentiation factors. *Cancer Cell* **26**, 521-533.

Vining, K. H. and Mooney, D. J. (2017). Mechanical forces direct stem cell behaviour in development and regeneration. *Nature reviews. Molecular cell biology* **18**, 728-742.

Yang, Z., Peng, Y. C., Gopalan, A., Gao, D., Chen, Y. and Joyner, A. L. (2017). Stromal hedgehog signaling maintains smooth muscle and hampers micro-invasive prostate cancer. *Disease models & mechanisms* **10**, 39-52.

Zhang, Y., Xie, P., Wang, X., Pan, P., Wang, Y., Zhang, H., Dong, Y., Shi, Y., Jiang, Y., Yu, R., et al. (2018). YAP Promotes Migration and Invasion of Human Glioma Cells. *Journal of molecular neuroscience : MN* **64**, 262-272.

APPENDIX

Table 2.3A List of genes with significant differential expressions ($p<0.05$, FDR<0.05, fold change >1.5).

Gene Symbol	P-value (Tumor vs. WT)	FDR step up (Tumor vs. WT)	Fold change (Tumor vs. WT)
Hoxc5	5.58E-06	2.71E-03	18032.52
Lppr4	2.71E-05	7.51E-03	8630.71
Hoxc8	6.38E-04	4.38E-02	5598.42
Hoxc6	1.06E-05	4.15E-03	4929.21
Has3	2.74E-06	1.63E-03	4143.30
Apol8	5.02E-05	1.04E-02	4021.21
Hotair	6.52E-10	6.02E-06	3993.11
Hoxa4	5.96E-05	1.20E-02	3505.57
Pydc4	1.53E-07	3.15E-04	3289.95
Col9a3	4.11E-04	3.57E-02	3175.37
AU040972	1.42E-04	2.04E-02	3047.99
Gm20758	3.72E-05	8.52E-03	3013.69
Hspb9	1.08E-11	1.99E-07	2949.93
Clec4n	3.00E-04	3.08E-02	2870.50
Mcm10	3.62E-05	8.52E-03	2607.49
Cyp3a41a	2.63E-05	7.49E-03	2343.74
Sall4	2.16E-05	6.59E-03	2291.24
Gfi1b	6.19E-06	2.79E-03	2089.07
Cd300ld	3.71E-05	8.52E-03	1925.99
Polq	5.23E-04	3.99E-02	1830.24
Gprc5d	1.58E-06	1.22E-03	1774.08
Trim67	1.48E-04	2.06E-02	1595.79
Actbl2	4.24E-04	3.60E-02	1590.05
Cd1d2	7.90E-05	1.41E-02	1353.41
Npb	2.41E-05	6.95E-03	1334.04
Gphb5	5.57E-04	4.13E-02	1297.87
4930502E09Rik	1.53E-05	5.34E-03	1176.84
Cyp3a41b	3.94E-05	8.88E-03	1116.74
Spem1	3.07E-04	3.12E-02	1017.34
Gm15350	1.16E-04	1.85E-02	929.04
Psmb11	8.79E-05	1.52E-02	829.12
Wnt3	1.23E-06	1.03E-03	803.99
1700001D01Rik	2.41E-04	2.69E-02	778.85
Platr7	1.75E-04	2.28E-02	748.43
Cst7	5.77E-05	1.18E-02	563.79
4930511A08Rik	3.51E-05	8.52E-03	548.58

Table 2.3A (Continued)

Gene Symbol	P-value (Tumor vs. WT)	FDR step up (Tumor vs. WT)	Fold change (Tumor vs. WT)
4930544G11Rik	3.51E-05	8.52E-03	548.58
Rnf151	3.51E-05	8.52E-03	548.58
Snora34	5.72E-07	8.13E-04	348.73
Matn4	1.58E-04	2.15E-02	17.07
A430090L17Rik	3.14E-04	3.14E-02	6.79
Adamts16	6.32E-04	4.36E-02	6.51
Hp	1.79E-04	2.30E-02	5.41
Fam166a	7.59E-04	4.91E-02	3.89
Snx29	3.98E-04	3.53E-02	3.76
Syne1	4.88E-04	3.85E-02	3.25
1700024P16Rik	5.07E-04	3.92E-02	3.21
Cdon	3.21E-04	3.17E-02	2.88
Cbx4	2.85E-04	2.95E-02	2.73
Sp110	1.52E-04	2.08E-02	2.69
Mycbp2	4.50E-04	3.73E-02	2.40
Fam193b	6.46E-04	4.40E-02	2.34
Zfp395	6.70E-04	4.50E-02	2.24
Lemd2	4.43E-04	3.70E-02	1.82
Ldb1	1.87E-04	2.35E-02	1.72
Rpe	2.40E-04	2.69E-02	-1.56
Tstd2	5.93E-04	4.23E-02	-1.57
Cbx5	4.44E-04	3.70E-02	-1.58
Pef1	1.45E-04	2.06E-02	-1.59
Sumo2	4.17E-04	3.60E-02	-1.59
Pus7l	2.23E-04	2.61E-02	-1.59
Ndufv2	1.66E-04	2.22E-02	-1.59
Gtf3c3	1.16E-04	1.85E-02	-1.60
Smdt1	4.06E-04	3.56E-02	-1.63
Cgrrf1	1.26E-04	1.90E-02	-1.64
Ssu72	5.20E-04	3.99E-02	-1.66
Cops3	3.78E-04	3.41E-02	-1.67
Atp6v0e	2.64E-04	2.86E-02	-1.68
Rps27l	2.44E-04	2.70E-02	-1.69
Psmd7	3.61E-04	3.33E-02	-1.71
Prelid1	5.14E-04	3.96E-02	-1.72
Abhd12	3.32E-04	3.24E-02	-1.72
Psmb2	6.02E-04	4.25E-02	-1.72

Table 2.3A (Continued)

Gene Symbol	P-value (Tumor vs. WT)	FDR step up (Tumor vs. WT)	Fold change (Tumor vs. WT)
Ciapin1	3.44E-04	3.31E-02	-1.75
Ndufa12	4.54E-04	3.73E-02	-1.75
Sike1	6.58E-04	4.45E-02	-1.77
Rbp1	3.60E-04	3.33E-02	-1.79
Fam63a	6.67E-04	4.50E-02	-1.80
Psma5	3.42E-04	3.31E-02	-1.80
Gskip	4.41E-04	3.70E-02	-1.80
Rab4b	6.08E-04	4.25E-02	-1.80
Rqcd1	1.81E-04	2.31E-02	-1.81
BC031181	1.67E-04	2.22E-02	-1.84
Msantd4	2.32E-04	2.67E-02	-1.87
Slc2a10	7.29E-04	4.76E-02	-1.88
Exoc3	7.31E-04	4.76E-02	-1.93
Gpx1	7.40E-05	1.36E-02	-1.94
Ran	2.37E-04	2.69E-02	-1.94
Psmd8	1.72E-04	2.27E-02	-1.97
Eif5a	7.03E-04	4.66E-02	-1.97
Cope	4.91E-04	3.85E-02	-1.99
Gng10	2.84E-04	2.95E-02	-2.00
Cox5a	3.49E-04	3.33E-02	-2.02
6030408B16Rik	1.48E-04	2.06E-02	-2.02
Fkbp1a	5.76E-04	4.20E-02	-2.04
Sgsm3	6.07E-04	4.25E-02	-2.07
Wdr1	5.89E-04	4.22E-02	-2.07
Suclg1	1.79E-04	2.30E-02	-2.08
Ptcd2	3.84E-04	3.44E-02	-2.08
Plp2	7.79E-04	5.00E-02	-2.08
Cers4	2.19E-04	2.60E-02	-2.10
Ccl7	2.42E-04	2.69E-02	-2.11
Nelfa	2.04E-04	2.51E-02	-2.11
Minos1	3.72E-04	3.39E-02	-2.11
Col6a1	2.46E-04	2.70E-02	-2.12
Prdx4	5.34E-04	4.06E-02	-2.13
Nme1	3.56E-04	3.33E-02	-2.16
Higd1a	4.07E-04	3.56E-02	-2.18
Ptpn14	5.86E-04	4.21E-02	-2.19
Alad	6.04E-04	4.25E-02	-2.25

Table 2.3A (Continued)

Gene Symbol	P-value (Tumor vs. WT)	FDR step up (Tumor vs. WT)	Fold change (Tumor vs. WT)
Rcl1	1.26E-04	1.90E-02	-2.26
Mrpl20	6.19E-04	4.28E-02	-2.36
Ccnd2	5.44E-04	4.11E-02	-2.45
Actg1	1.22E-04	1.89E-02	-2.80
B3gnt2	2.39E-04	2.69E-02	-2.86
Tpm1	4.70E-04	3.74E-02	-2.99
Anxa2	6.90E-04	4.60E-02	-2.99
Bok	2.21E-04	2.60E-02	-3.35
Synpo2	5.73E-04	4.20E-02	-3.50
Ociad2	3.21E-04	3.17E-02	-3.74
Ccnd1	6.72E-04	4.50E-02	-4.03
Lgals3	2.74E-04	2.92E-02	-4.04
Msmo1	5.86E-04	4.21E-02	-4.08
Pwwp2b	6.96E-04	4.62E-02	-4.20
Fdps	3.73E-05	8.52E-03	-4.26
Ucp2	1.17E-04	1.85E-02	-4.33
Hopx	5.60E-04	4.14E-02	-4.37
Id1	4.58E-04	3.73E-02	-4.55
B4galnt1	1.38E-04	2.01E-02	-5.36
Tubb4a	4.90E-04	3.85E-02	-5.46
S100a4	7.67E-04	4.94E-02	-5.65
Pde9a	8.77E-05	1.52E-02	-5.85
Nedd9	2.67E-04	2.87E-02	-6.55
Bhlhe40	4.10E-04	3.57E-02	-6.60
Cav1	4.18E-05	9.08E-03	-7.38
Tes	6.55E-04	4.45E-02	-7.44
Tmem132c	1.83E-04	2.31E-02	-7.58
Comp	1.74E-04	2.28E-02	-7.80
Cib2	7.19E-04	4.73E-02	-8.16
Adrb2	2.14E-04	2.55E-02	-8.18
Sqle	1.32E-04	1.95E-02	-8.27
Kdr	1.51E-05	5.34E-03	-8.84
Zdhhc14	7.04E-05	1.33E-02	-9.17
S1pr1	3.41E-04	3.31E-02	-9.88
Cx3cl1	5.85E-04	4.21E-02	-11.18
Pmaip1	1.05E-04	1.77E-02	-11.48
Perp	4.58E-04	3.73E-02	-12.97

Table 2.3A (Continued)

Gene Symbol	P-value (Tumor vs. WT)	FDR step up (Tumor vs. WT)	Fold change (Tumor vs. WT)
Gpc1	3.72E-04	3.39E-02	-13.11
Mboat2	6.02E-04	4.25E-02	-13.23
Etv1	5.81E-04	4.21E-02	-14.89
Efnb2	2.85E-04	2.95E-02	-19.02
Tinagl1	4.99E-04	3.88E-02	-24.84
Alpl	2.30E-04	2.67E-02	-28.08
Il34	1.83E-05	5.95E-03	-31.00
Aqp2	1.91E-04	2.38E-02	-31.06
Sbspon	4.60E-04	3.73E-02	-31.70
Tusc5	6.18E-04	4.28E-02	-36.97
Dner	2.05E-04	2.51E-02	-43.14
Rorb	4.56E-04	3.73E-02	-44.53
Pakap	6.17E-05	1.22E-02	-56.78
Apela	2.08E-04	2.52E-02	-82.60
Gfra1	5.66E-04	4.17E-02	-125.15
Ptn	7.11E-04	4.70E-02	-126.94
2610042L04Rik	1.04E-05	4.15E-03	-579.02
Wif1	2.21E-05	6.59E-03	-698.87
Defb2	3.62E-04	3.33E-02	-798.56
4933417G07Rik	6.83E-05	1.30E-02	-860.85
Sh2d1a	1.45E-04	2.06E-02	-999.55
Stap1	7.12E-07	8.77E-04	-1110.36
Mirt1	2.86E-04	2.95E-02	-1149.09
Cyyr1	3.21E-06	1.85E-03	-1221.16
Plekhd1	4.05E-04	3.56E-02	-1566.72
Pcdha9	7.45E-04	4.83E-02	-1706.91
Tox2	5.49E-04	4.11E-02	-1765.30
Vax1	8.99E-05	1.54E-02	-1800.58
Trim80	1.23E-04	1.89E-02	-1887.39
4930578C19Rik	5.87E-06	2.71E-03	-1896.19
Slc25a43	1.95E-04	2.42E-02	-1900.63
Clec4b1	1.32E-06	1.06E-03	-1959.60
Lmtk3	8.13E-09	5.01E-05	-1986.38
Ascl3	2.77E-04	2.94E-02	-2059.87
Pcdha12	3.78E-04	3.41E-02	-2081.92
Calcb	2.21E-05	6.59E-03	-2237.39
Plch2	5.49E-04	4.11E-02	-2471.70

Table 2.3A (Continued)

Gene Symbol	P-value (Tumor vs. WT)	FDR step up (Tumor vs. WT)	Fold change (Tumor vs. WT)
Dusp5	8.27E-07	8.90E-04	-2838.85
Col25a1	7.42E-05	1.36E-02	-2903.62
BC055402	2.79E-04	2.95E-02	-3003.59
Tmem54	4.68E-04	3.74E-02	-3080.46
Clcnka	2.32E-04	2.67E-02	-3159.52
Ecel1	4.65E-04	3.74E-02	-3443.70
1700049E15Rik	2.23E-06	1.55E-03	-3896.23
Serpina1c	1.21E-06	1.03E-03	-4075.91
Gimap1	3.59E-04	3.33E-02	-4164.47
Ms4a4c	1.19E-04	1.87E-02	-4302.21
H2-M2	7.24E-06	3.11E-03	-4373.50
Pcdha1	3.55E-04	3.33E-02	-4410.47
Prss16	4.50E-06	2.31E-03	-4705.61
Scnn1b	1.20E-05	4.51E-03	-4844.32
Gm14851	1.62E-04	2.19E-02	-4858.30
D030018L15Rik	4.23E-05	9.08E-03	-4876.66
Dach1	4.90E-04	3.85E-02	-5082.17
Tmeff1	2.47E-04	2.70E-02	-5132.64
Adgrl3	8.02E-05	1.41E-02	-5182.67
Drd4	2.77E-07	4.66E-04	-5661.51
Ms4a5	2.12E-05	6.59E-03	-5678.74
Padi2	1.36E-04	1.99E-02	-5730.72
Dgkg	3.09E-05	8.17E-03	-5795.94
2010107G23Rik	3.81E-06	2.07E-03	-5897.86
Dusp13	1.26E-04	1.90E-02	-5927.36
Pcyt1b	6.99E-06	3.07E-03	-5938.55
Klf8	3.06E-04	3.12E-02	-6230.26
Ptpn18	1.12E-04	1.84E-02	-6355.64
Fcna	4.03E-06	2.13E-03	-6367.38
Igsf21	3.27E-04	3.21E-02	-6554.08
4931429I11Rik	3.13E-04	3.14E-02	-6594.24
H60b	4.66E-04	3.74E-02	-6981.19
Spink11	7.45E-08	1.97E-04	-7155.25
Gimap8	5.47E-04	4.11E-02	-7156.39
Tmem255b	3.40E-07	5.24E-04	-7219.94
Galnt5	4.96E-08	1.83E-04	-7852.32
Fbxo40	1.08E-05	4.15E-03	-8034.29

Table 2.3A (Continued)

Gene Symbol	P-value (Tumor vs. WT)	FDR step up (Tumor vs. WT)	Fold change (Tumor vs. WT)
Pcp4	4.85E-06	2.42E-03	-8040.15
Chrm2	6.21E-05	1.22E-02	-8313.49
Sema7a	6.09E-04	4.25E-02	-8594.00
Scube1	1.34E-07	3.10E-04	-8835.23
Xkr5	7.99E-05	1.41E-02	-8955.12
6330403A02Rik	1.04E-04	1.76E-02	-9830.17
Gdnf	4.23E-04	3.60E-02	-9878.64
Samd5	3.02E-05	8.10E-03	-10392.51
Pbk	2.53E-06	1.59E-03	-10466.54
Emilin3	5.01E-05	1.04E-02	-10469.92
Slc27a6	9.44E-07	8.90E-04	-10541.08
Dscam	1.05E-05	4.15E-03	-10671.60
Mmd2	4.23E-05	9.08E-03	-10741.78
Rasd2	3.72E-05	8.52E-03	-11067.26
Mgat5b	4.13E-05	9.08E-03	-11142.79
Myct1	6.37E-05	1.24E-02	-11322.64
Sox6	1.59E-05	5.44E-03	-11343.24
Azgp1	6.58E-07	8.68E-04	-11502.03
Pitx2	9.37E-07	8.90E-04	-12077.02
H2-Ob	1.52E-04	2.08E-02	-12079.96
Mt3	2.15E-05	6.59E-03	-12586.50
Slc22a1	1.80E-05	5.94E-03	-12655.63
Madcam1	2.26E-08	1.04E-04	-13349.08
Vipr1	7.29E-04	4.76E-02	-13890.70
Cd209a	1.66E-05	5.56E-03	-13958.96
Hs3st3a1	4.18E-04	3.60E-02	-14359.28
Mfng	2.99E-05	8.10E-03	-15733.06
Dgkb	1.44E-05	5.23E-03	-15913.44
Lemd1	9.64E-07	8.90E-04	-16561.37
Egfem1	3.14E-04	3.14E-02	-16589.49
Mdga2	3.42E-05	8.52E-03	-16715.33
Npw	7.54E-05	1.37E-02	-16751.62
Frem2	2.09E-04	2.52E-02	-16815.37
Entpd3	4.94E-04	3.85E-02	-18157.82
Tlr12	9.52E-07	8.90E-04	-18866.90
Mall	7.62E-06	3.20E-03	-19208.91
Klk13	1.71E-07	3.17E-04	-19227.73

Table 2.3A (Continued)

Gene Symbol	P-value (Tumor vs. WT)	FDR step up (Tumor vs. WT)	Fold change (Tumor vs. WT)
Pcp4l1	6.81E-08	1.97E-04	-21601.93
Pdzk1ip1	2.72E-05	7.51E-03	-23010.27
Jakmip1	2.09E-06	1.54E-03	-24978.27
Emid1	6.45E-05	1.24E-02	-27218.54
Klk8	2.36E-06	1.56E-03	-28606.48
Plet1	3.47E-05	8.52E-03	-29569.98
Pkp3	5.52E-04	4.11E-02	-29640.43
Itga8	1.17E-04	1.85E-02	-29948.47
Wfdc6a	1.07E-04	1.77E-02	-30001.33
Sst	3.86E-04	3.45E-02	-30694.77
AU021092	5.85E-06	2.71E-03	-31208.27
Grb7	1.48E-04	2.06E-02	-32159.81
Rnf128	1.08E-04	1.77E-02	-33329.39
Abo	7.43E-05	1.36E-02	-33988.89
Krt5	3.72E-05	8.52E-03	-36991.00
Gm5615	1.28E-04	1.91E-02	-38033.02
Plekhs1	2.58E-06	1.59E-03	-50783.54
Ptgds	2.28E-05	6.70E-03	-77662.99
Pdyn	2.66E-04	2.87E-02	-90302.44
Kcnip1	3.50E-04	3.33E-02	-95679.59
Gsdma	2.27E-06	1.55E-03	-104113.40
Crmp1	3.80E-06	2.07E-03	-181236.20
Gja4	1.40E-05	5.17E-03	-287440.59